Design and Development of Clay-based Graphene/Polymer Composites for Extruded Cable Application

By

Sohrab AZIZI

MANUSCRIPT-BASED THESIS PRESENTED TO ÉCOLE DE TECHNOLOGIE SUPÉRIEURE IN PARTIAL FULFILLMENT OF THE REQUIREMENTS FOR THE DEGREE OF DOCTOR OF PHILOSOPHY Ph.D.

MONTREAL, May 10, 2019

ÉCOLE DE TECHNOLOGIE SUPÉRIEURE
UNIVERSITÉ DU QUÉBEC

BOARD OF EXAMINERS (THESIS PH.D.)

THIS THESIS HAS BEEN EVALUATED

BY THE FOLLOWING BOARD OF EXAMINERS

Mrs. Claudiane OUELLET-PLAMONDON, Thesis Supervisor
Department of Construction Engineering at École de Technologie Supérieure

Mr. Éric DAVID, Thesis Co-supervisor
Department of Mechanical Engineering at École de Technologie Supérieure

Mr. Michel FRÉCHETTE, Thesis Co-supervisor
Expert in Nanodielectrics, Retired from IREQ and currently associate professor at ETS

Mr. Mohamad JAHAZI, President of the Board of Examiners
Department of Mechanical Engineering at École de Technologie Supérieure

Mrs. Nicole DEMARQUETTE, Member of Jury
Department of Mechanical Engineering at École de Technologie Supérieure

Mr. Derek OLIVER, External Evaluator
Department of Department of Electrical and Computer Engineering at University of Manitoba

THIS THESIS WAS PRENSENTED AND DEFENDED

IN THE PRESENCE OF A BOARD OF EXAMINERS AND PUBLIC

ON APRIL 30, 2019

AT ÉCOLE DE TECHNOLOGIE SUPÉRIEURE

DEDICATION

Dedicated to:

To my beloved parents, Ali Azizi and Zivar Mohamadzadeh,

and my siblings, Yasin, Bahar, Morteza and Sajad

for their endless love and supports…

Without your encouragements, nothing was possible.

ACKNOWLEDGMENT

At the beginning, I am grateful of God.

Foremost, I would like to express my deepest gratitude to my thesis supervisor, Prof. Claudiane Ouellet-Plamondon, for accepting me as her Ph.D. student, and for her worthwhile supports and guidances. Under her supervision, it was a wonderful experience and opportunity to work hard to discover the world of composites.

I am also deeply thankful of my co-supervisors Prof. Éric David, Dr. Michel Frechette, and Phuong Nguyen-Tri. Their directions and support throughout the course of this research are greatly appreciated. What a professional experience working with them.

I would especially like to thank Professor Mohamad Jahazi, the president of my committee.

I also warmly thank Professor Nicole Demarquette and Professor Derek Oliver, the members of the jury.

A very special gratitude goes out to Natural Sciences and Engineering Research Canada (NSERC) for providing the funding for the work.

Special thanks to Dr. Behzad Ghafarizadeh, Emna Helal, Mohamad Saadati, Rafael Salles Kurusu, Hugues Couderc. Vincent Rohart, Mohsen Dastpak, Mr. Yvan Wilfried Tondji and Mrs. Lucie Banc.

I am also grateful to the following university staff: Mr. Nabil Mazeghrane, Radu Romanica, Olivier Bouthot for their endless assistance.

Conductivité Thermique et Électrique des Composites Polymère/Graphène

Sohrab AZIZI

RÉSUMÉ

Différentes techniques et stratégies sont présentées dans cette thèse afin de trouver des propriétés appropriées pour les composites polymériques conducteurs utilisables dans les câbles extrudés. Dans cette optique, des composites polymériques conducteurs flexibles et légers ont été développés. Les principaux aspects à considérer quand il est question de composites sont un processus de fabrication simple, accessible et des matériaux bon marché. Pour répondre aux besoins de l'industrie dans l'utilisation des câbles HV, deux polymères simples (polyéthylène basse densité et polyéthylène-acétate de vinyle) avec plusieurs charges conductrices carbonées ont été sélectionnés pour ce projet de doctorat. Les objectifs sont d'augmenter la conductivité thermique et électrique de plusieurs composites polymériques conducteurs en utilisant un graphène-hybride d'origine naturelle. Celui-ci a été obtenu à partir de sucre et d'argile.

Pour mener à bien ces objectifs, le polyéthylène basse densité a été combiné avec des charge de type graphene par un procédé de mélangeage fondu, comme matériau de référence. Les propriétés électriques caractérisées par spectroscopie diélectrique large bande ont révélées la formation d'un réseau conducteur pour une teneur en charges supérieure à 30 wt%. Le polyéthylène à basse densité/noir de carbone (LDPE/CB) avec plusieurs concentrations en charges de CB ont été préparés par mélange fondu. Une augmentation significative de la conductivité électrique a été obtenue avec une concentration de charge entre 15 et 20% en masse. La morphologie nanostructurée du composite avec une bonne dispersion et distribution des charges de noir de carbone sous forme sphérique a permis un bon contact entre les particules. Des chemins de charge ont alors pu se former en conséquence. Le LDPE/CB a montré une dépendance au champ magnétique et des phénomènes d'hystérèse. Le décalage du pic de polarisation interfaciale vers les fréquences les plus hautes a été observé et lié à la connexion entre agrégats à plus haut champ. L'ajout de 5% en masse de CB dans le LDPE a entrainé une augmentation du claquage diélectrique de 10% ce qui fait de ce matériau un bon choix pour les applications d'isolation électrique. Une augmentation significative de la conductivité thermique du composite LDPE/CB a été obtenue avec l'addition de 20% en masse de CB.

En changeant le polymère hôte non polaire par un polymère polaire, l'éthylène-acétate de vinyle a été mélange avec un graphène-hybride par une technique de coulée avec un solvant. Les investigations des propriétés électriques de l'EVA/graphène-hybride a montré un seuil de percolation entre 25 et 30 wt% de charge. Pour comparer la conductivité électrique des charges de graphène-hybride dans le composite polyéthylène-acétate de vinyle (EVA) avec des charges carbonées comme le CB ou du graphène (G) commercial était conducteur à des concentrations supérieures à 5 et 15% en masse respectivement. La technique de coulée-évaporation du solvant (« solvent casting ») et la taille nanométrique des particules de CB ont permis la

formation d'un réseau conducteur à basse concentration de charge (5% en masse). Au contraire, l'agglomération des particules micrométriques de graphène a entravé la formation du réseau conducteur jusqu'à 15% en masse. L'addition de CB et de graphène à l'EVA a systématiquement augmenté la conductivité thermique des composites.

Considérant les informations acquises sur le rôle des charges graphène-hybrides dans le LDPE et l'EVA, le LDPE/EVA a été mélangé avec des charges semblables au graphène par coulée-évaporation. Il a été montré que ce composite (LDPE/EVA/ graphène-like) était conducteur à 17,5% en masse de charge. Le taux de recuit du LDPE/EVA/ graphène -like était influent sur la conductivité du composite au seuil de percolation. De plus, une augmentation de la conductivité électrique d'un ordre de magnitude a été obtenue grâce à la formation d'un réseau conducteur durant le recuit. La réponse diélectrique du composite à été scannée sur une plage de fréquence de 10^{-1} à 10^{6} Hz et de température de l'ambiante à une température proche de la température de fusion. Les composites au seuil de sous-percolation ont révélé une dispersion de fréquence à basse fréquence et à une température élevée.

La conductivité effective du composite LDPE/CB, simulée numériquement, était en accord avec les valeurs expérimentales à de faibles concentrations de charges (jusqu'à 15% en masse). L'arrangement des particules dans le milieu a été simulé et les résultats ont mis en évidence une différence négligeable entre la morphologie aléatoire et ordonnée à basse concentration de charges. L'absorption d'eau par les particules de CB hydrophiles a augmenté la permittivité effective du composite de manière remarquable.

L'utilisation des charges conductrices dans les matrices polymériques pourraient permettre d'avoir des matériaux intelligents révolutionnaires pour les besoins de l'industrie. Par conséquent, il serait intéressant de faire des recherches supplémentaires sur le sujet.

Mots-clés : Composites conducteurs, conductivité électrique, conductivité thermique, graphène.

Electrical and Thermal Conductivity of Polymer/ Grapehene Composites

Sohrab AZIZI

ABSTRACT

Different strategies and techniques are reported in this thesis to meet appropriate properties for conductive polymeric composites applicable in extruded cables. In this regard, the following efforts have been conducted to develop and modify several lightweight and flexible conductive polymeric composites. Dealing with composites, manufacturing aspects such as easy processability, easy accessibility and designing low-cost materials are of the key elements that need to be considered. Therefore, to response the industrial needs in HV cable applications, two commodity polymers (low-density polyethylene and polyethylene vinyl acetate) with several carbon-based conductive fillers were selected for this Ph.D. project.

Our objectives were defined to increase the electrical and thermal conductivity of several conductive polymeric composites using naturally based graphene hybrids, obtained from clay and sucrose. To achieve our objectives, low-density polyethylene was combined with graphene-like filler by melt compounding technique, and the electrical properties, characterized by broadband dielectric spectroscopy, revealed the formation of a conductive network of graphene-like above 30 wt% of filler content. As benchmark, low-density polyethylene/carbon black (LDPE/CB) with several CB filler content was prepared via melt mixing. A significant increase in electrical conductivity was achieved at filler contents 15-20 wt%. The nanostructure morphology of the composite with well dispersion and distribution of sphere-shape carbon black led to adequate particle-particle contacts in which charge carrier pathways were formed as the consequence. LDPE/CB composite was found to show electric field-dependency and hysteresis behavior. The shift of interfacial polarization peak toward the higher frequencies was observed and related to the further intra-cluster connection at higher fields. Loading of 5 wt% of CB to the LDPE resulted in a 10% increase in dielectric breakdown which makes this material a good choice for electric insulating applications. Noticeable increase in thermal conductivity of the LDPE/CB composite was achieved with the addition of 20 wt% CB.

By changing the host polymer from a non-polar to a polar-polymer, ethylene vinyl acetate was mixed by graphene-like by means of solvent casting. The investigation of the electrical properties of EVA/graphene-like showed a percolation threshold between 25-30 wt% of the filler content. To compare the electrical conductivity of the graphene-like filler in EVA polymer, (EVA) composite with two carbonaceous fillers such CB and commercially available graphene (G) was found to be conductive at filler content of higher than 5 and 15 wt%, respectively. Selecting solvent-casting and nanosize CB particles, led to the formation of a conductive network at relatively low filler content (5 wt%), while filler agglomeration for microsize graphene flakes hindered conductive network formation up to 15 wt%. Addition of

carbon black and graphene to the EVA polymer continuously increased the thermal conductivity of the composites.

Considering the role of graphene-like filler in LDPE and EVA polymers, then low-density polyethylene/ethylene vinyl acetate (LDPE/EVA) was blended with graphene-like filler *via* solvent casting. The LDPE/EVA/graphene-like composite was found to be conductive at 17.5 wt% of the filler content. The annealing of the LDPE/EVA/graphene-like composite was found to influence the electrical conductivity of the composite at the percolation threshold. Indeed, one order of magnitude increase in electrical conductivity was obtained thanks to better conductive network formation during the annealing. Dielectric response of the LDPE/EVA/graphene-like composite was scanned over a wide range of frequency (10^{-1}-10^{6} Hz) and temperature from room temperate to near the melting point. Composites at sub-percolation threshold revealed a frequency dispersion at low frequencies and elevated temperature.

The effective permittivity of the LDPE/CB composite, simulated numerically, was found to be in relatively agreement with experimental values at low filler contents (approximately up to 15 wt%). The arrangement of the particles within the medium was simulated and the results evidenced negligible difference between the ordered and the random morphology when the filler content was likely low content. Water absorption by hydrophilic CB fillers was found to increase the effective permittivity of the composite remarkably.

The utilization of the graphene-like filler, obtained from renewable resources (clay and sugar), resulted in a rewarding candidate for production of polymeric composites for extruded cable application.

Keywords: Conductive composites, electrical conductivity, thermal conductivity, graphene.

TABLE OF CONTENTS

LIST OF TABLES

LIST OF FIGURES

Page

LIST OF ABBREVIATIONS

AC	Alternating current
AFM	Atomic force microscopy
BDS	Broadband dielectric spectroscopy
BD	Break down
CNTs	Carbon nanotubes
DC	Direct current
DMA	Dynamic mechanical analysis
DSC	Differential scanning calorimetry
E	Extrusion
EVA	Ethylene vinyl acetate
FTIR	Fourier transformed infrared spectroscopy
G-like	Graphene-like
GO	Graphene oxide
HDPE	High-density polyethylene
UHMPE	Ultra-high molecular polyethylene
LLDPE	Linear low-density polyethylene
XLPE	Cross-linked polyethylene
HV	High voltage
HR-SEM	High resolution scanning electron microscopy
MA	Maleic anhydride
MWS	Maxwell Wagner Sillars
HR-TEM	High-resolution transmission electron microscopy
T_g	Glass transition temperature
SM	Solvent-casting-melt mixing
LDPE	Low-density polyethylene
TGA	Thermogravimetric analysis
CPC	Conductive polymeric composites
rGO	Reduced graphene oxide
MWCNTs	Multiwall carbon nanotube

LIST OF SYMBOLS

ε^*	Complex dielectric permittivity
ε'	Real permittivity (dielectric constant)
ε''	Imaginary permittivity
Tan δ	Loss tangent or dissipation factor in BDS
ω	Angular frequency
$\Delta\varepsilon$	Dielectric strength
τ	Relaxation time
Σ	Conductivity modulus
T	Temperature
t	Thickness
λ	Thermal conductivity
G'	Storage Modulus
G''	Loss Modulus
η^*	Complex viscosity

INTRODUCTION

0.1 Context of research

Conductive polymeric composites (CPC) are known as the relatively new generation of conductive materials since the discovery of polyacetylene (Kondawar, 2015). Due to the promising properties of CPC materials, various applications have been suggested for those materials. For example, semiconductive layers in extruded cables are a key part which their electrical, thermal and mechanical properties need to be engineered carefully (Pleşa, Noţingher, Schlögl, Sumereder, & Muhr, 2016). With the development of electronic devices, the demand for CPC is growing extraordinarily (Kurusu, Helal, Moghimian, David, & Demarquette, 2018). CPCs are used in power transportation, solar systems, aeronautical devices, energy saving applications, microelectronics, and biomedical products as well (Burger et al., 2016; X. Huang & Zhi, 2016). Due to easy processing, adequate flexibility, noticeable heat sinking, and remarkable charge transport, some CPCs are used in extruded high voltage cables (Raju, 2016; Sadasivuni, Ponnamma, Kim, & Thomas, 2015). In addition, conductive polymeric composites are susceptible to be used in many electrical engineering fields.

Strengthen the HV cable against electrical failure or electrical treeing phenomena is significantly important in power industry, and remarkable attention has been made to prevent charge accumulation by creating a uniform electric field or balancing the distributed charge through the materials (Z.-M. Dang et al., 2012; Kondawar, 2015). Electromagnetic interference in electronic devices is another unwanted phenomenon that can be prevented by conductive polymeric composites. Conductive polymeric composites have also been identified as materials with high charge storage that can be used in capacitors (Raju, 2016). Recently, a new window has been opened to the automotive industry from the conductive polymeric composite materials by utilizing highly capacitive charge storage materials in hybrid cars (le Reinders, Verlinden, & Freundlich, 2017). Conductive polymeric composites have been used broadly in transducers by converting an electric signal to a mechanical signal (Klaus Friedrich, 2014). The electromechanical ability of the conductive composites provides the needs in biomedical application (Khobragade, Hansora, Naik, Njuguna, & Mishra, 2017). Additionally, conductive

composites are used in photovoltaic systems due to significant charge capacitive and thermal endurance (Bazaka, Jacob, & Ostrikov, 2015).

Graphene emerged as one of the most exceptional materials due to its extraordinary electrical, thermal and mechanical properties. Graphene with polymers has been extensively compounded and used in many applications, such as superconductive capacitors, thermally conductive composites, photovoltaic systems, as well as actuators (see Figure 0. 1). Even though graphene has been broadly studied with numerous polymers, but due to potential challenges, the topic is still significantly new, and needs to be developed. For instance, even though the graphene single layer has remarkable electrical, thermal and mechanical properties, some drawbacks that occur during manufacturing of the graphene/polymer composites, such as agglomeration, the filler structure needs to be manipulated or modified carefully.

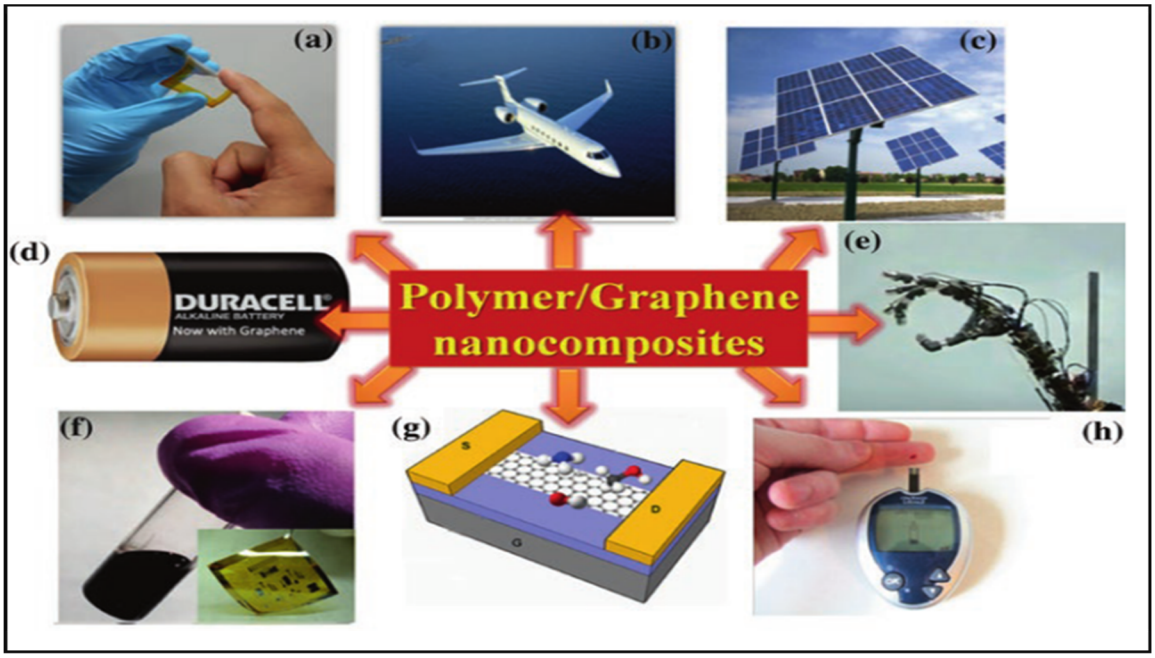

Figure 0. 1 Application of polymer/graphene composites in different fields: (a) flexible transparent electronic, (b) aeronautical field, (c) solar panel, (d) batteries, (e) actuators, (f) conductive inks, (g) gas sensors and (h) biosensors
Taken from Sadasivuni et al., (2015 p. 10)

CPCs are extensively used in high voltage AC and DC extruded transmission cables, particularly in underground transmission and distribution systems. CPCs have attracted significant attention in HVAC and HVDC cables applications due to low cost, reliability, and good electrical and mechanical properties. HVDC cable was used in power distribution for the first time in 1999 in Sweden (Mazzanti & Marzinotto, 2013). The new-introduced cable was capable of higher temperatures during power transmission. Moreover, those featured lower environmental issues due to oil leakage from the transmission system. Several polymers such as ethylene propylene rubber (EPR) and different grades of polyethylene (e.g. LDPE, HDPE and cross-linked polyethylene (XLPE)) have been used individually in HVDC extruded for the outdoor insulating layer. XLPE has shown good thermal stability up to 90 °C to be used in extruded cables. However, several drawbacks can avoid or limit the use of XLPE or EPR. For instance, the electric breakdown in the insulating part of the extruded cable can cause failure in power transportation (Mazzanti & Marzinotto, 2013). According to the studies, the origination of the electric breakdown mostly comes from the morphology of the materials (e.g. the existence of the voids, the crystallinity of the materials, etc.), Therefore, these materials need to be engineered carefully by controlling the quenching rate during polymer or composite manufacturing, or by the addition of some fillers to mitigate the charge accumulation. The addition of inorganic fillers such as carbon black, graphene and $BaTiO_3$ has been reported as another strategy in extruded cables to reduce the space charge. This is more predominant in HVAC cables when the use of semiconductive screen layer between the conductive core and the insulating layer diminishes the charge accumulation (see Figure 0. 2). As it can be seen, semi-conductive layer engineered by conductive additives can play a significant role by mitigating the charge accumulation in different layers of high-voltage extruded cables (Fréchette, Vanga-Bouanga, Fabiani, Castellon, & Diaham, 2015; C.-K. Kim, Sood, Jang, Lim, & Lee, 2009).

Some advantages make HDVC cables more desirable than the HVAC cables that can be summarized as follows:

- In absence of leakage current, the dielectric loss is lower in HVDC cables.
- HVDC cables can be designed for long length line.

- With respect to the HVAC, HVDC cables have lower induction effect on neighboring cables.
- The power flow in HVDC cables are more controllable than the HVAC cables.

HVAC cables features several disadvantages with respect to HVDC cable as follows:

- HVAC cables have higher dielectric loss than HVDC cables.
- The HVAC transmission cable is more expensive than the HVDC cable.
- Some elements such as inductive and capacitive of the overhead AC lines limits their applications
- HVAC cables are not susceptible of direct connection when it comes to the difference between the frequencies of the two cables.

HVDC cables are mainly used for undersea power transmission applications, and several categories of HDVC cables such as mass impregnated nondraining (MIND) cables, oil-filled (OF) cables, polypropylene paper laminate and polymer-insulated or extruded insulation cables have been introduced. The most suitable polymeric compounds used for the extruded cables are low-density polyethylene (LDPE), cross-linked polyethylene (XLPE) and high-density polyethylene (HDPE). Among the three grades of PE, high-density polyethylene is less applicable for HVDC application, due to the higher accumulation of space charge.

As earlier mentioned, HV cables are mainly prepared by extrusion technique. However, since the high-voltage cables are formed from several layers, the extrusion process of the layers performs simultaneously, and a following cross-linking step seems necessary to vulcanize the layers tightly together. A perfect vulcanization of the polymeric layers at high temperatures and pressures leads the extraction or the reaction of any remained monomer or gas molecule. The existence of any monomer, bubble, impurities and air severely reduce cable's performance in which some phenomenon such as electric breakdown, space charge accumulation and partial discharge might happen.

The inner semiconductor layer in high-voltage cable structure - which is also named conductor shield or semi-conductor screen- plays vital role in cable's performance. It uniforms the radial electric field around the conductive core and mitigate or eliminate the gap between the conductor and insulator interface, and prevent intensification of the electric filed and ultimately avoids occurrence of partial discharge, or current leakage through the vulnerable defects points. The inner semi-conductive screen layer usually is fabricated from the polymeric composites; mainly made of carbonaceous fillers such as carbon black, with the electrical conductivity of ~ 0.01- 100 S/m.

A second semiconductor layers which is called outer semiconductive layer is designed in HVDC cables with the same functionality as the inner screen layer, but to further contribute the radial electric field as well creation of an adherent layer between the insulation layer and the adjacent metallic screen.

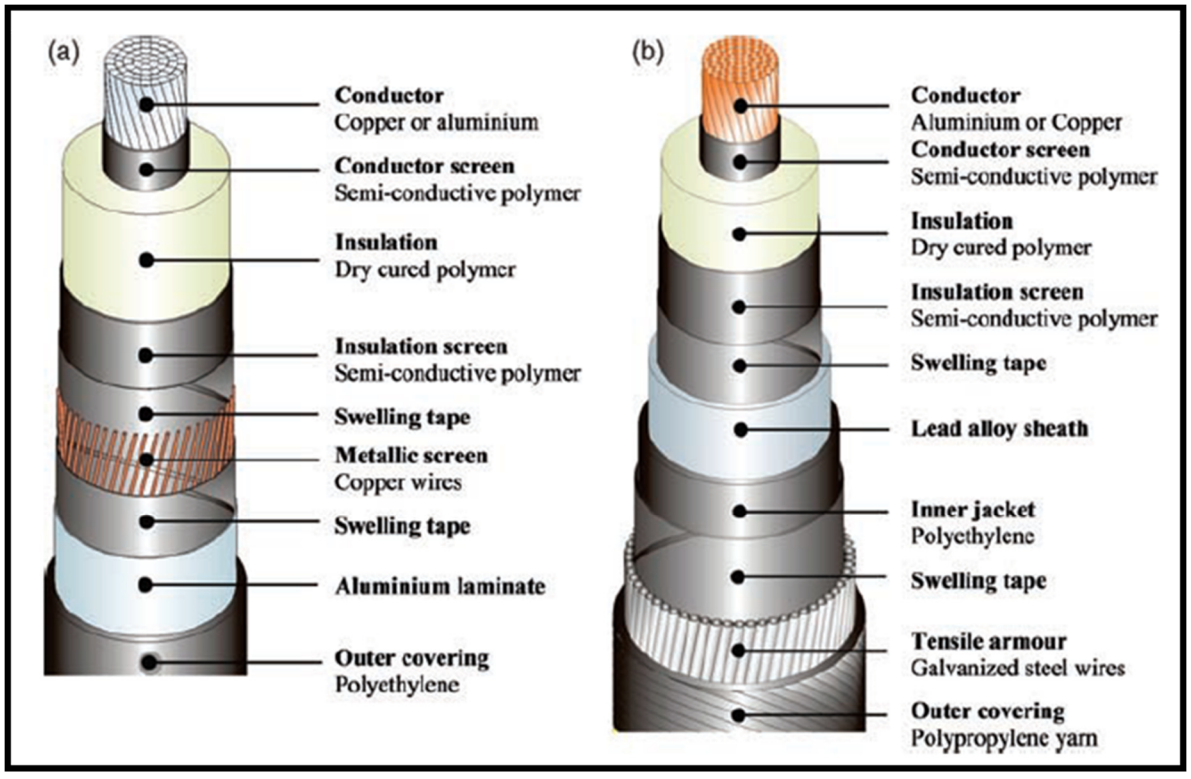

Figure 0. 2 HVDC cable structure used XLPE polymer for (a) land and (b) sea application
Taken from Mazzanti & Marzinotto(2013 p.76)

Among the CPCs materials, composites of polyolefin polymers such as polyethylene (PE) and ethylene vinyl acetate (EVA) compounded with conductive fillers were emerged thanks to their easy processability and accessibility (J. Yang et al., 2017). PE and EVA have arisen with suitable oxidation resistivity in atmospheric condition when used in coating insulating application (Burger et al., 2016; C. Wu et al., 2018; Xue et al., 2018). Promising resistance against electrical breakdown has led to significant attention for those polymers to be used in high-voltage applications (Raju, 2016; J. Yang et al., 2017).

Significant efforts have been dedicated to developing materials with desirable electrical, thermal and mechanical properties. In some circumstances, some aspects of materials were improved but the other properties were not developed or remained constant. The challenges in the development of the electrical and thermal properties might be related to the complexity of the system including the physicochemical properties of the components or the compounded materials. Despite having significant intrinsic electrical or thermal properties of the components, it would not eventually lead to a remarkable increase in electrical and thermal properties when those are combined. Thus, a broad range of parameters needs to be controlled during the processing. Therefore, appropriate selection of elements and proper fabrication methods need to be selected to engineer the morphology and the desired properties of the materials. The most frequent structure to achieve good properties was reported when the solid conductive fillers were dispersed and distributed uniformly (Burger et al., 2016; X. Huang & Zhi, 2016; Raju, 2016; Sadasivuni et al., 2015; Tkalya, 2012). Local agglomeration of the solid fillers in composite structure would result in weak mechanical performance, poor electrical properties or even worsening them. For instance, even though graphene is known as the most electrical and thermally conductive substance until now, but it remarkably tends to the agglomeration. So, only at good filler dispersion and distribution which forms a conductive network, a significant increase in electrical conductivity is expected. Therefore, as can be seen, comprehensive attention is required to design a desirable composite.

0.2 Research objective and approach

Considering significant growing demand for the conductive composite materials for many applications, during this Ph.D. project, efforts have been made to increase the electrical and thermal conductivity of composites with polyethylene and ethylene vinyl acetate polymers and carbonaceous fillers while the rest of the polymeric properties of the composite (e.g. flexibility, weatherability, etc.) are kept acceptable.

In this regard, **the main goal of this Ph.D. project was to utilize graphene-based filler in two commodity polymers such as low-density polyethylene and ethylene vinyl acetate to increase the electrical and thermal conductivity of the obtained composites for extruded cable application.** Therefore, different techniques were used to prepare polymer composites, and compare the desired properties as seen in Figure 0. 3.The details of the approaches are mentioned in the following sections.

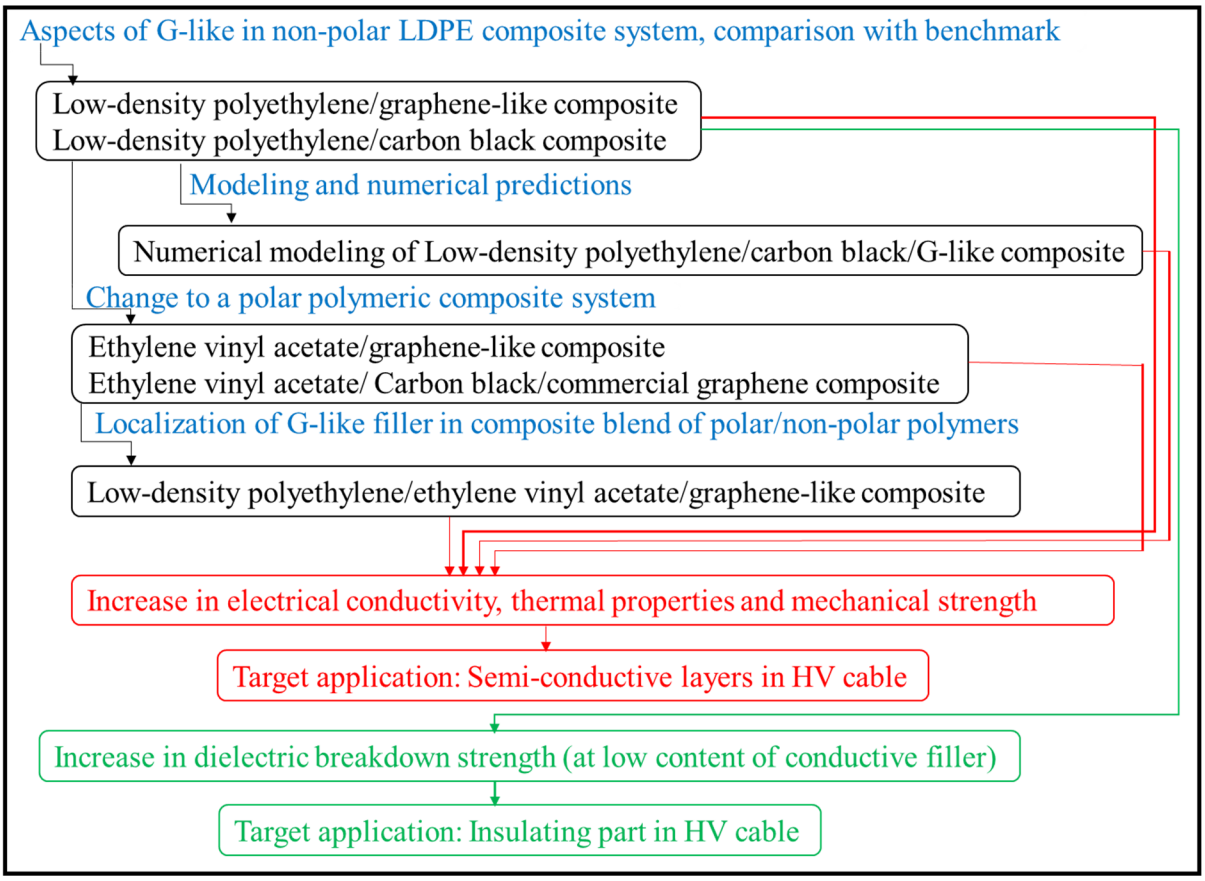

Figure 0. 3 Schematic of Ph.D. objectives with the reflection of the desired target properties and application

0.3 Syllabus of the Ph.D. thesis

This Ph.D. project was divided to three main investigations, reported in three articles, a numerical modeling of the prepared composites, the preparation and investigation of graphene-like and two further studies for the comparison that are shown in Figure 0. 4 and explained as follows.

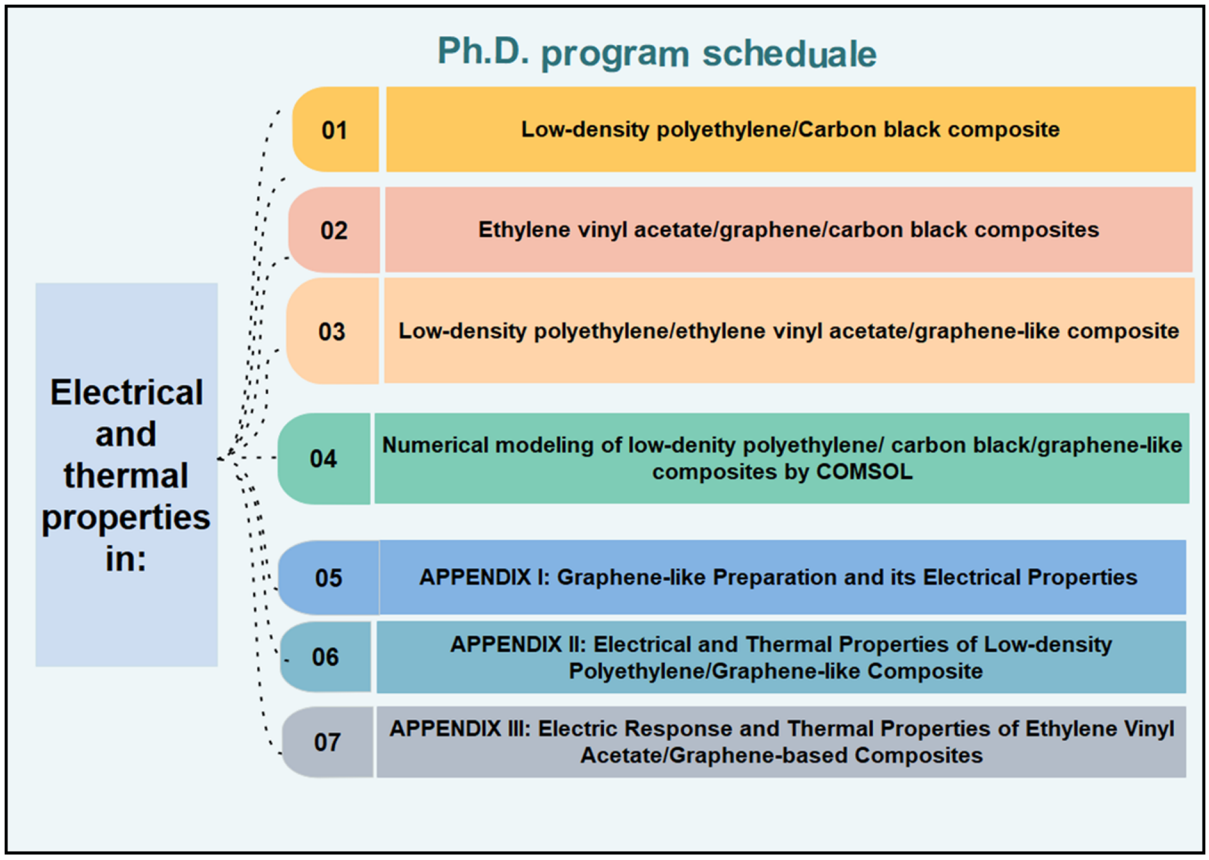

Figure 0. 4 The schematic of Ph.D. program divided projects

0.3. 1 LDPE/CB composite

LDPE thermoplastic polymer with suitable mechanical, thermal, and dielectric properties was made with highly conductive CB filler to be studied for high voltage cable used in power transportation. The acquired results led to the journal article I (Chapter 2) published in Journal of Applied Polymer Science (S. Azizi, David, Fréchette, Nguyen-Tri, & Ouellet-Plamondon, 2018).

0.3. 2 EVA/Commercial graphene/CB composite

The solvent-casting technique was chosen to compound EVA polymer with two conductive carbonaceous fillers (CB and commercially available graphene). The electrical, thermal and mechanical properties were investigated and the outcomes were compared. The findings of this

study were published in polymer testing journal as the second journal article II (Chapter 3) (S. Azizi, David, Fréchette, Nguyen-Tri, & Ouellet-Plamondon, 2018).

0.3. 3 LDPE/EVA/graphene-like composite

In this case study, the polymer blend of LDPE/EVA was composed with graphene-like filler to acquire a suitable composite of thermoplastic elastomer with adequate electrical, thermal and mechanical properties. The findings of this study resulted the journal article III (Chapter 4) has been submitted to Composite Part B Journal.
Parallel to the Ph.D. project, a numerical modeling and two experimental studies of the conductive composites was made as follows:

-Numerical modeling of LDPE composite with CB and G-like composite

The obtained results of the first and second study were compared and validated with the results of the simulation with finite element modeling of the composites. The outcomes are presented in chapter 5.

- LDPE/G-like composite

LDPE polymer as the most accessible, low-cost polyolefin with adequate flexibility for high voltage cable application was selected. Laboratory-made graphene-like from natural resources (clay and sucrose) possessing relative moderate electrical conductivity was used. Extrusion compounding and melt compression molding were chosen as fabrication techniques for the composite fabrication and sample disk preparation. The results of this study led to a conference article published in IEEE (S. Azizi, Ouellet-Plamondon, David, & Fréchette, 2017) and are presented in Appendix II.

- EVA/graphene-like and EVA

For this case study, solvent-casting technique was selected to prepare EVA composites. EVA copolymer with known VA content (28 %), was chosen and compounded with a commercial graphene and graphene-like, and the outcomes led to a conference article for CEIDP 2018 (S. Azizi, Ouellet-Plamondon, David, & Fréchette) which is presented in Appendix III.

To investigate the changes in the structure of the composites as well as the properties such as electrical, thermal, mechanical and rheological properties, several experiments and characterizations were performed. For example, the morphology of the composites was investigated by scanning electron microscopy (SEM), atomic force microscopy (AFM) or optical microscopy. The thermal properties of the test specimens were investigated by differential scanning calorimetry (DSC), thermal gravimetric analysis (TGA), and heat flux guard meter. Electrical properties were evaluated using broadband dielectric spectroscopy (BDS). Test specimens were also characterized by Fourier transform infrared (FTIR), Raman spectroscopy and X-ray diffraction.

0.4 The originality of the Ph.D. thesis

This Ph.D. program was defined as a research applied project to develop composites for electrical applications. To achieve our targets, a conductive filler such as graphene-based filler and carbon black were selected to compound with two commodity polymers. The whole project was divided into three main case studies.

Firstly, the graphene-like filler was used to increase the electrical and conductivity of the low-density polyethylene. Parallel to this case study, LDPE/CB composite was prepared to compare with its counterpart (LDPE/graphene-like composite). Secondly, graphene-like, commercially available graphene and carbon black fillers were compounded with ethylene vinyl acetate composite and the electrical and thermal conductivity were studied. Thirdly, graphene-like was mixed with a blend of LDPE/EVA, and the desired properties were investigated. The

achievements related to each study are reported as journal and conference article in detail in the following chapters.

CHAPTER 1

CONDUCTIVE POLYMERIC COMPOSITES INCORPORATED BY CONDUCTIVE FILLERS

This chapter explains the relevant fundamental aspects in the field of CPSs materials and the related phenomenon in their electrical properties. The former studies linking to polymeric composites applicable in HV cables are described. Afterward, the materials used for this Ph.D. project are shortly reviewed. Then, several fabrication methods of polymeric composites are presented. Finally, the investigated properties of the CPC during this thesis are discussed.

1.1 Fundamental aspects in electrical properties of CPCs

1.1.1 Electrical conductivity

Electrical conductivity defines as the ability of the material to transport charge carriers. Basically, the ratio of current density to the electric field allows to define the electrical conductivity and the units are the Siemens per meter (S/m). The electrical conductivity of a material depends strongly on the temperature. Generally, the increase of temperature leads to decrease in electrical conductivity for metallic materials due to the decrease of carrier mobility, but since polymeric composite materials possess a more complex structure, several more parameters, such as thermal expansion can influence on overall electrical properties of the composite.

1.1.2 Electrostatic charge carrier in dielectrics

Generally, when a dielectric is subjected to an electric (see field Figure 1.1), the action of the field on the bounded charges result in an electric phenomenon which is called polarization (Raju, 2016). For a capacitor consisting of a vacuum medium between a pair of parallel

electrodes with a surface area A and a distance between the electrodes (d), the capacitance (C_o) is given by:

$$C_o = \varepsilon_o \frac{A}{d} \tag{1.1}$$

where ε_0 is the vacuum permittivity.

Now, when a dielectric is placed between the two electrodes, the stored charge by the capacitor is now given by:

$$Q = \varepsilon_o \varepsilon A E \tag{1.2}$$

where ε is the relative dielectric permittivity of the dielectric. The amount of stored charge by vacuum also can be given as follows:

$$Q_o = \varepsilon_o A E \tag{1.3}$$

The dielectric dipole moment can be written as:

$$Q - Q_o = \varepsilon_o \varepsilon A E - \varepsilon_o A E \tag{1.4}$$

$$\mu = \varepsilon_o A E (\varepsilon - 1) d \tag{1.5}$$

Knowing that the polarization (P) equals the amount of the dipole moment per unit volume (Raju, 2016), we thus obtain:

$$P = \frac{\mu}{Ad} = E \varepsilon_o (\varepsilon - 1) \tag{1.6}$$

Where the part $(\varepsilon - 1)$ represents the electrical susceptibility of the dielectric and is usually represented by χ.

The flux density or the electric field displacement is given by:

$$D = \varepsilon_o \varepsilon E \tag{1.7}$$

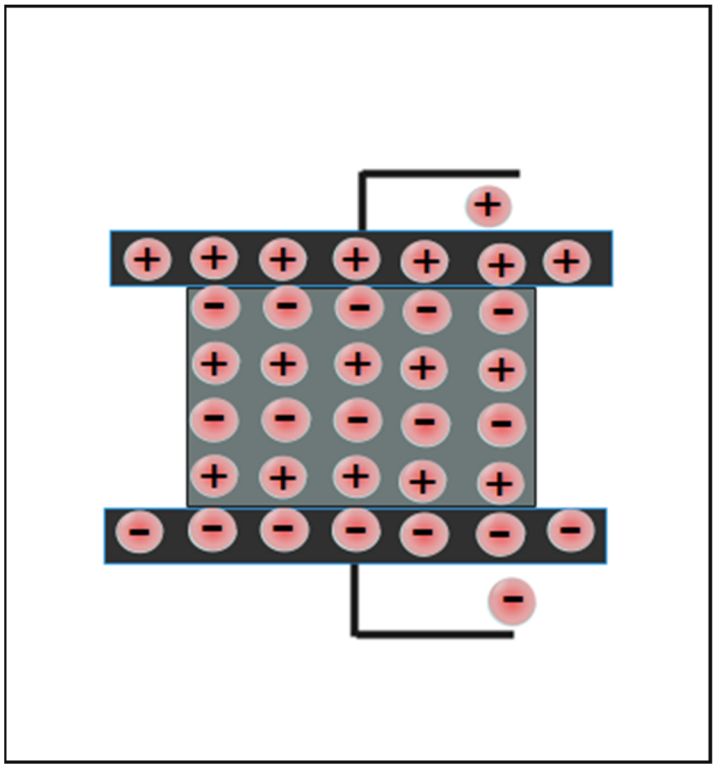

Figure 1.1 Polarization of the mounted dielectric between two electrodes, subjected toan electric field

1.1.3 Percolation threshold

Generally, polymers feature an insulating behavior since free charges are not available to be carried along the materials. However, when a conductive filler such as carbon black, carbon nanotubes or graphene is composed with polymers, at a certain filler content, a transition occurs in electrical conductivity of the composites and suddenly, charge transportation can occur (Raju, 2016). The minimum filler content for which this happens is called the percolation threshold. This increase in electrical conductivity for the composite can be expressed by a power law as follows:

$$\sigma = k(\varphi - \varphi_c)^t \tag{1.8}$$

where σ is the electrical conductivity of the composite, φ and φ_c are filler volume fraction and filler volume fraction at percolation threshold, k is the constant quantity and t represents an exponent related to the filler geometry (Isayev, 2016) (see Figure 1.2). The mechanism of charge transport in percolating composite relays in part in the tunneling of the electrons from particle to particle through the connected conductive particle network. Therefore, the existence of a conductive network is necessary to reach a conductive composite.

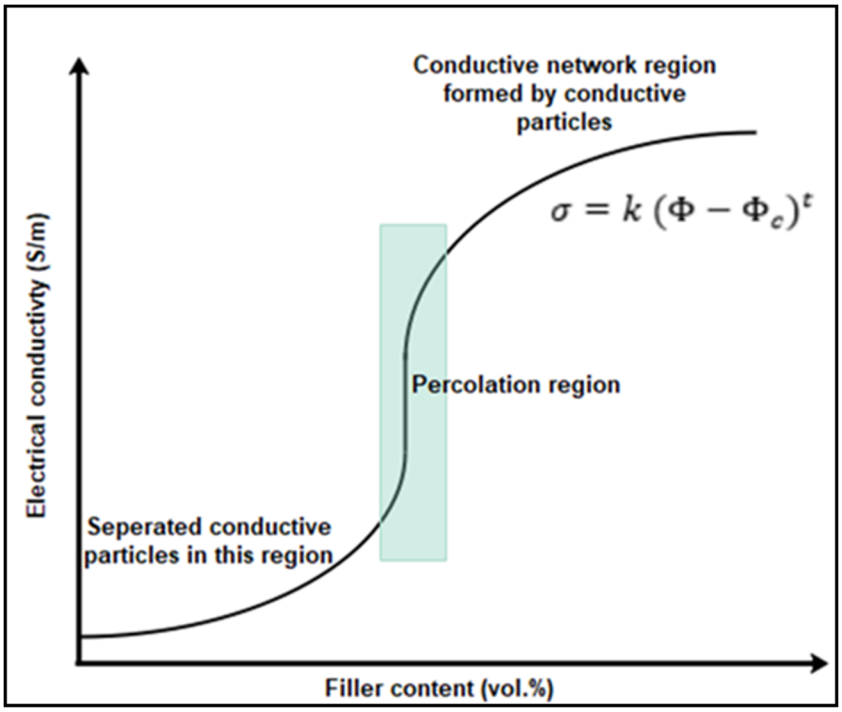

Figure 1.2 Variation of electrical conductivity as a function of filler content, a significant increase in electrical conductivity at percolation threshold region
Taken from Ram, Rahaman, Aldalbahi, & Khastgir (2017 p. 82)

1.1.4 Mechanisms of the polarization

Several polarization mechanisms can occur in the material when it is subjected to an electric field. The different type of polarization is characterized by an activation frequency (or equivalently a relaxation time) of the applied AC electric field (see Figure 1.3). In the

following, the electronic, ionic, orientation and interfacial polarization mechanisms are discussed.

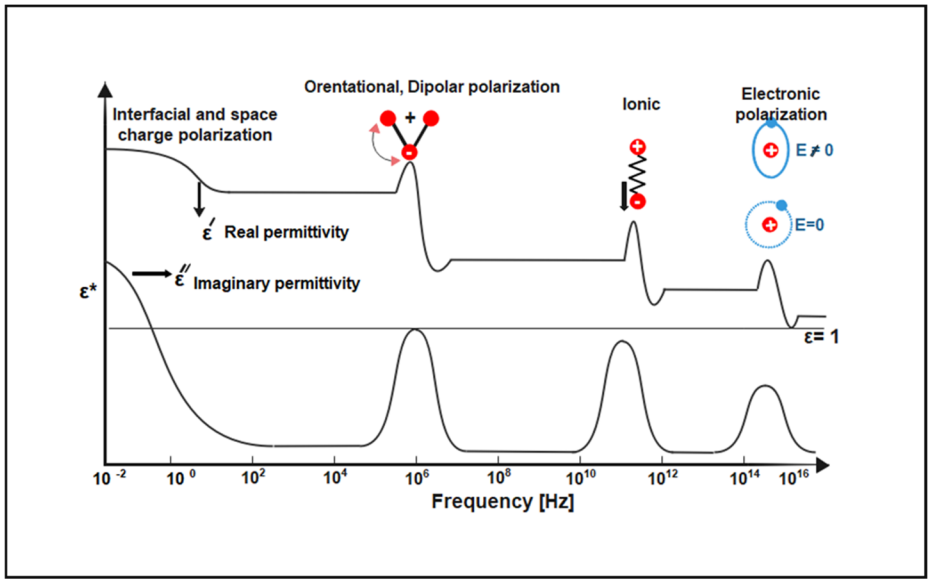

Figure 1.3 Various types of electrical polarization in materials
Adapted from X. Huang & Zhi (2016 p.13)

1.1.4.1 Electronic polarization

Basically, an atom which forms of positive charges (protons) and cloud negative electron revolving around the positive nuclei, is susceptible to the motion of the electron. Therefore, when, an atom is subjected to an electric field at very high frequency, the center of the cloud electron which coincided to the nuclei, shifts toward the applied external electric field. The resulting electron cloud distortion is called electronic polarization.

1.1.4.2 Ionic polarization

Ionic polarization occurs in two ways. The first is an intrinsic polarization that occurs due to the dissociation of polymer chains or attached groups to the backbone followed by electron or proton transfer in the polymer. The second is an extrinsic polarization which occurs due to the

presence of impurities, free radicals, antioxidants or cross-linking agents in the matrix. Ionic polarization happens at high frequencies (~10^{12} Hz).

1.1.4.3 Orientation polarization

Materials with asymmetrical molecules can have a permanent dipole even in the absence of an external electrical field. For example, carbon monoxide has a dipole moment as opposed to carbon dioxide which is a symmetrical molecule. Therefore, when, an asymmetrical molecule with a permanent dipole moment is subjected to an external electric field, the permanent dipole is displaced and oriented in the direction of the applied electric field and causes dipole polarization.

1.1.4.4 Interfacial polarization

In nonhomogeneous polymers or composites, interfacial polarization might happen at low frequencies. The boundaries between crystalline regions and amorphous area as well as the interface between the particles and medium are highly susceptible to the charge accumulation. The accumulated charges lead to interfacial polarization or Maxwell–Wagner– Sillars (MWS) effect that causes a remarkable increase in the apparent permittivity of the composite material.

1.2 Literature review

Electrical and thermal properties of polyolefin-based composites containing of graphene-based additives have been frequently studied. The role of filler content, the use of functionalizing agents, influence of fabrication method and the use of compatibilizer in electrical and thermal properties have been investigated. For example, the use of pre-coated graphene nanoplatelet in LDPE composites prepared by melt mixing resulted in a conductive composite with a percolation threshold of 5 wt% and the graphene nanoplatelet filler in LDPE host polymer was dispersed non-uniformly, in turn, led to different values of electrical properties in different directions (Gaska, Xu, Gubanski, & Kádár, 2017). The functionalized

graphene filler was compounded with LDPE polymer by means of ball milling and compression molding, and the electrical properties were characterized by broad banded dielectric spectroscopy. The outcomes revealed an undesirable graphene agglomeration, where, a conductive network in composite was obtained at high filler content (Pirondelli et al., 2016).

The role of graphene oxide in electrical conductivity of LDPE polymer composite was also studied by Pirondelli et. al. and the electrical response of the characterized composite revealed a higher dielectric loss, thanks to higher polarity of graphene oxide (Pirondelli et al., 2016). The role of processing parameters on electrical properties of LLDPE/graphene nanoplatelet composites, prepared by melt extrusion, were investigated by Khanam et al. and their findings revealed the significant role of screw speed on filler dispersion. In addition, an increase in thermal conductivity of the LLDPE/graphene nanoplatelet was seen due to the incorporation of highly thermally conductive filler (Khanam et al., 2016). Furthermore, graphene nanoplatelet increased the thermal stability of the composites with the addition of 10 wt% graphene nanoplatelet filler (Khanam et al., 2016).

Anh et al. reported the formation of an electrically-conductive network in LDPE/commercial graphene composite structure with the loading of 12 wt% filler. However, with the same processing conditions in composite preparation (melt extrusion), LDPE with graphene-like, the formation of the electrically conductive network was formed at higher filler (Anh, Fréchette, David, & Ouellet-Plamondon, 2016). An electrical percolation threshold of 8.4 wt% was found for polyethylene composite containing graphene nanosheet (Fim, Basso, Graebin, Azambuja, & Galland, 2013). However, graphene agglomeration remained an issue, where a non-homogenous morphology was observed by scanning electron microscopy. In addition, graphene nanosheets increased thermal stability (20 °C at 15 wt%) as well as the mechanical properties of the composite (Fim et al., 2013).

Expanded graphite was blended by maleic anhydride grafted polypropylene to obtain a conductive composite. Electrical response evidenced a significant increase in electrical

conductivity of the composite at an extremely low filer content of expanded graphite (0.67 vol.%). The electrical conductivity of the composites with carbon black, graphite and carbon nanofiber was evaluated by Ezquerra et al., and their findings revealed a lower percolation threshold and higher electrical conductivity for the graphite-contained composites due to smaller particle size of the filler, while filler alignment in carbon fiber-based composites give significant rise in electrical conductivity along the extrusion (Ezquerra et al., 2001).

Polystyrene/ expanded graphite was prepared by in situ polymerization following by rapid hating for better graphite intercalation to obtain a conductive composite. The results showed a very low critical percolation threshold at around 1.8 wt% of the filler content with around 10 orders of magnitude increase in electrical conductivity (G. H. Chen, Wu, Weng, He, & Yan, 2001). The effect of filler content, filler type and co-filler loading on the electrical conductivity of HDPE composite incorporated graphite and carbon fiber was investigated (Thongruang, Spontak, & Balik, 2002), and the outcomes showed a further increase for the co-filler composites with respect to the single-loaded filer composites. Fillers having large aspect ratio such as carbon nanotube and graphene nanosheets increased the electrical conductivity of the polystyrene acrylonitrile composites (Göldel, Kasaliwal, & Pötschke, 2009), however, possessing large surface area did not lead low percolation threshold due to undesirable filler agglomeration. In situ polymerization of ultrahigh molecular weight polyethylene composite containing thermally reduced graphene resulted in extremely low percolation threshold (0.66 vol.%) (D.-X. Yan et al., 2014). Morphological structure of the UHMWPE/reduced graphene revealed uniform segregation of dispersed filler within throughout the composite. Lisunova reported an extremely low critical percolation threshold of 0.0004-0.0007 vol.% for the ultrahigh molecular weight polyethylene/multiwall carbon nanotube composite. In addition, UHMWPE/MWCNTs composites showed a strong dependency on heat, where, the external stimulation by heat could change the electrical properties (Lisunova, Mamunya, Lebovka, & Melezhyk, 2007).

The electrical conductivity of ethylene vinyl acetate/graphene platelet composite was investigated by Soheilmoghaddam et al., and the orientation of graphene platelet and suitable

filler dispersion led to the formation of an electrically conductive network at ~ 3 wt% (Soheilmoghaddam et al., 2017). Yousefzade and his colleagues studied the electrical conductivity of several EVA composites with expanded graphite filler and their outcomes revealed a lower percolation network for the composites prepared from a diluted masterbatch followed by a melt mixing rather than directly extruded composites (Yousefzade, Hemmati, Garmabi, & Mahdavi, 2016). Electrical and thermal conductivity of ethylene vinyl acetate/ expanded graphite was investigated by Sefadi et al. and to achieve a proper filler dispersion, expanded graphite was chemically treated by anionic surfactant sodium dodecyl sulfate. Their findings showed a low percolation threshold of 8 wt% of the filler content. In addition, one further step of electron beam (EB) irradiation of the chemically modified filler was conducted, however, EB irradiation did not improve filler dispersion, and a higher percolation threshold of 10 wt% was obtained (Sefadi, Luyt, Pionteck, Piana, & Gohs, 2015).

A comparison study of ethylene vinyl acetate composites incorporated by pristine carbon nanotube and modified carbon nanotube was conducted by VALENTOV ´A et. al, and their results evidenced that surface modification of MWCNTs resulted in a better filler dispersion and stronger interaction between the host polymer and inclusions. Furthermore, EVA/MWCNTs composite demonstrated a conductive network at 6 wt% of the filler content (Valentová et al., 2014). The effect of vinyl content in EVA composites containing thermally reduced graphene oxide was reported in (Ratzsch et al., 2014), and the vinyl content varied from 0 to 70 % in EVA host polymer. It was shown that rising the VA content increased the electrical conductivity of the polymer. In addition, a lower percolation threshold was obtained for the EVA polymer with higher VA content. Utilizing ethylene–propylene in EVA/carbon black composite system resulted a suitable filler localization in composite structure in which the conductive network demonstrated uniform dispersion within the composite, and led to a lower percolation threshold (Gkourmpis et al., 2013).

The combination of reduced graphene oxide and polyaniline with EVA by means of solvent casting was suggested as an effective strategy to reach a conductive composite at low filler content (N. Yuan, Ma, Fan, Liu, & Ding, 2012). In this regard, the loading of 4 wt% of rGO

and 8 wt% PANI in EVA host polymer showed 13 orders of magnitude increase in electrical conductivity. Wu el. Al. showed a significant reduction of the percolation threshold in EVA composite by involving graphene filler obtained from graphene nanosheets via solution mixing technique. Functionalized graphene filler by octadecyl amine led to a noticeable improvement in the electrical and thermal properties of EVA/functionalized graphene composite (Kuila, Khanra, Mishra, Kim, & Lee, 2012). Klaudia et. al. studied the role of carbon nanotube filler in EVA host polymer prepared via solvent casting and their results showed the formation of a 3D network of CNT filler in which a significant rise in electrical conductivity was observed at percolation threshold (Czaniková, Špitalský, Krupa, & Omastová, 2012). A summary of conductive composite incorporated with conductive fillers is listed in Table 1.1.

Table 1.1. Summay of the experimental studies of the conductive composites incorporated with cabron-based fillers

Host polymer	filler	Preparation method	Percolation threshold	Refs
LDPE	CB	Dry mixing	1 vol. %	(Wycisk, Poźniak, & Pasternak, 2002)
HDPE	Graphene nanosheet	Solvent mixing	0.95 vol.%	(Ghislandi et al., 2013)
HDPE	rGO-CNT-Fe	In situ reaction	2.8 wt%	(Nisar et al., 2017)
HDPE	CB	Extrusion	3.8 wt%	(Ren et al., 2014)
HDPE	CB	Extrusion	1-2 wt%	(Q. Yuan & Wu, 2010)
PP	CB	Extrusion	2-3 wt%	(Q. Yuan & Wu, 2010)
PE	GNP	Extrusion	5.99 wt%	(Rizvi & Naguib, 2015)
PE	MWCNTs	Extrusion	6 wt%	(Rizvi & Naguib, 2015)
Chlorinated PE	Carbon nanofiber	Solution+ Extrusion	4.2 wt%	(Mondal et al., 2017)
PS	Graphene nanosheet	Latex technology	0.15 vol.%	(C. Wu et al., 2013)
PS	Graphene nanosheet	Latex technology	0.08 vol. %	(Long et al., 2013)
LLDPE (50)/HDPE(50)	Graphite	Melt mixing	35 wt%	(P. Zhang & Wang, 2018)
EVA	Graphene	Solution	3 wt%	(Soheilmoghaddam et al., 2017)
EVA	Expanded graphite	Extrusion	6-8 wt%	(Yousefzade et al., 2016)
EVA	Expanded graphite	Extrusion+ irradiation	8 wt %	(Sefadi et al., 2015)
EVA	Graphene nanoplatelet	Solution	17 phr	(Dash, Achary, & Nayak, 2015)
EVA	Thermally reduced graphene	Extrusion	3-5 vol. %	(Ratzsch et al., 2014)
EVA	CB	Extrusion	~ 30wt%	(Gkourmpis et al., 2013)

1.3 Review of the materials

1.3.1 Low-density polyethylene (LDPE)

Polyethylene is known as a commodity polymer and belongs to the polyolefin family. The long backbone of the covalently bonded carbons with a pair of hydrogen atoms attached to each carbon forms the polyethylene structure (see Figure 1.4). Depending on the length and the number of defects existing in chains, the crystallinity of the polyethylene varies. Polyethylene with fewer branches is more crystalline. The greater the crystallinity, the higher the density. Therefore, different grades of polyethylene such as ultra-high molecular polyethylene (UHMPE), high-density polyethylene (HDPE), linear low-density polyethylene (LLDPE), LDPE and cross-linked polyethylene (XLPE) exist. LDPE possesses numerous ethyl and butyl groups, which are attached to the backbone and its density is around 0.9–0.94 g/cm^3. Low-density polyethylene has no free electron in its structure, thus, it is an insulating material. In addition, when low-density polyethylene is subjected to an electric field, negligible dipolar polarization would be expected due to the weak polarity of the carbon-carbon as well as carbon-hydrogen bonds. Low-density polyethylene with a dielectric constant of 2.25–2.35 and relatively low dielectric loss is extensively used as an insulating wall for medium and high-voltage cables. For this application, significant attention should be paid to the material's thermo-mechanical properties since when it is used in high-voltage application systems, a significant amount of heat can be generated during power transmission.

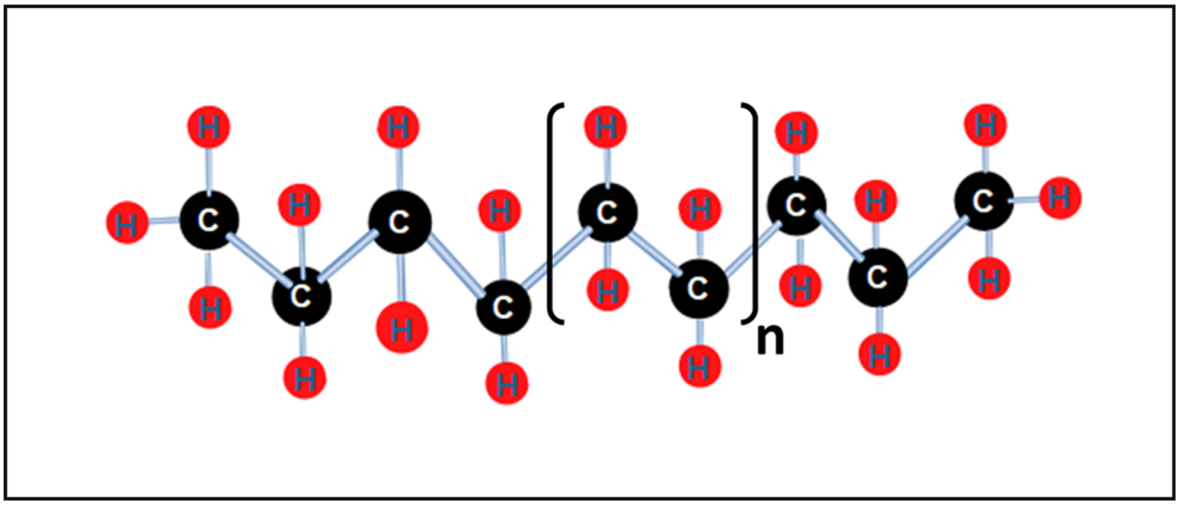

Figure 1.4 Polyethylene structure showing the repeating units of ethylene

1.3.2 Ethylene vinyl acetate (EVA)

Ethylene vinyl acetate is a polar polymer due to the acetoxy groups which are linked to the olefins backbone (see Figure 1.5). It is a semicrystalline copolymer for which the vinyl acetate content varies up to 60 %. Due to sliding groups of acetate, it is more flexible than the rest of its polyethylene-based counterparts (Peacock, 2000). Notably, EVA is a good candidate to be blended with numerous polymers such as polyethylene, polypropylene, etc. It has been used in a broad range of applications such as packaging, drug delivery systems, tissue engineering, and cable coatings (Ponnamma, Sadasivuni, Wan, Thomas, & AlMa'adeed, 2015). Water repellency is a desirable property of EVA, which makes it an excellent choice for outer coatings in electrical applications. At moderately high temperature, EVA shows suitable resistance against thermal degradation (Sabu, Visakh, Jasma, & Nikolic, 2011).

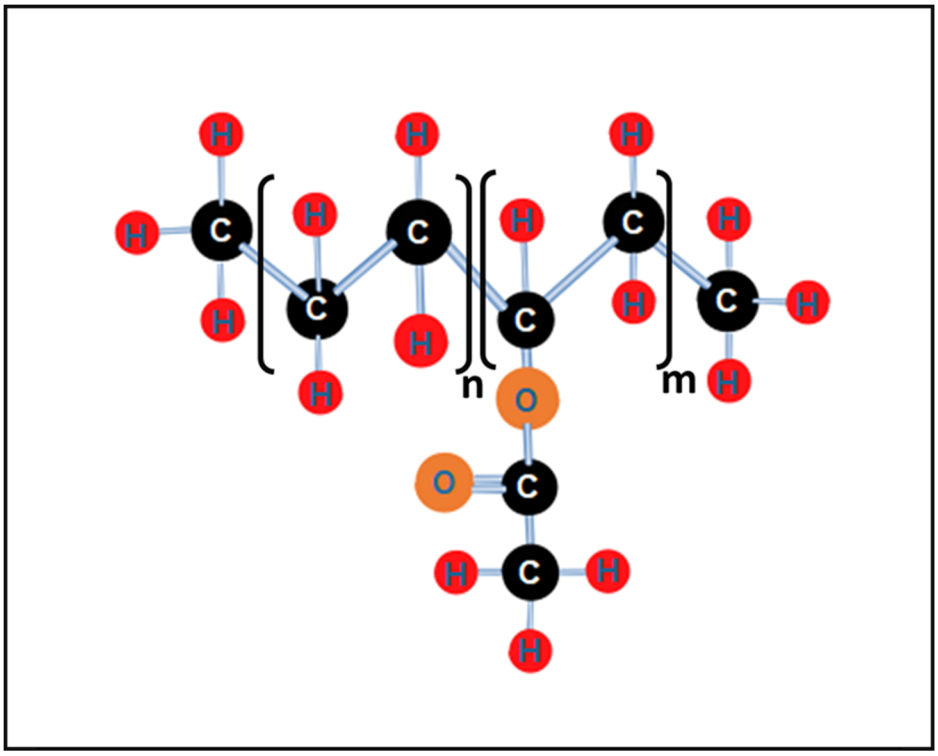

Figure 1.5 The spatial structure of the ethylene vinyl acetate copolymer

1.3.3 Graphene-like filler

Graphene, a single layer of carbon, structurally formed in a hexagonal lattice, is known as the most electrically and thermally conductive materials. Numerous methods such as modified Hummer's methods, chemical vapor deposition, etc. have been reported to prepare graphene. Environmental issues due to the usage of solvent, low scale production, and time-consuming were the most drawbacks of those traditional preparation techniques. However, the most recent method to prepare graphene was established based on the carbonization of hybrid clay sucrose in a free solvent way (Ruiz-García, Darder, Aranda, & Ruiz-Hitzky, 2014; Ruiz-Hitzky et al., 2016b). The main idea of this technique is to generate carbon atoms within the prose or in intracrystalline regions of the solids. Thus, an inorganic material such as clay-based material as the support template is impregnated by sucrose, and the caramel clay is heated under an inert atmosphere. The obtained material was characterized as a graphene-clay composite (Ruiz-Hitzky et al., 2016b).

1.4 Composites preparation techniques

Polymeric composites can be prepared by several techniques depending on the polymer properties, the amount of the filler content, processing possibility, environmental and health considerations. Therefore, in the following the four most frequently used preparation techniques are briefly explained as melt compounding, solvent casting, direct compounding by high-energy mechanical ball milling.

1.4.1 Melt compounding

Most of the thermoplastic composites are prepared by melt compounding techniques. A schematic of this technique is shown in Figure 1.6. This technique is based on applying shear stress on solid filler and polymeric chains in a molten state to form a uniform structure. The most remarkable aspects of this technique are the simplicity and being environmentally friendly which lead to being known as an industrial friendly method. In most of the fabricated composites by melt mixing, an adequate filler dispersion can be achieved (Paul & Robeson, 2008). Several extrusion parameters such as melting zone temperature, residence time, screw speed and die diameter can influence the composite properties. In addition, the morphology of the composite would significantly be dependent to the length of the extrusion zone and the type of screw such as co-rotating or counter rotating (K. Wang, Liang, Du, Zhang, & Fu, 2004). The dispersion of the nanoparticles into the host polymer is controlled by two major parameters which are called dispersive and distributive parameter. In hybrid systems, the dispersive parameters refer to the reduction of cohesive minor component. The distributive parameter represents the process that minor components extend into the matrix to create an adequate dispersion. These two parameters may occur during extrusion, simultaneously or gradually. The dispersion of the particles into the polymer matrix depends on both the dispersive and distributive factors. In other words, a good dispersion takes place among filler and host polymers when a reasonable thermodynamic relationship occurs (Frache, Monticelli, Ceccia, Brucellaria, & Casale, 2008). As a drawback for this technique, melt mixing is not a suitable method at high filler content owing to the high viscosity of the melt and poor processability.

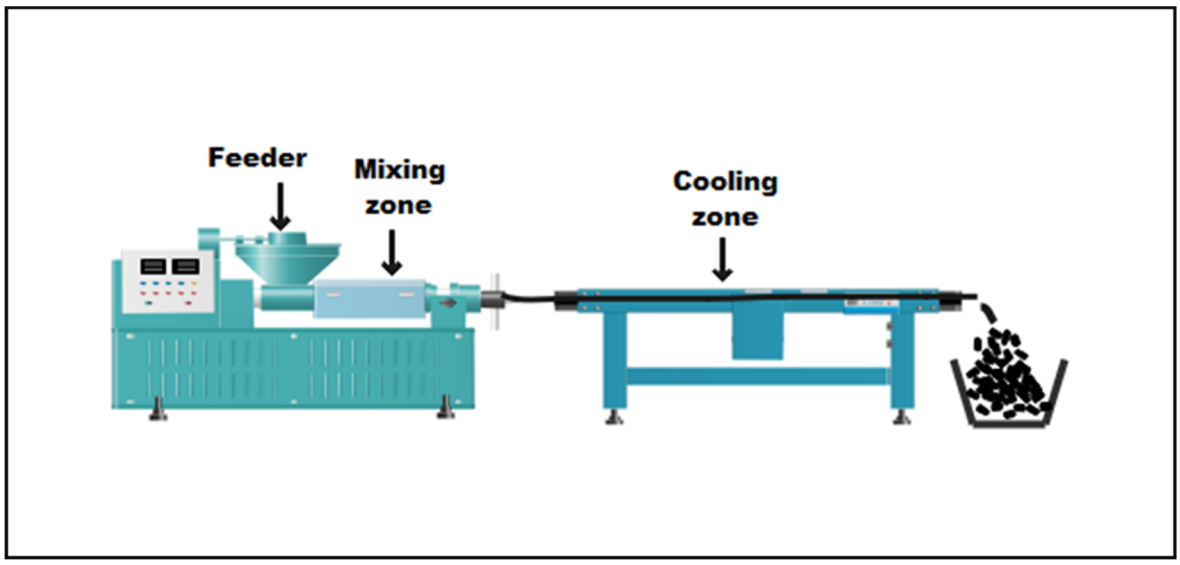

Figure 1.6 The schematic process of melt-compounding technique to prepare polymeric composite materials

1.4.2 Solvent-casting

Solvent-casting is known as the oldest processing technique in plastic film manufacturing. In this technique, the polymer must be soluble in a volatile solvent or water. In addition, a stable composite after removing the solvent should be obtained. Moreover, since the casting process is usually done over a plate or film, releasing the remained composite must be possible (Siemann, 2005). Therefore, to meet these key elements in solvent casting technique, several tricks such as co-solvent casting, dissolving components in a high-pressure system, selecting a polymer with suitable molecular weight, using plasticizers and releasing agent might be necessary. It should be noted that the filler size is a critical key in the solvent-casting technique (Yin, Niu, & Chen, 2012). The filler dispersion and distribution substantially depend on the viscosity of the solution. Therefore, rheological parameters, mechanical stress such as shear stress, and thermal condition must be strictly monitored. An uncontrolled thermal condition or shear stress can dramatically lead to chain degradation in the polymer structure. Thus, the room temperature up to the boiling point of the solvent might be used for this method. A filler content of up to 40 or 50 % can lead to an 80,000 mPas viscosity during the solution process and this value should not be further exceeded. Dissolution can be done vertically or horizontally

depending on the viscosity of the solvent (Siemann, 2005). A schematic of solvent casting can be seen in Figure 1.7.

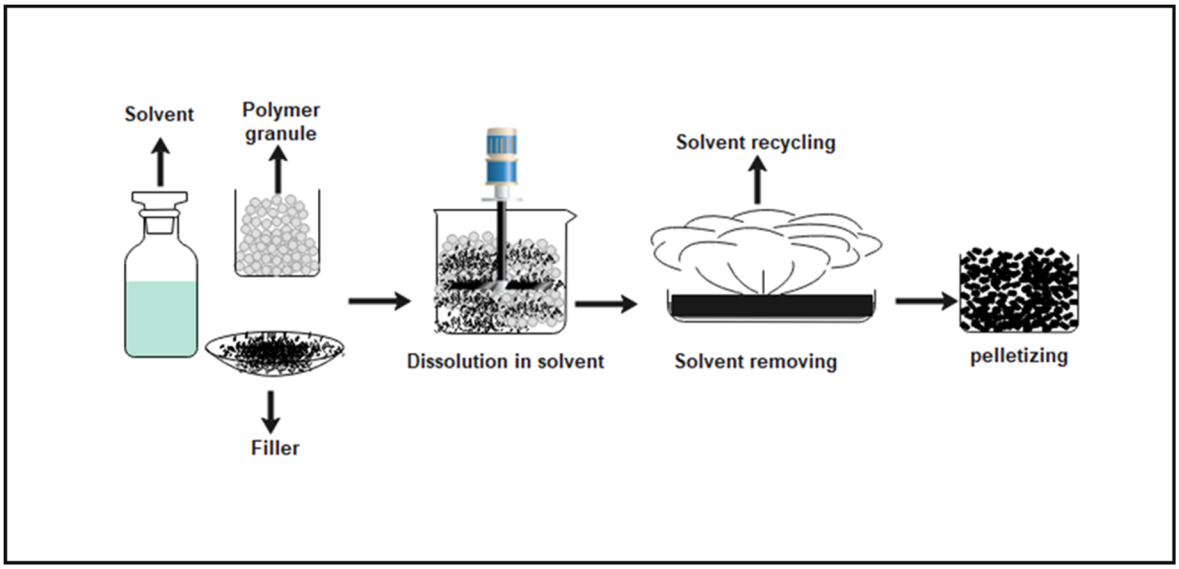

Figure 1.7 Schematic of solvent casting technique to produce well-dispersed nanofillers in a composite structure

1.4.3 Direct compounding by high-energy mechanical ball milling

This technique was suggested in the half-second of the last century for the first time when metallic oxides such as Al_2O_3 was used with powders to alloy metallic composites (Koo, 2006). In this method, polymeric powders and fillers are mixed and subjected to high-energy mechanical forces. As a result, polymeric powders are coated by nano or micro-sized particles and dispersed uniformly. In addition, by applying high-energy mechanical shear stress, mass transformation between phases are possible, where the filler particles migrate into the softest phase (polymer part) (Isayev, 2016). Chemicals can be loaded in the mixing chamber (for example planetary miller) to introduce functional groups on the surface of the components for better filler dispersion and further possible chemical interactions. Several factors such as milling time, rotational speed, the size of the balls and the ratio of the ball volume to the volume of the used filler influence strongly the filler dispersion (Sopicka-Lizer, 2010). The main advantages of this technique are the easy operation as well as using a high volume of the filler.

However, due to the high mechanical force during the rotational process, the structure of the filler can significantly be damaged (Dong, Umer, & Lau, 2015).

1.4.4 In-situ reaction compounding

In situ polymerization of composites relays on a chemical reaction between low molecular weight molecules such as monomers, dimers, trimers and so on to form a continuous matrix into which particles are being embedded within the polymer chains (see Figure 1.8) (L. Yang, Toh, & Lu, 2014). It is generally believed that in-situ polymerization is carried out in two steps. The first step, which is called the growth step, includes the dispersion of the filler to reach a good dispersion. This is more predominant for fillers such as carbon nanotubes and graphene, which intrinsically tend to the agglomeration. In this step, some reactive sites of nanoparticles can react with functional groups in monomers or play initiator role in the polymerization reaction. The second step is the chain growth in which monomers react together and form polymer chains. Consequently, particles are exfoliated uniformly among the polymer chains and can form a conductive network (Mittal, 2011). Thermoset nanocomposites are the most suitable candidate to be compounded by this technique. The process is usually conducted using an initiator and/or a curing agent to proceed the reaction (Kontopoulou, 2011). This technique is also suitable for more insoluble polymers as well as thermally unstable polymer composites, which cannot be processed by solvent casting or melt processing (Han & Fina, 2011). In addition, this technique is particularly suitable for the preparation of highly loaded filler composites which leads to very good miscibility with almost any types of polymers (Kuilla et al., 2010).

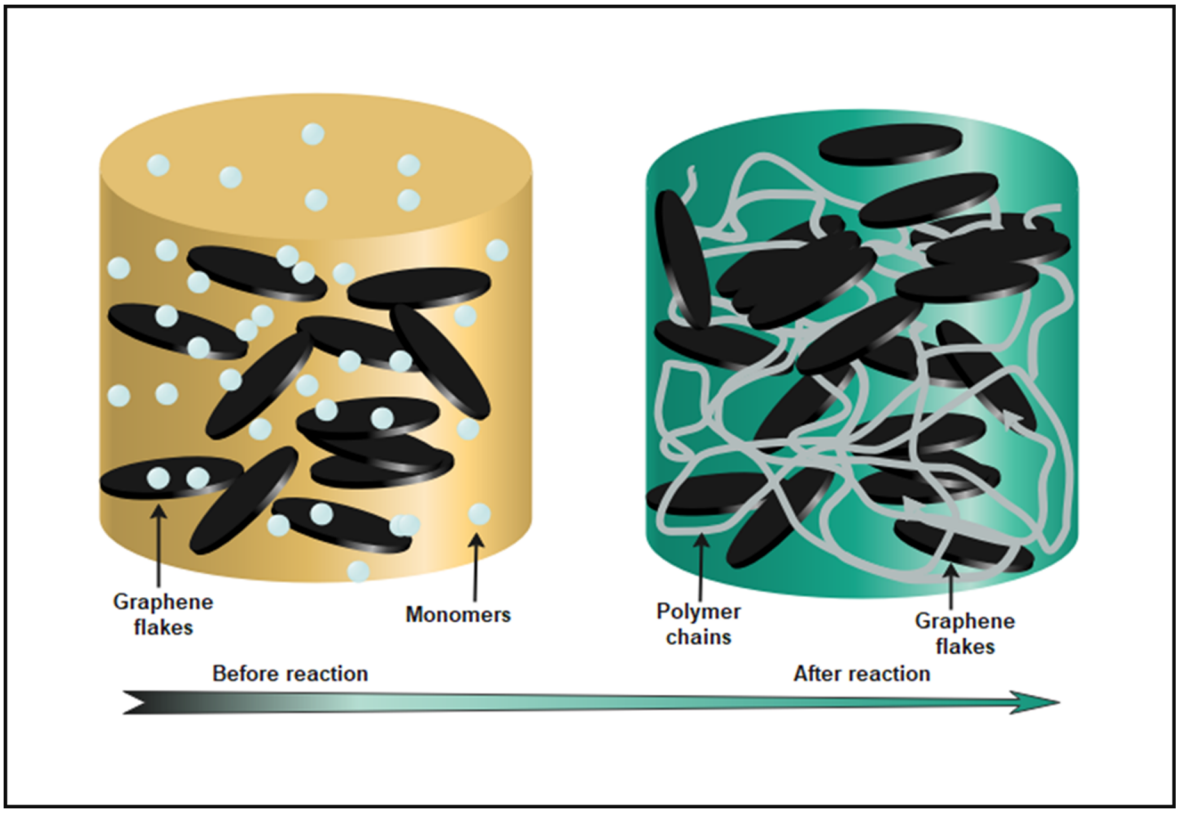

Figure 1.8 Schematic of in situ polymerization, composite manufacturing during the polymerization reaction

1.5 Vital aspects of polymeric composites

1.5.1 Composite structure

Composites are one of the most ancient materials that humankind has made. The evidence proving this is the addition of straw to mud for building stronger mud walls. Therefore, a composite is a material that is formed from a bulk continuous phase (matrix) and one or more non-continuous solid materials (reinforcement) which are embedded throughout the matrix. The bulk phase is similar in all composite in terms of embracing the fillers, but the filler morphology varies from zero D (spheres) to 1D (fibers or tubes) and 2D (sheets) (Sabu et al., 2011). Depending on the type of filler geometry, the properties of the composites along the different directions can change significantly. The interface zone between the filler and bulk matrix is an important region in a composite structure that plays a significant role in ultimate

composite properties. The interface is remarkably important when the possible chemical bonds (moderately strong covalent bonds) or physical interactions (weak Van der Walls forces) occur between the components (X. Huang & Zhi, 2016). The wettability of the fiber, particle or sheet is a key element that increases the surface area in composite morphology (Klaus Friedrich, 2014). Coupling agents or compatibilizers are known as wetting agents in composite systems. The geometry of the filler in composite also strongly determines the anisotropy or isotropy of the composite structure.

1.5.2 Morphology of the filler

The aspect ratio of the filler is a key parameter that can substantially influence on composite's properties, composite's morphology and manufacturing parameters. The higher the aspect ratio, the more intense the interfacial interactions will be (L. Yang et al., 2014). This becomes more predominant when electrical conductivity is the desirable property. Indeed, higher aspect ratio results in lower percolation threshold. Therefore, a lower percolation threshold is expected for the composites with carbon nanotubes (CNTs) and graphene as compared to amorphous carbon black. It should be noted that even though CNTs and graphene possess an aspect ratio of 100-10000, the significant tendency of CNT and graphene to agglomerae remain a challenging issue that must be overcome.

1.5.3 Miscibility of the blends

Technically, a stable mixture of two or more polymers which forms a homogeneous phase is called a miscible blend. A miscible blend is expected to show the macroscopic properties of a single-phase polymer. Therefore, several properties such as light transparency, glass transition temperature, melting temperature are expected to be obtained from different domains of the polymer blend similarly (Olabisi, 1981; Schultz, 2017). Miscibility is important when a blend of two polymers or more is needed. The purpose of the polymer blending is to acquire new material with desirable properties. The properties of miscible polymer blends are expected to lay between those of the two unblended polymers. For instance, the ductility of a polymer

blend is expected to be closer to the one with the higher portion into the polymer blend (Coleman, 2017).

1.5.4 Effect of intrinsic polymer properties on composite properties

Several dominant factors in the polymer matrix can strongly influence composite properties. Crystallinity is one of the key parameters that can ease or hinder suitable filler dispersion. In other words, amorphous regions trap particles further than crystalline regions. Thus, a lower percolation threshold would be expected for the same polymer with a higher degree of crystallinity than a polymer having lower crystalline regions. The second important factor is the melt flow index (MFI). This parameter has essentially the same effect as viscosity, where polymer with lower viscosity (higher MFI) allows to reach the lower percolation threshold than the one with higher viscosity (Kontopoulou, 2011). Polar polymers are more susceptible to react and link with reactive sites of functionalized carbon-based fillers (Tkalya, 2012). Ultimately, greater wettability of a polymer leads to lower interfacial tension between polymer and filler, then thus better filler dispersion can be achieved (L. Yang et al., 2014).

1.5.5 Homogeneity (dispersion and distribution)

When it comes to electrical conductivity in polymer composite materials, filler dispersion and distribution are of great importance, since a poor filler dispersion and distribution would not lead to a significant increase in electrical conductivity. We can assume three filler arrangements in the composites (Sumita, Sakata, Asai, Miyasaka, & Nakagawa, 1991). As can be seen in Figure 1.9a, graphene flakes neither dispersed perfectly nor distributed, and several non-ordered agglomerated regions are seen in the composite structure. This filler morphology would not lead a suitable charge carrier through the materials. Figure 1.9b shows a suitable filler distribution but poor dispersion. This filler arrangement cannot either allow charge transmission through the bulk. The last filler arrangement shows a good distribution as well as good filler dispersion (see Figure 1.9c). Enough filler content is required as well to have a

particle-particle connection network in composite with uniform filler dispersion and distribution (Gulrez et al., 2014; Z. Yan, Martin, Guillon, & Bouvard, 2013).

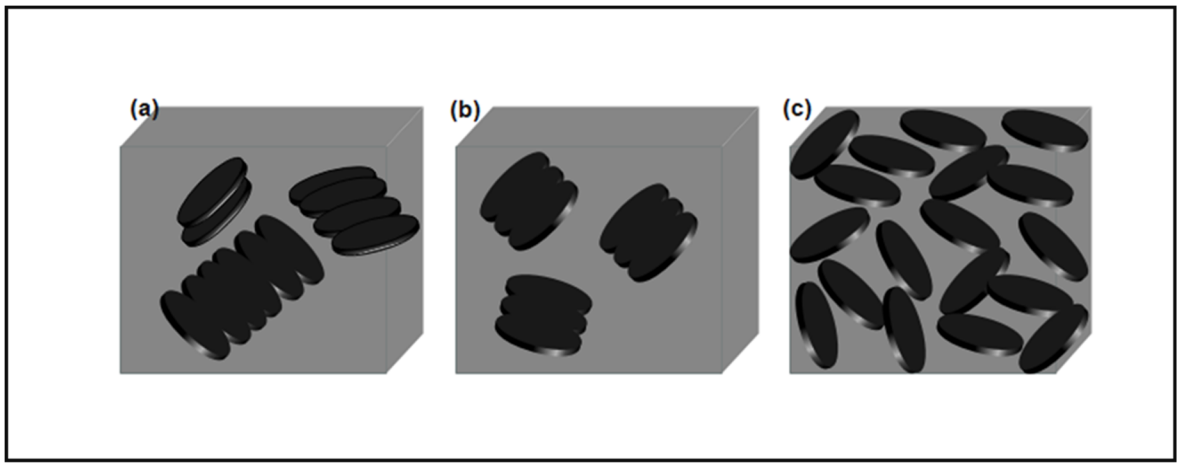

Figure 1.9 Composite's morphology with (a) poor dispersion and distribution, (b) good distribution but poor dispersion, (c) appropriate distribution and dispersion

1.6 Physical properties of polymeric composites

1.6.1 Dielectric breakdown

Dielectric breakdown in an insulating material is a catastrophic, destructive and irreversible phenomenon in which an intense current surge causes a narrow breakdown channel between the electrodes. Generally, four breakdown mechanisms have been reported in dielectrics. Electric breakdown, thermal breakdown, electromechanical breakdown and partial discharges-induced breakdown which involves different physical processes but lead to the same ultimate result. The electrical breakdown usually occurs in semiconductive composites. The electron avalanches by tunneling effect to the conduction band lead to electric breakdown. This incident happens in a very narrow conjunction in the materials at strong electric fields. Similarly, when an insulating material is subjected to a high electric field, a significant amount of heat can be generated due to dielectric losses. If the generated heat overtakes the released heat by conduction and/or convection, a thermal runaway occurs leading to ultimately thermal breakdown. Electromechanical breakdown happens when the applied compression load due to

the Colombian forces decreases the thickness of the insulating wall and thus increases the electrical field, which in turn increases the mechanical stresses and so on. Accordingly a mechanical runaway can occur similarly to the thermal runaway previously described (Dissado & Fothergill, 1992). Partial discharge breakdown occurs in dielectric materials due to the existence of voids (David & Fréchette, 2013). Those voids or more importantly the gases inside the voids are vulnerable to the act as local spots as partial discharge source. Erosion of the cavity walls due to the partial discharges and subsequent electromechanical fractures eventually can lead to a complete breakdown. Overall, all kinds of breakdowns lead to local melting of the sample, polymer carbonization or vaporization of the dielectric. Figure 1.10 shows a schematic of the setup used for dielectric strength measurement. To avoid flashover, the sample to be tested is immersed in a dielectric liquid such as mineral transformer oil.

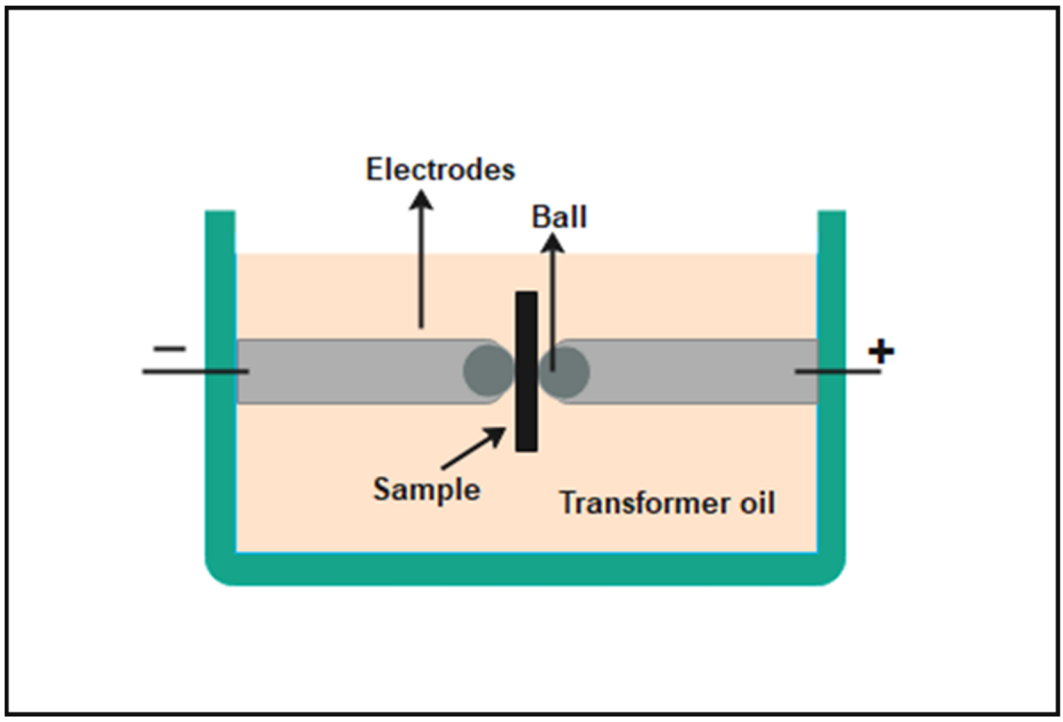

Figure 1.10 The schematic of dielectric breakdown strength measurement setup

1.6.2 Resistance to corona discharge exposure

Corona discharge is an electrical phenomenon that occurs in high-voltage systems where the surrounded medium of a conductor is ionized and the potential gradient (electric field) around the conductor is large enough for partial ionization but not high enough to lead electrical breakdown or arcing. The surface of the material subjected to partial discharge or corona undergoes several physicochemical degradation processes. These changes are induced by the combined effect of the generated heat, the electronic bombardment and the chemical action of the reactive gases created by the corona activity. For example, degradation of polymer chains or oxidation can result from corona discharge exposure, which leads to deterioration of the material properties. Corona discharge only forms when the electric field (potential gradient) at the surface of the insulator exceeds a critical value. Poor engineering of insulators and the existence of water droplet on the surface of the insulator subjected to high field boost corona discharge. A schematic of the setup used for the measurement of the resistance to corona discharge exposure is shown in Figure 1.11.

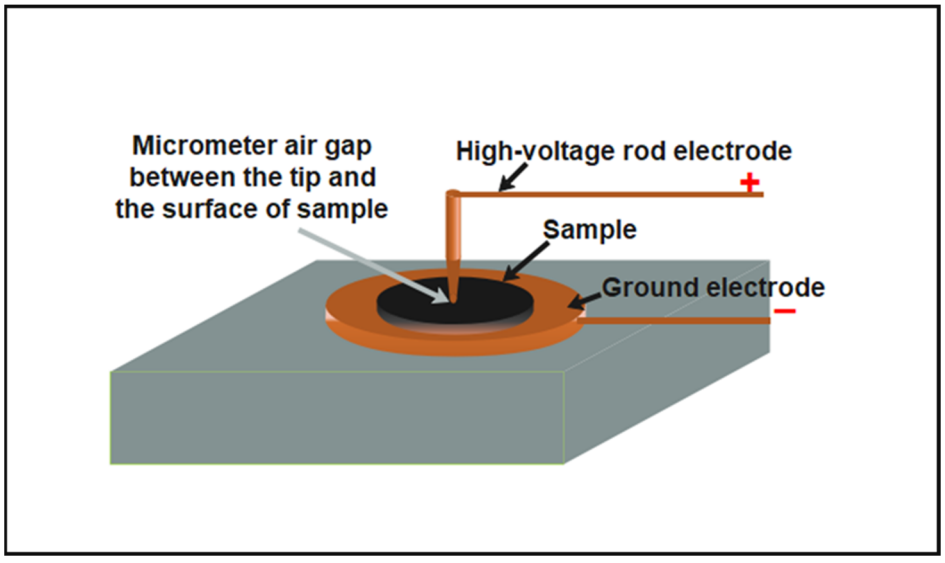

Figure 1.11 Schematic set-up of the corona discharge exposure on the surface of the composite

1.6.3 Thermal properties

Several thermal properties in polymer composites are significantly important. In this regard, glass transition temperate (T_g) which is related to the transition from glassy to rubbery and melting point (T_m) which is linked to the change from solid state to semi-viscous state can significantly influence material properties (Crompton, 2012). In addition, when high-temperature applications are concerned, attention should also be paid to the thermal degradation temperate. Differential scanning calorimetry (DSC) and thermogravimetric analysis (TGA) are the most widely used technique to analyze and estimate the above-mentioned properties. The former technique (DSC) is based on the amount of the released or absorbed energy per unit of mass needed to increase (or decrease) the material temperature. The heat flow which is entered (endothermic) or exhausted (exothermic), will be measured as a function of temperature or time. The latter technique (TGA), is according to the weight loss which is occurred during the heating in the sample (Sabu et al., 2011).

1.6.4 Dynamic mechanical properties

Dynamic mechanical properties of the polymeric systems and composites play a significant role in processability and end-use performance of the designed materials. Intrinsic properties of the materials, modification, blending, the addition of reinforcement fillers and compounding can influence the resulting dynamic mechanical properties. To investigate the dynamic mechanical properties, a material needs to be subjected to an external load. Two important characteristic properties are considered for dynamic mechanical analysis; the externally applied load stress (σ), and the resulting deformation from the imposed stress, the deformation or strain (ε). The correlation between the stress and strain represents the material mechanical properties. Depending on the intrinsic structure of the test specimen, different mechanical responses can be expected. In addition, depending on the way of applying a stress (shear, tension, and compression), the type of potential deformation would be different. Depending on the phase shift between the stress and the lagging strain, the material can have an elastic or viscous behavior. Polymeric systems usually remain between these two extreme

behaviors, and therefore would expect to show a viscoelastic behavior (Kremer, Huwe, Schönhals, & Rózanski, 2012).

In the dynamic mechanical analysis, a material is subjected to sinusoidal stress, then the resulted strain and phase shift are measured. As previously explained, depending on the material structure, the applied stress may partially store, and the rest of the stress would release after a certain time (relaxation time). The viscous part is defined as storage part (storage modulus) and the elastic part which is in phase with the occurred strain is counted as a loss modulus. Thus, it is expectable from a thermoplastic polymer to store some part of the imposed stress as well as some loss as heat for the elasticity part. These values could be varied depending on the morphology of the polymer.

1.6.5 Rheological properties

The rheological properties of the molten polymers are significantly important, particularly from the designing of the processing equipment standpoint. The complex viscosity of the molten polymer as a function of shear rates reveals significant information about the macroscopic interaction between the filler and polymer as well as the formation of the solid network within the molten polymers. When a molten polymer is subjected to shear stress, resistance against the shearing exists which is called viscosity as follows:

$$\eta = \frac{shear\ \text{stress}}{Shear\ \text{rate}} = \frac{\tau}{\dot{\gamma}} \tag{1.9}$$

where η denotes complex viscosity, τ is the shear stress and $\dot{\gamma}$ represents the shear rate.
The above-mentioned equation is known as Newton's law. Due to the complexity of the structure in polymers, the viscosity is strongly dependent on the shear rate. The molten polymers show a pseudo-plastic behavior where the viscosity decreases with increasing the shear rate. Several parameters such as the average molecular weight or the distribution of molecular weight influence on the rheological properties (Rudolph & Osswald, 2014).

Loading of the inorganic filler to polymers leads to new rheological behavior due to the mesoscopic structure of nanocomposite and the strength of the interfacial interactions between polymer and particles. Thus, nanocomposites at different filler content and frequency feature different viscoelastic behaviors. At low filler content or in composites with weak interaction between the polymer and the particles, the storage modulus (G') is proportional of ω^2. When the molten nanocomposite switches from liquid-state to solid-state due to the formation of a solid network, the viscoelastic behavior of the composite show a plateau region and the storage modulus is proportional of ω (Kontopoulou, 2011).

1.6.6 Thermal conductivity

The thermal conductivity of composites has been extensively studied and significant efforts have been devoted to engineer composite's morphology to increase the heat conductivity of materials. Polymers depict a thermal conductivity between 0.1 to 0.5 W/m.K, which is fairly low to be used in some applications such as cable insulation and electronic devices (Han & Fina, 2011). Several factors have been noted influencing thermal conductivity of polymer composites. Crystalline polymer shows higher thermal conductivity than the amorphous one. The alignment of the polymer chains during melt compounding can increase the thermal conductivity of the composite or polymer. Blending of the polymers with additives with higher thermal conductivity can remarkably increase the thermal conductivity of composite (Han & Fina, 2011). Filler concentration in composite plays a noticeable role in the thermal conductivity of the composite. At low filler content, due to the lack of a filler network, a significant rise in thermal conductivity of composites would not be expected. However, upon forming a percolation network by particles, a dramatic increase in thermal conductivity can be achieved. Interchain coupling of the polymer chains can enhance thermal conductivity. Homogenous composites feature higher thermal conductivity than non-homogenous (C. Huang, Qian, & Yang, 2018). Despite better distribution of filler within the composite with using functionalized fillers, functionalizing can reduce thermal conductance due to higher thermal resistance at the interface layer. Therefore, each factor that might lead to phonons scattering, results in lower thermal conductivity in polymer composite (see Figure 1.12) (C.

Huang et al., 2018). The major mechanism of thermal conductivity in polymer composites can be expressed briefly as:

1. Transformation of heat by the polymer chains on the surface;
2. Transmission of the heat wave to the subsequent layers and so on.

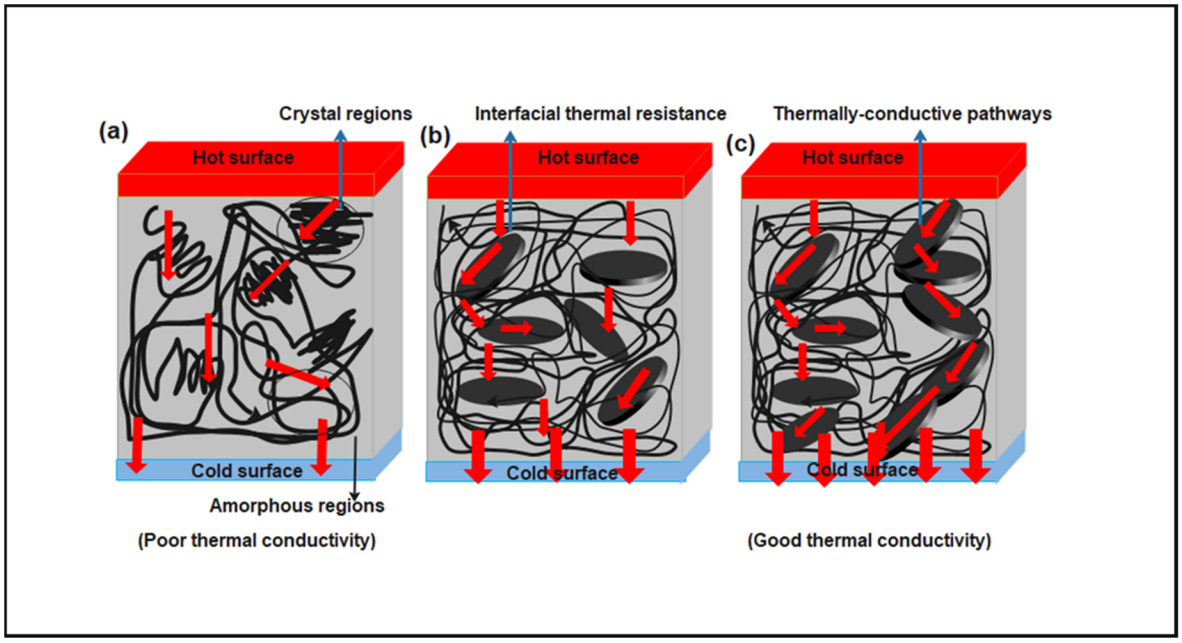

Figure 1.12 Illustration of the thermal conductivity through the polymer and composite with crystalline regions and conductive fillers, (a) semicrystalline polymer, (b) composite with low filler content with slight incorporation of thermal conductivity by fillers, (c) heat conduction by conductive channels,
redraw from (C. Huang et al., 2018) p.9)

The thermal conductivity is a physical property of the material which defines as the amount of the energy that is passing through a material in a certain time. Therefore, according to the Fourier law:

$$q_x = -KA\frac{dT}{dx} \tag{1.10}$$

where q_x is the transferred heat across the material along x direction, K is the capacity of the material to conduct heat, A is the perpendicular surface area to the heat transfer direction, dT is the temperature difference across a distance dx.

1.7 Methodology

Figure 1.13 shows an overall schematic of the composite preparation and characterization techniques for the treated samples during this doctorate project. To investigate the micro- or nanostructure of the composites, a cryofractured cross-sectional of the sample was prepared and the morphology of the composite was studied by scanning electron microscopy (SEM) and atomic force microscopy (AFM). The electrical properties of the test specimens were investigated by broadband dielectric spectroscopy (BDS), electrical breakdown tester (BD) and corona discharge exposure tester. The thermal properties of the composites were evaluated by differential scanning calorimetry (DSC), thermogravimetric analysis (TGA) as well as thermal conductivity measurement tester. FT-IR spectroscopy was used to evaluate possible chemical interaction between components in composites structure. The crystallinity of the composites was investigated by XRD experiment. More details regarding each experiment is explained in the following.

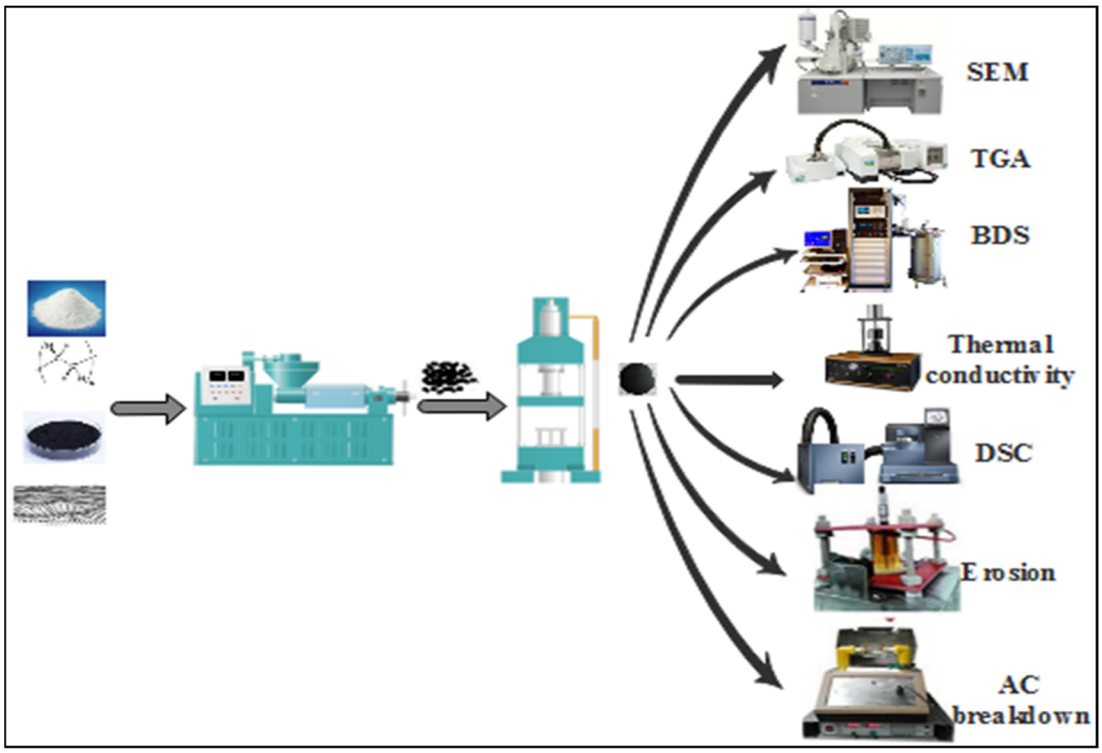

Figure 1.13 The schematic of experiments, including composite preparation and material's properties evaluation

CHAPTER 2

ELECTRICAL AND THERMAL PHENOMENON IN LOW-DENSITY POLYETHYLENE/CARBON BLACK NEAR THE PERCOLATION THRESHOLD

Sohrab Azizi[1], Eric David[1], Michel F. Fréchette[2], Phuong Nguyen Tri [1, 3], Claudiane M. Ouellet--Plamondon[1,]

[1] École de technologie supérieure (Université du Québec), 1100 Notre-Dame St W, Montreal, QC H3C 1K3 Canada
[2] Xi'an Jiaotong University, Shaanxi Sheng, 28 Xianning W Rd, JiaoDa ShangYe JieQu, Beilin Qu, China
[3] Department of Chemistry, Université du Montréal, 2900 Edouard Montpetit Blvd, Montreal, QC H3T 1J4, Canada

Paper published in *Journal of applied polymer science*, July 2018

Abstract

Low-density polyethylene (LDPE)/carbon black (CB) composites were fabricated via melt-compounding technique. The percolation threshold was found to be around 20 wt % CB, and an electrical network formed by conductive CB was proven by scanning electron microscopy investigation. Dielectric responses depicted an interfacial relaxation peak at 20 wt % CB content. LDPE/CB composites showed an electric field-dependent conductivity and a hysteresis behavior around the percolation threshold region. The CB particles with high thermal conductivity increased the heat conductance of the LDPE/CB20 up to 56%. The dynamic mechanical analysis of the LDPE/CB composites exhibited a noticeable contribution of CB throughout the composites, increasing the storage and loss modulus. The physical interactions between CB particles in the filler network enhanced the thermal stability of the LDPE/CB25 composite for more than 76 °C. The maximum breakdown strength of the LDPE/CB composites appeared with an approximately 10% improvement for LDPE/CB5 than pure LDPE.

Keywords: composites; conducting polymers; dielectric properties; extrusion; thermal properties.

2.1 Introduction

Carbonaceous conductive fillers have attracted a vast part of composite research due to a large number of potential industrial applications. A wide range of applications dealing with electromagnetic radiation shielding, self-regulating heaters (Feller, Bruzaud, & Grohens, 2004; Villacorta, Ogale, & Hubing, 2013; Q. Yuan & Wu, 2010), high-voltage and high-temperature devices, high-performance electromagnetic (EMI) shielding materials (Mondal et al., 2016; Nisar et al., 2017; Villacorta & Ogale, 2014), and electrical field grading have been proposed for polyethylene (PE)/CB composites (Foulger, 1999). LDPE composites loaded with CB are attractive materials for EMI shielding applications thanks to their cost-effectiveness, lightweight, high resistance to corrosive conditions, and easy processability (Mondal et al., 2016). These composites, at low filler concentration, can also be used for applications where the material remains insulating but in which electrical charges are allowed to slowly leak out of the material bulk to avoid space charge accumulation (S. Azizi et al., 2017; B. Li, Xu, Li, & Song, 2008). HVDC cables and spacecraft dielectrics are examples of such applications (Mazzanti & Marzinotto, 2013; Ryden & Hands, 2017). Therefore, possible applications for LDPE/CB composites cover the whole range of concentrations from low concentration for dielectric applications to intermediate concentration (near percolation threshold) for stress grading applications and up to high concentrations for EMI-shielding or semi-conductive screen applications.

Several studies have been conducted to investigate the electrical and thermal properties of LDPE/CB composites. Due to the role of finite and infinite CB clusters on the electrical conductivity of LDPE/CB composite, samples subjected to an electric field featured different behaviors. A non-ohmic trend at filler concentration close to the percolation threshold was observed due to the onset of current tunnels between CB clusters (Nakamura & Sawa, 1998). At the percolation threshold, a conducting pathway was formed resulting in a sharp increase in

electrical conductivity. The application of a magnetic field on LDPE/CB nanocomposites prepared by thermoforming technique was found to increase the degree of crystallinity and reduce the electrical conductivity (Ma, Han, Wang, & Jiang, 2009). The DC electrical conductivity of PE/CB nanocomposites was also found to decrease with the increase in temperature, particularly near the melting point (Hindermann-Bischoff & Ehrburger-Dolle, 2001; Hao Tang, Chen, & Luo, 1997). These conductivity changes were linked to the positive temperature coefficient (PTC) factor of the composites and affected by the filler concentration (Di et al., 2003; Hindermann-Bischoff & Ehrburger-Dolle, 2001; Hao Tang et al., 1997). The multi-walled carbon nanotubes-core/thiophene polymer composite fabricated by chemical oxidative polymerization indicated a significant electrical and thermal conductivity enhancement as the results of π-π interaction between polymer and filler (Reddy, Jeong, Lee, & Raghu, 2010). The compounded composite with carbon nanotubes (CNTs) and polycaprolactam (PA6) illustrated a lower percolation threshold than the one with thermally reduced graphene oxide (TrGO). Furthermore, due to the presence of impurities within the TrGO, the electrical conductivity of TrGO composites was found to be lower than that of CNTs composites (Méndez et al., 2017). In the study done by Son et al., the thermally reduced graphene created an electrically conductive network throughout the polyester and poly (butylene terephthalate) (PBT) composite in which the electrical conductivity followed a power low at percolation threshold, leading to an increase of around 8 orders of magnitude with addition of ~ 0.2 -0.4 vol.% (Son, Raghu, Reddy, & Jeong, 2016).

The thermal conductivity of polymeric composites containing high thermally conductivefillers, such as CNTs and graphene as well as carbon fillers has been widely investigated. The thermal conductivity of composites has been related to many factors such as filler morphology and concentration, the strength of bonding between polymer and filler, the volume of side groups of the host matrix, defects, inherent thermal conductivity of filler and host polymer and processing conditions (Han & Fina, 2011; Kochetov, Andritsch, Morshuis, & Smit, 2012). For example, the particle size of graphite in high-density polyethylene (HDPE) was found to play a predominant role in the thermal conductivity of the composite; graphite

with a diameter larger than 15 μm significantly intensified thermal conducting (Ye, Shentu, & Weng, 2006).

According to these studies, several drawbacks such as poor miscibility and inappropriate filler dispersion have been reported for polyolefin-based/carbon-based composites. In this regard, additives play a predominant role. Thus, in comparison to different allotropes of carbon, CB provided a more uniform distribution, higher apparent density, and faster flowrate during manipulation (B.-Y. Chen & Hwang, 2010). For this reason, the LDPE/CB remains an economic system that serves as a benchmark for polymer blends and nanoparticles. To the best of our knowledge, the hysteresis electrical effect and electrical field-dependency of LDPE/CB composites, as well as, their thermal conductivity have not so far been studied. The aims of this study are to investigate the thermal conductivity of LDPE composite containing highly conductive CB and their dielectric response to different electric field. In this regard, CB particle dispersion within the host matrix was investigated by scanning electron microscopy (SEM) and atomic force microscopy (AFM). Electrical field dependency, composite's memory behavior subjected to the electrical field, and resistance of LDPE/CB composites at low CB content to high AC electrical fields was also examined. Thermal properties of the composites were assessed via differential scanning calorimetry and thermogravimetric analysis (TGA). Finally, the dynamic mechanical properties of the composites were investigated.

2.2 Experimental

2.2.1 Materials

LDPE powder (XDS34P500) with a density of 0.922 g/cm^3, a melt flow index of 0.4 g/10 min and an average molecular weight of 102,000 was purchased from Marplex Australia. Commercial CB particle (VXC500) possessing excellent electrical and thermal conductivity and low sulfur content was provided from Cabot (USA), with an apparent density of 1.7-1.9 g/cm^3 at 20 °C and an average particle size of 10 micrometers or less in diameter.

2.2.2 Sample preparation

CB additive with different concentrations was blended with LDPE and the samples were labeled according to Table 2.1. All samples were fabricated with a twin screw co-rotating extruder (Haake MiniLab II) at a 140 °C melting zone temperature and a 110 rpm screw rate. To obtain a better dispersion, the extruded compound was recycled through the internal bypass existing in the extruder. Each batch of the compound was extruded and recycled for 5 min. Polymer films with an average thickness of 0.3 mm were subsequently prepared by hot pressing at 155 °C and 6.5 MPa of loading pressure.

Table 2.1 Formulations of the low-density polyethylene/carbon black composites prepared by melt compounding technique

Sample	LDPE (wt %)	Carbon Black (wt %)
Pure LDPE	100	0
LDPE/CB5	95	5
LDPE/CB10	90	10
LDPE/CB15	85	15
LDPE/CB20	80	20
LDPE/CB25	75	25
LDPE/CB30	70	30

2.2.3 Measurements

The morphology of the composites was investigated by scanning electron microscopy (SEM) using a Hitachi microscope (SU-8230 FE-SEM). The sample specimens were cryo-fractured by microtome in -100 °C liquid nitrogen and coated with a 2 nm platinum using the turbo-pumped sputter (Q150T).

The composite morphologies were analyzed by atomic force microscopy (AFM) using a digital instrument multimode AFM (Veeco multimode) on a cross-section thin film prepared by

cryogenic microtoming. These observations were carried out at room temperature and the data were acquired in the height, amplitude and phase modes with a scan rate of 1 Hz and areas of 4×4, 2×2 and 0.65 ×0.65 μm^2.

The dielectric response of LDPE/CB composites was measured using a flat disk with a diameter of 40 mm and an average thickness of 300 μm. The measurements were performed with a broadband dielectric spectrometer (Novocontrol) in a wide range of frequencies, ranging from 0.01 Hz to 1 MHz at 20 °C with an AC excitation voltage of 3 Vrms. The real part (ε'), the imaginary part (ε'') and the complex permittivity (ε^*) are given by Equation 2-1 (Håkansson, Amiet, Nahavandi, & Kaynak, 2007):

$$\varepsilon^*(\omega) = \varepsilon'(\omega) - j\varepsilon''(\omega) \tag{2.1}$$

The AC breakdown strength (ACBD) of LDPE/CB composites at low filler contents was obtained with a Bauer DTA100 tester. These measurements were conducted according to the procedures described in the ASTM D149-09(2013) standard. A thin sheet was positioned between two ball-tip electrodes with a diameter of 4 mm and immersed into dielectric mineral oil. A short-term test consisting of 60 Hz voltage at a rising rate of 2 kV/s was employed for each measurement. The reported values were calculated from the average of ten trials in the same condition for each sample.

The resistance of the neat LDPE and LDPE/CB5 to erosion due to exposure to corona discharges was investigated by a handy-setup erosion tester. This type of test consisted of applying 10 kV rms at a frequency of 300 Hz for 35 h on a titanium ball with a diameter of 4 mm that was separated from a disk-shaped sample with a diameter of 40 mm by a gap of 10 μm between the ball tip and the sample surface. More information on this type of test and on the experimental setup can be found elsewhere (Heid, Fréchette, & David, 2015).

The structure of neat LDPE and its composites comprising CB filler was characterized using an X-ray diffractometer (PANanalytical X'Pert Pro). The scanning was conducted with Cobalt tube with Kα radiation (λ = 1.792 Å) in the range of 2θ from 15 to 65°. An accelerating voltage of 40 kV, a step size of 0.0668° and a counting time of 150 ms per step was applied.

The degree of crystallinity and melting temperature of LDPE/CB composites were obtained using differential scanning calorimetry (DSC) (Q20, TA instrument). To remove the thermal history of composites, the test specimen was first heated with a ramp of 10 °C/min from 0 to 150 °C. It was cooled down from 150 to 0 °C with a rate of 10 °C/min, and again, subsequently, the sample was heated similarly to the previous heating step. The DSC thermograms for the thermal properties assessment were obtained from the second heating cycle. The melting temperature as well as the specific fusion's enthalpy (ΔH_m) of the composites were extracted from the DSC thermograms, which allows the calculation of the degree of crystallinity (X_c) from Equation (2-2) (Suñer, Joffe, Tipper, & Emami, 2015).

$$X_c = \frac{\Delta H_m}{\Delta H_m^o} \frac{1}{(1-w)} \times 100 \tag{2.2}$$

where w is the filler content and ΔH_m^o (293.6 J/g) is the specific fusion's enthalpy of a perfect crystal of PE. (Ratanakamnuan & Aht-Ong, 2006)According to the variant of the Thomson-Gibbs equation for a lamellar crystallite of large lateral dimensions, the lamellar thickness (l) of pure LDPE and its composites is given by Equation 2-3, as follows (Psarski, Piorkowska, & Galeski, 2000):

$$l = \frac{2\sigma_e}{\Delta H_m^0} \times \frac{T_m^o}{T_m^0 - T_m} \tag{2.3}$$

where, T_m^o is the thermodynamic melting point of infinite perfect crystals (418.6 K), T_m is the melting temperature, and σ_e is the fold-free surface energy (90.4 mJ.m^{-2}) (Furushima et al., 2015).

The thermal stability of LDPE/CB composites, as well as the content of CB in the samples, were measured by thermogravimetric analysis (TGA) using a diamond TG/DTA instrument (Perkin Elmar). TGA experiments were carried out with samples around 10 to 13 mg in weight. The heating was performed with a ramp of 20 °C/min from 200 to 800 °C under N_2 atmosphere and then the temperature was kept at 800 °C under air for 10 min.

The thermal conductivity of LDPE/CB composites was investigated using a guarded heat flow meter (DTC-25 TA instrument). Measurements were conducted according to the ASTM E1530-11(2016) standard, by applying a pressure of 20 psi from the upper surface on the sandwiched disk placed between two heating and cooling brass plates. The differential temperature between the heated and cooled brass plates was set to 25 °C. For each sample, the measurement was conducted on two replicates consisting of a circular disk with a diameter of 50.8 mm and a thickness of about 300 µm. To ensure the thermal stabilization of the sample chamber, the thermal conductivity measurement was performed after 2 h. The heat flowing across the sample was measured by a heat flux transducer which is located in the lower plate, and the thermal conductivity can then be inferred by Equation 2-4 (Heid et al., 2015):

$$\lambda = \frac{Q.t}{A.\Delta T} \tag{2.4}$$

where Q represents the heat flux through the sample, A is the sample area, ΔT is the differential temperature between upper and lower plates and t is the sample thickness.

The dynamic mechanical properties of LDPE/CB composites were measured by a DMA Q800 (TA Instruments). Measurements were carried out in the tension mode with a standard rectangular sample having dimensions of 30×7×0.3 mm^3 at a frequency of 1 Hz, deformation amplitude of 20 µm and a force track of 120 %. Each measurement was performed in a wide range of temperatures, ranging from -100 to 100 °C with a ramp of 5 °C/min.

2.3 Result and discussion

2.3.1 SEM imaging

Figure 2.1 shows the cross-section morphology images of LDPE/CB composites at two magnifications. As indicated, the spheroid-shaped CB particles throughout the LDPE/CB composites at below the percolation threshold (LDPE/CB15) were dispersed somehow uniformly, and the connections between particle-particle were not sufficient to form a conductive pathway (Figure 2.1a and Figure 2.1b). The addition of more CB particles was

found to form a connected network within the composite for LDPE/CB20 (at percolation threshold). At this filler content (LDPE/CB20) the chain-shaped CB particles were seen clearly, leading bridges between the upper and lower electrode, and ease charge carrier (Figure 2.1c, Figure 2.1d). At higher filler content (LDPE/CB25), a conductive network of the CB particles as well as several islands of the agglomerated CB particles was observed. Apparently, the CB particles acted as the nucleating agents in which caused some micron-sized filler agglomerations within the composite (Figure 2.1e and Figure 2.1f).

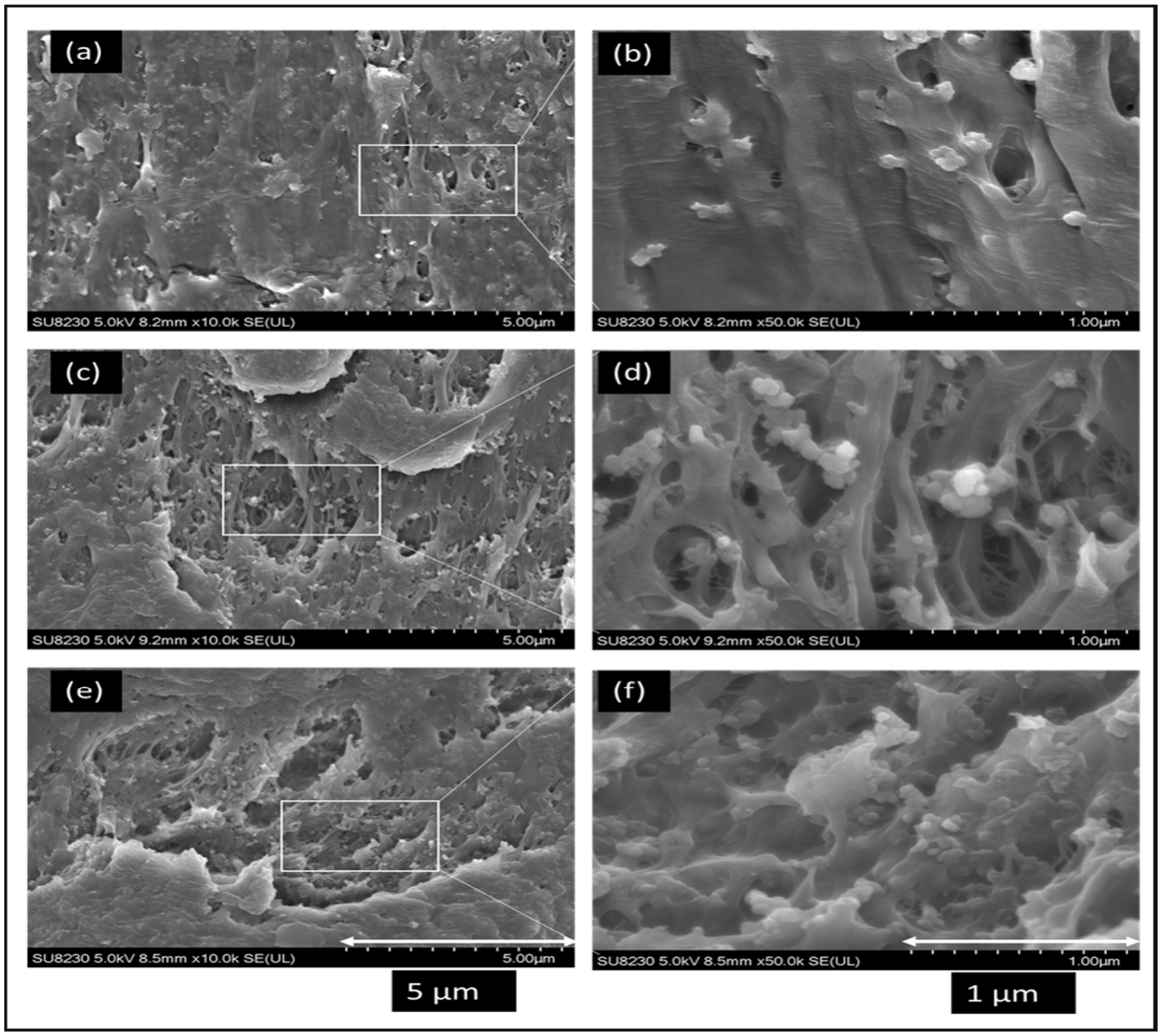

Figure 2.1 SEM images of the cross-sectioning cut of the LDPE/CB composites : (a, b) LDPE/CB15, (c, d) LDPE/CB20 and (e, f) LDPE/CB25 at 10k and 50k magnifications, respectively

2.3.2 AFM imaging

The cross-sectional cut surface morphology of LDPE/CB composites was observed by the AFM below (LDPE/CB15) and above (LDPE/CB25) the percolation threshold (Figure 2.2). The phase imaging in AFM showed rather uniform filler dispersion in the whole composite sample. The yellow and brown region in the phase images indicate the polymer matrix while the bright dots illustrate the CB particles. At filler concentrations below the percolation threshold (Figure 2.2a and Figure 2.2b) some agglomerations were observed but overall, the CB particles were still mostly isolated. Beyond the percolation threshold (LDPE/CB25), the CB particles were connected together, forming some conducting pathways in the polymer matrix (Figure 2.2c and Figure 2.2d), and, as expected, a higher number of particle-to-particle connections were observed here than in the case of the composite containing 15 wt % CB. Further physically-connected particles in the composite with high filler content (LDPE/CB25) will influence on electrical, mechanical and thermal properties of composites that will be explained later.

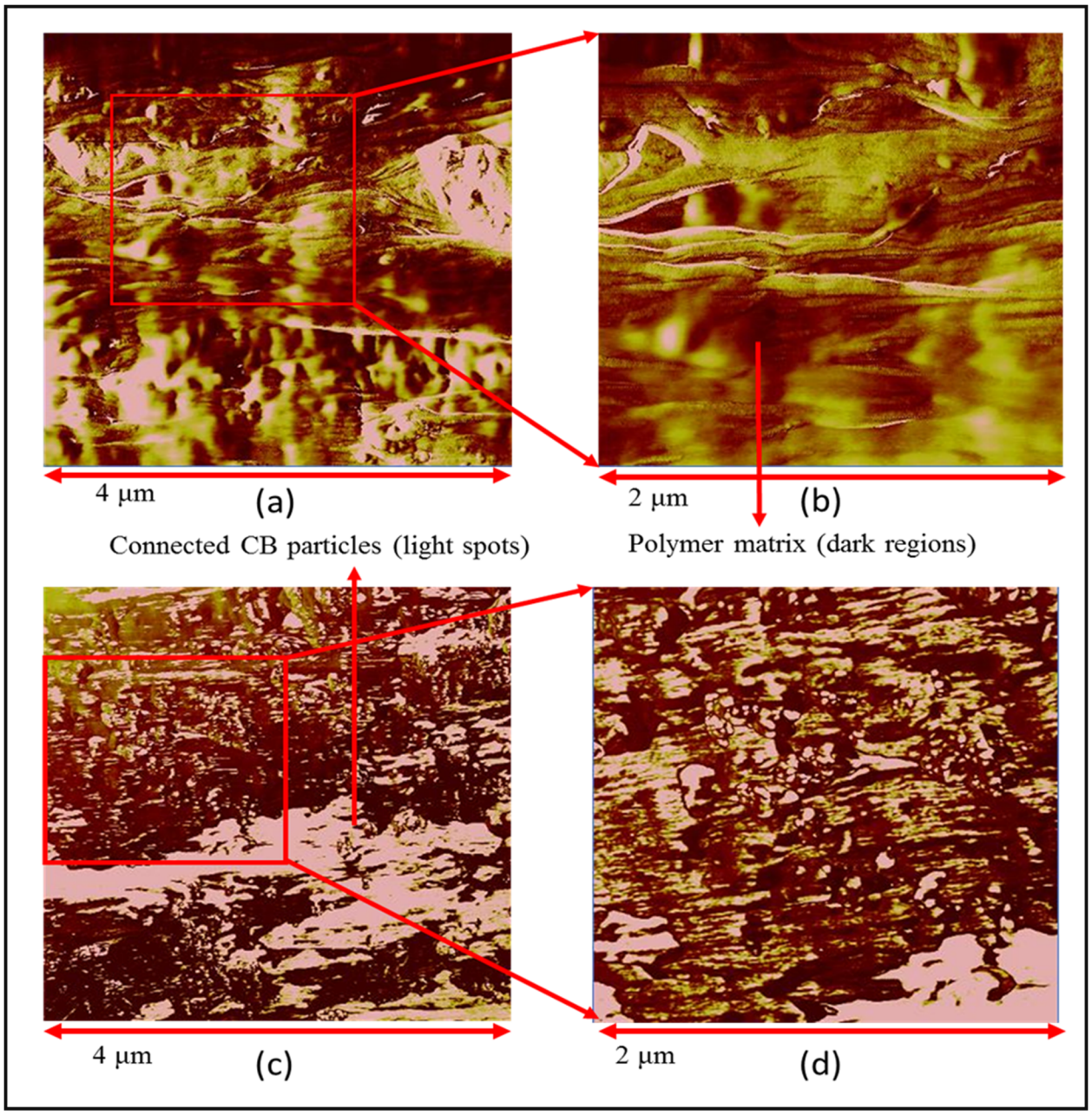

Figure 2.2 AFM phase images at different magnifications: (a, b) LDPE/CB15, (c, d) LDPE/CB25

2.3.3 Dielectric properties

The frequency-domain dielectric response of LDPE/CB composites at 20 °C is shown in Figure 2.3 (real part, Figure 2.3a, and imaginary part, Figure 2.3b). At low filler concentrations (under 20 wt%), a conductive network bridging both electrodes was not achieved,(Zhou,

Hrymak, & Kamal, 2017) but at filler content around 20 wt%, while the DC conductivity remained very low, some conductive structures within the composite bulk started to form and gave rise to high dielectric losses featuring an interfacial loss peak in the vicinity of 1 Hz. This was in good agreement with SEM and AFM observations explained previously. This interfacial polarization mechanism in the composite led to a stepwise increase of the real permittivity part, as imposed by the Kramers-Kronig relations (Z.-M. Dang et al., 2012; Kremer et al., 2012). The interfacial relaxation mechanism, also known as Maxwell-Wagner-Sillars effect (Burger et al., 2016), was a result of the accumulation of charge carriers at the interface of the slightly conductive clusters within the composites that were not yet bridging both electrodes' (Yu et al., 2005; Q. Yuan & Wu, 2010). When the filler concentration reached the percolation threshold (CB content between 20-25 wt %), the electrical conductivity of the composite switched from that of an insulating material to a semi-conductive one (Mysiukiewicz, Sterzyński, Ławniczak, & Rogodzińska, 2017; Ren et al., 2014). Thus, the conductivity of the LDPE/CB25 composite was found to increase by about 11 orders of magnitude compared to that of pure LDPE, as can be seen in Figure 2.4.

Comparative value of the electrical conductivity and the percolation threshold of several composites are presented in Table 2.2. Composites prepared by solvent casting were found to be conductive at extremely lower filler content than the melt compounding one. Due to the existence of some impurities such as oxygenated groups in the graphene-based fillers, composites with CB additive revealed higher electrical conductivity. In this regard, comparing our LDPE/CB composite with its counterparts indicate good electrical conductivity with respect to other referred composites.

Table 2.2 Comparison of electrical conductivity of various composites with different carbonaceous fillers

Composites	Mixing procedure	Percolation threshold	Electrical conductivity (S/m)	Reference
PA6/CNT	Melt blending	~ 2-3 wt %	10^{-5} at 2 wt %	(Méndez et al., 2017)
PA6/TrGO	Melt blending	~ 5-10 wt %	10^{-5} at 10 wt %	(Méndez et al., 2017)
TRG/PBT	Solvent-casting	0.22 vol %	10^{-2} at 0.4 vol %	(Son et al., 2016)
TRG/PEE12	Solvent-casting	0.27 vol %	10^{-3} at 0.7 vol %	(Son et al., 2016)
TRG/PEE30	Solvent-casting	0.31 vol %	10^{-3} at 0.7 vol %	(Son et al., 2016)
TRG/PEE35	Solvent-casting	0.36 vol %	10^{-3} at 0.7 vol %	(Son et al., 2016)
CPE/CB	Solvent-casting	10 wt %	10^{-2} at 10 wt %	(Mondal et al., 2016)
LDPE/CNT	Roll mixing	-	10^{-9} at 2 wt %, 0.1 kV/mm	(Ma et al., 2009)
HDPE/CB	Grinding mill	0.1 vol %	10^{-1} at 0.11 vol %	(Hindermann-Bischoff & Ehrburger-Dolle, 2001)
LDPE/CB	Melt blending	2-7 wt %	10^{-7} at 7 wt %	(Di et al., 2003)
PEDOT/ MWCNTs	Solvent-casting	-	293 S/m at 27 wt %	(Reddy et al., 2010)
LDPE/CB	Melt compounding	20-25 wt %	10^{-1} at 25 wt %	Our work

In order to better understand the origin and contribution of the charge carrier and charge accumulation in the interface of inclusions, the imaginary permittivity of the LDPE/CB20 composite at 20 °C was fitted according to Equation 2-5 (Kremer et al., 2012),

$$\varepsilon^*(\omega) = -i\left[\frac{\sigma_o}{\varepsilon_o \omega}\right]^N + \frac{\Delta\varepsilon}{(1+(i\omega\tau)^\alpha)^\beta} + \varepsilon_\infty \tag{2.5}$$

where the first term represents the contribution from the charge carriers and the second term is the general empirical expression, the Havriliak-Negami function, used to model a relaxation process. σ_o and N are the material's parameters related to the conduction process, with N = 1 leading to special case of direct conduction, $\Delta\varepsilon$ denotes the dielectric strength of the relaxation peak, τ is the relaxation time and the parameters α and β are the slopes of the low-frequency side of the relaxation peak and the asymmetry parameter, respectively.(Kremer et al., 2012) As can be seen in Figure 2.5, the use of Equation 2-5 gave a reasonable fitting of the relaxation peak of the LDPE/CB20 composite with a time constant of 6.2 x 10^{-2} s and a dielectric strength of 8.2. The parameters α and β are given in Table 2.3 as well as σ_o with N = 1 (direct conduction). At higher frequencies than the peak frequency of the relaxation process, Equation 2-5 predicts a rapid decrease to essentially zero of the dielectric losses and consequently cannot fit anymore the experimental data that exhibits an unusual constant-loss dielectric response. The complete fitting of the dielectric spectrum shown in Figure 2.5 can be achieved by the addition to Equation 2-5 of a third term, similar to the first one but with a low value of N in the vicinity of ~ 0.1.

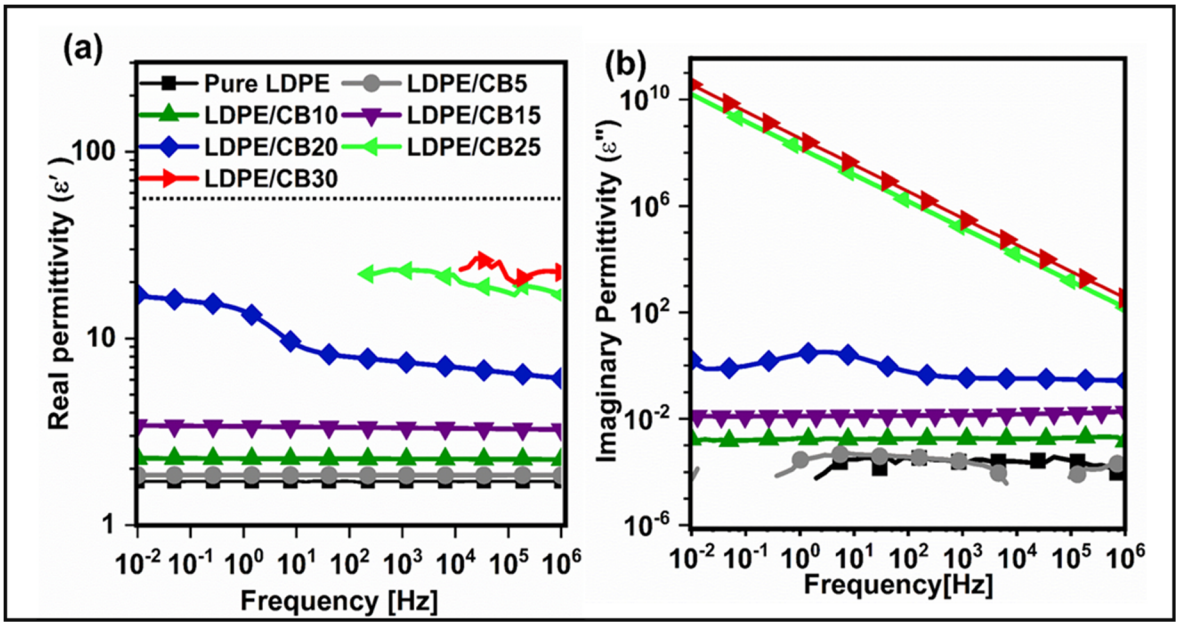

Figure 2.3 Real (a) and imaginary permittivity (b) of LDPE/CB composites at 20 °C as a function of frequency

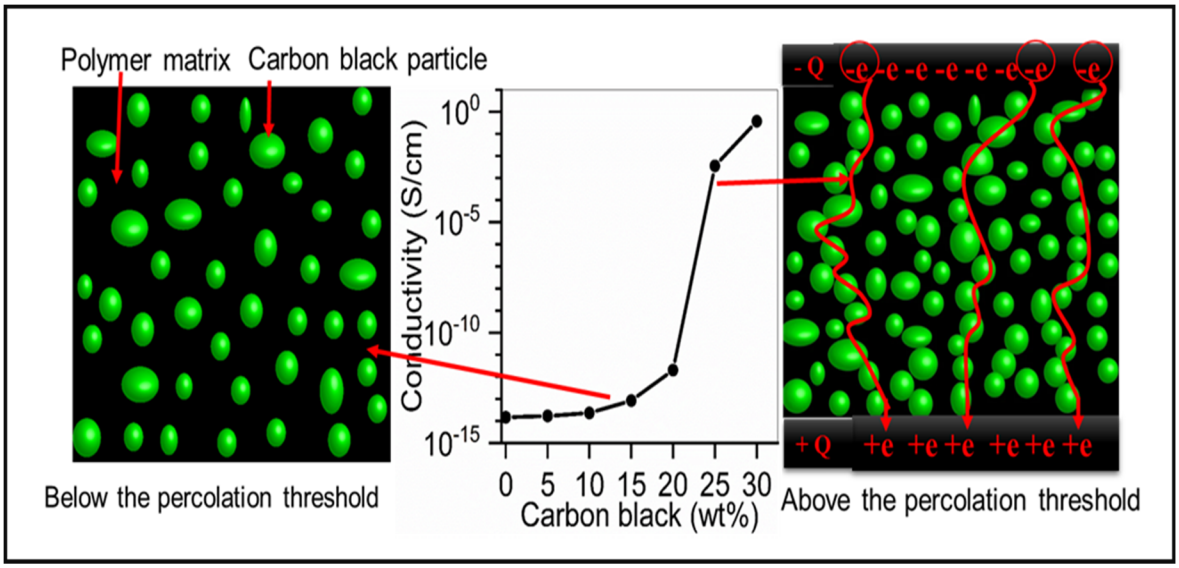

Figure 2.4 Charge carrier diagram and electrical conductivity of LDPE/CB composite as a function of CB concentration

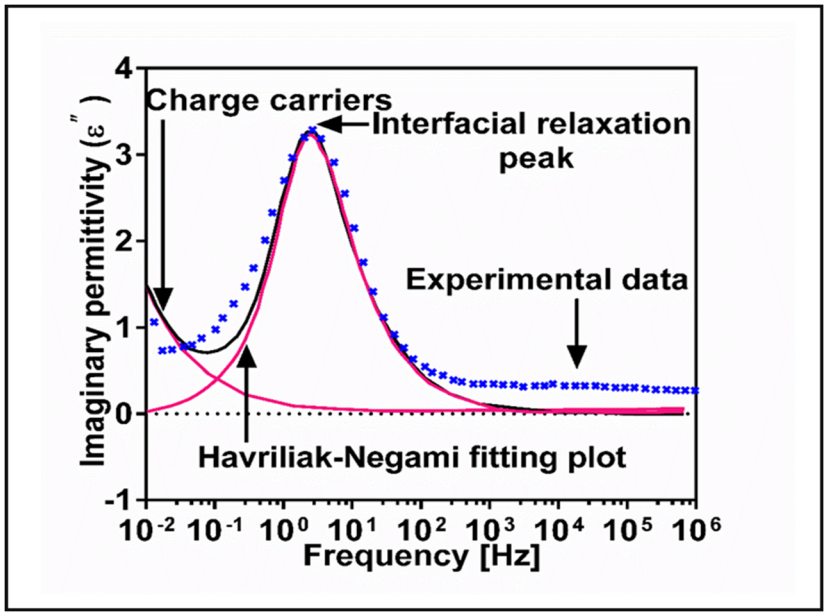

Figure 2.5 Imaginary permittivity of LDPE/CB20 as a function of frequency at 20 C, fitted with equation 2-5, the black curve representing the sum of the contribution from the DC conductivity and the interfacial relaxation process

Table 2.3 Fitting Parameters for Dielectric Response of LDPE/CB20 Composite at 20 °C according to equation 2-5

DC conductivity ($S.cm^{-1}$)	Exponent N	$\Delta\varepsilon$ at 20 °C	τ (s)	α	β
8.50×10^{-14}	1.0	8.20	0.065	0.854	0.955

2.3.4 Effect of temperature on the electrical responses

The electrical responses of the LDPE/CB composite at percolation threshold (LDPE/CB20) were investigated at different temperatures from 30 °C to approximately the polymer melting point (100 °C) (Figure 2.6). The findings showed a significant decrease in the dielectric losses with increasing temperature and a constant or "flat" dielectric loss behavior. This behavior, which has been known for decades for various solid materials such as glasses and ferroelectric crystals (Andrzej K Jonscher, 1996), is still poorly understood. One possible reason for the decrease of dielectric losses with the increase of temperature might be the release of the absorbed moisture forming an interlayer between the hydrophilic particles and the hydrophobic

matrix (David & Fréchette, 2013). However, when the measurements were conducted for the second run at 40 and 30 °C consecutively after the elevated temperature (100 °C) run, the dielectric losses were found to increase again at approximately the same level than for the first run. Accordingly, the main contribution of the lowering of the dielectric losses was found to be linked to the thermal expansion of the composite for which the increase of temperature (50 to 100 °C) causes a slight separation of previously connected particles (Hindermann-Bischoff & Ehrburger-Dolle, 2001; Shen, Wang, Yang, & Meng, 2011; Traina, Pegoretti, & Penati, 2007; Yacubowicz & Narkis, 1986; P. Zhang & Wang, 2018). When the dielectric response was measured for the second run (at 40 and 30 °C), due to the shrinkage of the composite, the electrical connectivity between closely located carbon particles increases, forming larger aggregates. As a result, both the real and imaginary parts of the complex permittivity of the LDPE/CB20 were found to increase significantly. Thus, the volume fraction of the CB particles (ϕ_{CB}) within the composite, as well as the microstructure, was affected by thermal expansion, which plays a remarkable role in the electrical properties of the composite (Bueche, 1973; Dudić, Škipina, Dojčilović, Novaković, & Kostoski, 2011; Webb, Bloor, Szablewski, & Atkinson, 2014). The changes in the location of the interfacial relaxation peak with increasing temperature can be explained in a similar fashion by the disruption of the previously conductive aggregates (for 40, 50 and 60 °C). At higher temperatures up to 100 °C, the contribution of charge fluctuation throughout the composite bulk starts to be predominant at low frequency and leads to the usual low-frequency dispersion behavior (E Helal, Pottier, David, Fréchette, & Demarquette, 2018).

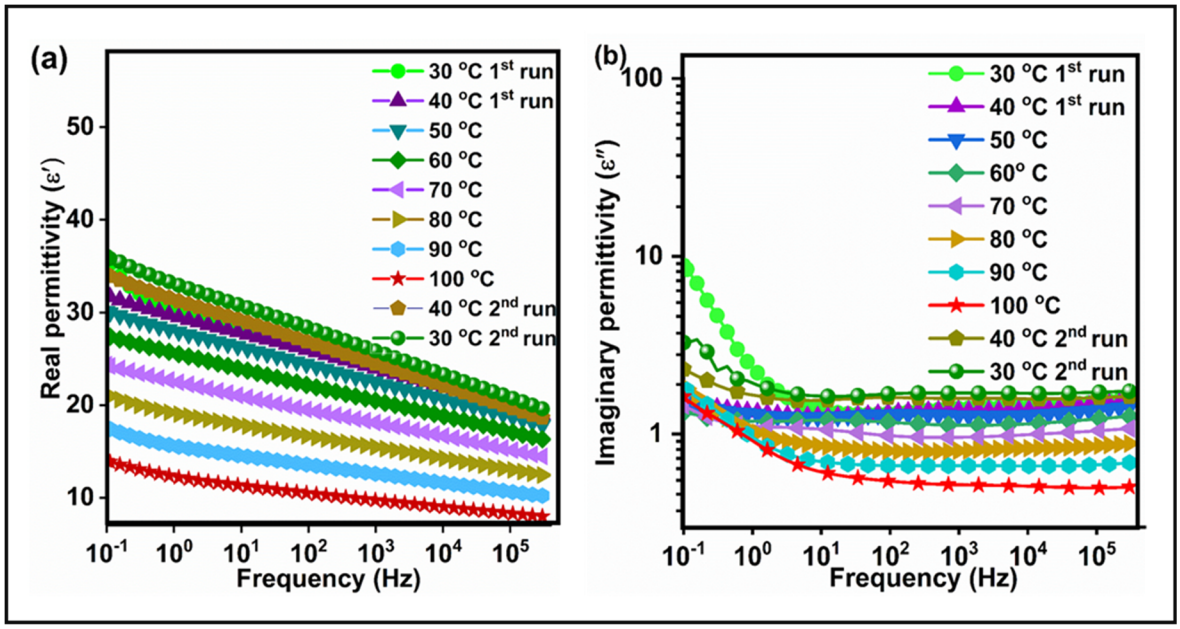

Figure 2.6 Real and imaginary parts of the complex permittivity of LDPE/CB20 as a function of frequency at various temperatures

2.3.5 Non-linearity and hysteresis

Electrical field-dependency of the dielectric response of pure LDPE and LDPE/CB composites was studied over the 10^{-1}-10^{-4} Hz frequency range. Measurements were conducted using different electrical fields, ranging from 17 to 1100 V/mm (first run) and then lowering the electrical field to the initial value of the electrical field (second run). For LDPE/CB25 and LDPE/CB30, the measurements were carried out only at 17 and 178 V/mm. The composites were found to exhibit significant electrical field-dependency in their dielectric response in the vicinity of the percolation threshold, as illustrated in Figure 2.7a. In fact, the LDPE/CB20 composite featured a non-linear conductivity and a counterclockwise hysteresis behavior. Figure 2.7b illustrates the imaginary permittivity of LDPE/CB20 as a function of applied electric field. As can be observed, a low-frequency interfacial relaxation peak occurred at the low electrical field during the first run but then moved towards higher frequencies as the field was increased. The peak disappeared when the field was further increased, and the contribution of the DC conductivity started to dominate the low-frequency dielectric response. This shift of MWS peak towards higher frequencies is due to the increase of the intra-cluster connections

leading to a more conductive cluster and consequently a lower relaxation time (Song, Zheng, & Yi, 2004). When the field reached values above 300 V/mm, cluster-to-cluster connections started to appear and ultimately charge transportation through the material occurred (Donzel, Greuter, & Christen, 2011; He & Tjong, 2011).

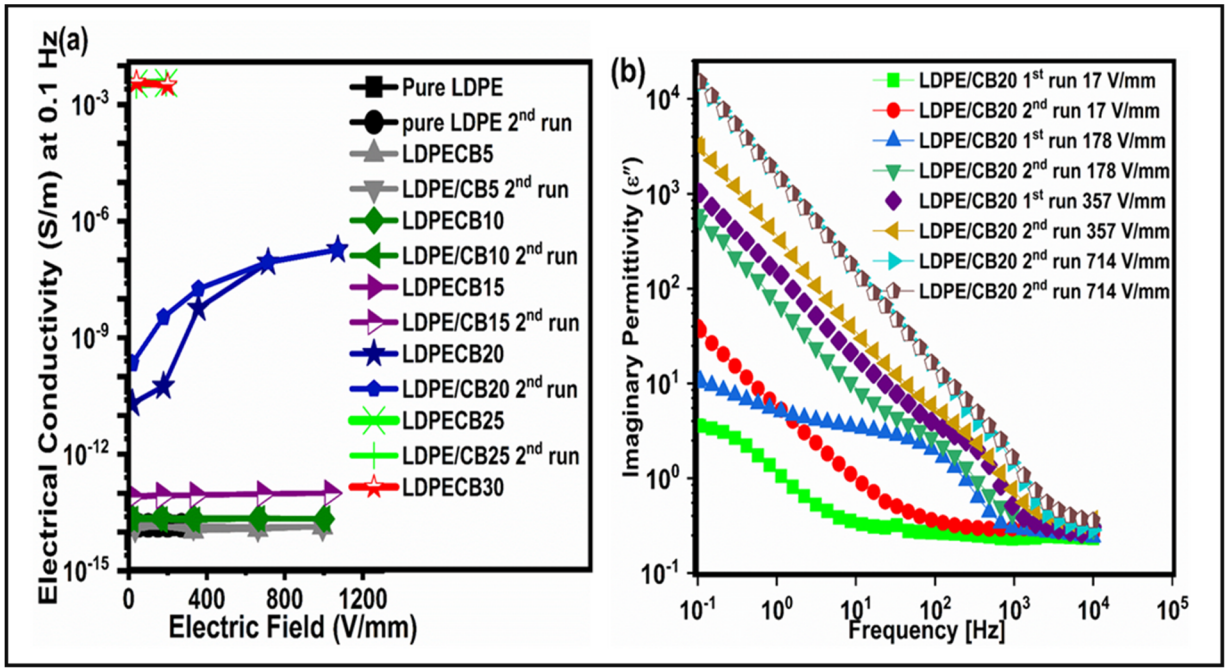

Figure 2.7 Real part of the complex conductivity at 0.1 Hz for several LDPE/CB composites as a function of electric field for the first two runs and (b) imaginary permittivity of the LDPE/CB20 composite at various electric fields

2.3.6 AC breakdown

Dielectric AC breakdown strength was analyzed with the two-parameter Weibull distribution, and results are shown in Figure 2.8. According to this distribution, the failure probability under an increasing ramp of AC voltage is given by Equation 2-6:

$$P(E) = 1 - \exp[-(\frac{E}{\alpha})^{\beta}] \tag{2.6}$$

where $P(E)$ represents the cumulative failure probability at an electrical field E, α is the scale parameter or the characteristic breakdown strength, which is the field for which 63.2 % of the samples have failed, and β is the shape parameter which is related to the scattering of the data

obtained during the BD measurements (Heid et al., 2015). A characteristic breakdown strength (α) of 117 kV/mm was found for the LDPE/CB5 sample which was about 10 % higher than the one obtained for pure LDPE. This increase can be linked to the trapping of charge carriers, generated in the composite matrix at high electrical field (Z.-M. Dang et al., 2012; Emna Helal, Demarquette, David, & Fréchette, 2016). Further addition of CB nanoparticles led to a reduction of dielectric breakdown strength due to the formation of conductive clusters and consequently tunneling current between particles and clusters (Tian, Lei, Wang, & Wang, 2012).

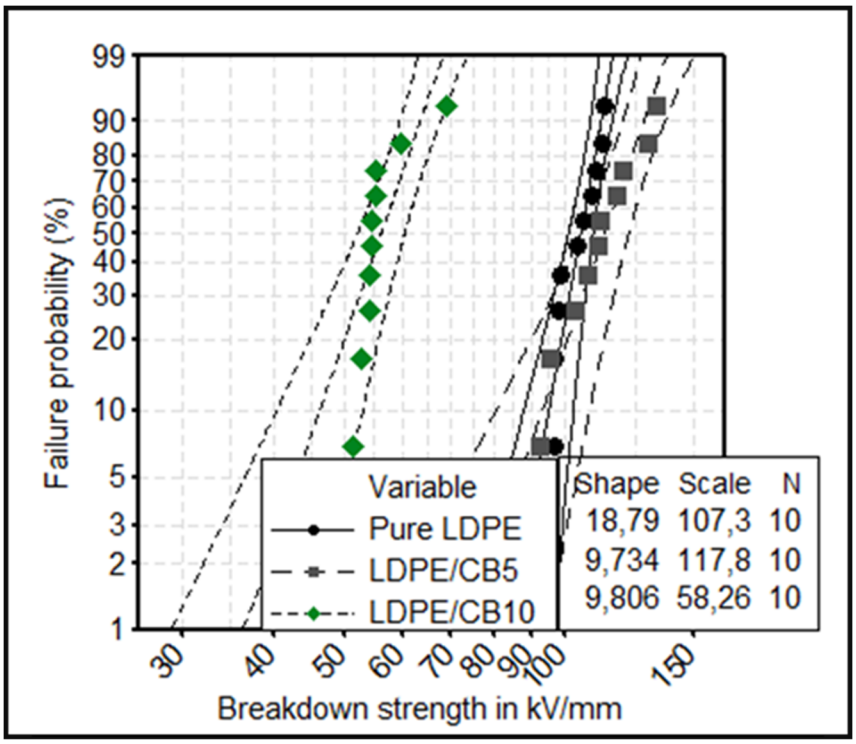

Figure 2.8 Weibull plots of the breakdown strengths with 95% confidence intervals for the pure LDPE, LDPE/CB5, and LDPE/CB10 composite

2.3.7 Resistance to corona discharges

The eroded volume after exposure to corona discharges was subsequently evaluated by the use of a mechanical profilometer for the neat LDPE and two composite samples (LDPE/CB5 and LDPE/CB10). The erosion test was stopped after 10 h for LDPE/CB10 due to sample failure.

Figure 2.9 shows the profiles of the eroded surfaces for LDPE and LDPE/CB5 after the erosion test was completed. As can be observed, the eroded areas were highly symmetrical around the tip of the HV titanium electrode. The resistance to corona discharges was evaluated based on the calculation of the eroded volume and it was found to decrease when 5 wt% CB was added to the LDPE polymer matrix. Indeed, the eroded volume, as measured by the profilometer, was found to be 3.05 $\times 10^9$ μm^3 and 3.88 $\times 10^9$ μm^3 for LDPE and LDPE/CB5, respectively, corresponding to a decrease of about 27 % in erosion resistance.

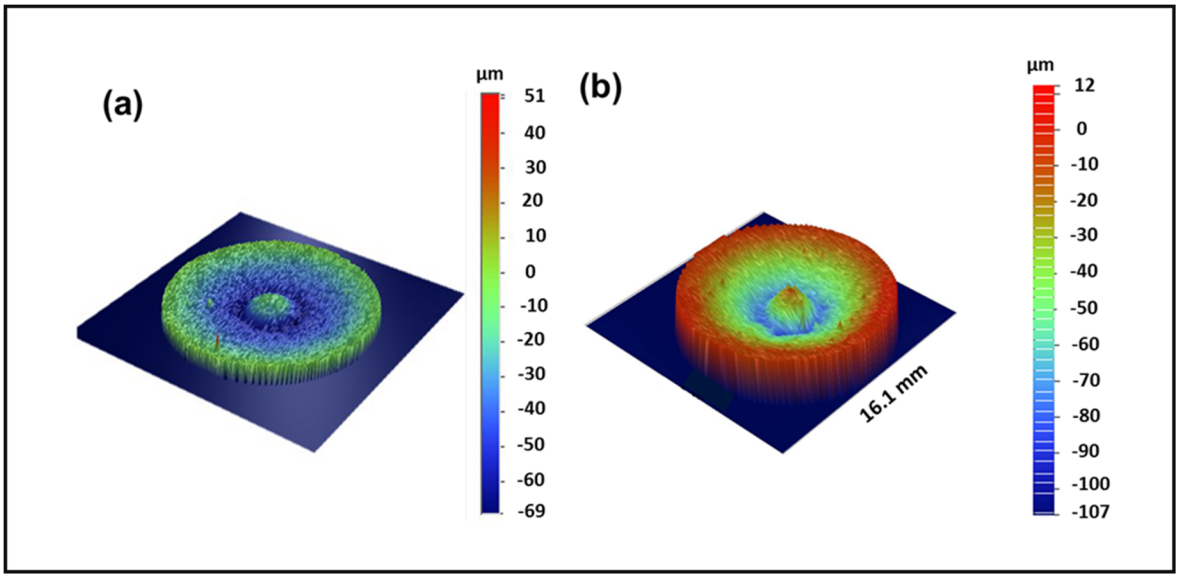

Figure 2.9 Eroded areas of the samples subjected to corona condition: (a) pure LDPE, (b) LDPE/CB5 composite

2.3.8 Dispersion of CB in LDPE investigating by XRD

XRD experiment was carried out to evaluate the CB dispersion in LDPE polymer. As indicated in Figure 2.10, the XRD patterns did not feature any diffraction peaks derived from CB in the LDPE/CB composites, illustrating suitable dispersion of CB particles in the matrix. CB illustrated two broad reflections at 28.5° and 52°, revealing extremely lower crystallinity with respect to the observed sharp-peak for the semicrystalline LDPE polymer at 24.3 ° (Hu et al., 2013) Additionally, due to high surface specific area of the CB, re-stacking of the CB was occurred, and resulted broad reflection peak. The broad peak at 28.5° corresponds to the (002)

of the CB. Pure LDPE and its composites with CB indicated two peaks at 24.3 ° and 27.5° corresponding to (110) and (200) lattice planes. The appeared peaks were found to be fixed in their locations, indicating adequate exfoliation of polymer chains and poor particles agglomeration (Lei et al., 2016).

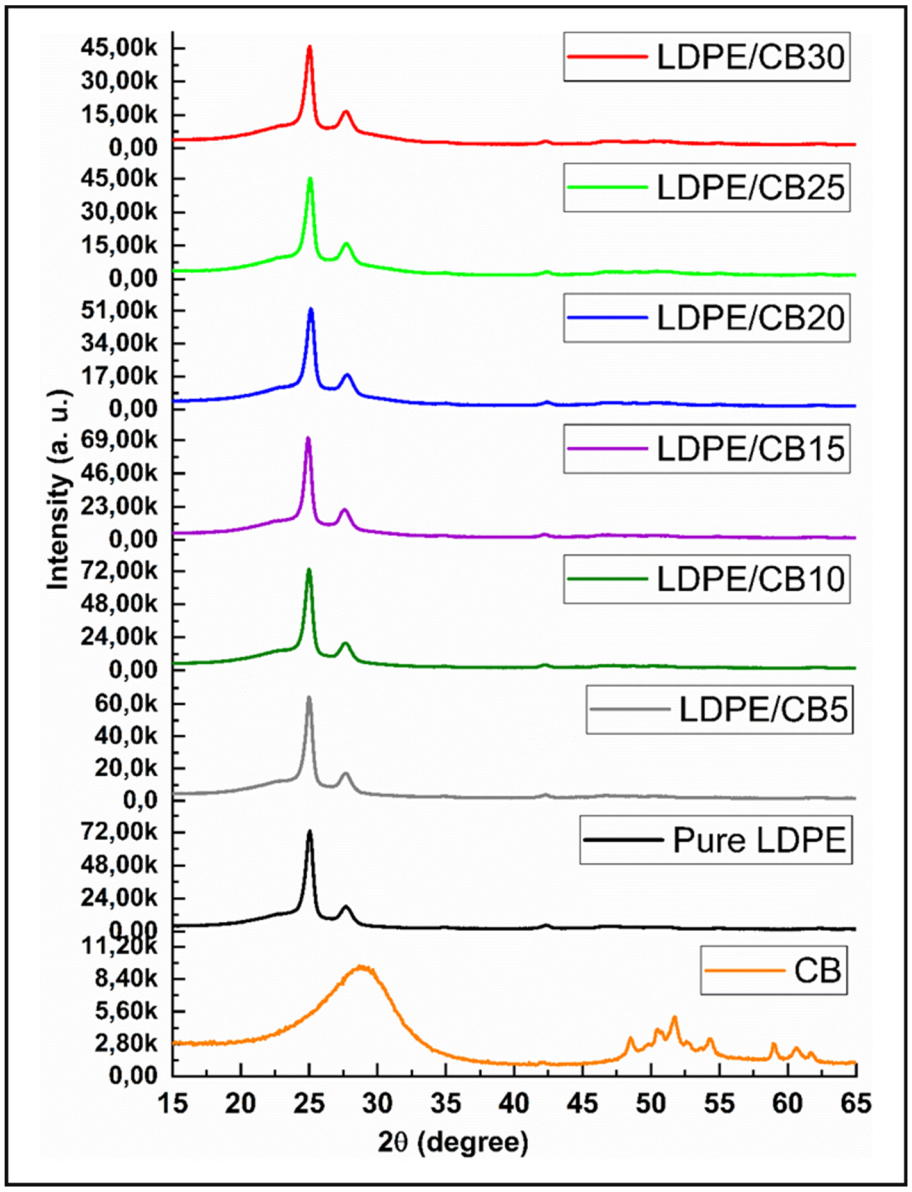

Figure 2.10 XRD patterns of CB, pure LDPE, and its composites at differentCB contents

2.3.9 Thermal properties

The incorporation of CB into the pure LDPE was not found to significantly alter the composite's melting point (T_m), indicating a broad melting range, commencing from ~ 40 °C (Figure 2.11). Furthermore, the addition of CB particles did not increase the degree of crystallinity (X_c), as the crystallinity percentage was found to remain almost constant with a negligible change within two percent with respect to the pure LDPE. The lamellar thickness (l) of the ordered regions was deduced from the melting temperature and calculated according to Equation 2-3. Similar values of lamellar thickness were found for pure LDPE and their composites, which again corroborates the fact that the incorporation of CB did not lead to significant change in the matrix morphology (Table 2.4). TGA measurements were conducted showing that pure LDPE started to undergo pyrolysis at about 375 °C and then undergoes a rapid decomposition down to basically no ash content (Ruvolo Filho, Menezes, & Scarpa, 2008). The onset temperature ($T_{5\%}$), corresponding to 5 % of sample weight loss, the $T_{50\%}$ corresponding to 50 % of sample weight loss and the final remaining mass at 550 ^{o}C are given in Table 2.4 for each composite. CB loading was found to increase the onset decomposition temperature, particularly in the case of the LDPE/CB25 sample. This enhancement of the thermal properties can be explained by possible weak physical interactions between particles (C. L. Huang, Chen, Wang, Tu, & Liao, 2013; Kuilla et al., 2010) and the formation of a filler network within the composite. Decomposition temperature was also found to increase by the addition of CB, from 464 °C for the pure LDPE to about 500 °C and 492 °C for the LDPE/CB25 and LDPE/CB30 composites, respectively. This increase may due to the high thermal stability of CB itself (Crompton, 2012) and the lower mobility of the polymer chains close to the additives (Gabbott, 2008; S. Yang, Taha-Tijerina, Serrato-Diaz, Hernandez, & Lozano, 2007). The residual content at 550 °C was in good agreement with the nominal values, initially calculated during the formulation.

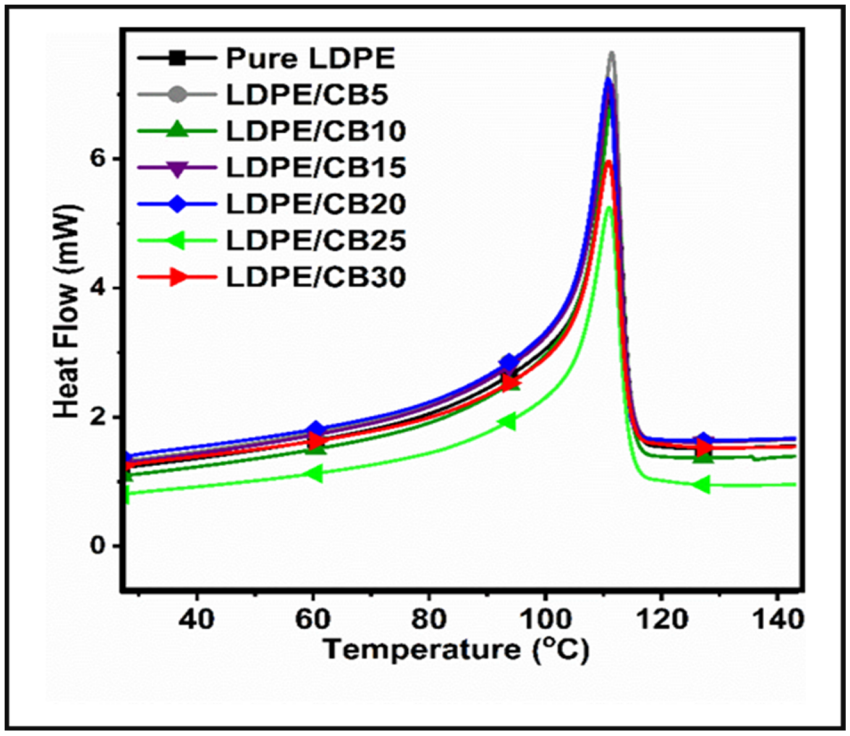

Figure 2.11 The heating thermograms of the pure LDPE and LDPE/CB composites, featuring the onset temperature and melting points.

Table 2.4 The Melting Point, Degree of Crystallinity, Lamellar Thickness, Onset temperature, and the Degradation Temperature of the LDPE/CB Composites Measured by DSC and TGA

DSC results				TGA results		
Sample	T_m (°C)	X_c (%)	l (nm)	T at 5 wt% loss (°C)	T at 50 wt% (°C)	Residue (wt) % at 550 °C
Pure LDPE	111.61	41	7.62	376	464	0.26
LDPE/CB5	111.39	41	7.57	401	491	5.90
LDPE/CB10	111.30	40	7.55	404	479	9.11
LDPE/CB15	111.15	42	7.52	403	493	15.39
LDPE/CB20	110.80	43	7.44	401	498	20.16
LDPE/CB25	111.02	40	7.49	452	501	24.13
LDPE/CB30	110.85	40	7.45	409	492	29.37

2.3.10 Thermal conductivity

Thermal conductivity measurements of LDPE/CB composites were in good agreement with what was found for the electrical conductivity, featuring a significant increase only for concentrations at or above the percolation threshold (Figure 2.12). Neat LDPE showed a thermal conductivity of 0.28 W/m.K which is mainly due to phonon transportation as the electronic contribution is negligible. The amorphous regions and free volumes in the LDPE scatter phonons, which reduces thermal transportation.(X. Huang, Jiang, & Tanaka, 2011) Since the DSC results did not show much change in the polymer morphology for the composites, it was expected that the thermal transportation done by the crystalline regions would also be predominant for the composite below percolation and would increase due to the contribution of the CB conductive network from the percolation point. In fact, the thermal conductivity of LDPE/CB composites at low filler content up to 15 wt% was found to slightly decrease (Figure 2.12), probably due to the thermal resistivity at interfacial layers between the particles and the host polymer and due to the additional scattering of the phonons. (Burger et al., 2016; Ghose et al., 2008). Increasing CB content above 15 wt% was found to raise the thermal conductivity significantly as can be seen for the LDPE/CB20, LDPE/CB25 and LDPE/CB30 composites. The enhancement of the thermal conductivity at high filler content was observed due to the dominant contribution to the thermal conductivity of electronic transport and phonons transportation through the network formed within the composite.

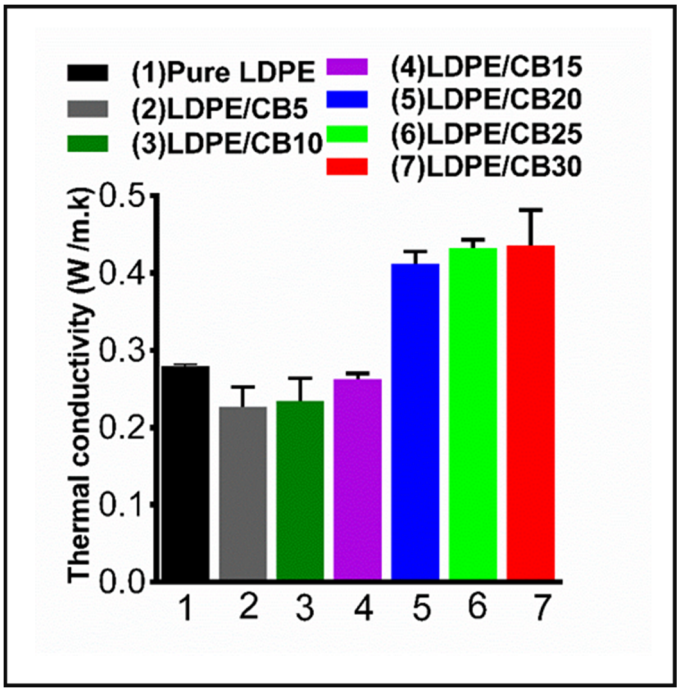

Figure 2.12 The thermal conductivity of LDPE/CB composites at different carbon black contents

2.3.11 Dynamic mechanical properties

The influence of CB inclusions on dynamic mechanical properties was investigated in terms of storage modulus (E'), loss modulus (E'') and damping factor (δ), and the results are shown in Figure 2.13. The storage modulus that expresses the stiffness of the composite, and the loss modulus that is related to the absorbed energy are shown as a function of temperature. Both properties were strongly temperature-dependent. The reduction of storage modulus with increasing temperature is related to the increase of the mobility of the amorphous regions within the semicrystalline composites (Menard, 2008). The addition of CB to pure LDPE increased the storage modulus of composites. This can be attributed to the possible Van der Waals interactions between CB particles (Mondal et al., 2016). The loss modulus and damping factor (tan δ) (Figure 2.13b and Figure 2.13c) showed two relaxation peaks over the temperature range from -100 to 100 ºC. The first relaxation peak, around 60 °C (Figure 2.13c), is related to the fading of crystalline regions, and consequently the loss of the composite's mechanical strength. The second relaxation peak (Figure 2.13b) at about -25 °C, is related to

the mobility of entire polymer chain motions in the amorphous regions (Yuqiang Huang, Jiang, Wu, & Hua, 2004). The loss modulus of all LDPE/CB composites were higher than that of the pure LDPE, which might be because of the mesophases created between CB particles and polymer that causes the applied external energy by frictional forces between polymer and particles to dissipate (Yuqiang Huang et al., 2004). The enhancement of the mechanical properties of composites with higher filler content with respect to their counterparts with lower contents showed the contribution of the CB particles to the material's mechanical strength (Fathi, Hatami, & Grady, 2012; G. Wu, Zheng, Zhang, & Hou, 2006).

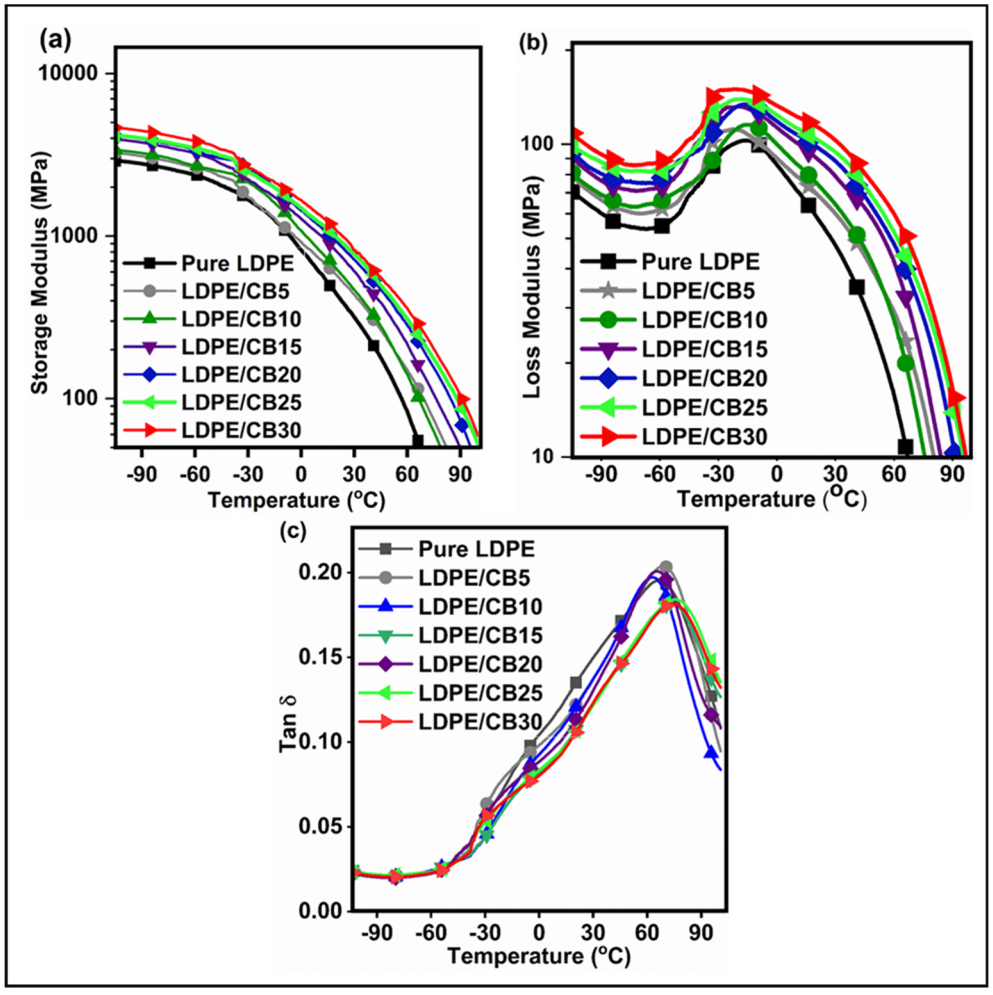

Figure 2.13 The log scale of the storage (a), loss (b) modulus and the tan δ (c) of LDPE/CB composites as a function of temperature (°C)

The comparison of the storage modulus of several polymeric composites compounded with carbonaceous fillers is reported in Table 2.5. As indicated, different carbon-based fillers revealed the different value of storage modulus at the same filler content. In comparison with the reported references, our CB/LDPE composite illustrated higher mechanical storage modulus than its counterparts. It might be related to the better dispersion, higher intrinsic mechanical properties of the filler or greater mechanical strength of the matrix.

Table 2.5 Comparison of storage modulus of different carbonaceous-based composites with different matrices

Composites	Mixing procedure	Storage modulus	Reference
PA6/TrGO	Melt blending	~ 3.6 GPa at 10 wt%	(Méndez et al., 2017)
PA6/CNT	Melt blending	~ 2.8 GPa at 10 wt%	(Méndez et al., 2017)
CPE/CB	Solvent-casting	~ 2.5 GPa at 10 wt% CB	(Mondal et al., 2016)
LDPE/CB	Melt compounding	~ 4.2 GPa at 10 wt% CB	Our work

2.4 Conclusions

In summary, LDPE/CB composites compounded by means of melt compounding featured a sharp increase in electrical conductivity with the addition of 20 wt% or more of CB particles. SEM investigation and AFM phase imaging showed the formation of conducting pathways within the LDPE/CB composite at high filler concentration, while at low filler content, no connected pathways were seen. The storage modulus of LDPE/CB composites increased with the incorporation of CB within the polymer matrix. The composite thermal decomposition temperature increased considerably thanks to the high thermal stability of CB and formation of the CB network in LDPE polymer. LDPE/CB composites showed electrical field-dependency and hysteresis in their electrical properties at filler concentration around the percolation threshold. The dielectric breakdown strength was found to increase by around 10% with the addition of 5 wt% CB, which makes LDPE/CB composites a suitable material at low concentration for applications requiring insulation. The addition of CB to LDPE did not enhance the resistance of the composite to erosion due to corona exposure. LDPE/CB

composites with the electrical conductivity of about 10^{-4} S/m (above the percolation) are suitable materials for semiconductive applications, having appropriate mechanical and thermal properties.

Acknowledgment

The Natural Sciences and Engineering Research Council of Canada is acknowledged to support this study

CHAPTER 3

ELECTRICAL AND THERMAL CONDUCTIVITY OF ETHYLENE VINYL ACETATE WITH GRAPHENE AND CARBON BLACK FILER

Sohrab Azizi[1], Eric David[1], Michel F. Fréchette[1] , Phuong Nguyen-Tri[1,2], Claudiane Ouellet-Plamondon[1]

[1] École de technologie supérieure (Université du Québec), 1100 Notre-Dame St W, Montreal, QC H3C 1K3 Canada
[2] Department of Chemistry, Université du Montréal, 2900 Edouard Montpetit Blvd, Montreal, QC H3T 1J4, Canada

Paper published in *Polymer testing Journal*, September 2018

Abstract

Ethylene vinyl acetate (EVA) composites, including two different carbonaceous conductive fillers, carbon black (CB) and commercially available graphene (G), were fabricated by solvent-casting and melt compounding methods. The effect of additives and process conditions on electrical and thermal properties of composites was investigated. The dielectric responses of EVA composites were characterized by a percolation threshold of 15 wt % for EVA/G prepared by solvent-casting. However, as the EVA/G15% was also subsequently extruded, the applied shear stress induced by extrusion caused deterioration of the electrical network and reduced the composite's electrical conductivity. A percolating network was found for the EVA composites containing CB at around 5-7 wt % with 10 orders of magnitude increase in electrical conductivity with respect to the neat EVA. The thermal conductivity of EVA/CB7% and EVA/G15% increased 16 and 22 % respectively, in comparison to the neat EVA. Both additives increased the electrical and thermal conductivity of composites to be appropriate as jackets for high-voltage cables.

Keywords: Electrical properties; Thermal conductivity; Ethylene vinyl acetate; Carbon black; Graphene.

3.1 Introduction

Ethylene vinyl acetate (EVA), a random copolymer, is made from ethylene and vinyl acetate monomer via continuous bulk polymerization or an emulsion process (Henderson, 1993). The vinyl acetate (VA) content in EVA copolymer ranges from 1-50 wt% (Shafiee & Ramazani, 2008), depending on the desired mechanical and physical properties. The inclusion of higher VA content in EVA decreases the average molecular weight of EVA copolymer, which consequently changes the copolymer properties. For instance, the stiffness modulus, surface hardness, crystallinity, melting point and softening point of the EVA polymer are reduced due to the higher VA content (Henderson, 1993; Q. Wang, Meng, Wang, & Guo, 2017). Although the increase in VA content undermines some properties, it leads to several improvements for electrical applications such as high dielectric strength, high volume resistivity against low and moderate voltages, and suitable compatibility with polar polymers for blending. (Henderson, 1993; Khobragade et al., 2017; Sheng, Liu, Zhang, & Chen, 2013; H Tang et al., 1994; Xuebao Wang et al., 2018)

Ethylene vinyl acetate (EVA) and its conductive composites are widely used in electrical cables (Kuila et al., 2012), self-regulating heaters and sensors (Hou, Zhang, & Rong, 2003; Hou, Zhang, Rong, Yu, & Zeng, 2002), electronic devices in the automotive industry (Çopuroğlu & Şen, 2005; Takidis, Bikiaris, Papageorgiou, Achilias, & Sideridou, 2003), and electromagnetic interference shielding (EMI) applications (Henderson, 1993; Jyoti, Kumar, Dhakate, & Singh, 2018). The use of neat EVA copolymer without additives features some drawbacks involving low electrical and thermal conductivity and sometimes inadequate mechanical properties. Accordingly, the combination of the pure EVA with conductive additives such as graphene-based materials can serve to increase the electrical conductivity. An improvement in the electrical conductivity of EVA was reported by the addition of 4 and 8 wt % of reduced graphene oxide and polyaniline, respectively (N. Yuan et al., 2012). Also,

the thermal stability and electrical conductivity were found to be improved by 42 °C and 10 orders of magnitude, respectively, with the addition of 8 wt% functionalized graphene additive to the pure EVA (Kuila et al., 2012). The effect of VA content in EVA on graphene dispersion and the percolation network in EVA/G nanocomposite indicated that the lowest percolation threshold is found for VA content at approximately 20 wt% (Ratzsch et al., 2014). Furthermore, according to Yang et al., the electrical conductivity of EVA-based nanocomposite including a carbonaceous filler is dependent on the VA content, as well as the nano-additive concentration in the vicinity of the percolation threshold (Q. Q. Yang & Liang, 2010).

The particle shape, the morphology of additive, the inherent electrical conductivity of the nanofiller as well as the aspect ratio of conducting fillers can all significantly influence the final electrical and thermal conductivity of nanocomposites (George, Bhadra, & Bhowmick, 2010). Thus, it is relevant to study the effect of several carbonaceous nanofillers with different shapes and physical properties. Moreover, the fabrication method and the incorporation of functionalizing or compatibilizer agents can play a dominant role in determining the properties of the fabricated composite (M. Azizi, Ramazani, Etemadi, & Shirzaei, 2013). Therefore, in this study, more or less spherical and highly conductive CB filler has been selected as reference filler for comparison with commercially available graphene.

Oxygenated groups such as hydroxyl or ester groups exist more or less in carbonaceous derivatives such as graphene-like materials (Boussaboun, Azizi, & Ouellet-Plamondon, 2017), and are expected to be fairly compatible with the polar part (VA part) of the EVA copolymer, Therefore, the compatibility of the graphene-like and carbon black plays a significant role in composite properties. However, the influence of fabrication method is often dominant over the chemical affinity and the dispersion of the particles in impacting the final properties of composites (M. Azizi, Zolfaghari Sharak, et al., 2013; Kurusu et al., 2018; Méndez et al., 2017; Pajoumshariati et al., 2018; Soheilmoghaddam et al., 2017). Hence, the effect of melt compounding after solvent-casting on the electrical, thermal and mechanical properties of EVA/G composites at the percolation threshold is investigated in this study.

To the best of our knowledge, most of the previous studies on EVA and the corresponding nanocomposites were focused on the effect of VA content, interactions of additives with EVA matrix, the blending of EVA with different polymers, or using compatibilizers, as well as the surface modification of the particles (Badiee, Ashcroft, & Wildman, 2016; Khobragade et al., 2017; Pu et al., 2017; Sefadi et al., 2015; Soheilmoghaddam et al., 2017; Q. Wang et al., 2017; Yousefzade et al., 2016). Few studies investigate the dominant influence of the compounding procedure on the particles' reorientation and the resulting properties. In this study, the EVA matrix was blended with two conductive additives, CB and graphene, via solvent-casting technique. One of the samples featuring a critical filler concentration was further processed by extrusion. The thermal properties and the morphology of the composites, as well as the low field dielectric response, were investigated.

3.2 Experimental

3.2.1 Materials

EVA copolymer was provided by Repsol Company with 28 wt% VA content and a density of 0.950 g/cm3. The commercially available graphene filler (heXo-GV20) was obtained from NanoXplore Inc (Montreal, Canada). This is a versatile and large-scale graphene product with nanoplatelets with an average thickness of 20 nm (40 layers) and a flake size of 50 μm. The spheroid-shape CB filler (VXC500 grade, CABOT, USA) with an apparent density of 1.7-1.9 g/cm3 at 20 °C is suggested as a high electrical conductivity additive with 0.05 wt % sulfur content and 16.7 ppm total ionic. The toluene solvent was purchased from Sigma-Aldrich with 99.5 % purity. All the materials were used as received.

3.2.2 Sample fabrication

The sample fabrication steps are schematically shown in Figure 3.1. Briefly, the labeled composites with different filler concentrations (Table 3.1) were fabricated via solvent-casting as well as melt compounding. The pure EVA was dissolved in toluene for 30 min by stirring

at 100 °C and 600 rpm. The additives were suspended in toluene with the same fabrication conditions. Both dissolved and suspended solutions were then mixed together and again stirred at 600 rpm and 100 °C for 30 min. Afterward, the obtained dissolved samples were cast on aluminum foil and dried at room temperature in a fume hood until the remained weight became constant. One of the samples was further compounded in a co-rotating screw mini-extruder (Haake MiniLab II) for 5 min of extrusion-circulation time and at 130 °C in the melting zone. To fabricate the disc-shaped samples, the blends were pressed using a hot press (Accudyne Engineering & Equipment Company, Los Angles, USA) at 155 °C and 8 MPa.

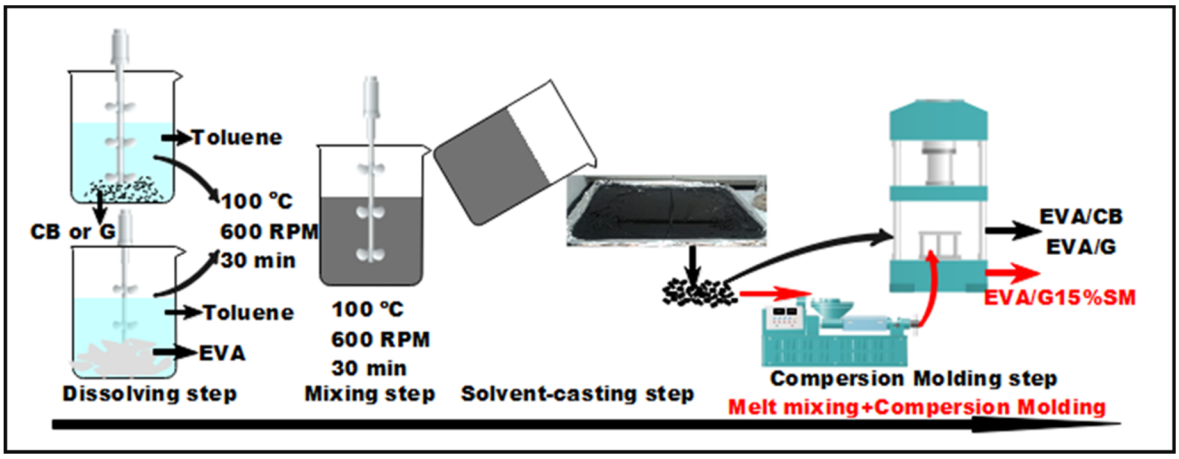

Figure 3.1 Schematic of composite preparation by solvent-casting and further melt mixing for one sample

Table 3.1 Labeled samples with additive content and fabrication method

Sample	EVA (wt %)	G (wt %)	CB (wt %)	Fabrication method
Pure EVA	100	0	0	Solvent casting
EVA/CB5%	95	0	5	Solvent casting
EVA/CB7%	93	0	7	Solvent casting
EVA/CB10%	90	0	10	Solvent casting
EVA/G10%	90	10	0	Solvent casting
EVA/G15%	85	15	0	Solvent casting
EVA/G15% SM	85	15	0	Solvent casting + Melt mixing

3.2.3 Characterization

To investigate the additive dispersion and distribution within the composites, the morphology of the EVA copolymer and EVA composites with CB and graphene was investigated using a scanning electron microscope (Hitachi, SU-8230 FE-SEM, Japan). The specimens' cross-sections were prepared using a cryogenic microtome and the thin films were subsequently coated with approximately 2 nm of platinum under vacuum using a turbo-pumped sputter coater/carbon coater (Q150T, Guelph, Canada).

The dielectric response of the composites was measured via frequency-domain broadband dielectric spectroscopy (BDS - Novocontrol, Montabaur, Germany) on disk samples with a diameter of 4 cm and an average thickness of 0.5 mm. Each specimen was mounted between the two brass electrodes forming a typical electrode-dielectric-electrode sandwich. Isothermal scans were performed over a wide range of frequencies ranging from 0.01 Hz to 10^5 Hz at various temperatures under an applied voltage of 3 Vrms. The relative complex permittivity ε^* is expressed in terms of relative real permittivity (ε') and relative imaginary permittivity (ε'') as expressed by: (Kochetov et al., 2012)

$$\varepsilon^*(\omega) = \varepsilon'(\omega) - i\varepsilon''(\omega) \tag{3.1}$$

To investigate the thermal properties of composites such as melting point and the degree of crystallinity (Xc%), differential scanning calorimetry (DSC) (Q20, TA Instruments, New Castel, USA) was conducted 0-160 °C with a ramp of 10 °C/min under 50 mL/min of nitrogen flow rate. The degrees of crystallinity of all samples were calculated according to Equation 2, (Gaska et al., 2017)

$$X_c(\%_{Crystallinity}) = \frac{\Delta H_m}{\Delta H_m^o \times (1 - W_f)} \times 100\% \tag{3.2}$$

where ΔH_m is the fusion enthalpy of the sample, $\Delta H_m^o$is the melting enthalpy of 100 % crystalline polyethylene (277.1 J/g) (Badiee et al., 2016; Shi, Zhang, Jin, & Chen, 2008) and W_f is weight fraction of fillers in the composite. The lamellar thickness (l) of the pure EVA and EVA composites with CB and graphene were calculated from the Thomson-Gibbs formula given by Equation 3, (Gill, Moghadam, & Ranjbar, 2010)

$$l = \frac{2\sigma_e}{\Delta H_m^o} \times \frac{T_m^o}{T_m^o - T_m} \quad (3.3)$$

where T_m^o is the thermodynamic melting point of the infinite perfect crystals (418.6 K), and σe is the fold surface energy (90.4 mJ/m2) (Furushima et al., 2015).

The dynamic mechanical properties of the EVA composites were measured by using a DMA Q800 (TA Instruments, New Castel, USA). A rectangularly shaped specimen (30×7 mm) with a thickness of approximately 0.5 was tested for each sample. The DMA measurements were conducted in tensile mode at a frequency of 1 Hz and at a temperature range from -50 °C to 70 °C with a ramp of 5 °C/min. An amplitude of dynamic deformation of 20 μm and force track of 120 % with a preload force of 0.02 N was applied on each specimen.

The thermal stability of the composite samples was investigated by thermogravimetric analysis (Diamond TG/DTA, PerkinElmer technology, Shelton, CT, USA). The measurements were conducted under a nitrogen atmosphere with a heating ramp of 20 °C /min from 200 °C to 600 °C and then 10 min at 600 °C under air atmosphere. A sample with a weight from 10 to 15 mg was selected for each measurement.

The thermal conductivity of composites was measured using a guarded heat flux meter, DTC-25 (TA Instruments, New Castel, USA). A 5 cm in diameter disk sample was mounted between the isothermally cold and hot brass electrodes, applying 137.89 kPa load and 25 °C differential temperature between the two plates.

3.3 Results and discussion

3.3.1 Scanning electron microscopy

Figure 3.2 shows the SEM micrographs of the pure EVA and EVA composites with CB and graphene at 5 and 7 wt% of CB content. Figure 3.2a and Figure 3.2b reflect the morphology of pure EVA at 5 k and 10 k magnification. The CB particles were dispersed throughout the composite randomly and appeared well distributed at 5 wt% CB content (Figure 3.2c and

Figure 3.2d). The further addition of CB to 7 wt% leads to the onset of connection between the particles, with an individual particle size less than 100 nm and an agglomerate size of ~ 100–300 nm (Figure 3.2e and Figure 3.2f). In that case, CB particles are more in contact, forming a continuous carbon network within the composite. This will be further discussed in the following section. Figure 3.3 exhibits the morphology of EVA composites with 10 and 15 wt% of graphene contents. At 10 wt % of the graphene, some isolated flake sheets were seen, but most of the individual flakes were found to be piled together due to the intrinsic tendency of graphene to agglomerate (Figure 3.3a and Figure 3.3b) (S. Azizi et al., 2017). With further addition of graphene, more particle-particle connections and graphene flakes overlapping were found, resulting in some agglomerations at the micrometer scale (Figure 3.3c and Figure 3.3d). For the EVA/G15% compounded by solvent-casting followed by extrusion, the additional extrusion step was found to cause deterioration of the well-connected graphene network, resulting in additional agglomeration of the graphene flakes as some larger agglomerates of ~ 30–40 μm were observed.

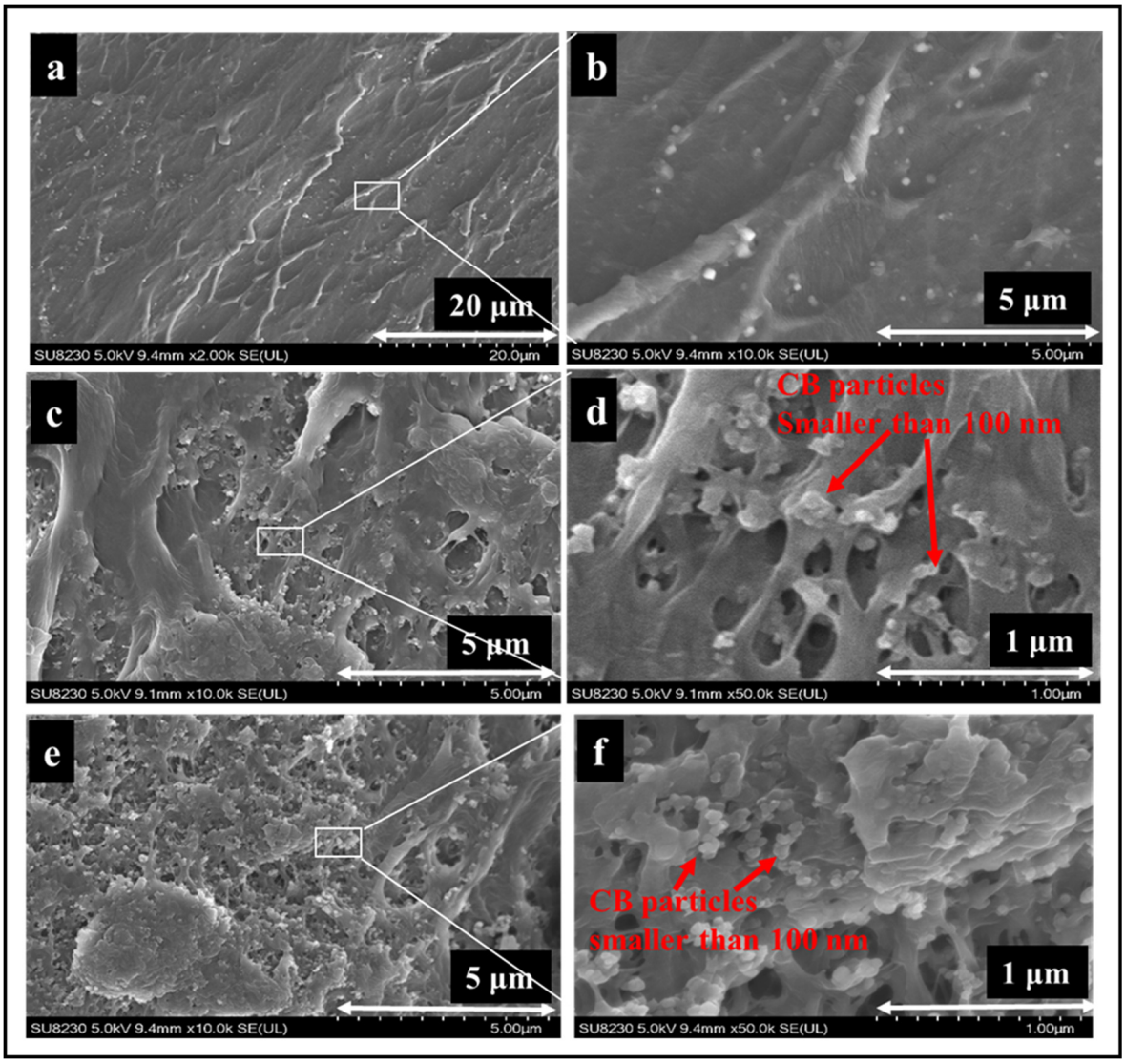

Figure 3.2 SEM micrographs at two different magnifications of pure EVA (a, b), EVA/CB5% (c, d) and EVA/CB7% (e, f)

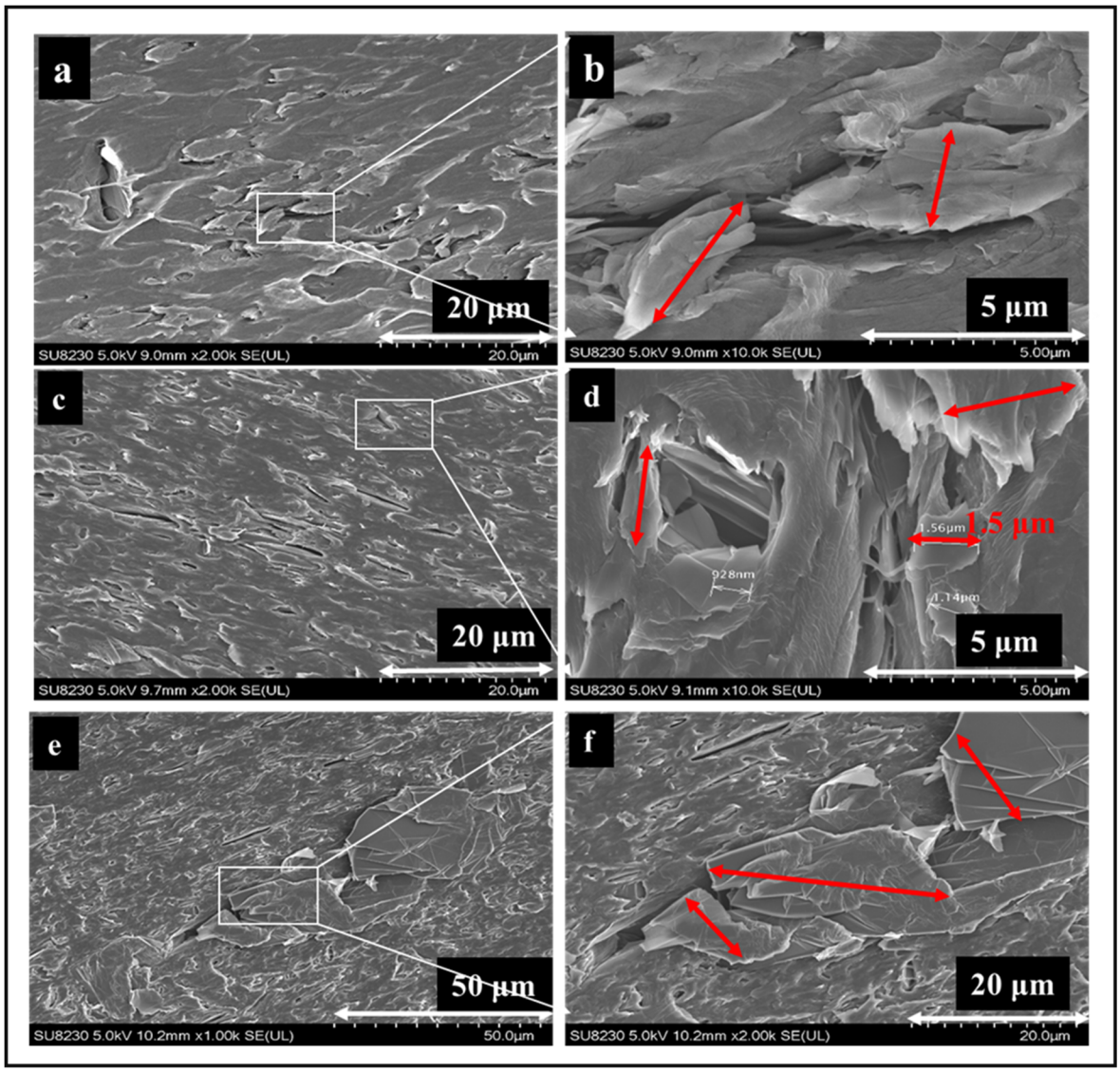

Figure 3.3 SEM images at two different magnifications of EVA/G10% (a, b), EVA/G15% (c, d), and EVA/GV15% SM composites (e, f)

3.3.2 Dielectric properties

Figure 3.4a and Figure 3.4b describe the frequency-domain dielectric responses (real and imaginary permittivity, respectively) of the pure EVA and EVA composites with CB and graphene. The inset in Figure 3.4a is the modulus of the complex conductivity as a function of frequency. The EVA composites containing CB additive featured a percolation threshold between 5 and 7 wt%. The dielectric response of the EVA/CB7% was dominated by direct

electrical conduction over the whole frequency range. The dielectric response of EVA/CB5% exhibited high frequency-independent dielectric losses, so-called flat dielectric loss behavior (Andrew K Jonscher, 1999), accompanied by a noticeable increase of the real permittivity. This is quite an intriguing result since flat dielectric loss behavior normally occurs for low loss material (such as neat polyethylene or polypropylene). A possible explanation relates to the wide distribution of interfacial relaxation mechanisms due to the wide distribution of agglomerate size and morphology (L. A. Utracki & Wilkie, 2002). This would lead to a dielectric response consisting of the superposition of a large number of Debye-type relaxation processes with a broad distribution of relaxation times. The superposition of the relaxation peaks in dielectric losses would result in a negligible change of maximum one decade over the whole frequency range. At low filler concentration, below the percolation threshold, the EVA composites remained an insulating material with an AC conductivity in the vicinity of 10^{-15} S/m at 0.01 Hz, as shown in the inset. When the concentration is increased above the percolation threshold, the conductivity sharply increases, as explained by the percolation theory (Das, Chaki, & Khastgir, 2003; X. Huang & Zhi, 2016; Kondawar, 2015; Sadasivuni et al., 2015; Yousefzade et al., 2016) for which the conductivity can be expressed by (Mondal et al., 2017; Rizvi & Naguib, 2015; Yousefzade et al., 2016)

$$\sigma_{DC} = k\left(\varphi - \varphi_c\right)^t \tag{3.4}$$

where k is a constant quantity, t is the critical exponent, φ is the volume filler concentration and φ_c is the volume concentration at the critical concentration (Mondal et al., 2017). The direct current (DC) conductivity is not equivalent to the alternating current (AC) conductivity, shown in the inset for nonconductive samples, the DC conductivity is typically lower than the lowest value of the AC conductivity (the one at 0.01 Hz). However, it is convenient to use the AC conductivity, as it can be readily measured both for conductive and insulating samples and this value converges on the value of the DC conductivity as soon as the material starts to become slightly conductive. Using the values of the AC conductivity at 0.01 Hz, it can be seen that the electrical conductivity increases by 10 orders of magnitude when the conductive network starts to form (if the real values of the DC conductivity had been used instead, this increase would have been even larger). The conductive network in the EVA composites containing CB formed at lower filler concentration than for EVA with graphene. The reason

might be related to the smaller size of CB (nano-sized) compared to the graphene (micro-sized) (Klaus Friedrich, 2014). The other reason might be related to the formation of agglomeration of graphene during the composite fabrication (Z.-M. Dang et al., 2012; Singh, Ohlan, & Dhawan, 2012; Soheilmoghaddam et al., 2017; Tkalya, 2012); thus, a higher loading of graphene is needed to achieve a percolating network (N. Yuan et al., 2012). To understand the effect of processing conditions on the electrical conductivity of the composites, the dielectric properties of EVA/G15% SM were also studied with the same frequency-domain type of measurement. Surprisingly, this investigation revealed a non-conductive composite, whereas the equivalent solvent-cast sample was found to be conductive. The reason might be the interruption of the percolating network within the composite due to additional agglomeration induced by the melt compounding process (Bellucci, Fabiani, Montanari, & Testa, 2010; Tjong & Mai, 2010).

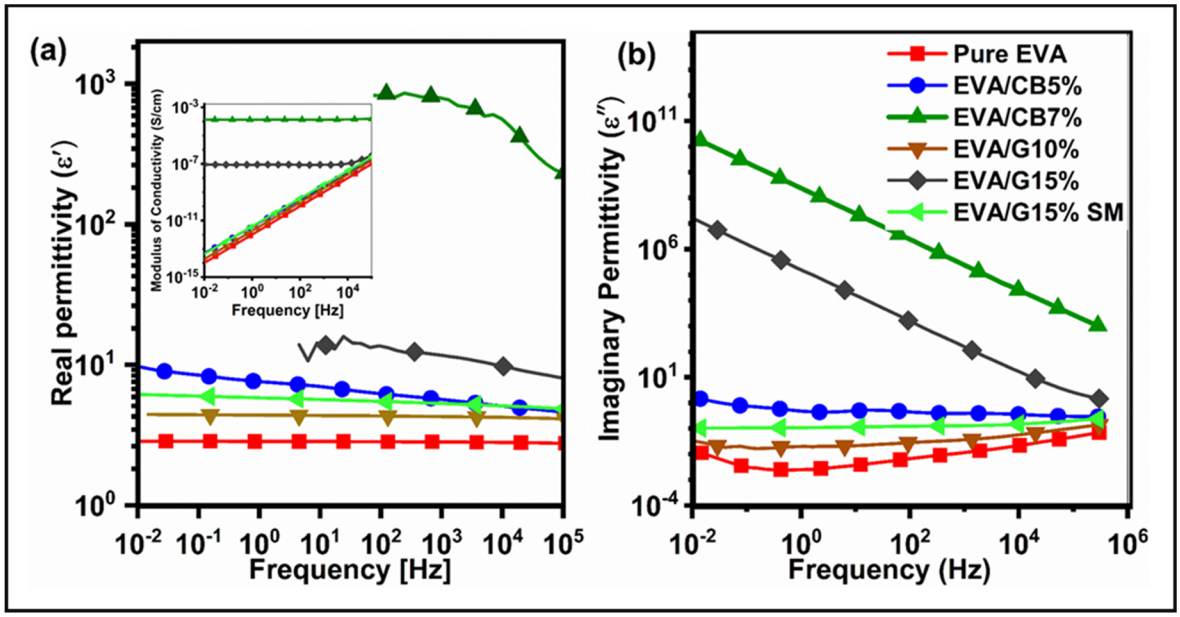

Figure 3.4 Dielectric response of the pure EVA and EVA composites, real permittivity (a) and imaginary permittivity (b) as a function of frequency

The dielectric responses of the pure EVA, EVA/CB5% and EVA/G15 % were also assessed over the same range of frequencies at different temperatures, and the results are shown in Figure 3.5 in terms of three-dimensional plots of the imaginary permittivity as a function of frequency and temperature. The pure EVA revealed its two main relaxation peaks (Figure

3.5a). The sub-glassy peak is conventionally called the β-relaxation process. This appears at low temperature around 1 kHz and it is linked to the micro-Brownian motions of the acetate side groups (Alegria & Colmenero, 2016). As the temperature increased, the β-relaxation shifted toward the higher frequencies and merged with the α relaxation peak. This polarization mechanism is the main polarization phenomenon in EVA and originates from the reorientation of dipoles due to the segmental motion of the main chains (Alegria & Colmenero, 2016; Raju, 2016). Scanning the dielectric response of the EVA polymer at higher temperatures (near the melting point) reveals a significant increase of dielectric loss at low frequency. This sharp increase of dielectric loss is due to the contribution of the charge carrier, leading to low frequency dispersion (Andrew K Jonscher, 1999) with some possible contribution from ionic impurities creating electrode polarization. The dielectric loss of the EVA/CB5% composite (Figure 3.5b) at different temperatures and frequencies revealed almost constant values for which the losses are not particularly low. This type of behavior has also been reported for ferroelectric materials and p-n junction (Andrew K Jonscher, 1999), but its physical origins are not well understood. It seems that sub-percolating material might be another class of material exhibiting this behavior. Despite the global increase of the losses, it was still possible to observe both α and β relaxation mechanisms, as well as the contribution from charge carriers. The addition of 15 wt% of graphene to pure EVA leads to a dielectric response dominated by the DC conductivity for the whole temperature and frequency range, as shown in Figure 3.5c.

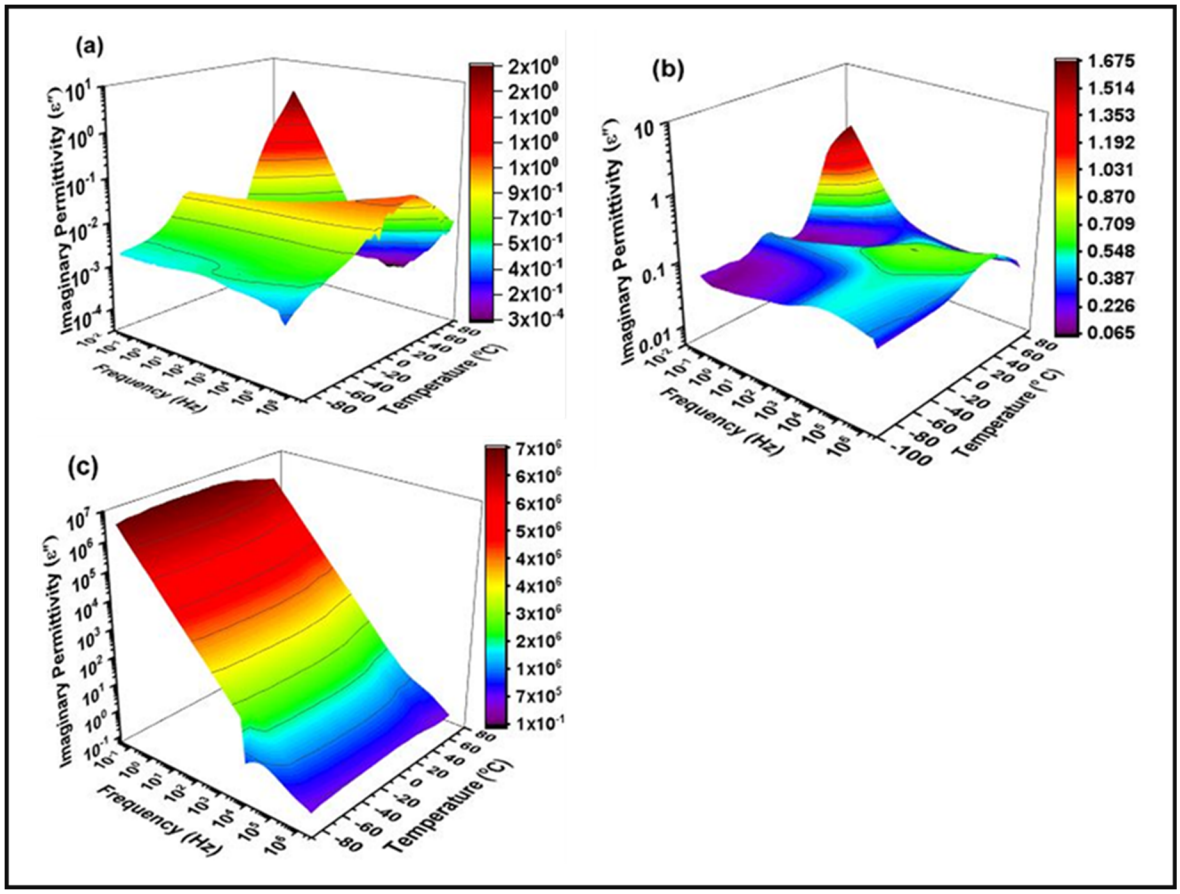

Figure 3.5 3D plots of the dielectric loss of EVA composites at different temperatures and frequencies: (a) pure EVA, (b) EVA/CB5% and (c) EVA/G15%

3.3.3 DSC and TGA results

The role of CB and graphene fillers on the thermal properties of the EVA composites was investigated by differential scanning calorimetry (DSC). The obtained results are presented in Table 3.2. The melting point, the degree of crystallinity and the lamellar thickness of the EVA composites including CB additive or graphene flakes were not found to change significantly with respect to the pure EVA copolymer. These results are in line with those recently reported (Bahmanyar, Ramazani SA, & Baniasadi, 2015; Borisova & Kressler, 2003; Pu et al., 2017; Q. Q. Yang & Liang, 2010).

Table 3.2 Thermal properties and the lamellar thickness of EVA composites comprising CB and graphene fillers.

Samples	Melting point °C	Crystallinity (%)	Lamellar thickness (nm)
Pure EVA	87.0	20.4	4.40
EVA/CB5%	87.2	20.3	4.42
EVA/CB7%	87.4	20.7	4.30
EVA/CB10%	87.8	20.5	4.43
EVA/G10%	87.2	19.4	4.42
EVA/G15%	87.3	19.6	4.42
EVA/G15%SM	87.3	19.5	4.41

Figure 3.6a and Figure 3.6b show the TGA thermograms and derivative thermal analysis (DTA) of the pure EVA and EVA composites with CB and graphene for temperatures from 200 °C to 600 °C. The results show two stepwise thermal degradations of the specimens. As can be seen, the first onset of degradation started at approximately 300 °C. This weight loss is related to the deacetylation process (Badiee et al., 2016; Kuila et al., 2012; N. Yuan et al., 2012) in which almost 10 wt% loss was seen for all specimens (losing acid acetic). The second weight loss starting from 450 °C corresponds to the degradation of the backbone chain (CH2 groups) in EVA polymer (Costache, Jiang, & Wilkie, 2005; Sabet, Soleimani, & Hosseini, 2018; H. Wu, Zhao, & Chen, 2012; N. Yuan et al., 2012). The addition of CB and graphene did not significantly increase the thermal endurance of the fabricated composites. The amount of remaining ash at 550 °C is given in Table 3.3. The obtained values were in good agreement with the labeled filler content.

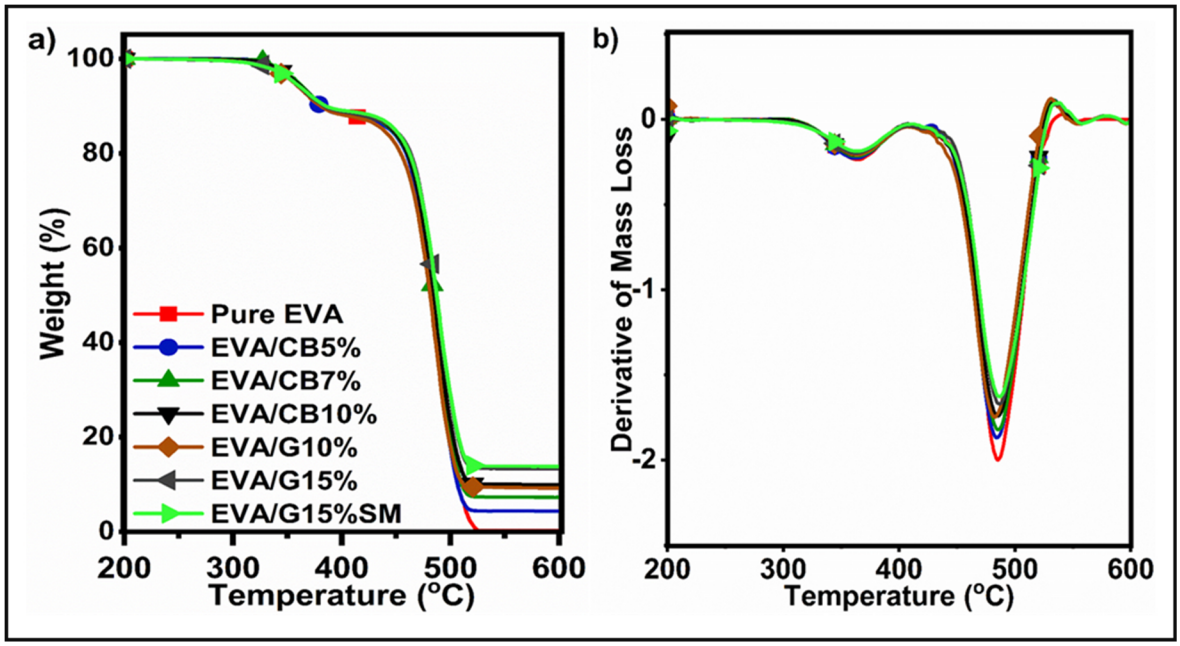

Figure 3.6 TGA thermograms of pure EVA and EVA composites (a) weight loss (b) the derivative of mass loss as a function of temperature.

Table 3.3 TGA data, T onset at first and second degradation and ash content.

Sample name	$T_{-10\%}$ (°C)	$T_{-50\%}$ (°C)	Ash content at 550 °C
Pure EVA	381	482	0.20
EVA/CB5%	382	483	4.30
EVA/CB7%	384	483	7.30
EVA/CB10%	384	486	10.1
EVA/G10%	385	481	9.30
EVA/G15%	384	486	13.8
EVA/G15% SM	385	488	13.9

3.3.4 Mechanical properties

The mechanical properties of the EVA composites, such as storage modulus (Figure 3.7a), loss modulus (Figure 3.7b), and tan δ (inset in Figure 3.7b), were obtained by dynamic mechanical analysis over a wide range of temperature. The addition of graphene and CB fillers

to the EVA copolymer was found to increase both dynamic mechanical properties (storage and loss modulus) over the entire glassy and rubbery regions of the composites. The rise of mechanical properties corresponded to the incorporation of filler in the composite structure and possible physical contact between filler parts (Mensah et al., 2018). A drastic reduction in the storage modulus was found as an increase in the temperature occurred from -50 °C to 0 °C. This can be explained by the EVA transition from glassy to the rubbery state (Badiee et al., 2016). Corresponding to this drop in the modulus, an obvious peak was seen around -20 °C in the tan δ versus temperature graphs. Another peak at higher temperatures (20–40 °C) was observed in the tan δ curve, which represents the vanishing of the crystalline parts of the polyethylene as the hardest part in the composite (Das et al., 2003; Jacob George, Bandyopadhyay, & Bhowmick, 2008; Kuila et al., 2012). Less area under the tan δ curve for the EVA/CB composites with respect to the EVA/G composites corroborates with better filler dispersion of the CB filler (Yousefzade et al., 2016). Additionally, the movement of the second peak in tan δ toward higher temperatures suggests suitable particle dispersion within the matrix (Stark & Jaunich, 2011).

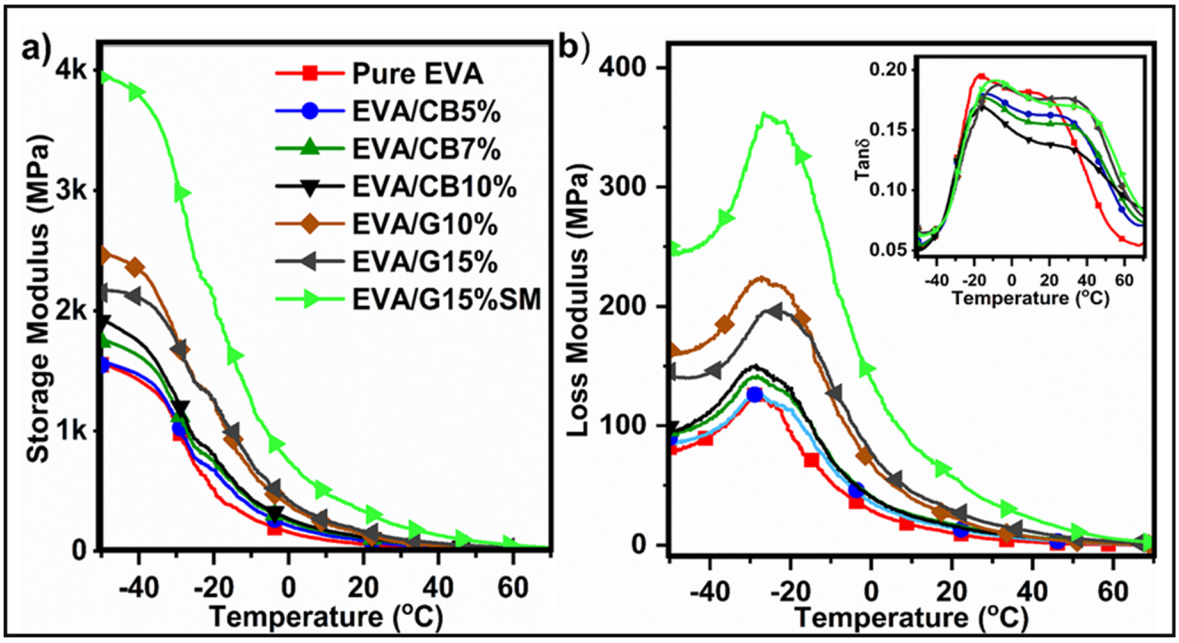

Figure 3.7 Mechanical properties of the EVA composite (a) storage modulus (b) loss modulus (c) tan δ as a function of temperature.

3.3.5 Thermal conductivity

The thermal conductivity of the pure EVA and EVA composites with CB and graphene are shown inFigure 3.8. The thermal conductivity of all composites was found to increase with addition of conductive particles thanks to the large thermal conductivity of particles (J. George & A. K. Bhowmick, 2008; J. J. George & A. K. Bhowmick, 2008; Sefadi et al., 2015). The mechanisms of thermal conduction in the composites are linked to the degree of crystallinity, the concentration of the particles, their size and shape (H. S. Kim, Bae, Yu, & Kim, 2016; Xiao Wang, Zhao, Jin, & Song, 2017), their thermal conductivity, as well as the polymer matrix and processing conditions (Ghose et al., 2008; Sefadi et al., 2015). Thus, since significant change did not occur in the crystallinity of composites, the determining factor is the parameters related to the fillers. The reduction of the thermal conductivity for the extruded EVA composite (EVA/G15% SM) compared with the non-extruded one (EVA/G15) can be explained by the interruption of the conducting network within the composite formed by solvent-casting due to the shear forces from fabrication, thus reducing the contribution from the electronic conduction to the thermal conduction process. Another factor that influences the thermal conductivity is the thermal interface resistance within the composite; as long as the uniform network within the composite is discontinuous, the number of separated individual particles is increased and, consequently, the value of interface resistance between particles and host polymer will grow and cause phonon scattering or even phonon backscattering (Burger et al., 2016; Sun, Ramesh, Itkis, Bekyarova, & Haddon, 2010).

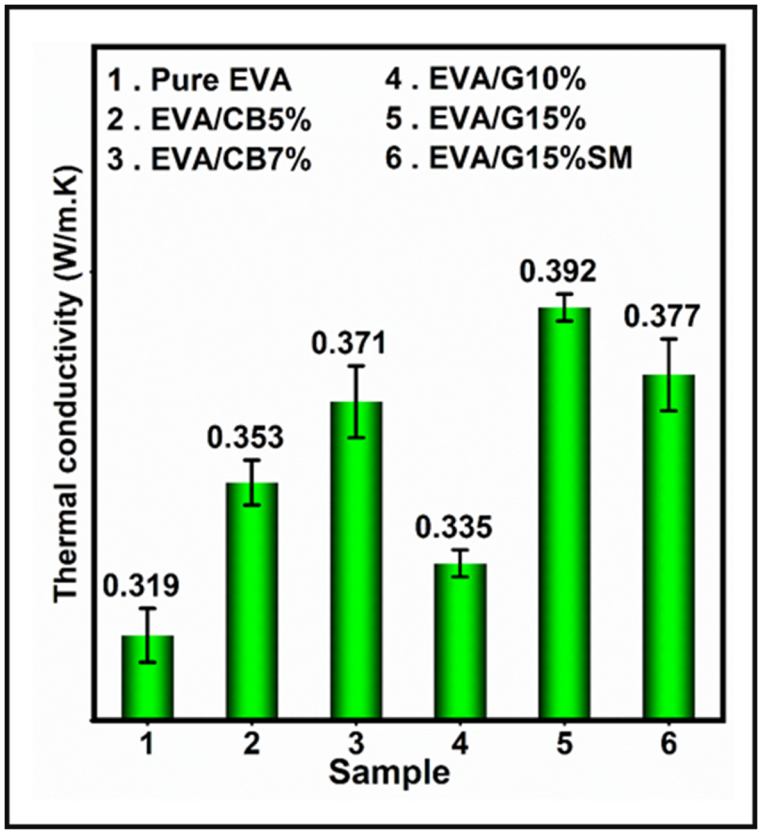

Figure 3.8 Thermal conductivity of the EVA composites at different filler content.

3.4 Conclusions

The electrical properties of EVA composites containing carbonaceous additives demonstrated significant dependency on the type of the conductive additive as well as the manufacturing method. Mechanical properties were also found to be affected by the fabrication process. The percolation threshold for EVA composites with CB was found to be lower than for EVA composites containing graphene. Below the percolation threshold, the composites exhibited a high constant loss behavior that is also observed for different classes of dielectric. The onset of the melting temperature, as well as the crystallization point, was not significantly affected by the filler content. The same observation was made for thermal degradation temperatures that were not significantly affected by the addition of the conductive fillers. The composites of EVA containing CB and graphene additives showed slightly higher thermal conductivity than

pure EVA. Analysis of electrical and thermal conductivity suggests that the dispersion, distribution, and orientation of the filler strongly impact the above-mentioned properties.

Acknowledgment

The authors thank Natural Sciences and Engineering Research Council of Canada for financial support.

CHAPTER 4

ELECRICAL, THERMAL, AND RHEOLOGICAL PROPERTIES OF LOW-DENSITY POLYETHYLENE/ETHYLENE VINYL ACETATE/GRAPHENE-LIKE COMPOSITE

S. Azizi[1], E.David[1], P. Nguyen Tri[1,2], M. Fréchette[1], C. Ouellet-Plamondon[1]

[1] École de technologie supérieure (Université du Québec), 1100 Notre-Dame St W, Montreal, QC H3C 1K3 Canada
[2]Department of Chemistry, Université du Montréal, 2900 Edouard Montpetit Blvd, Montreal, QC H3T 1J4, Canada

Paper submitted for publication in *Composite Part B Journal*.

Abstract

Low-density polyethylene (LDPE)/ethylene vinyl acetate (EVA)/graphene-like composites were prepared via solvent–casting technique. Graphene-like, obtained from hybrid clay-sucrose mixture, was used. Electrical percolation threshold was measured using frequency-domain broadband dielectric spectroscopy and was found to be somewhere between 16 and 17.5 wt% of graphene-like loading. Thus, graphene-like can act as an appropriate conductive filler for the fabrication of electrical conductive LDPE/EVA blends to be used as semiconducting screens in extruded high voltage cables. The annealed composite close to the percolation threshold showed a higher electrical conductivity (approximately one order of magnitude) than the same non-annealed composite. Due to charge transport and electrode polarization, the sub-percolating composites exhibited low frequency dispersion, particularly at elevated temperatures. Blending EVA elastomer to LDPE thermoplastic and graphene-like fillers led to a higher storage modulus and thermal stability composite.

Keywords: LDPE/EVA blend, electrical properties, graphene-like, rheological properties.

4.1 Introduction

Polymer blend and composites have increasingly been studied for their electrical and thermal properties since the 1990s. In this respect, significant efforts have been spent to modify the existing polymers and/or to tailor different thermoplastics to elastomers. In addition, several complex and novel manufacturing techniques with/without fillers have been used to produce desirable materials with advanced properties for electrical and thermal applications (Haurie et al., 2007; Jia, Yan, Cui, Ji, & Li, 2016; Silva et al., 2018; Xiaoming & Shuangnan, 2001; Zarandi & Bioki, 2013). Blending can provide materials with desired properties by tuning and controlling the components content and their morphologies. In addition, from an economic standpoint, a set of low-cost products can be obtained by blending process (L. A. Utracki, 2010; L. A. Utracki & Wilkie, 2002). However, in some cases, the favorable properties for the final products cannot be acquired by the blending process, so, the need for another alteration such as using micro/nanostructure fillers is crucial. The blending of binary/ternary polymer blends or multi-component composites is complex processes to be carried out due to their incompatibility. Thus, coupling agents are often needed in order to improve the compatibility of blend components by raising interfacial adhesion and reducing surface tension with fillers for non-compatible components (Sadasivuni et al., 2015).

Among the thermoplastic polymers, polyethylene with different grades has been widely used in various industrial fields thanks to its low-cost, easy processability and suitable practical functions (S. Azizi et al., 2017; Yuqiang Huang et al., 2004). Low-density polyethylene (LDPE) is a semi-crystalline polymer with a typical 40% degree of crystallinity, soluble in some nonpolar organic solvents at approximately 100 °C. Polyethylene features α, β, and γ–relaxation occurring at different frequencies depending on the applied temperature and the morphology of the polymer. The α–relaxation is linked to the mobility of the crystalline regions at elevated temperature, the β–relaxation ascribed to the branched ties to the main polymer chains which relax at modest temperature (10 °C), and the γ–relaxation attributed to the crankshaft motion of amorphous regions (Bellucci et al., 2010; Kremer et al., 2012; Raju, 2016;

Tjong & Mai, 2010). These processes can be monitored in dynamic thermo-mechanical experience but are hardly seen in dielectric relaxation spectroscopy because of the non-polar nature of the polymer. Low-density polyethylene (LDPE) which is one of the most widely–used grades of polyethylene, is known as an insulating polymer with a relative permittivity of 2.3 (S. Azizi, David, Fréchette, Nguyen-Tri, et al., 2018; E Helal et al., 2018). When loaded with conductive fillers, it has been used in numerous applications, such as conductive layers in high-voltage cables, as well as, electromagnetic shielding products (Khanam et al., 2016). Ethylene vinyl acetate (EVA) as a commodity thermoplastic elastomer is widely used in biomedical engineering (Bakar, Chee, Abdullah, Ratnam, & Ibrahim, 2015), insulating applications (Sonnier et al., 2016; Yan Zhang et al., 2016), photovoltaic application (de Oliveira, Diniz, Viana, & Lins, 2017), as well as, conductive sensors (Calegari et al., 2017). The VA content in EVA structure has been reported from ~ 15 up to 70 % (Henderson, 1993). EVA shows a glass transition temperature around 30 °C and is soluble in some aromatic solvents at high temperatures (~ 90 °C). EVA features two relaxation peaks when it is subjected to an electric field, the α– and β–relaxation peaks. The former is related to the micro–Brownian peak (at low temperatures) due to the side groups attached to the main chain and the latter is related to the re–orientation of dipoles created by segmental motions at around the glass transition temperature (J. C. Huang & Wu, 2000; X. Huang & Zhi, 2016; Raju, 2016; L. A. Utracki & Wilkie, 2002). Mechanically, EVA copolymer is known as a soft material with an amorphous structure, which displays comparatively low stiffness and mechanical properties. In comparison with polyethylene, the permittivity of EVA is higher than the LDPE due to the VA groups which are highly polarizable, particularly at high frequencies. However, EVA features suitable dielectric strength and it can be used in low and medium voltage applications (Henderson, 1993).

Conductive inorganic additives that feature extraordinary properties are of great importance for the development of functional polymeric composites. Graphene, as a versatile filler, with a two-dimensional (2D) geometry and honeycomb crystal structure (H. Kim, Abdala, & Macosko, 2010; Kuilla et al., 2010; X. Li, Cai, Colombo, & Ruoff, 2009; Yuanbo Zhang, Tan, Stormer, & Kim, 2005), is known to possess high carrier mobility of 200,000 cm^2/Vs and a

high thermal conductivity of 3000 W/m.K (Ray, 2015; Stankovich et al., 2006; Q. Wang et al., 2017). Accordingly, numerous efforts have been done to produce graphene using different techniques (Boussaboun et al., 2017; Qiu, Guan, Luo, & Wang, 2017; Ruiz-Hitzky et al., 2016a; S. Wang et al., 2017). In some cases, the obtained graphene-like is enough electrically conductive to be used as filler in conducting composites. For instance, the conductive graphene-like filler prepared from natural resources (bentonite and sucrose) (Boussaboun et al., 2017) was used to increase the electrical conductivity of LDPE (S. Azizi et al., 2017). The LDPE/graphene–like composite was found to be conductive at filler content roughly higher than 30 wt%, where the multilayered graphene-like showed a significant agglomeration within the composite. This agglomeration is deemed to prevent the formation of the electrical network in the composite at low filler content. Furthermore, LDPE/graphene–like composite featured a non-linear behavior as it was subjected to several electric fields. The electrical conductivity of LDPE composites with commercial graphene and graphene-like was studied and it was found that the commercialized graphene containing composites are conductive at lower filler content than the graphene-like containing composites due to the less agglomeration, as well as, oxygenated groups within the filler (Anh et al., 2016). The LDPE composite with functionalized graphene and graphene-like prepared by ball–milling featured an electrical conductivity only at high filler content due to the poor filler dispersion in the composites (Pirondelli et al., 2016). LDPE/graphene composite with few attached oxygenated groups to the graphene showed a non–ohmic behavior (Mancinelli et al., 2014). The EVA/reduced graphene oxide composites prepared by in situ polymerization showed an electrical conductivity of 2.7×10^{-3} S/cm with the addition of 6 wt % of the filler (N. Yuan et al., 2012). The electric percolation threshold of EVA composite prepared by solvent–casting was reported at 17 per hundred rubber (Dash et al., 2015). PE/EVA blend was compounded with carbon black and carbon nanotube to investigate the electrical conductivity of composites in several studies, but only a few studies have been conducted so far with the addition of graphene. For example, Fouleger *et al.* added 4 wt % carbon black filler to HDPE/EVA immiscible blend, and the electrical conductivity of the composite increased from 10^{-14} to 10^{-3} S/cm (Foulger, 1998). A percolation threshold was observed at around 15 wt % of CB content for EVA/LDPE/CB composite, for which the electrical conductivity of the composite reached 10^{-}

^{3} S/cm (M. Q. Zhang, Yu, Zeng, Zhang, & Hen, 1998). To localize and disperse graphene flakes in EVA/LLDPE/graphene composite, two processing methods (fast quenching and annealing) were used by Kurusu *et al.* (Kurusu et al., 2018). The findings revealed a significant reduction in the percolation threshold for composite with respect to LDPE/graphene or EVA/graphene composites. In addition, annealing (gradual cooling down during hot press-molding) was found to lower the electrical percolation threshold of EVA/LDPE/graphene composite compared to faster cooling, thanks to better graphene layered migration between polymer chains.

The formation of the carbon-based conductive network within the composite with minimum filler content has always been the main objective of the aforementioned studies, but the limitations in filler's intrinsic properties, compounding conditions, and chemical composition of polymers, led to change the strategies to overcome these manufacturing issues. Consequently, graphene-like is suggested as a conductive filler to be processed and localized into the LDPE/EVA blend by solvent-casting technique.

Herein, electrical, thermal and rheological properties of LDPE/EVA/G composite were investigated. The morphology of the as-prepared composites was firstly observed by scanning electron microscopy (SEM) to have a clue about the dispersion and distribution of the graphene-like fillers throughout the composite. Thereafter, possible chemical interactions of LDPE/EVA blend and its composites owing to the use of LLDPE-g-MA compatibilizer was assessed *via* FT-IR spectroscopy. Then, the electrical properties of the composite were investigated by broadband dielectric spectroscopy (BDS). The effect of the filler content on crystallinity, as well as the melting point of the composite, was studied to corroborate the role of local changes on overall properties of the composites. Moreover, TGA experiments were conducted to measure the alteration of the thermal stability caused by the inclusion of the graphene-like filler. The accuracy of the filler content within the composite was assessed by the TGA test. Eventually, the rheological behaviors of the composite in the molten state were investigated to obtain a comprehensive view regarding the role of the fillers in the composite.

4.2 Materials and processing

Low-density polyethylene (LDPE) powder used for this study was purchased from Marplex Company with a density of 0.922 g/cm^3 and a melt flow index of 0.4 g/10 min. Ethylene vinyl acetate copolymers (EVA) was obtained from Repsol Company with 28% VA content and a density of 0.950 g/cm^3. Xylene and toluene were supplied from Sigma-Aldrich Company with 99.5 % purity. Graphene-like was produced in the university's laboratories from natural resources (clay and sucrose). The fabrication process can be found elsewhere (Boussaboun et al., 2017). Briefly, one part of bentonite and five parts of table sugar was mixed. Each gram of bentonite and sugar was dissolved in 1.2 and 0.5 ml of DM water, respectively. Mixing was conducted at 400 rpm mixing speed for 20 min and the obtained caramel-clay was kept in an oven for a week at 50 °C. Ultimately, the mixture was heated in a furnace at 800 °C and the monolith sample was reduced to reaching a micro-size filler. Linear low-density polyethylene grafted maleic anhydride, LLDPE-g-MA, was provided from DuPont (Fusabond M603) company. All purchased materials were used as received.

4.2.1 Sample preparation

LDPE/EVA/G composites were produced using the solvent casting method with different graphene-like filler contents (see Table 4.1). Solvent casting technique was selected for better filler dispersion (Siemann, 2005). Annealing (A) and non-annealing (NA) steps were applied during hot press molding and the samples are labeled accordingly. LDPE and EVA were respectively dissolved in xylene and toluene solvent at high temperate (90 °C). LLDPE-g-MA compatibilizer was added to LDPE during dissolution. The graphene-like filler was also mixed in the solution and then, dissolved blends and suspended graphene-like were compounded using 600 rpm stirring at 90 °C for 2 h at the same as former steps. Eventually, the compounded viscous materials were subjected to ultrasonic mixing (1 min) with a Qsonica sonicator (Q700). Prepared composites were dried on an aluminum foil until no more changes in weight were observed. The obtained composites were then pelletized using a Brabender pelletizer. Subsequently, the annealed composite disks were fabricated by hot press molding at 155 °C

and 7 MPa load for 5 min and then, while the same load was maintained, cool down to room temperature gradually. The non-annealed composites were molded at 0.8 MPa at 155 °C for 2 h and then quenched in tap water.

Table 4.1 Composites labeling according to the component concentration

Sample	LDPE (wt %)	EVA (wt %)	Graphene-like (wt %)	LLDPE-g-MA (wt %)
LDPE/EVA_A or NA	47.5	47.5	0	5.0
LDPE/EVA/G5_A or NA	45.1	45.1	5.0	4.7
LDPE/EVA/G10_A or NA	42.7	42.7	10.0	4.5
LDPE/EVA/G15_A or NA	40.3	40.3	15.0	4.2
LDPE/EVA/G16_A or NA	39.9	39.9	16.0	4.2
LDPE/EVA/G17.5_A or NA	39.1	39.1	17.5	4.1
LDPE/EVA/G20_A or NA	38.0	38.0	20.0	4.0

4.2.2 Characterizing and property measurement

The graphene-like structure was observed using high-resolution transmission electron microscopy (HR-TEM JEOL 2170F) at a 200 kV acceleration voltage. The morphology of the composite was investigated by a high-resolution scanning electron microscope (Hitachi SU-8230 FE-SEM). The test specimens were cryo-fractured by immersing in liquid nitrogen using a microtome and then the prepared cross-sections were coated with ~ 2 nm platinum layer under vacuum condition using a turbo-pumped sputter coater/carbon coater (Q150T). The morphology of the specimens was observed at different magnifications.

The particle distribution size of the prepared graphene-like was evaluated by laser granulometry technique, using Mastersizer 3000 Malvern, by dispersing graphene-like filler in DM water at 3000 rpm agitation speed and 90 % sonication.

The conductivity of the graphene-like powder was measured suing a laboratory setup. A sample holder was filled by 5 g graphene-like and the powder was subjected to several mechanical loads using universal testing machine. The conductivity of the powder was measured at different loads using a 4-cable ohmmeter.

The chemical interaction of LDPE polymer with EVA in presence of LLDPE-g-MA compatibilizer was assessed by performing Fourier transforms infrared spectroscopy (FT-IR) test. FT-IR experiments were conducted in the absorbance mode over a wide range of wavelengths from (400–4000 s^{-1}) with Nicolet 6700 FT-IR Spectrometer.

Broadband dielectric spectroscopy was conducted using Novocontrol dielectric spectrometer to measure the electrical response of the polymer blend and composites over a wide range of frequencies and temperatures. A 0.5-mm thick sample disk with a diameter of 4 cm was mounted between two electrodes (made of brass) and subjected to an excitation voltage of 3 Vrms. The frequency-domain electrical responses at different temperatures were obtained.

Differential scanning calorimetric (DSC) measurements were performed to analyze the change of melting point, as well as the crystallinity rate of composites. The experiment was conducted with a Perkin Elmar Pyris1 DSC apparatus at a heating ramp of 10 °C/min from 20 to 150 °C under a 50 ml/min flow of argon, followed by a cooling step at the same rate to 20 °C, and consecutively, another heating step at 10 ^{o}C/min.

Thermogravimetric analysis (TGA) was conducted using Diamond TG/DTA (Perkin Elmer technology via SII) with test specimens around 10 mg. The composite samples were heated under a nitrogen atmosphere with a heating ramp of 20 °C/min from 100 °C to 600 °C.

To investigate the viscoelastic properties of the composite at molten state, rheological experiments were conducted at a processing temperature of 155 °C. Small Amplitude Oscillatory Shear (SAOS) test was conducted using Anton Paar MCR 501 in strain-controlled

mode on test specimens of the diameter of 25 mm. A strain value of 0.03 % with a range of frequency from 0.01 to 300 rad/s was applied.

4.3 Result and discussion

4.3.1 Graphene-like properties

High-resolution transmission electron microscopy (HR-TEM) images of caramelized hybrid clay which was graphitized in an inert atmosphere are shown in Figure 4.1. Graphene-like filler composed of bentonite layers, as well as multilayered graphene layers (white arrows in Figure 4.1), were seen. Caramelization of bentonite by sucrose, and consequently graphitization led to greater layer spacing of graphene than the initial bentonite layers. The regional graphene layers, including several pilled-graphene layers, can be seen clearly in the graphene-rich region. The electrical conductivity of the graphene-like was measured and reported in our previous work (Boussaboun et al., 2017). The particle size distribution of the graphene-like is shown in Figure 4.2. As can be seen, the significant portion of particle's size ranging from 800 nm to 10 μm. The electrical conductivity of the prepared graphene-like powder was measured at different mechanical loading and the result is seen in Figure 4.3. At low loads, due to the low contacts between the particles, and the existence of the air, the measured conductivity was fairly low. However, at higher loads, up to a non-compressible powder, a conductivity between 100 to 165 S/m was obtained.

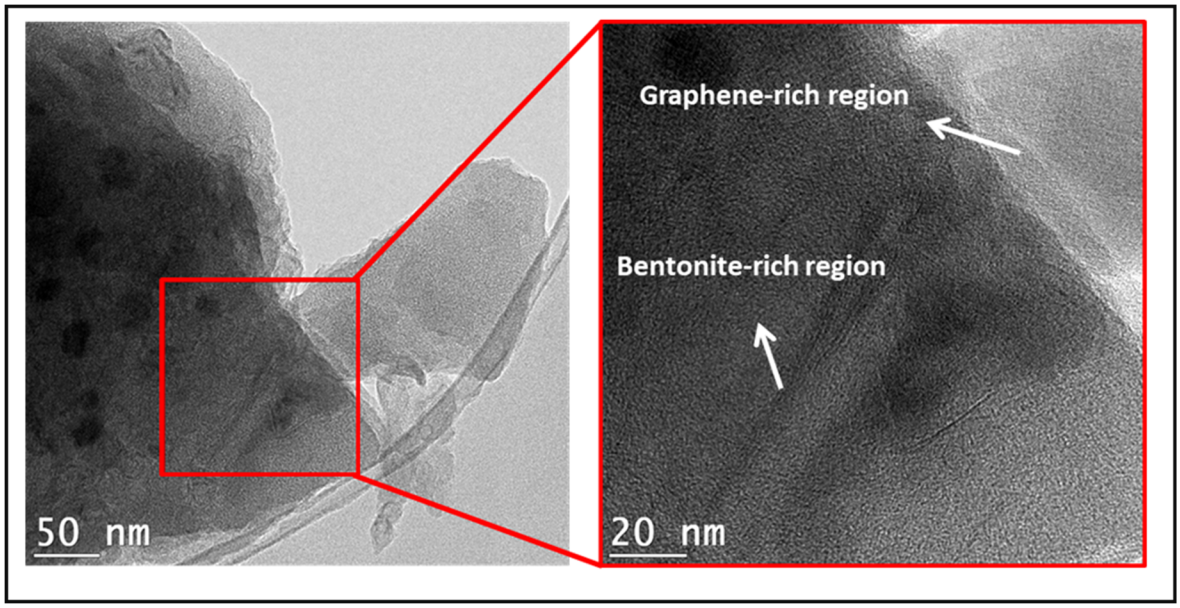

Figure 4.1 High-resolution transmission electron microscopy (HR-TEM) images of graphene-like layers

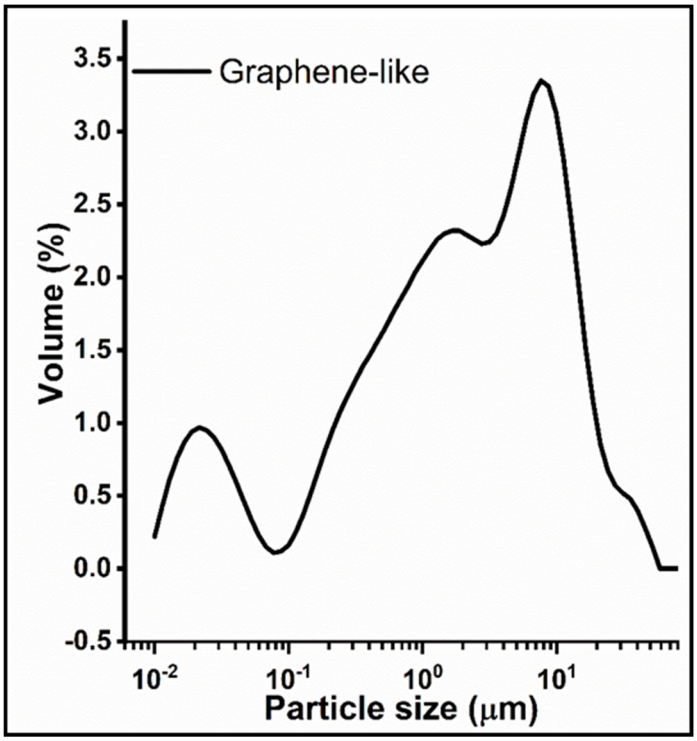

Figure 4.2 Particle size distribution of graphene-like

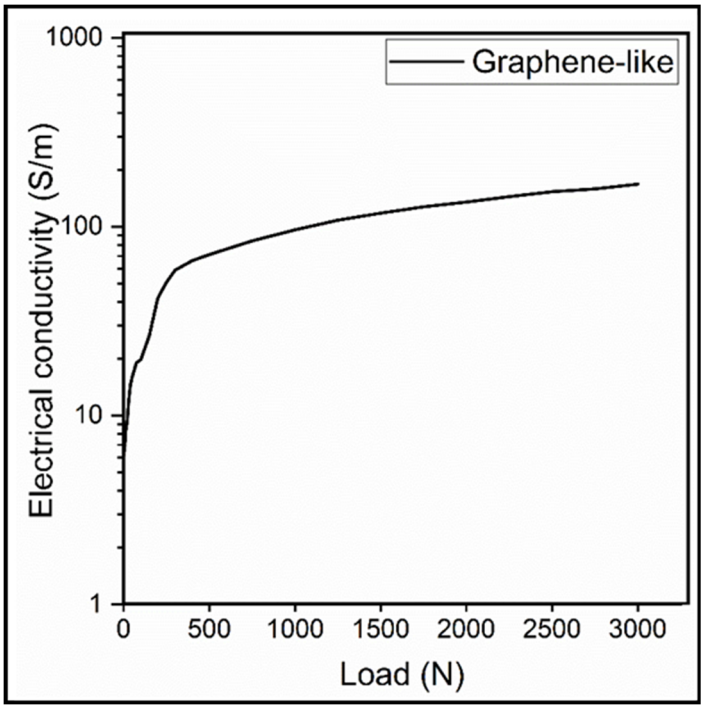

Figure 4.3 Electrical conductivity of graphene-like powder as a function of pressure

4.3.2 Scanning electron microscopy (SEM) images

Figure 4.4 shows the SEM micrographs of LDPE/EVA_A blend and its composites with graphene-like filler. The SEM micrograph at a 2K magnification of LDPE/EVA/G15_A (Figure 4.4c) shows agglomerated graphene-like flakes which are nearly stacked together and feature islands of particles, distributed within the composite with respect to the LDPE/EVA/G20_A at the same magnification (Figure 4.4e). As the filler content reached 20 wt%, the number of contacts between graphene-like fillers raised, and a network was formed throughout the composite as it can be clearly seen in Figure 4.4e. The SEM image of the LDPE/EVA/G20_A with higher magnification shows a suitable dispersion as well as the distribution of graphene-like layered within the composite with the particle size of up to 2 μm.

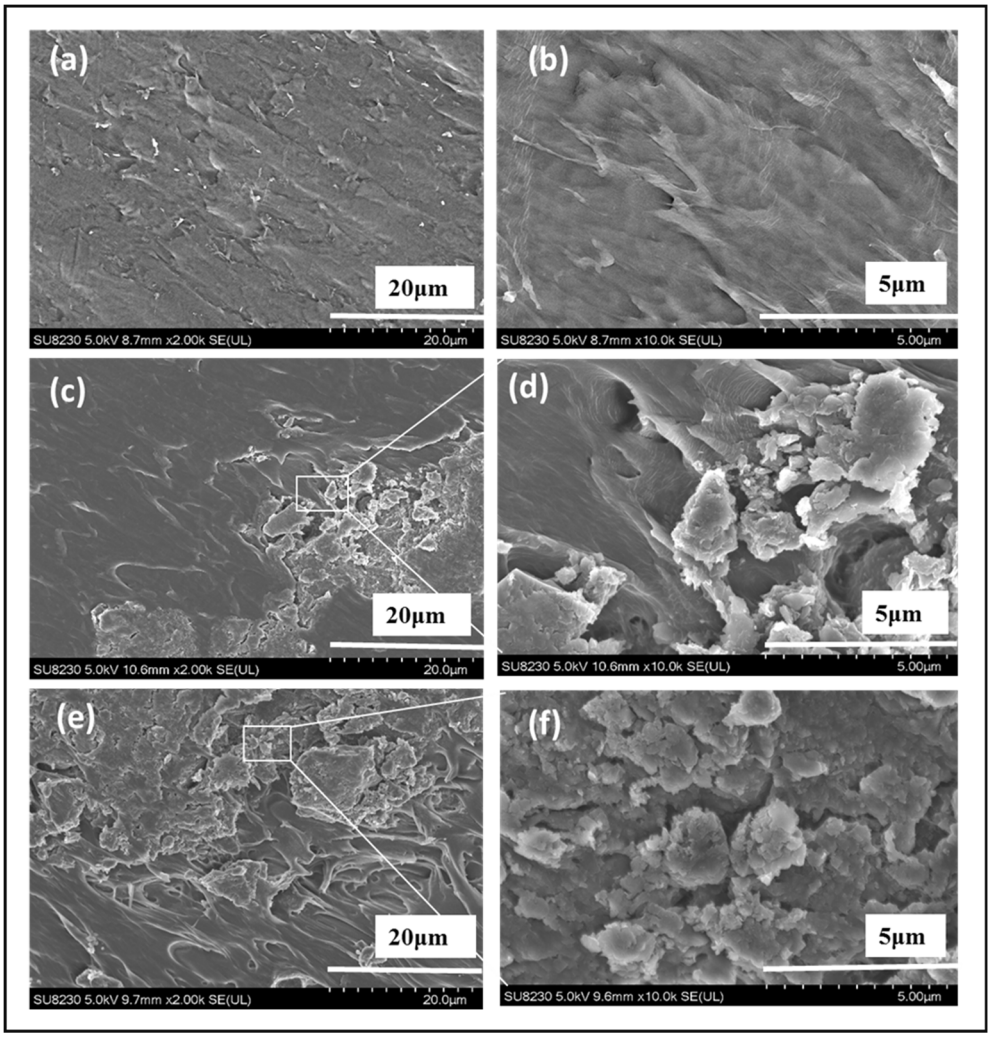

Figure 4.4 SEM micrographs of (a, b) LDPE/EVA_A blend,
(c, d) LDPE/EVA/G15_A and (e, f) LDPE/EVA/G 20_A

4.3.3 FT-IR results

Figure 4.5 represents the FT-IR spectra of the neat LDPE, neat EVA, LDPE/EVA_A blend, and LDPE/EVA/G_A composites compounded with LLDPE-g-MA as a compatibilizer. As FT-IR spectra represent information about the chemical structures of components, as well as the conformation and configuration, FT-IR spectra indicate that no significant chemical interaction between the polymer blend and graphene. Indeed, the FTIR spectra of the graphene, containing composites essentially showed the same absorption bands than the neat polymers (LDPE and EVA). EVA spectrum exhibited two sharp peaks at 1720–1745 cm^{-1} and 1100–

1200 cm^{-1}, which are attributed to the stretching vibration of C=O and C–O bonds, respectively (Shokri, Yegani, Heidari, & Shoeyb, 2015; Zarandi & Bioki, 2013). The FT-IR spectra revealed two intensive peaks at 2850 and 2910 cm^{-1} for all samples, which are assigned to the ethylene groups existing in both the LDPE and EVA components. The intensity of both the peaks (2850 and 2910 cm^{-1}) decreased with an increase of graphene-like content and/or the decrease of ethylene groups. Therefore, the lower intensity confirms that the bulk value of the graphene-like in the membrane of the polymer has increased (Hojjat & Mahmood, 2015; Meszlényi & Körtvélyessy, 1999; Shokri et al., 2015).

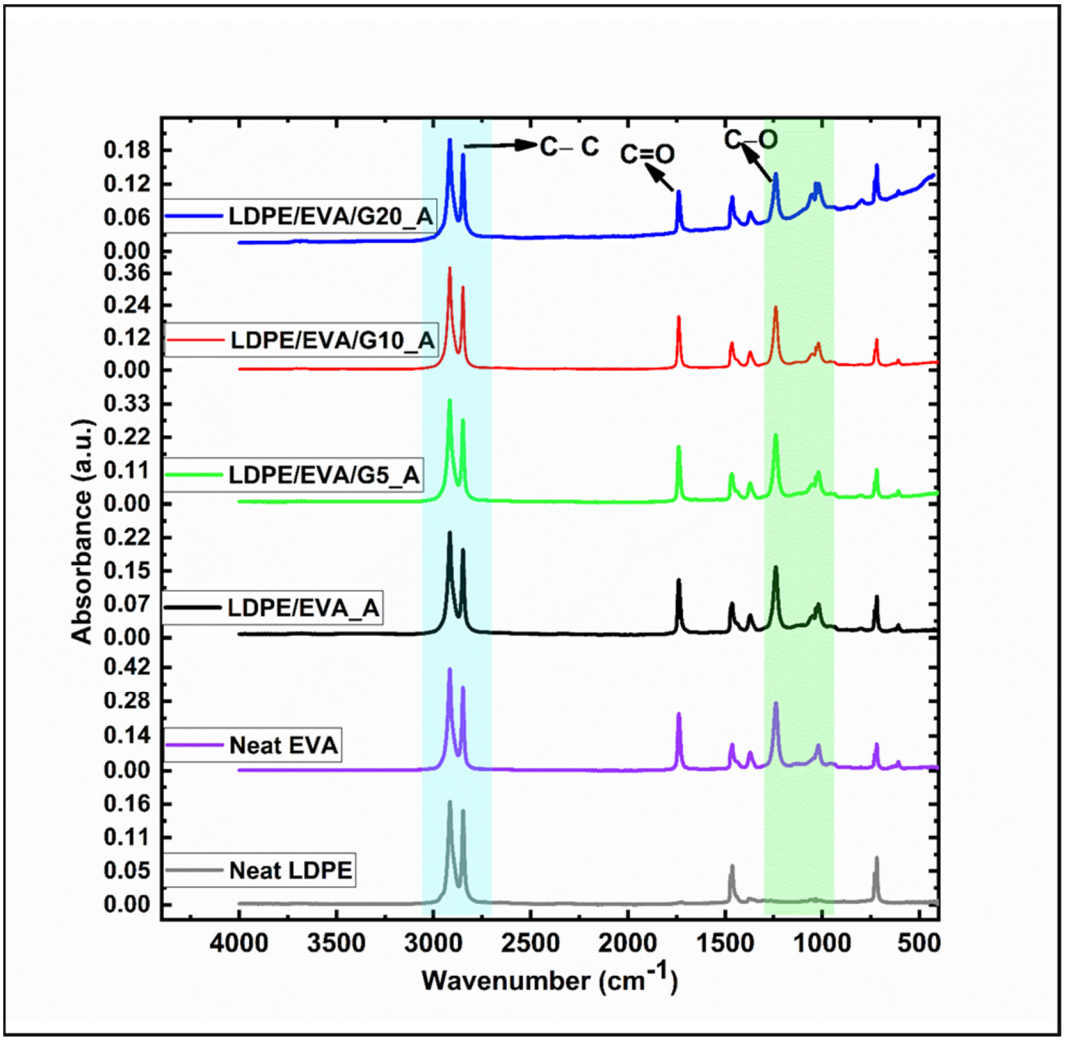

Figure 4.5 FT-IR spectra of the LDPE, EVA, LDPE/EVA_A blend and LDPE/EVA/G_A composites over the range of wavelengths of 400 to 4000 s^{-1}

4.3.4 Electrical characterization

The dielectric responses of the LDPE/EVA/G composites at room temperature prepared via annealed and non-annealed techniques are shown in Figure 4.6 and Figure 4.7, respectively. As illustrated, the addition of graphene-like filler to LDPE/EVA blend did not significantly increase the real part of the permittivity (the dielectric constant) of annealed and non-annealed composites at low filler contents. However, a tremendous change in electrical conductivity of the composites was found for both annealed and non-annealed composites with the addition of 17.5 wt% of graphene-like which correspond to the electrical percolation threshold for both systems. The annealed composites were found to be more slightly conductive than the non-annealed ones near the percolation threshold (one order of magnitude) due to better graphene layered arrangement within the polymer chains which was addressed by Kurusu et al. as well (Kurusu et al., 2018) (Figure 4.8).

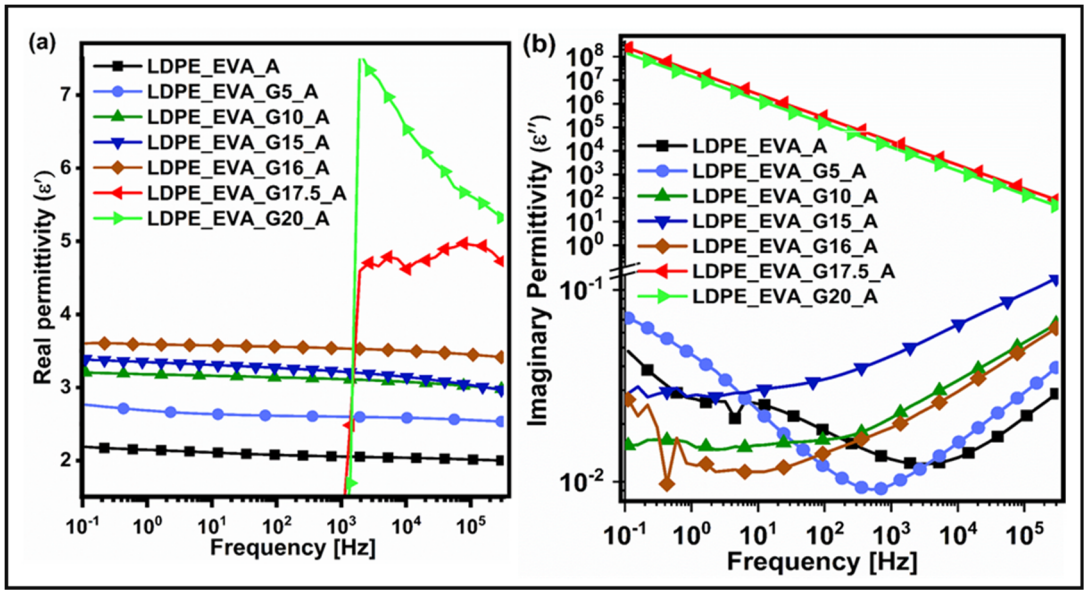

Figure 4.6 Real and imaginary part of the LDPE/EVA/G_A composites at room temperature

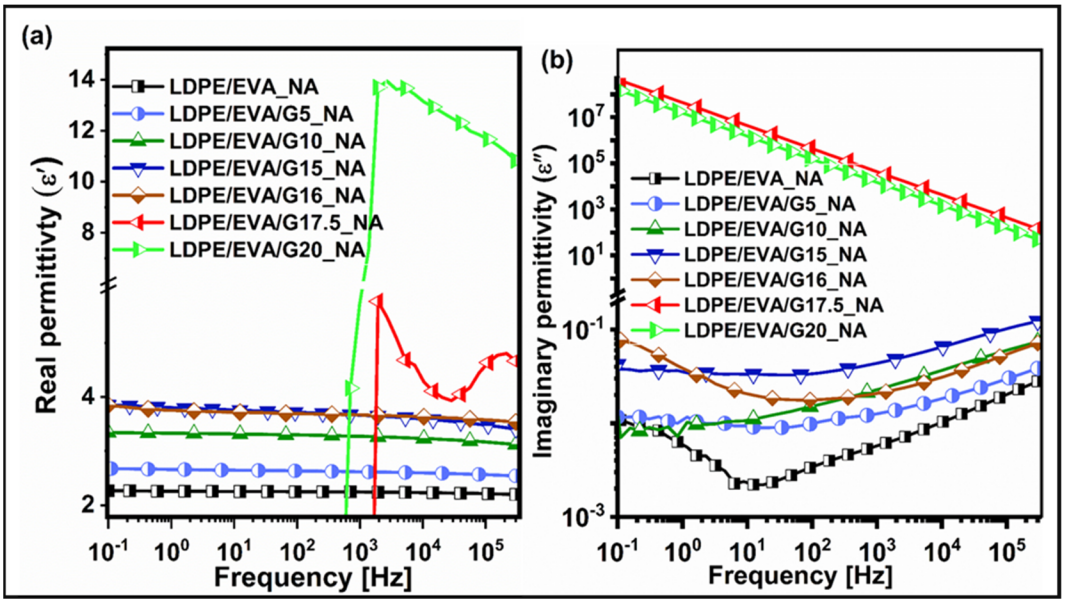

Figure 4.7 Real and imaginary part of the LDPE/EVA/G_NA composites at room temperature

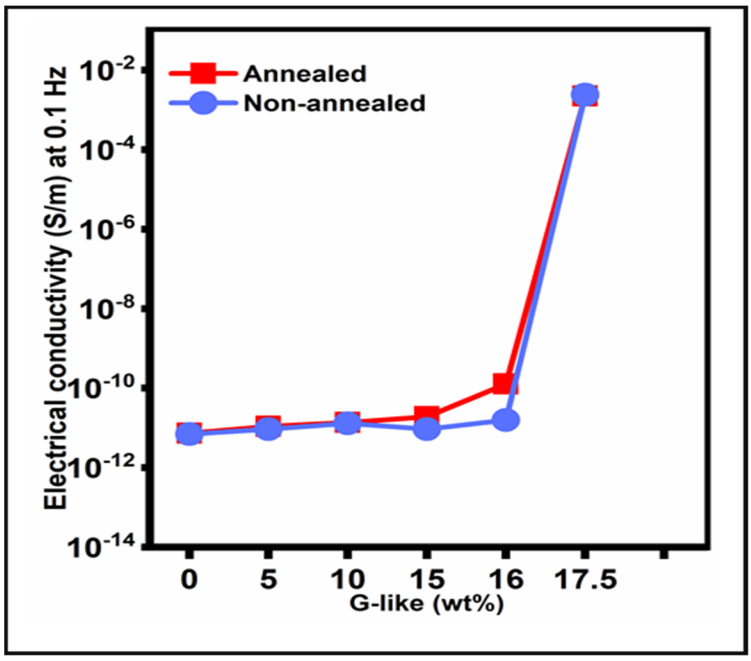

Figure 4.8 Electrical conductivity of LDPE/EVA/G composites at different filler contents prepared via annealing and non-annealing methods

Figure 4.9 shows the loss part of the electrical response of the LDPE/EVA/G composite at a frequency range of 100 mHz to 100 kHz at different temperatures starting from room

temperature to 85 °C. The complex permittivity of a material is expressed by Equation 4-1, where ε' represents storage part and ε" denotes the loss part,

$$\varepsilon^*(\omega) = \varepsilon'(\omega) - j\varepsilon''(\omega) \tag{4.1}$$

For a pure Debye relaxation process, the complex permittivity (real and imaginary part) is given:

$$\varepsilon' = \varepsilon_\infty + \frac{\varepsilon_s - \varepsilon_\infty}{1 + \omega^2\tau^2} \tag{4.2}$$

$$\varepsilon'' = \frac{(\varepsilon_s - \varepsilon_\infty)\omega\tau}{1 + \omega^2\tau^2} \tag{4.3}$$

where τ is the time constant of the process. For many processes, its temperature dependency follows an Arrhenius behavior given by:

$$\tau = A\exp(\frac{-Q}{RT}) \tag{4.4}$$

Accordingly, the imaginary part of the dielectric response varies with the temperature. These changes originate from changes in the relaxation times (τ) which invariably decrease with temperature increases (Dakin, 2006; Raju, 2016). Faster polarization at higher temperature can be linked with lower viscosity of the material at high temperature, for which charges have more freedom to be transferred or dipole to rotate. In addition, higher temperatures ultimately lead to a sharp increase of the imaginary part at low frequency due to charge transport processes leading to a mixture of direct conductivity and electrode polarization processes (Figure 4.9a–d). The dielectric relaxation peaks in polymer blends seem to be broader than the ones for neat polymers. As can be seen in Figure 4.9f, LDPE/EVA/G17.5 annealed composite has become semi-conductive and the transition from the insulating to the conductive regime was found to occur at a filler content between 16 to 17.5 wt%.

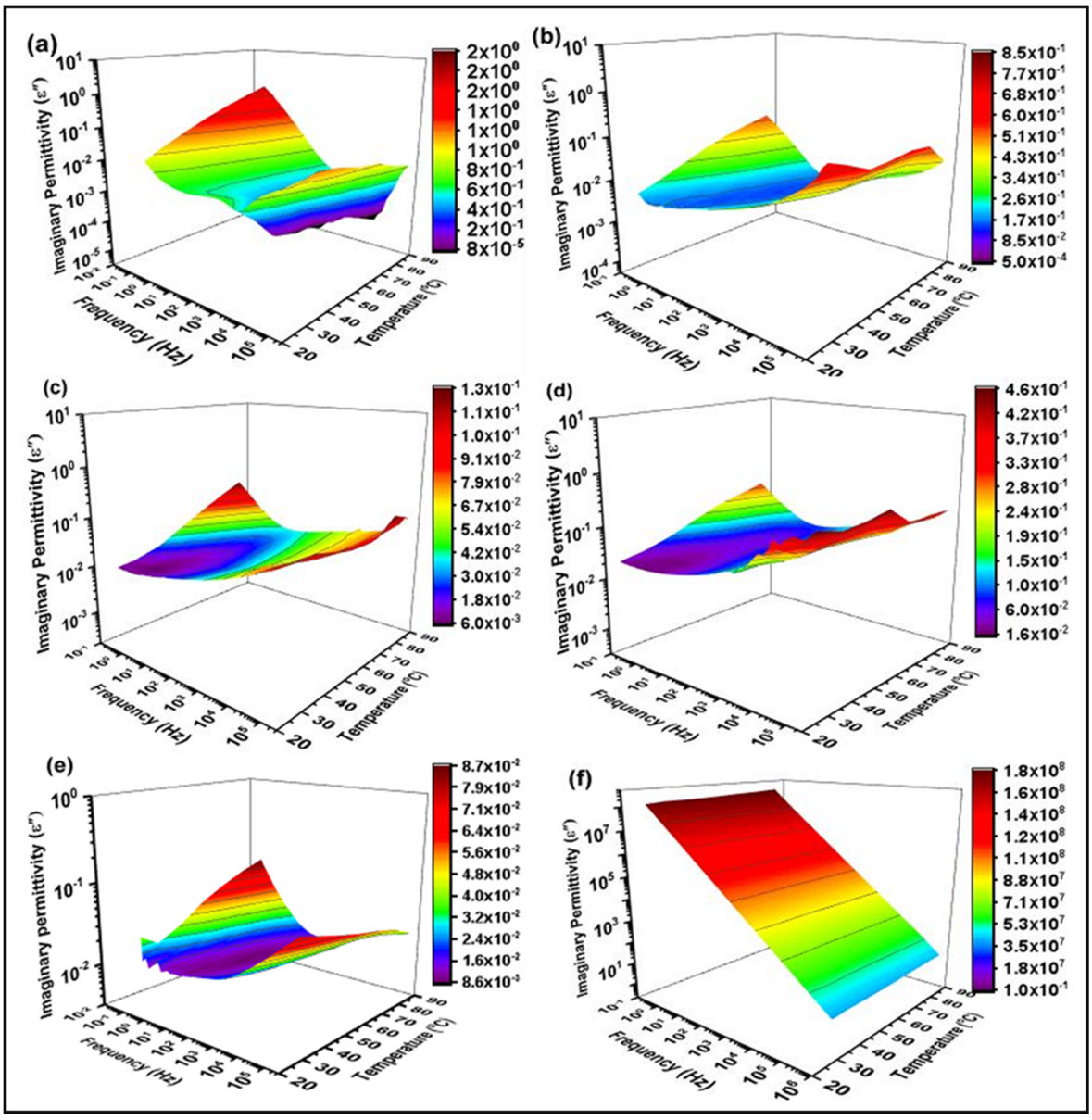

Figure 4.9 Imaginary part of electric response of LDPE/VEA/G composite at different temperatures over the wide range of frequency, (a) LDPE/EVA_A blend, (b) LDPE/EVA/G5_A, (c) LDPE/EVA/G10_A, (d) LDPE/EVA/G15_A, (e) LDPE/EVA/G16_A and (f) LDPE/EVA/G17.5_A

4.3.5 Thermal characterizations (DSC and TGA)

The DSC thermograms of LDPE/EVA/G composites are shown in Figure 4.10a, Figure 4.11a (melting endotherms) and Figure 4.10b, Figure 4.11b (crystallization endotherms). The heating thermograms showed a wide peak, starting from 40 °C to 95 °C which is attributed to

the melting of EVA crystals. This peak overlapped with the second peak which was found to lay between 105 °C to 117 °C. The second peak originating from the melting of PE crystals was found to be greater than the previous one due to the larger crystallinity of LDPE than EVA (Stark & Jaunich, 2011). The absorbed energy (fusion's enthalpy) of the composites was found to be greater than the polymer blends due to the nucleation effect of the graphene-like filler (Gil-González et al., 2018; Mofokeng, Ray, & Ojijo, 2018; Sabet et al., 2018; Tarani et al., 2016; P. Xu, Luo, Zhou, Yang, & Ding, 2017). The cooling plots showed a modest peak (~ 70 °C), which is linked to the vinyl acetate crystal formation, and another peak (~ 95 °C), which is related to PE crystal formation (Faker, Aghjeh, Ghaffari, & Seyyedi, 2008). The addition of graphene–like filler did not shift neither the melting point nor the crystallization temperature for all the annealed and non–annealed composites.

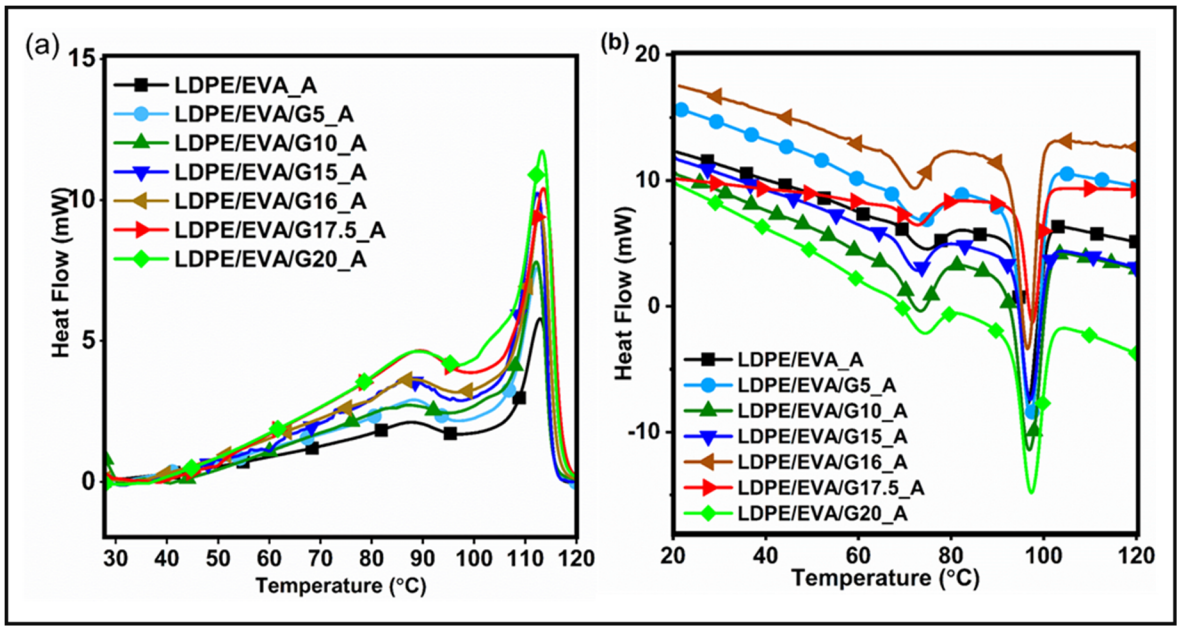

Figure 4.10 DSC thermograms of the LDPE/EVA_A polymer blend and its composites (a) heating curves and (b) cooling curves

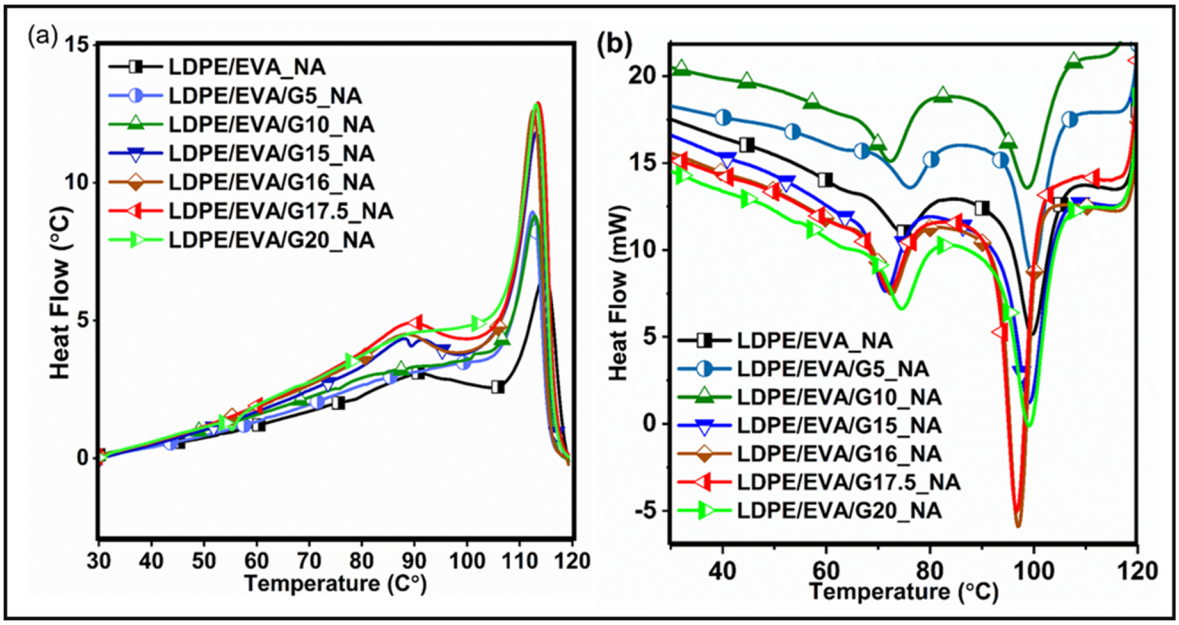

Figure 4.11 DSC thermograms of the LDPE/EVA_NA polymer blend and its composites (a) heating curve and (b) quenching curve

The thermal stability of the composites and the actual filler content were investigated by the means of TGA measurements. Figure 4.12 shows the TGA thermograms of LDPE/EVA composites with graphene-like filler in the range of temperature from 100 to 600 °C. Two decompositions were clearly seen in which the first weight loss starting from 300 °C, and is related to the division of vinyl acetate chains (deacylation) (Haurie et al., 2007). The second weight-loss occurred at ~ 370, 430 and 450 °C can be attributed to the pyrolysis of the LDPE/EVA_A, LDPE/EVA/G10_A, and LDPE/EVA/G20_A polymer chains (Dalai & Wenxiu, 2002). An increase of 80 °C was seen in the thermal stability of the composite containing 20 wt% graphene-like with respect to the polymer blend, thanks to the filler network formed throughout the composite which is acting similarly to the cross-linked matrix (M. Tang et al., 2016; Youssef, Senna, & Eyssa, 2007). A slight weight loss at higher temperatures (higher than 550 °C) is observed which is assigned to the existing oxygenated groups within the graphene-like filler (Paredes, Villar-Rodil, Martínez-Alonso, & Tascon, 2008). The remained ash at 520 °C for the composites proved the accuracy of the filler content in the labelled samples.

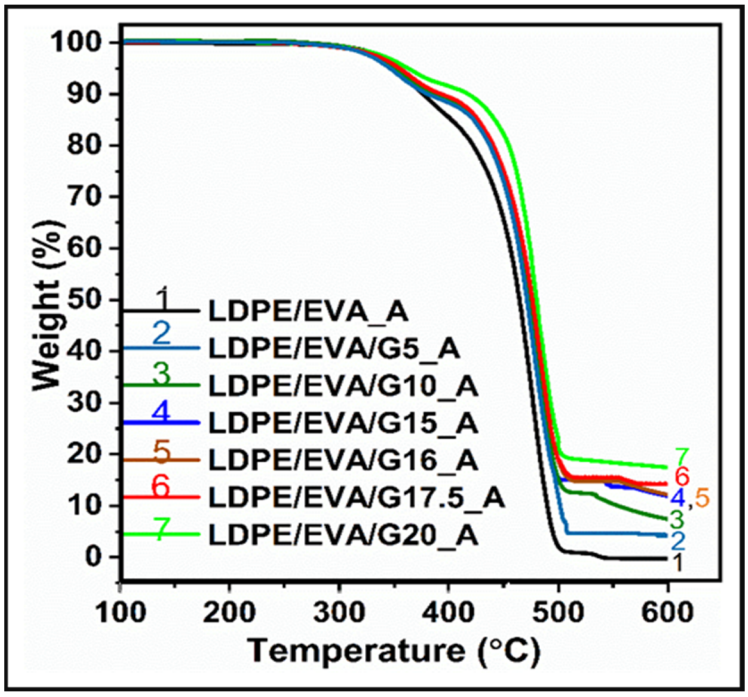

Figure 4.12 TGA thermograms of LDPE/EVA_A blend, LDPE/EVA/G10_A and LDPE/EVA/G20_A

4.3.6 Rheological properties

To obtain an overview in the structure of LDPE/EVA blend and its composites, rheology experiments were performed in the small amplitude oscillatory shear (SAOS) mode as a function of angular frequency (ω). The rheological results are shown in Figure 4.13a (storage modulus, G') and Figure 4.13b (complex viscosity modulus, η^*). The linear viscoelastic response of polymeric composites at filler content below the percolation threshold essentially depicts a terminal behavior at low frequency in which the storage modulus (G') is proportional to ω^2 (Peon, Vega, Del Amo, & Martınez-Salazar, 2003). As the content of filler increases, the slope of the storage modulus versus angular frequency decreases, and the materials subjected to shear stress show a non-terminal behavior displaying a plateau region for the storage modulus at low frequency (Carastan & Demarquette, 2006). Below percolation, LDPE/EVA/G_A composites the storage modulus (G') is proportional of ω^2 for which a negligible interaction between the blend and graphene-like can be observed. Therefore, the storage modulus was not found to increase significantly with the increase of G-like. At 20 wt%

(LDPE/EVA/G20_A) a transition occurred, the material showing a pseudo–solid-like curve which is related to the formation of strong particles networks throughout the composite, leading to a noticeable increase of storage modulus, similarly to what was found in (Krishnamoorti & Giannelis, 1997). This also led to a remarkable increase in complex viscosity of the molten composite (Faker et al., 2008; L. Utracki, 1991). These changes in the structure of the composite at molten state are in a good agreement with the electrical properties, thermogravimetric results as well as SEM micrographs, corroborating, the formation of the electric network, higher thermal stability, and connected particles network.

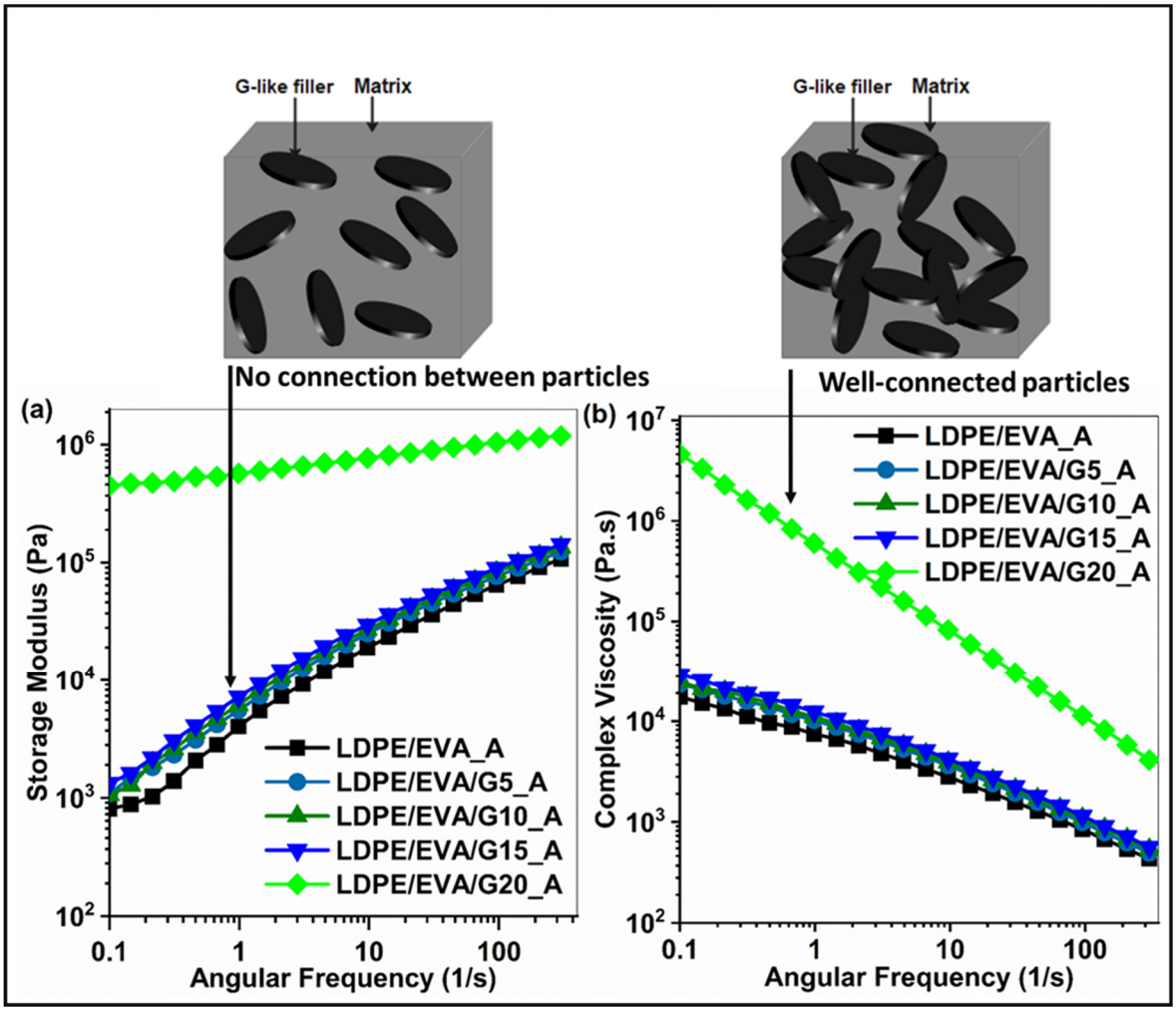

Figure 4.13 Small amplitude oscillatory shear measurements of LDPE/EVA_A polymer blend and its composites with graphene-like: (a) storage modulus ($G^{'}$) and (b) complex viscosity modulus (η^{*}) as a function of angular frequency

4.4 Conclusions

In this study, the aim was to increase the electrical conductivity of the LDPE/EVA composite using semiconductive graphene-like filler. LDPE, a non-polar thermoplastic polymer from one hand, and EVA, an elastomer polymer from the other hand were selected as the blend used for the polymeric matrix. The conductive network was achieved for the LDPE/EVA/G composite with the addition of more than 16 wt % of the natural-resource-based graphene-like filler. The electrical conductivity of the polymer blend was found to increase from 10^{-14} to 10^{-6} S/cm at 17.5 wt% of graphene-like, which makes LDPE/EVA/G composite a suitable candidate for semi-conductive and antistatic applications. Annealing of the LDPE/EVA/G composites led to a higher electrical conductivity near the percolation threshold with respect to the non-annealed composites. Addition of 20 wt % graphene-like to the LDPE/EVA blend increased the thermal stability of the composite by 80 °C. Eventually, graphene-like obtained from natural resources is an interesting candidate among the various conductive fillers to tailor the electrical properties of a variety of the polymers for conductive or semi-conductive applications.

Acknowledgment

The authors thank Natural Sciences and Engineering Research Council of Canada for the support.

CHAPTER 5

NUMERICAL SIMULATION OF EFFECTIVE PERMITTIVITY OF LDPE COMPOSITES FILLED BY CARBON BLACK AND GRAPHENE-LIKE FILLER

Abstract

The effective permittivity of low-density polyethylene (LDPE) with conductive carbon black (CB) was modeled by COMSOL. The impact of CB content on the electric properties of the composites with different geometry of the inclusions was investigated. The modeling outcomes evidenced that the simulation was in good agreement with experiment results at low-filler concentration, but at high filler content, the numerical modeling did not lead to a suitable prediction. The effect of moisture on the effective permittivity of the composites was also investigated, and the results were found to be significantly dependent on the absorbed moisture by the inclusions.

Keywords: Numerical modeling, Dielectric properties, Permittivity, Finite element.

5.1 Introduction

Great attention is paid to binary or multicomponent composite materials comprising conductive particles due to their suitable electrical properties for electrical applications. Numerous experimental researches have been performed to investigate the effect of the inclusion of conductive particles on the effective permittivity of composites (Cai et al., 2017b; Moalleminejad & Chung, 2015; Nilsson, Gedde, & Hedenqvist, 2011; Nilsson et al., 2016; Serdyuk, Podoltsev, & Gubanski, 2005). Although the conducted experiments are worthwhile and valuable, they are fairly time-consuming and expensive. Thus, numerical and analytical modeling of the composites is an appropriate way to predict and estimate the electrical properties of the composites. The composites are formed from a matrix loaded with one or more type of inclusions. These materials were considered as heterogeneous systems with their effective electrical properties (e.g. effective complex permittivity) being highly dependent on

the filler geometry (Yanhui Huang et al., 2014), filler content, filler dispersion and distribution (Bao, Meguid, Zhu, & Meguid, 2011), interfacial interaction between matrix and particles (Amini & Bahreyni, 2012; J. Xu, Zhong, & Yao, 2010) and the inherent properties of the inclusions and the matrix (Atif & Inam, 2016; Jylha & Sihvola, 2005; Mora, Han, & Lubineau, 2018; Tanaka, Kozako, Fuse, & Ohki, 2005; Z. Wang, Nelson, Hillborg, Zhao, & Schadler, 2013; Zare & Rhee, 2017). Furthermore, the distribution of the distance between the particles, and the number of contact points between them are two determining parameters for the effective electrical properties (Hoang, Leung, & Zhu, 2018; Louis & Gokhale, 1996; Shenogin, Lee, Voevodin, & Roy, 2016). Taking into account the above-mentioned parameters, the electrical properties of the composites such as the dielectric response can be somehow predicted by varieties of theories and models. For instance, the electrical properties of the composites with conductive particles can be approximately anticipated with providing the actual geometry and/or the spatial arrangement of the inclusions in the matrix.

The effective permittivity of the composites can be estimated and was reported based on the filler orientation within the matrix. It was suggested that the minimum value could be achieved by a laminated structure for which the phases are in series as follows (Jylha & Sihvola, 2005; Sihvola, 2000; Torquato, 2000):

$$\varepsilon_{\min,C} = \frac{\varepsilon_f \varepsilon_m}{\varepsilon_f \varphi_f + \varepsilon_m \varphi_m} \tag{5.1}$$

and that the maximum value is obtained when the laminates are in parallel (with respect to the electrical field) as follows:

$$\varepsilon_{\max,C} = \varepsilon_f \varphi_f + \varepsilon_m \varphi_m \tag{5.2}$$

where ε represents the effective permittivity, Φ the volume fraction, and the indexes f and m corresponding to the filler and matrix respectively. The aforementioned models give a global viewpoint of the effective permittivity of the composite but do not provide the exact bounds. Vargas-Bernal and his coworkers modeled the DC electrical conductivity of binary composites using Kirkpatrick's Model with more influential parameters. Based on this model, the DC electrical conductivity of the composite depends on the probability of the contacts between

particles within the composite, which leads to an alteration of the property of the matter from an insulating to a conductive one based on a power law as follows:

$$\sigma_{DC} = k\left(\varphi - \varphi_c\right)^t \tag{5.3}$$

where σ_{DC} is the conductivity of the composite, φ is the volume filler concentration and φ_c is the volume concentration at the critical concentration, k is a constant and t is the critical exponent (Stepashkina, Tsobkallo, & Alyoshin, 2014). The AC conductivity of PMMA with antimony tin oxide (ATO) filler was modeled and estimated by Jin and Gerhardt (Jin & Gerhardt, 2014). Their findings revealed that a perfect network of the connected fillers is more conductive than a random path connected. Both mentioned arrangements were also more conductive than the one with randomly distributed particles below the percolation threshold. The macroscopic electrical conductivity of CNT-polymer composite materials was simulated using multiscale approach by Shenogin et al (Shenogin et al., 2016). They reported that the metallization of the CNT-CNT contact-point leads to 150 to 500 times improvement in electrical conductivity. Monte Carlo model was used by Coelho et al. (Coelho, Armellini, & Morales, 2017) to estimate the percolation threshold of the individual and hybrid composite materials with carbon black and carbon nanotube particles. Their modeling results indicated that the percolation threshold of the composites including individual filler is corresponding to the experiments. However, for the multi-particle composites, the experimental results were not in good agreement with the modeling. Nevertheless, the best arrangement of the inclusion with the lowest percolation threshold was obtained.

In this work, the effective permittivity of the LDPE-based composites was analyzed numerically. The structure of the composite was designed and modeled according to the real morphology of the composites obtained by SEM images. The simulations were conducted for LDPE composites with carbon black (CB) and graphene-like (G-like) fillers with different arrangements (ideal and real orientation). The effect of the absorbed moisture on the electrical properties of the composites was also investigated. The obtained results were compared with the experiments.

5.2 Models and methods

The effective permittivity of the composite was evaluated based on filler orientation and arrangement. The modeling was also compared the effect of the particle size on effective permittivity for the composites with the same filler concentration.

A periodic geometry was chosen thus neglecting edge effect at boundary conditions. In the 3-D representative element, the 4 parallel surface boundaries along the Z direction were selected as periodic surfaces. The applied electrical field was set along the Z direction by setting to 5 V the potential of the top surface and to zero the potential of the bottom surface. The modeling was performed in the frequency-domain with harmonic electrical field condition. The effective permittivity of the composite was obtained from the equation (5-4) (Myroshnychenko & Brosseau, 2005; Venkatesulu, Jonsson, Edin, & Norgren, 2013; Zazoum, David, & Ngô, 2014)

$$\varepsilon_c = \frac{\langle D \rangle}{\langle E \rangle \varepsilon_o} \tag{5.4}$$

where ε_c is composite effective permittivity, $\langle D \rangle$ is the average electric flux density, $\langle E \rangle$ is the average of electric field over the selected cubic element and ε_o is the vacuum permittivity. It should be noted that these 3 values are in general complex values.

In the present study, highly conductive carbon black (CB) with an electrical conductivity of 100 (S/m) and a dielectric constant (real part of the complex permittivity) of ε = 30 (Hotta, Hayashi, Lanagan, Agrawal, & Nagata, 2011) at the frequency of 10^6 Hz was used for the numerical simulation. The electrical prosperities for the other phases are given in Table 5.1. The imaginary part of the permittivity (other than the one coming from the conductivity) for PE, CB and G-like was assumed to be negligible for the investigated frequency range.

Table 5.1 Electrical properties of the materials used for the simulation

Material	Electrical conductivity (S/m)	Complex permittivity at 10^6 Hz including the contribution of the conductivity	Reference for the obtained data
PE	10^{-15}	$\varepsilon^* = 2.3$	Our measurement
CB	100	$\varepsilon^* = 30 - 1.80 \times 10^6 i$	Our measurement
G-like	10	$\varepsilon^* = 100 - 1.80 \times 10^5 i$	Our measurement
Deionized water	5.5×10^{-6}	$\varepsilon^* = 80 - 0.0988i$	(Renaudot et al., 2013)

5.3 Results and discussion

5.3.1 Effective permittivity of LDPE/CB composites

5.3.1.1 Filler content

In order to understand the dispersion and distributions of CB particles in composite's structure, a cross-section SEM image of the LDPE/CB composite containing 15 wt.% of CB was taken and is shown in Figure 5.1. As illustrated, the CB particles are characterized by a somewhat spheroidal geometry. Furthermore, the CB particles seem to be randomly distributed within the composite. The effective permittivity of the composite as a function of the filler fraction (weight %) is shown in Figure 5.2 (dried CB filler randomly dispersed in matrix was assumed here). As shown, the effective permittivity of the composites was found to increase with the addition of the conductive CB. The computed values of the permittivity were found to be in reasonably good agreement up to 15 wt% and then were clearly underestimating the experimental values. In fact, at this critical filler concentration (percolation threshold), the conductivity of the composite was also found to sharply increase. In order to compare the numerical results with experimental findings, we considered the bulk density of LDPE and CB as 920 and 1120 kg/m^3, respectively, in order to convert the volume fraction used in the

numerical simulations in weight fraction. For example, the experimental percolation threshold of LDPE/CB composite fabricated by melt compounding was ~ 20 wt%, which is equal to 18.3 vol %. The effective permittivity of simulated composites at low filler contents featured closer values to the experimental results, but at high filler contents, the difference was noticeable which means the modeling cannot correctly predict electrical properties of the composites at high filler contents. The surface plots of the magnitude of the electric displacement field within LDPE/CB composites are shown in Figure 5.3. An enhancement of the electrical field was found at the interface of inclusion medium which is in good agreement with the analytic solution of the single inclusion problem. In addition, decreasing the particles size (and increasing their number to keep the same volume fraction) throughout the composites was found to increase the electric displacement field in which the maximum electric field density was found in the case of 20 vol. % (4.2×10^{-3} C/m^2). The higher electric displacement field can be addressed by the equation 5-5 (Z. M. Dang, Yuan, Yao, & Liao, 2013)

$$J = \int_0^{D_{max}} EdD \tag{5.5}$$

where J denotes the energy storage density, E stands for the electric field, D is the electric displacement and D_{max} represents the highest value of the electrical displacement. Therefore, based on (5), the rise of the total energy of the material would intensify the electric displacement field (Cai et al., 2017a).

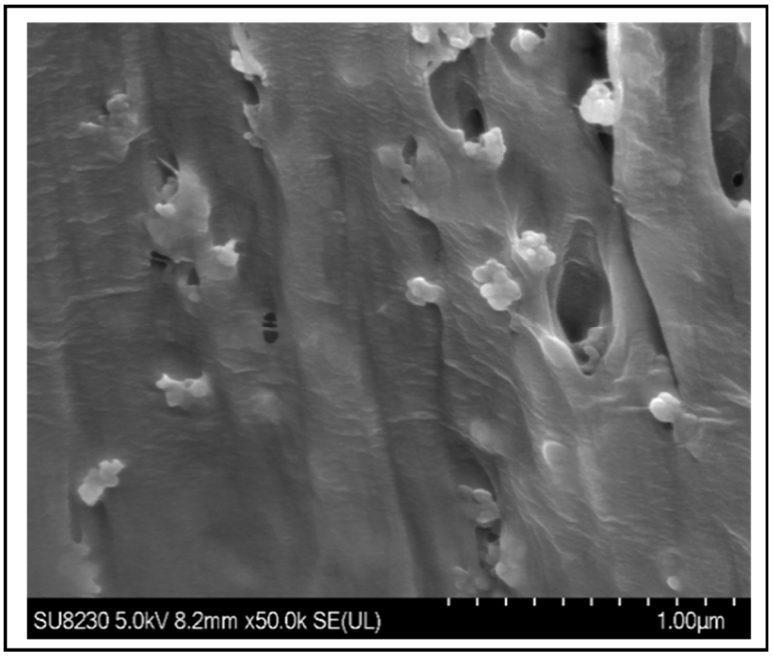

Figure 5.1 SEM micrograph of LDPE/CB15 wt% at
50 K magnification

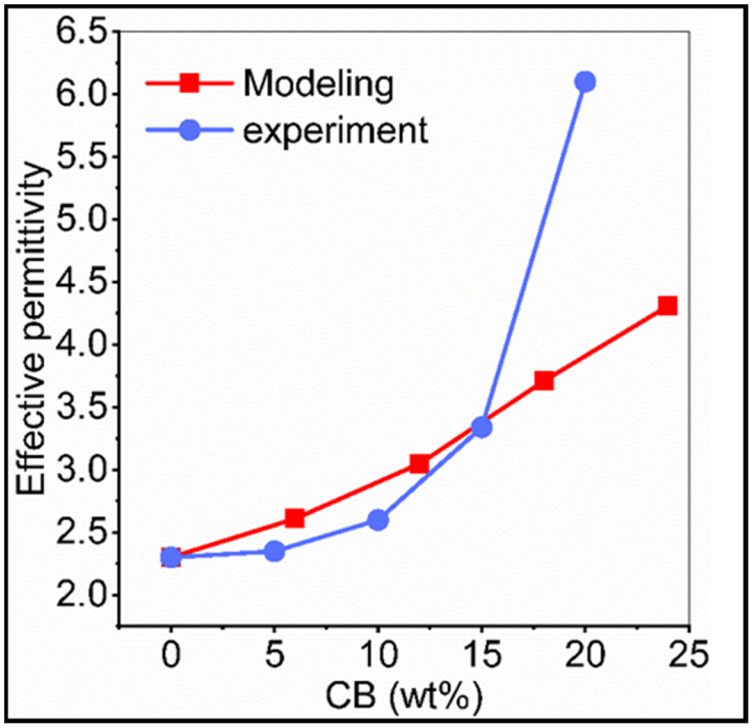

Figure 5.2 Effective permittivity of the LDPE/CB
composite at different filler contents
(CB without moisture, with a random dispersion)

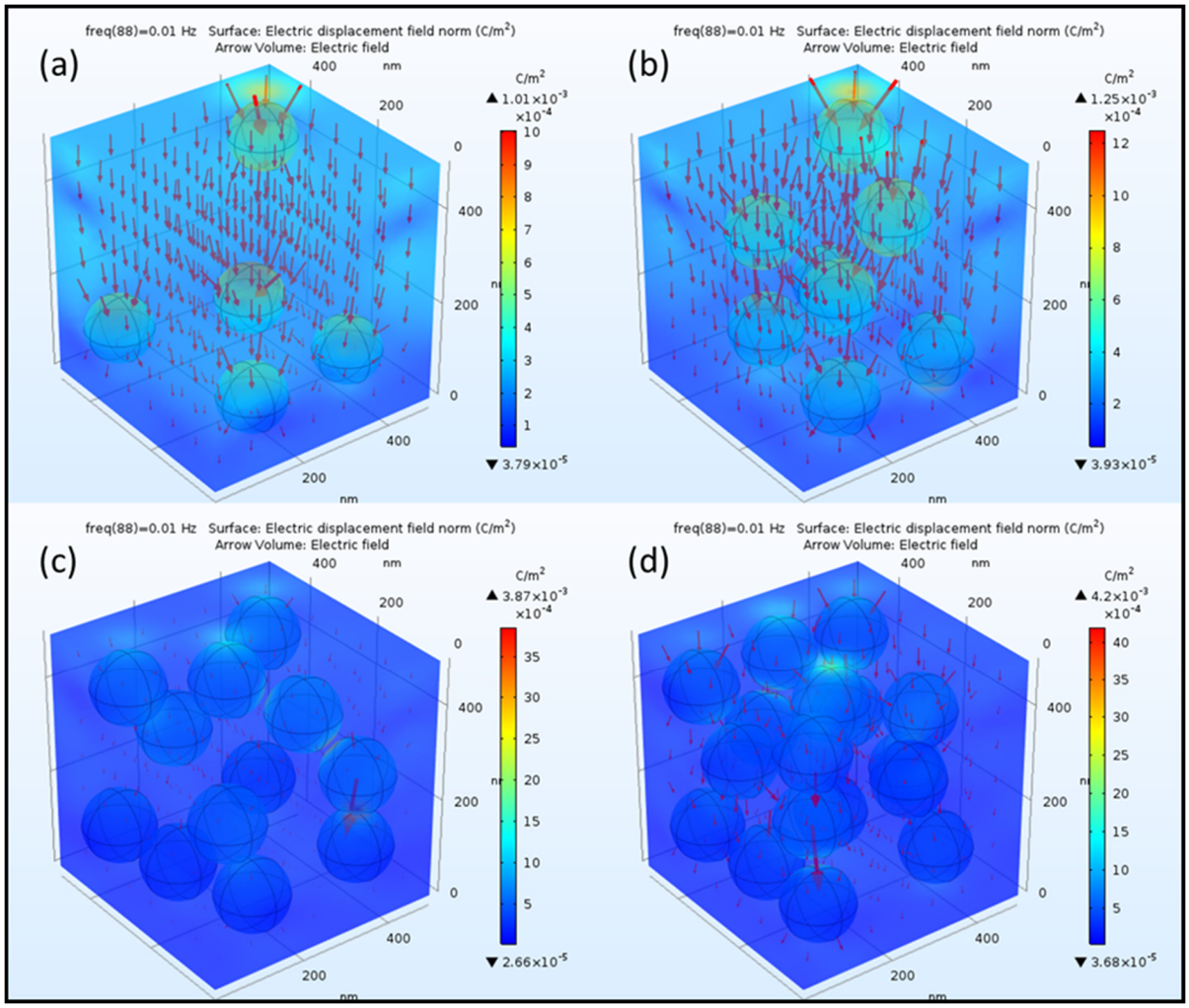

Figure 5.3 The surface plots of the electric displacement field norm of LDPE/CB composites with a random distribution of particles comprising of (a) 5, (b) 10, (c) 15 and (d) 20 vol. % of carbon black with the particle size of 106 nm

5.3.1.2 Orientation effect on the permittivity of composites with constant filler content

The role of particle distribution and particle size on the electrical properties of the composite was studied. In this respect, the LDPE/CB10 vol. % was selected, and the CB particles were either distributed randomly or placed in a regular order to form a symmetrical pattern. As can be seen in Table 5.2, at the same volume fraction of CB, the number of particles did not lead to significant change and the resulting electrical properties remained essentially unchanged. The surface plots of the magnitude of the electrical field of the modeled LDPE/CB10% with ordered and random filler distribution are illustrated in Figure 5.4 and Figure 5.5, respectively.

As can be seen, an increase of the electrical field is observed on the surface of the particles, particularly in the Z direction. At the same filler content, the highest value of the electric field magnitude was observed for the composite containing 36 particles randomly dispersed. The effective permittivity of the LDPE/CB 10 vol. % with 36 particles is slightly greater than the others with the same volume content of the CB. The particle size's can be extracted based on the number of particles and filler content.

Table 5.2 Effective permittivity of LDPE/CB composites containing 10 vol. % filler content with different particle distribution

Effective permittivity (ε)		
Particle number	Ordered dispersion	Random dispersion
1	3.050	3.027
8	3.061	3.023
27	3.075	3.065
36	-	3.088
64	3.071	-

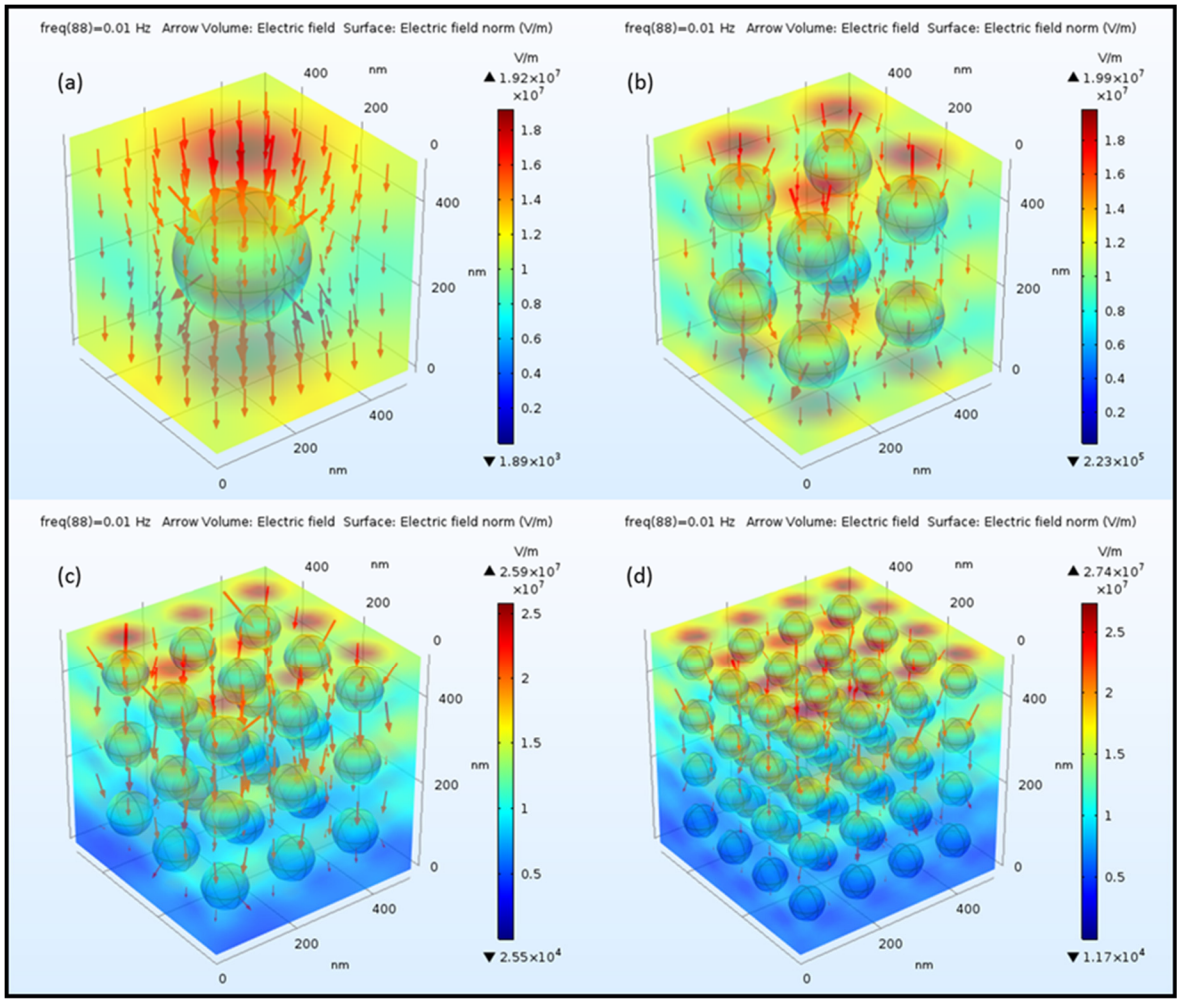

Figure 5.4 The surface plots of electric field norm of the LDPE/CB 10 vol. % composite with different particles number, (a) 1, (b) 8, (c) 27, and (d) 64, with ordered distribution.

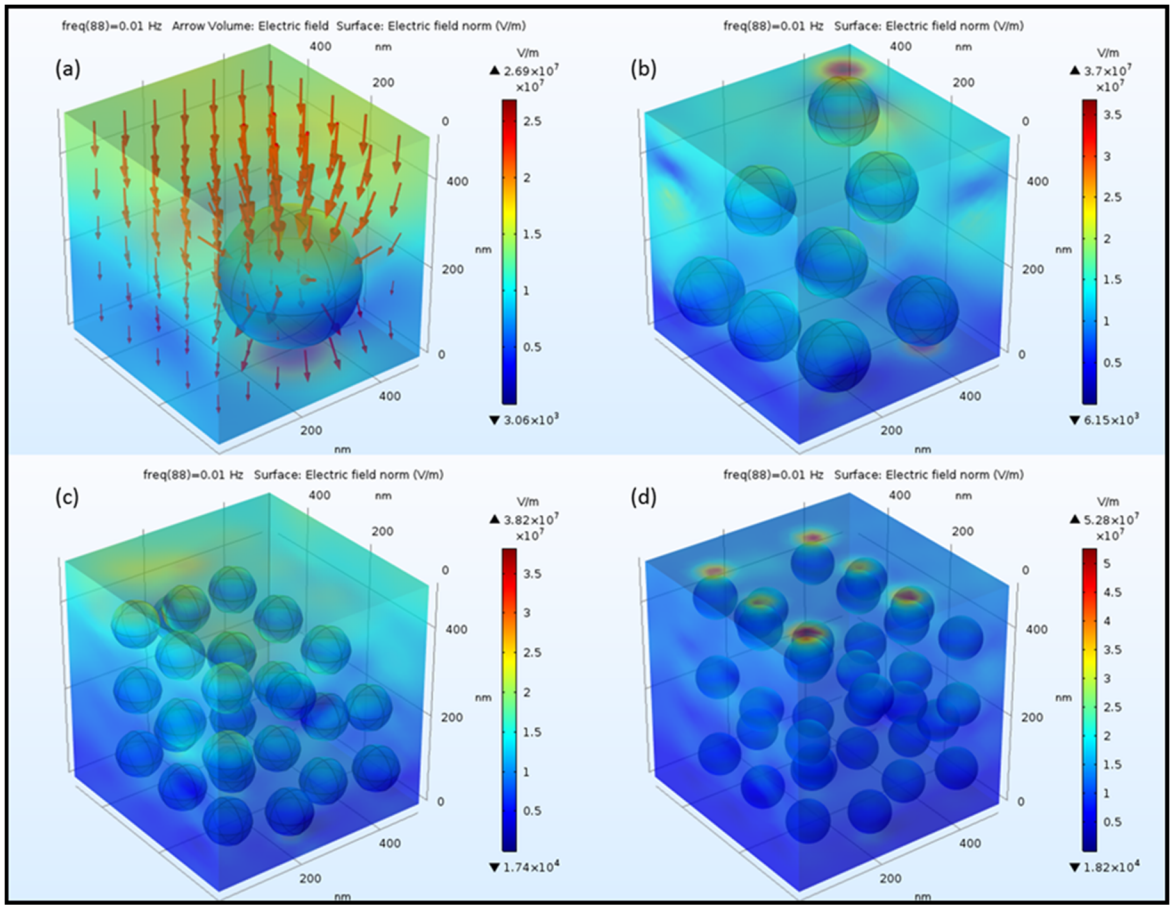

Figure 5.5 The surface plots of electric field norm of the LDPE/CB 10 vol. % composite with different particles number, (a) 1, (b) 8, (c) 27, and (d) 36, with random distribution at the applied electric field of 5 V

5.3.1.3 Effect of moisture

The hydrophilic behavior of CB particle was experimentally found to have a significant impact on the composites electrical properties. In this section, a thin membrane of moisture was created around the particles and the role of moisture on the effective permittivity of composites was evaluated. The effective permittivity of LDPE/CB10 vol. % with and without moisture as a function of the number of particles are shown in Figure 5.6. The water with effective permittivity of 80 and significant electrical conductivity (5.5×10^{-6} S/m) with respect to the insulating polymer engendered a significant synergies effect on the effective permittivity of the composites. Thus, significant increae in effective permittivity of the composites was

obtained. Furthermore, the composites with more particles were more susceptible to absorb moisture, and the more moisture caused a significant increase in effective permittivity. The experimental findings are in good agreement in where the conducted BDS at two successive runs. Performing a BDS measurement at room temperature after exposure to 100 ºC in order to remove absorbed moisture allowed to clarify the role of absorbed water since the resulting permittivity of composites was decreased.

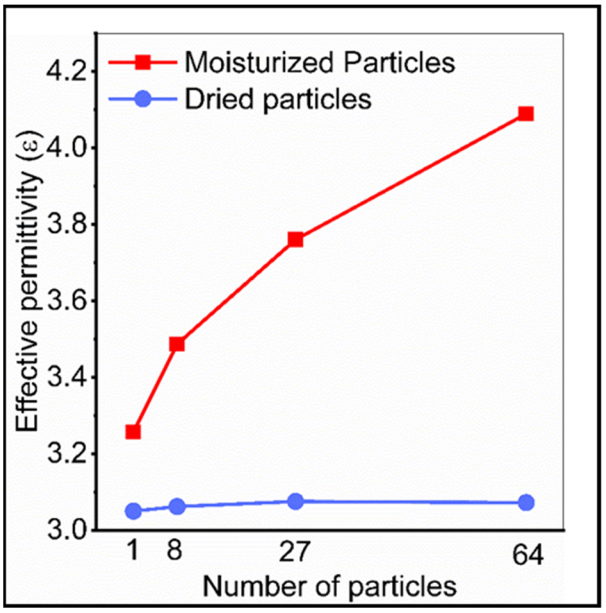

Figure 5.6 Numerical effective permittivity of LDPE/CB 10 vol. % composite with different dried and moisturized particles.

5.3.2 LDPE/graphene-like

5.3.2.1 Effective permittivity at different filler contents

The effective permittivity of G-like embedded randomly throughout the LDPE polymer was investigated. For this purpose, pellet-shaped G-like particles with a radius of 73 nm and a thickness of 10 nm were designed. The conductivity of the G-like was considered to be 10 S/m as measured in the compact state. Accordingly, the permittivity of the powder was set to $\varepsilon = 100 - 1.797e5i$ and the permittivity of the LDPE was as usual $\varepsilon = 2.3$. The effective

permittivity as a function of G-like content is shown in Figure 5.7. As can be seen, the effective permittivity of the composite was found to increase with the addition of G-like, as expected. The effective permittivity of the LDPE/G-like 7% obtained experimentally in our study (S. Azizi et al., 2017) was found to be much lower than the outcome of the numerical modeling. Comparing the effective permittivity of LDPE composite containing either CB or G-like, the composites with G-like filler exhibited a percolation threshold at much lower filler content than CB. This can be explained by the significant difference between the aspect ratio of the G-like with respect to the CB. As it can be seen, LDPE/G-like composite exhibited an effective permittivity of 3.78 at 7 vol. %. The surface plots of the magnitude of the electric displacement field of the composites are shown in Figure 5.8. The interconnection between the G-like particles led to a significant rise of electric field displacement. The maximum electric field displacement was obtained for the LDPE/G-like composite with 7 vol. % (4.5 $\times 10^{-3}$ C/m^{-2}).

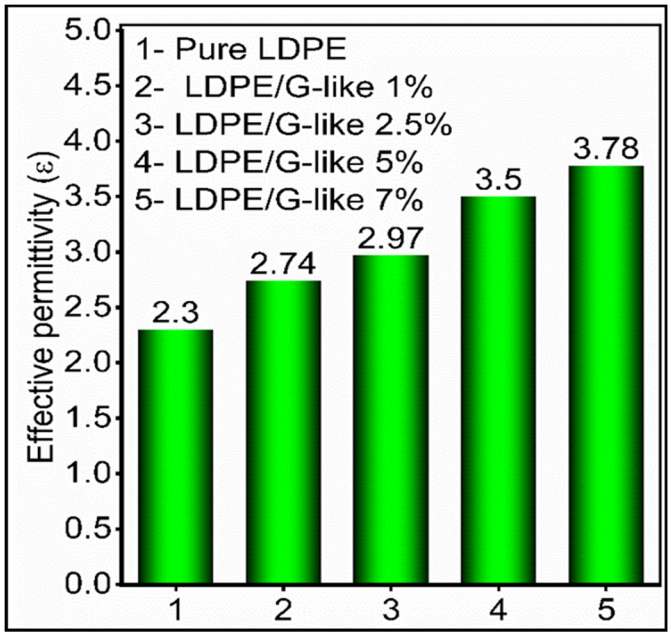

Figure 5.7 The numerical effective permittivity of the LDPE/G-like composite at different filler content with a random distribution of filler throughout the composite

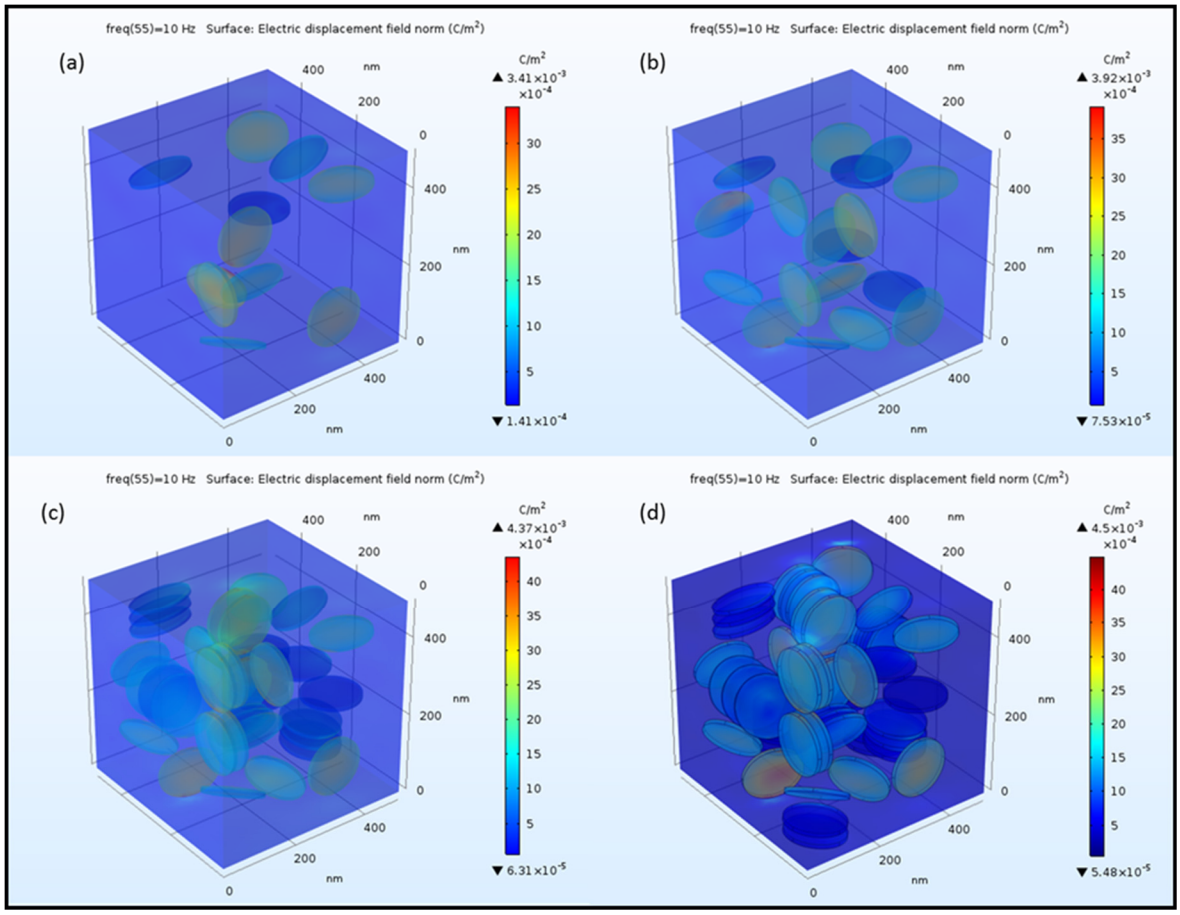

Figure 5.8 The surface plots of the electric displacement field norm of the LDPE/G-like composites at different filler contents; (a) with 1.5, (b) 2.5, (c) 5 and (d) 7 vol. %. Pellet-shaped G-like particles with a radius of 73 nm and a thickness of 10 nm

5.4 Conclusions

The nanostructure LDPE composites with either CB or G-like filler were designed and their effective permittivity was estimated by finite element modeling. Filler geometry and arrangement were found to have a significant influence on the electrical properties. Moisture absorption by CB particles was found to significantly increase the effective permittivity of the LDPE/CB composite. The effective permittivity of the LDPE composite obtained by numerical modeling was found to be in good agreement with the experimental results at low filler content. However, the numerical outcomes for the LDPE-G-like were not in good agreement with the experimental values and it might be because of the complexity and non-homogeneity of the composites microstructure.

Acknowledgment

The authors would like to thank École de technologie supérieure (ÉTS) and Natural Sciences and Engineering Research Council of Canada (NSERC) for their financial support.

CHAPTER 6

DISCUSSION AND CONCLUSION

6.1 DISCUSSION

During this Ph.D. study, carbonaceous fillers such as graphene-like, commercial graphene and carbon black were utilized to increase the electrical and thermal conductivity of the polymeric composites. In this context, several parameters need to be controlled, tuned or engineered to reach the desirable properties. Several key factors in polymers such as processability, compatibility, and miscibility need to be considered carefully. Sometimes, the initial properties of the polymers, for example, the flexibility, is particularly important and needs to be maintained for the considered application. For instance, conductive composites might be subjected to static or dynamic mechanical loading which requires adequate flexibility. In addition, in some situations, the high thermal stability of the composite is required, or great dielectric strength is needed in insulating applications. Moreover, the high electrical and thermal conductivity of polymeric composites is needed to be used as semiconductive screens for HV extruded cable applications. Therefore, the role of filler dispersion, processing condition, the type of polymers, the use of polymer blends can significantly affect the resulting electrical and thermal conductivity. To achieve our target, two commodity polymers (low-density polyethylene and ethylene vinyl acetate) and several types of conductive fillers were used. Two preparation methods (melt compounding and solvent casting) were used to obtain composites with the desired properties.

6.2 CONCLUSION

In the following, the achievements reached in this thesis as well as some limitations and challenges are discussed separately for each composite.

6.2.1 Low-density polyethylene/ carbon black composite

Commercially available carbon black was used to increase the electrical and thermal conductivity of the LDPE/CB composite. Different content of CB filler was combined with LDPE polymer via melt compounding technique. In this context, suitable dispersion of the nanosized carbon black filler led to the formation of a uniform network throughout the LDPE matrix. Thus the following results were obtained:

-A conductive network was found at filler content around 20 wt%, where LDPE/CB composite switched from an insulating material to a conductive one. This change led to an increase of 11 orders of magnitude in electrical conductivity and the LDPE/CB20 composite showed an electrical conductivity of 10^{-2} S/cm which can be used as inner semiconductive layer in HV cables.

-The electric response of the LDPE/CB composite was significantly dependent on the temperature where the LDPE/CB20 (at percolation threshold) was found to show a lower electrical conductivity at higher temperatures. The decrease in electrical conductivity of the LDPE/CB composite at elevated temperatures is attributable to the thermal expansion of the composites, which leads to the disruption of the previously formed CB network. Evaporation of the possible absorbed moisture at the interface of the filler and polymer might reduce the electrical conductivity of the composite as well.

-Loading of the CB filler resulted in the improvement in thermal conductivity of the LDPE/CB composite where an increase of 56 % was reached at 20 wt% filler. The increase in heat conductivity of the composite is linked to the incorporation of the CB particles having a high thermal conductivity. However, at low filler content, a slight decrease in thermal conductivity was observed, and this is linked to the significant thermal resistance at the interfacial region between the filler and polymeric matrix.

-A significant improvement in mechanical properties (storage and loss moduli) of the LDPE/CB composite was obtained by incorporating the CB filler. At low temperatures, LDPE/CB composites featured remarkable mechanical strength while with increasing temperature, a reduction of the storage and loss modulus of the composite was observed.

-Thermal properties of the LDPE/CB composite such as melting point and the degree of crystallinity were found to remain almost constant. The incorporation of the CB filler in LDPE/CB composite enhanced the thermal stability of the polymer. With 25 wt % of CB, a 76 °C increase in onset degradation temperature was achieved with respect to the LDPE polymer. This enhancement is usually attributed to the formation of some connected carbon-carbon pathways as well as some weak physical interactions between the inclusion and the polymer.

-The role of CB filler in dielectric strength breakdown of the LDPE/CB composite was investigated and the outcomes revealed that at 5 wt % content of CB, around 10 % increase in dielectric breakdown strength was obtained with respect to the LDPE polymer. However, upon further increase of CB content, the dielectric breakdown strength was found to dramatically decrease.

-The electrical conductivity of the LDPE/CB composite at the percolation threshold (LDPE/CB20) varied with increasing the electric field, showing a counterclockwise hysteresis when the electrical field was increased and then decreased. A relaxation peak related to interfacial polarization occurred at low frequency and, with an increasing electrical field, it was shifted toward higher frequencies. Due to the movement of the relaxation peak toward higher frequencies, a non-linearity and hysteresis effect was observed for the LDPE/CB20 composite.

-LDPE/CB composite with 5 wt% of the CB filler was evaluated in terms of resistance to corona discharge and the results did not show an enhanced behavior with respect to the LDPE polymer. Indeed, after a 35 h exposure to corona discharges, the eroded area for the LDPE/CB5 was 27 % greater than the LDPE. The resistance to corona discharge was also investigated for

the LDPE/CB10 composite but, due to an electrical arc, the measurement was stopped after 10 h.

-The imaginary part of the complex permittivity of the LDPE/CB20 was fitted to Havriliak–Negami functions in order to better understand the physical process leading to relaxation mechanisms.

-The main achievement of this study was the formation of a conductive network by carbon black filler at reasonable filler concentration for which a sharp increase in electrical conductivity of composite was obtained. LDPE/CB composite with 20 wt% filler content **meets desirable electrical and thermal conductivity** to be used as **semi-conductive screen layers in extruded high-voltage cable applications**.

6.2.2 Ethylene vinyl acetate/graphene and carbon black composite

EVA copolymer with graphene and carbon black fillers were blended via solvent casting. Different content of filler was used to prepare the composites. Nanosized carbon black particles were observed by SEM imaging and appeared fairly well distributed within the EVA polymer. However, graphene multilayers were randomly distributed and shown some agglomerated regions. The following findings were obtained:

-When carbon black was added to the EVA copolymer, a conductive composite was obtained at a filler content around 5-7 wt%. At 7 wt% of CB content, a significant increase in electrical conductivity was obtained to reach 10^{-2} S/m, around 10 orders of magnitude with respect to the neat EVA (10^{-12} S/m).

-An electrical percolation threshold was obtained for the EVA/graphene composite upon the addition of 15 wt% graphene filler. The tendency of the graphene layers to agglomerate resulted in a higher percolation point than for CB.

-Loading of graphene and carbon black filler to the EVA copolymer increased the thermal conductivity of the composite continuously in both cases. A 16 and 12 % increase in thermal conductivity of the EVA composites was obtained by adding 5 wt% CB and 15 wt% of graphene, respectively.

- A comparison between two composites with 15 wt% graphene, one prepared by solvent casting and one prepared by solvent casting followed by melt compounding was performed and it was found that solvent casting only resulted in a conductive composite, while, further compounding by melt blending led to a deterioration of the previously conductive network. This reveals that melt compounding can enhance the tendency of the graphene layer to agglomerate and thus prevents the formation of a conductive path at low filler content.

-Dynamic mechanical analysis of the EVA/graphene 15%wt prepared by solvent casting and further extruded, revealed a significant increase in storage modulus with respect to its counterpart. This might be due to the alignment of the graphene layers along the extrusion axis.

-The main finding of this study was the establishment of the graphene-network and carbon black fillers throughout the EVA copolymer. This conductive network enabled direct current conductivity within the composite. In addition, the increase in thermal conductivity of the EVA composites with CB and graphene provides a suitable material for several applications.

6.2.3 Low-density polyethylene/ Ethylene vinyl acetate/graphene-like composite

LDPE/EVA/graphene-like composites were prepared by solvent casting. The prepared composites were molded by annealing and non-annealing method. The role of graphene-like filler in electrical, thermal, mechanical and rheological properties was investigated. The results are presented in the following:

-An electrical percolation threshold was reached at ~ 16 to 17.5 wt% of graphene-like filler, at which concentration a significant change in electrical conductivity of LDPE/EVA/graphene-like was found. The SEM imaging of the composite structure showed the formation of microsize graphene layers throughout the composite.

-It was found that annealing the LDPE/EVA/graphene samples after the molding step enhances the formation of conductive paths within the composites. For example, the electrical conductivity at the percolation threshold was found to be one order of magnitude higher for the annealed sample with respect to the non-annealed one.

-The dielectric response of the LDPE/EVA/graphene composites was investigated over a wide range of temperatures and frequencies. The relaxation peaks, originating from the polar groups in the EVA structure as well as interfacial polarization peaks, were merged together at the percolation threshold and formed a wide peak over the entire temperature range. At low frequencies and high temperature, a significant rise in electrical losses was observed, which is related to charge carriers fluctuations.

-DSC measurements revealed unchanged values for the thermal properties of the LDPE/EVA/graphene-like composites. Melting points and degree of crystallinity remained almost unchanged, either with annealing or non-annealing preparation method.

-The continuous increase in thermal stability of the LDPE/EVA/graphene-like composites was detected with increasing the graphene-like filler content, particularly with 20 wt% filler content, 80 °C increase in thermal stability was resulted due to higher physical interaction between the fillers and the matrix.

-Rheological measurements corroborated SEM imaging and electrical response of the LDPE/EVA/graphene, where a rheological transition was seen at about the same point that the electrical percolation threshold. In other words, when a solid network of the graphene-like

filler was formed within the composite, it resulted in a significant increase in storage modulus as well as a remarkable enhancement in electrical conductivity.

-The significant achievement of this part was to **obtain a semi-conductive composite with the addition of a natural-based conductive filler to LDPE/EVA blend**. This composite blend meets electrical and mechanical requirements for the semi-conductive layer in high voltage extruded underground cables.

6.2.4 Numerical simulation of effective permittivity of LDPE composite filled by carbon black and graphene-like filler

-The effective permittivity of the LDPE/CB composite was modeled numerically, and the results were compared with the experimental data. At concentration below the percolation threshold, the numerical results were in good agreement with the experiment result.

-The role of filler dispersion in LDPE/CB composite was also studied numerically, and the modeling evidenced that below the percolation threshold, no significant difference in the electrical properties can be found between the random and ordered arrangement.

-Water absorption by CB filler was also numerically investigated by creating a thin membrane around the embedded particles within the medium, and the outcomes revealed that the presence of a water film leads to a significant increase in effective permittivity of the LDPE/CB composite.

Therefore, the numerical modeling of the LDPE composites with CB and G-like created a paradigm for better understanding of the role of filler concertation, the role of filler arrangement, the role of particle size, the role of moisture absorption on electrical properties. The outcome corroborated the obtained experimental results in low filler content of the CB, and this model can be optimized to predict the electrical properties of the composites with some similarities in component’s properties and morphology.

6.3 RECOMMENDATIONS

In this doctorate thesis, different techniques and preparation methods were used in order to obtain a good distribution of conductive carbonaceous filler within a polymeric matrix. However, as far as the graphene filler is concerned, agglomeration between the graphene layers was found to almost inevitably occur. Therefore, here in the following several recommendations are suggested:

6.3.1 Low-density polyethylene/ carbon black composite

The inclusion of carbon black allowed to successfully form a conductive network within LDPE polymer, but changes in composite preparation technique are suggested to reduce the percolation threshold. In addition, some agglomerates of the carbon black filler were seen in SEM images and more efforts are needed to achieve an optimal distribution. Diluting a PE/CB masterbatch to the desired concentration may reduce the percolation threshold. The existence of moisture on the surface of the carbon black filler was detected by the frequency-domain spectroscopy and this should be further investigated.

6.3.2 Ethylene vinyl acetate/ graphene/carbon black composite

Solvent casting is suggested as a technique to obtain a composite with at least one-decade lower filler concentration with respect to melt-compounding for the same composites. However, the solvent-casting was not found to successfully disperse graphene layers within the EVA chains. This may be because of the high graphene surface energy. Thus, a proper selection of solvent, solvent concentration, steering speed, and ultra-sonication energy is required. Therefore, all the aforementioned parameters need to be investigated and optimized. Moreover, as we have seen, nanosized carbon black resulted in low percolation threshold, and consequently, a finer particle size of graphene (around nanometer) might lead to lower percolation threshold, higher electrical and thermal conductivity.

6.3.3 Low-density polyethylene/ Ethylene vinyl acetate/ graphene-like composite

In this investigation, both LDPE and EVA polymer were dissolved separately and then mixed with dispersed filler. As a suggestion, premixing of the graphene-like filler in either LDPE or EVA and then incorporating in LDPE/EVA blend might facilitate the migration of the filler at the LDPE/EVA interface and thus lead to lower percolation threshold. Agitation of the graphene-like filler for a longer time (24 h) in the solvent may result in better exfoliation of graphene-sheets and then cause a lower percolation threshold. Precise control of the temperature of the mixer during the composite preparation may lead a better filler dispersion and ultimately lower filler concentration. In addition, it would be interesting to compound different ratio of the LDPE with EVA in presence of graphene-like filler.

It is also worth mentioning that the experimental conditions such as atmospheric moisture, temperature, etc. can influence electrical measurement. Therefore, precise control of the BDS sample holder by nitrogen flow would result outcomes that are more accurate.

APPENDIX I

GRAPHENE-LIKE PREPARATION AND ITS ELECTRICAL PROPERTIES

In order to prepare graphene-like filler via a green-eco-friendly way, different portions of natural-source materials such as clay (bentonite) and sucrose were caramelized with the required water portion (more details regarding graphene-like preparation can be found in (Boussaboun et al., 2017) . The mixture was heated under an inert atmosphere (see Figure AI. 1). Graphene-like material was reduced for 10 min in a grinder at 1000 rpm, and ultimately the reduced monolith carbon was sieved to reach the particle size smaller than 75 µm. The particle size distribution was measured by granulometry analysis using mastersizer 3000 Malvern (see Figure AI. 2). The electrical conductivity of the graphene-like was measured and compared with several commercially available graphene (see Figure AI. 3).

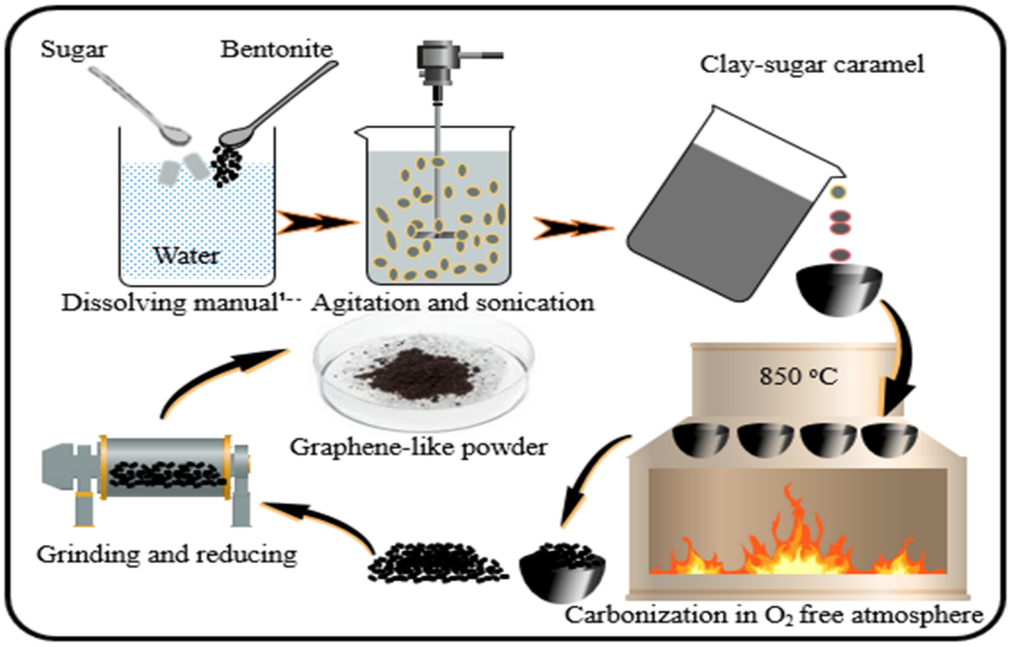

Figure AI. 1 Schematic of graphene-like fabrication from natural resources (bentonite and sucrose)

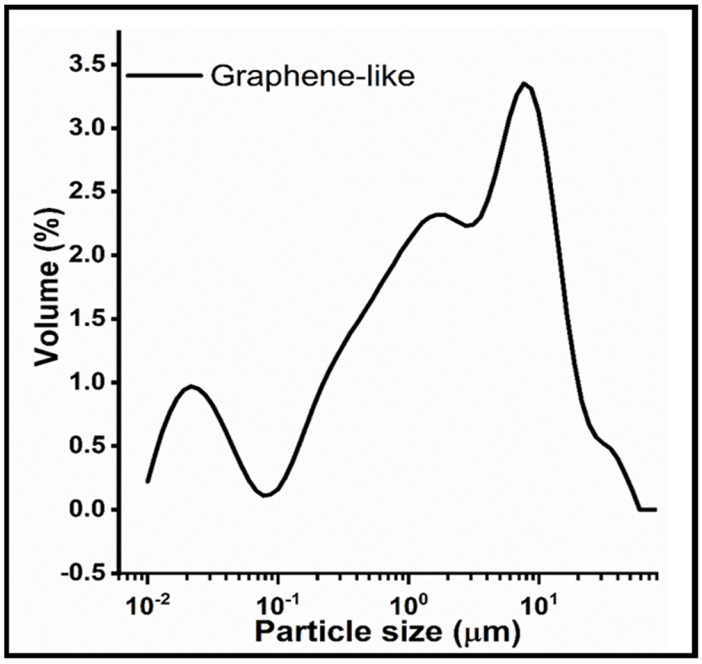

Figure AI. 2 Particle size distribution of graphene-like

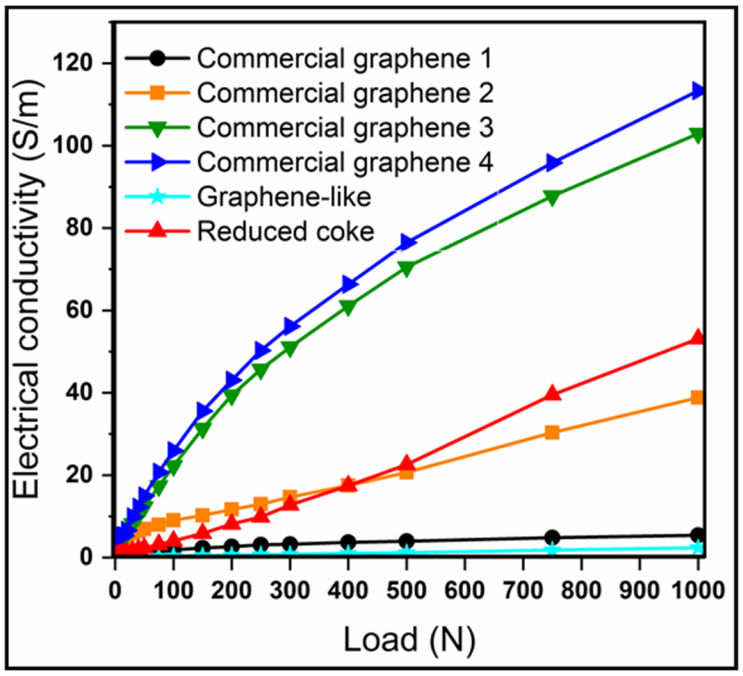

Figure AI. 3 Electrical conductivity of the graphene-like powder and several carbonaceous fillers as a function of load.

APPENDIX II

ELECTRICAL AND THERMAL PROPERTIES OF LOW-DENSITY POLYETHYLENE/GRAPHENE-LIKE COMPOSITE

S. Azizi[1], C. Ouellet-Plamondon[1], E. David[1], M. F. Fréchette[2]

[1] École de technologie supérieure (Université du Québec), 1100 Notre-Dame St W, Montreal, QC H3C 1K3 Canada
[2] Hydro-Québec's research institute (IREQ), Varennes, 1800 Boulevard Lionel-Boulet, Varennes, QC J3X 1S1 QC, Canada

Conference paper published in the 2016 CEIDP conference proceeding:

Abstract

Low-density polyethylene/graphene-like composites were prepared via melt-intercalation compounding technique. Then, the extruded composites were molded by compression molding. Differential scanning calorimetric measurements showed a negligible reduction of the melting point and the degree of crystallinity for the LDPE/G30 with respect to its neat polymer. The dielectric response of composites was found to exhibit the formation of a percolation network at higher loading than 30 wt%. The dielectric behavior of the composite at different electric fields featured a significant electric-field dependency.

1.Introduction

Graphene, a single-sheet thick of sp^2 bonded of carbon atoms with honeycomb structure has been frequently studied from the electrical, thermal and mechanical properties aspect (Anh et al., 2016; H. Kim et al., 2010; Pirondelli et al., 2016). In the recent decade, it has been observed that graphene-based composites have allocated for a large part of energy storage materials (Stoller, Park, Zhu, An, & Ruoff, 2008), chemical sensors, electromagnetic shielding products,

and semiconductive layers in cables. Graphene-based composites have also featured tremendous potential applications in electronics, bioproducts, automotive, photovoltaic and aerospace industry (Jiang & Drzal, 2012). Polyethylene as the most widely used polymer due to its easy processing, non-toxic, easy-accessible and cost-effectiveness has raised in the research studies abundantly. Melt intercalation compounding is one of the most popular technique from the industrial aspect for the manufacturing of thermoplastic-based composites with the nano-additives. Particularly, the platelets and sheet-type nano additives can be dispersed within the polymer chains with shear stress by an extrusion technique. In this regard, obtaining the best filler dispersion is the most important target and challenge during composite fabrication (Khanam et al., 2016; Mancinelli et al., 2014; Pirondelli et al., 2016; Zhu et al., 2010). The improvement of the filler dispersion has been addressed via the interfacial interaction between additives and host polymer. Several methodologies and techniques such as chemical functionalization of the host polymer and/or nanoadditive, a physical linkage between polymer matrix and filler using compatibilizer or applying shear stress have been already reported. Despite the excellent electrical and thermal properties of the graphene additive, the intrinsic tendency of this additive to form agglomeration and aggregates has hindered the formation of an appropriate electrically conductive network within the nanocomposite at low filler concentration.

In this research study, low-density polyethylene with different filler concentrations of graphene-like additive was compounded by melt compounding and then molded with a hot press. To analyze the morphology of the samples and also the thermal properties, differential scanning calorimetric (DSC) measurements were performed. Electrical properties of the composites were investigated over a wide range of frequencies with broadband dielectric spectroscopy (BDS). The material resistance under corona discharge condition was also investigated by an erosion test.

2. Experimental

2.1 Materials

Low-density polyethylene (LDPE) was purchased from Marplex with the bulk density of 0.992 g/cm^3 and melt flow index of 0.4 g/10 min with an average dimension of the powder grains with 95% lower than 500 μm. The graphene-like additive was prepared from natural resources such as sugar and bentonite with the ratio of 5:1. The average dimension of powder particles was 90% lower than 22 μm and the electrical conductivity of 1.2 S/cm at an apparent density of 4 g/cm^3.

2.2 Fabrication and characterization

Low-density polyethylene nanocomposites with different filler concentrations, which are labeled and presented in Table AII. 1, were fabricated by a twin screw co-rotating mini-extruder Haake MiniLab II with melting temperature zone 140 °C and 5 min recycling time in order to enhance the platelets dispersion as much as possible. The extruded composite then was molded under 7 MPa load at 150 °C molding temperature for 5 min. A 5-min annealing time was used in order to fix the crystalline structure of the composite.

Thermal properties and morphology structure of the composites were evaluated by differential scanning calorimetric (DSC) (Q20, TA instrument) test. The measurement was performed with two heating cycles and a cooling cycle. A ramp of 10 °C/min from 0 °C to 150 °C during the heating cycle and from 150 °C to 0 °C for cooling step, was applied. Dry nitrogen gas with 50 mL/min flow rate was used during the measurement.

Table AII. 2 Composite label and composition concentration

Sample code	Polymer concentration (wt %)	Filler concentration (wt %)
LDPE	100	0
LDPE/G1	99	1
LDPE/G10	90	10
LDPE/G30	70	30

The degree of crystallinity (Xc) was calculated by:

$$X_c = \frac{\Delta H_m}{(1-w)\,\Delta H_m^o} \times 100 \qquad \text{(AII.1)}$$

where ΔH_m is the experimental specific enthalpy of fusion of composite, w is the weight fraction of filler, and ΔH_m^o (293.6 J/g) (Fréchette et al., 2016) is the specific enthalpy of fusion of totally crystalline polymer.

Dielectric spectroscopy measurements were conducted using disk-shaped samples with a diameter of 4 cm and an average thickness of 0.3 mm. Each specimen was put between two brass electrodes and the measurement was performed with a Novocontrol dielectric spectrometer in a wide range of frequencies from 0.1 Hz to 104 Hz with an excitation AC voltage of 3 Vrms. The complex permittivity ε^* is given by

$$\varepsilon^* = \varepsilon'(\omega) - j\varepsilon''(\omega) \qquad \text{(AII.2)}$$

where $\varepsilon'(\omega)$ and $\varepsilon''(\omega)$ are the frequency-dependent real and imaginary part of the complex permittivity.

The erosion tests were performed on specimens with a diameter of 40 mm exposed to a continuous partial discharge activity. A 4 mm of diameter tungsten carbide ball tip was connected to an AC high voltage supply and the position of the tip was adjusted so the gap between the high voltage tip and the sample surface was 100 µm. A sinusoidal voltage with 10

kV rms at a frequency of 300 Hz was applied for 35 h. The eroded area of the samples was measured using a mechanical profilometer.

3.Results and discussion

The melting point and the degree of crystallinity calculated using Eq. (AI-1) is shown in Figure AII. 1. As can be seen from the DSC thermograms, the samples featured a melting peak around 110 to 111°C in the heating cycle which is related to the melting point of the LDPE and its composites. The degree of crystallinity obtained by (AII-1) illustrated a 6% reduction from 41% crystallinity to 34 % for the LDPE and LDPE/G30, respectively. The lowering of the degree of crystallinity is ascribed to the graphene-like nanoparticles which have refrained crystalline regions formation and facilitated the formation of a percolating network (S. Yang et al., 2007).

Dielectric responses of LDPE and its composites are shown in Figure AII. 2a and Figure AII. 2b. As it can be observed, the addition of 30 wt% graphene-like nanoparticle still could not form a conducting network within the polymer matrix and it can be predicted that percolation threshold will be found at higher filler concentration. The most probable reason which can be claimed that at this filler concentration the conducting network has not been formed yet, is the agglomeration of graphene sheets during melt compounding fabrication (Kalaitzidou, Fukushima, & Drzal, 2006; Tsekmes, Kochetov, Morshuis, & Smit, 2013; Zhu et al., 2010).

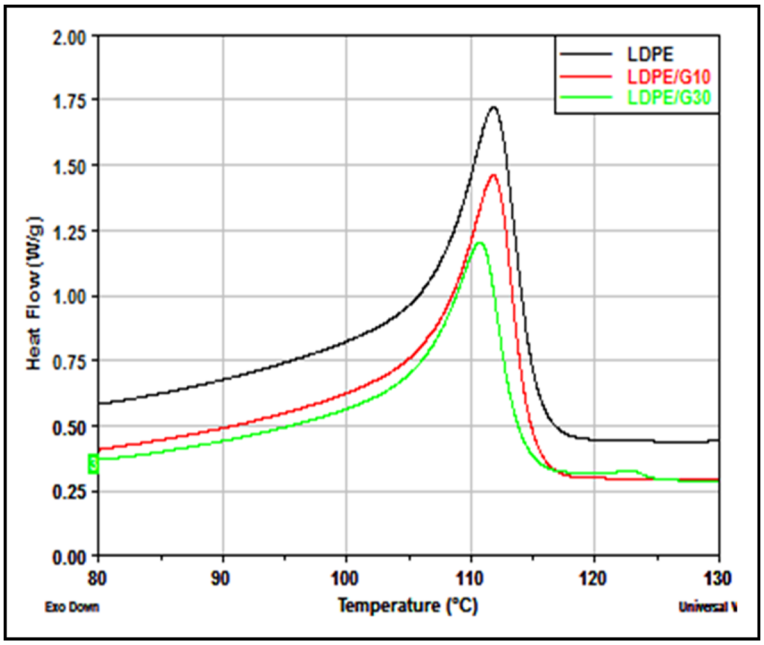

Figure AII. 1 DSC thermograms of LDPE and its composites including graphene-like additive

Table AII. 3 Thermal properties of LDPE and its composites

Sample	Melting point (°C)	Crystallinity (%)
LDPE	111.3	41
LDPE/G10	110.5	40
LDPE/G30	110.2	34

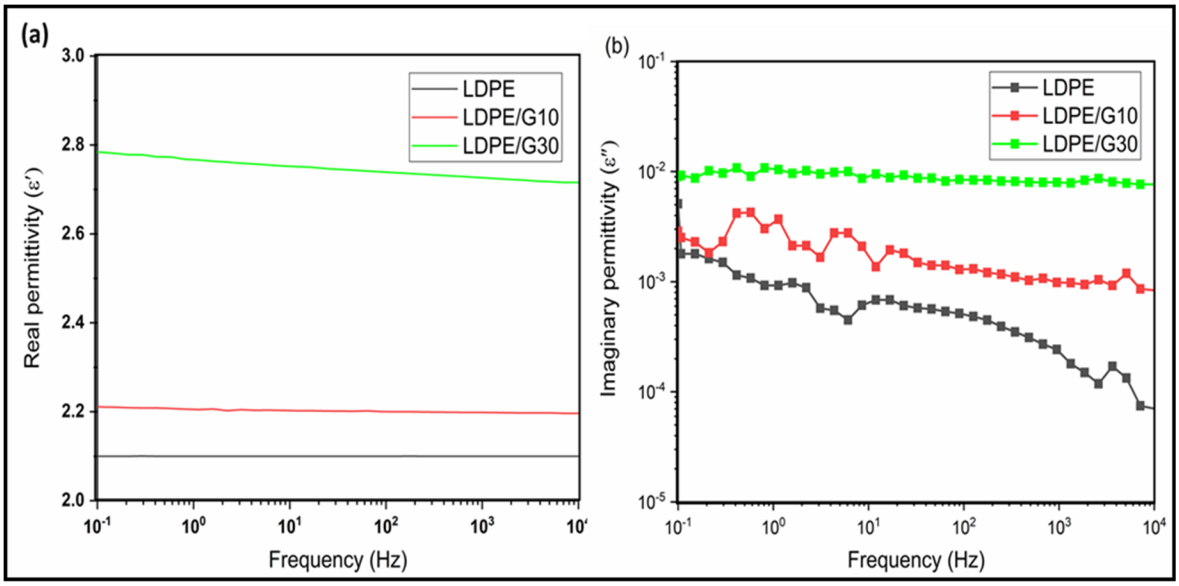

Figure AII. 2 Dielectric response (real part (a) and imaginary part (b)) of LDPE and its composites including different graphene-like filler concentration at room temperature

The non-linearity behavior of the LDPE/graphene-like composite at three different electric fields was investigated. The imaginary part of the complex permittivity at frequencies from 0.1 to 104 Hz under different applied electrical fields is shown in Figure AII. 3. The measurement at low electrical field (187 V/mm) exhibited a broad relaxation peak at about 1 Hz in addition to a smaller one at a higher frequency (~ 200 Hz), both related to the interfacial relaxation peaks. These peaks were also observed at higher electrical fields at about the same frequency for the low frequency peak and at a slightly higher frequency in the case of the high frequency peak and in both cases, with a higher magnitude. This reveals the non-linearity aspects of the composite. Since this electrical field-dependency typically appears in the vicinity of the percolation threshold for composites containing carbonaceous additives (Christen, Donzel, & Greuter, 2010), it can be claimed that some conduction path within the composite bulk is created when the electrical field is increased.

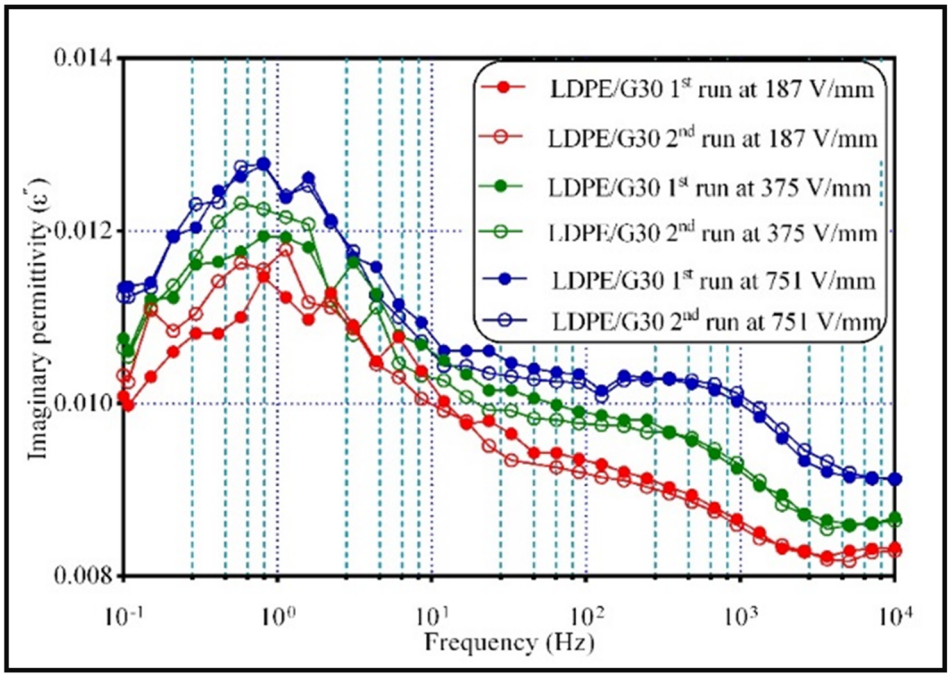

Figure AII. 3 Dielectric loss part of the complex permittivity as a function of frequency at room temperature at different electric fields.

The eroded sample patterns under corona condition after 35 h are shown in Figure AII. 4a and Figure AII. 4b. The assessment of the eroded volume was performed with a mechanical profilometer. As it can be observed, the eroded area in the case of both LDPE and LDPE/G1 composites is symmetrical around the tip of the HV electrode exhibiting circular patterns. The symmetry of the eroded area can be related to the uniformity of the host polymer as well as LDPE/G1 composite. The value of the eroded volume of LDPE and LDPE/G1 are shown in Table AII. 4. As can be seen, the addition of 1 wt% of the graphene-like nanoparticle to the LDPE increased the material eroded by corona discharges. For 3wt% of graphene-like, a breakdown occurred before the end of the erosion test (35 h).

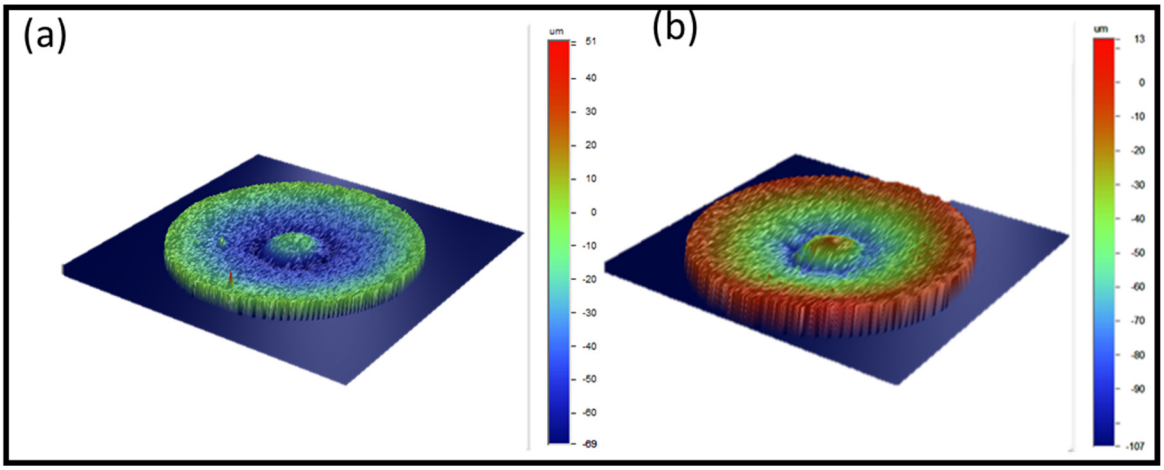

Figure AII. 4 Eroded patterns of LDPE and LDPE/G1 after 35 h obtained by DEKTAK profilometer.

Table AII. 5 Eroded value of the low filler content of graphene-like filler and low-density polyethylene after 35h

Sample	LDPE	LDPE/G1
Net missing volume (μm^3)	3.05×109	3.8×109

Conclusion

The thermal properties of low-density polyethylene/graphene-like composite fabricated by melt compounding were evaluated by differential scanning calorimetric and a decrease of the polymer crystallinity was observed in the graphene-like filled composite with 30 wt% of the additive. The dielectric properties were investigated by broadband dielectric spectroscopy and featured a non-linear behavior of composite containing 30 wt% of the additive. Modification of neat LDPE with graphene-like additive did not lead to an increased surface resistance against partial discharges.

ACKNOWLEDGMENT

The authors would like to warmly thank the École de technologie supérieure (ÉTS) and Hydro-Québec's research institute (IREQ) for their financial support.

APPENDIX III

ELECTRIC RESPONSE AND THERMAL PROPERTIES OF ETHYLENE VINYL ACETATE/GRAPHENE-BASED COMPOSITE

S. Azizi[1], C. Ouellet-Plamondon[1], E. David1, M. F. Fréchette[2]

[1] École de technologie supérieure (Université du Québec), 1100 Notre-Dame St W, Montreal, QC H3C 1K3 Canada
[2] Hydro-Québec's research institute (IREQ), Varennes, 1800 Boulevard Lionel-Boulet, Varennes, QC J3X 1S1 QC, Canada

Conference paper published in the 2018 CEIDP conference proceeding:

Abstract

Ethylene vinyl acetate/Graphene (EVA/G) composites containing two different types of graphene were prepared by solvent-casting. The EVA/commercial graphene (CG) composites featured a percolation threshold at slightly higher than 20 wt% of CG content, while, the EVA/G-like was found to be conductive at 30 wt%. Below the percolation threshold, a constant dielectric loss behavior was observed for most of the graphene-containing composites. Closer to the percolation, interfacial loss peaks were observed and their frequential position was found to shift toward the higher frequencies when the temperature was increased.

1.Introduction

In the last decades, carbonaceous-based/polymeric composites have received considerable attention thanks to their electrical conductivity (Badiee et al., 2016; Dash et al., 2015; Sefadi et al., 2015), adequate mechanical properties (Bahmanyar et al., 2015) and increased thermal conductivity (Burger et al., 2016; Han & Fina, 2011). Among the different allotropes of carbon, graphene (G) or expanded graphite (EG) with a 2D honeycomb structure of carbon is an

interesting material due to its good electrical and thermal properties (Ruiz-Hitzky et al., 2016a; Sadasivuni et al., 2015) combined with better flame retardant properties than conventional carbon black-based materials [9]. Ethylene vinyl acetate/graphene-based (EVA/G) composites feature different electrical properties, depending on graphene properties, concentration and processing. For instance, greater aspect ratio of EG leads to higher electrical conductivity for EVA/EG composites (Yousefzade et al., 2016). Vinyl acetate (VA) content in the EVA composite containing expanded graphite was found to play a tremendous role on the percolation threshold for which the minimum percolation network was achieved for the EVA containing 20 % of VA (Ratzsch et al., 2014). Chemical modification of expanded graphite using anionic surfactant sodium dodecyl sulphate suppressed the formation of electrical network inside the EVA/EG composite even at high filler content (Sefadi et al., 2015). Although there have been ongoing studies on EVA/G-based composites in terms of electrical properties, it seems there is a lack of understanding regarding the dielectric properties of EVA/G composite, particularly below the percolation concentration. Investigation on the electrical and thermal properties of graphene-based composites with EVA copolymer are reported in this paper.

2. Experimental

2.1 Materials

Pure EVA pellets with a density of 0.950 g/cm3 and 28% of VA content were purchased from Repsol Company. G-like was fabricated at ETS from natural resource, and the CG was obtained from NanoXplore. More details on the fabrication of G-like are given in (Boussaboun et al., 2017). Toluene solvent was provided from Sigma-Aldrich Company with 99.5 % purity.

2.2 Composite Preparation and Characterizing

EVA/G-like x% and EVA/CGx% S+E composites (x= 0, 15, 20, 25 and 30 wt% graphene, S = solvent-casting, E = extrusion) were prepared by solvent-casting technique. The EVA was

dissolved in toluene and graphene was suspended also in toluene at 90 °C. Magnetic stirring at 600 rpm for 2 hours was applied in both cases. Then, both solutions were mixed together, and the stirring was conducted with the same above-mentioned conditions. The compounded samples were then cast and dried under a fume hood at room temperature until the complete removal of the solvent. The pelletized composites were then pressed under 5 MPa at 150 °C and maintained 5 min under this load and temperature to obtain flat disks having a thickness around 0.5 mm. A batch of EVA/G15% was further extruded and then molded.

Electrical properties were investigated using frequency-domain broadband dielectric spectroscopy, with a sample disk of 0.5 mm of thickness and 30 mm in diameter and under an excitation voltage of 3 Vrms and a frequency window from 0.1 to 100 kHz at different temperatures. The thermal properties were measured by differential scanning calorimetric (DSC) and thermal gravimetric analysis (TGA).

3. Results and discussion

The degrees of crystallinity for the pure EVA and its composites measured by DSC are given in Table AIII- 1. Adding graphene was found to not change significantly, neither the melting point nor the degree of crystallinity of the composites. The thermal stability of the samples investigated by TGA also did not feature significant change, which might be because of insufficient connection between polymer and graphene particles (Bahmanyar et al., 2015).

Table AIII- 1: Thermal properties of EVA/G-like and EVA/CG composite obtained by DSC and TGA.

DSC results			TGA results		
Sample	Melting point, Tm (°C)	Xc (%)	T at 5 wt% loss (°C)	T at 50 wt % (°C)	Residue (wt) % at 550 °C
Pure EVA	87.0	20	378	482	0.2
EVA/G-like 20%	87.5	21	395	505	19.4
EVA/G-like 25%	86.9	22	397	507	24.1
EVA/G-like 30%	86.9	22	401	509	28.9
EVA/CG15%	87.5	21	385	486	14.6
EVA/CG15% S+E	87.6	21	384	485	14.5
EVA/CG20%	88.0	23	388	490	19.1
EVA/CG25%	89.0	23	389	493	24.3

The cross-section morphology images of EVA/G-like composites are shown in Figure AIII. 1. The addition of 25 wt% G-like formed some isolated/agglomerated regions within the composite, but the connections between the conductive fillers were not sufficient to form a conductive network (Figure AIII. 1c and Figure AIII. 1d). The conductive network was achieved for the EVA/G-like at a loading of 30wt%. As observed, the G-like flakes were overlapped together, and ultimately, the interconnection between particles led to the formation of a conductive network within the composite (Figure AIII. 1e and Figure AIII. 1f).

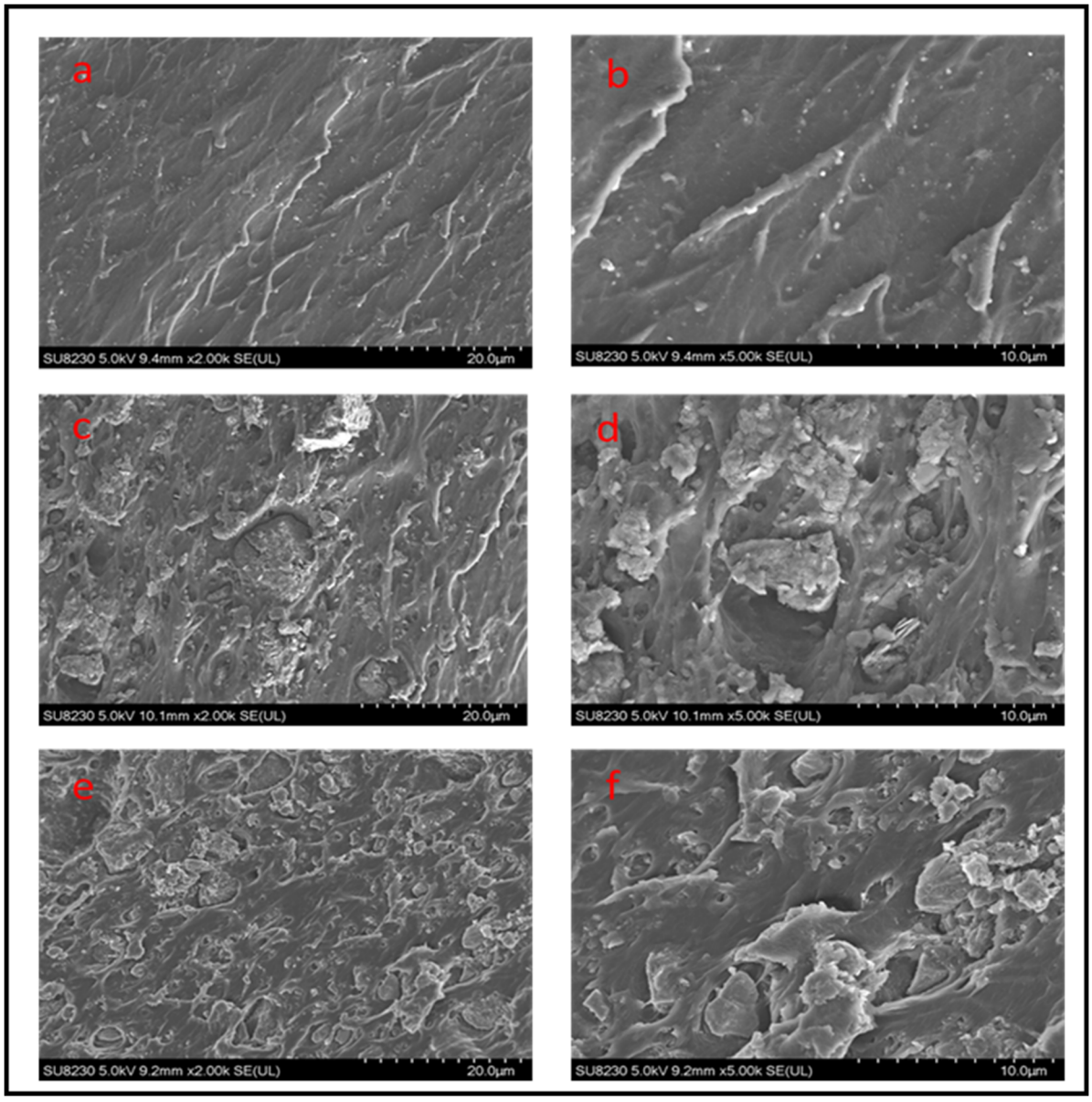

Figure AIII. 1 The SEM cross-section images of the pure EVA (a, b), the EVA/G-like 25% (c, d), and the EVA/G-like 30% (e, f) at 2K and 5K magnification for all samples

The real and imaginary permittivity of EVA/G-like composites is shown in Figure AIII. 2. As can be seen, below the percolation, the inclusion of G-like particles led to an increase of the dielectric losses, but with these losses staying relatively flat over the entire frequency range Figure AIII. 2b. The existence of the oxygenated groups in the G-like chemical structure (S. Azizi et al., 2017) and the intrinsic tendency of the graphene sheets to agglomerate prevented the formation of electric network up to 30 wt%. At 30wt% of G-like, a sharp increase of the

conductivity was observed as it can be seen in Figure AIII. 2b in the form of a significant rise of imaginary permittivity towards low frequencies.

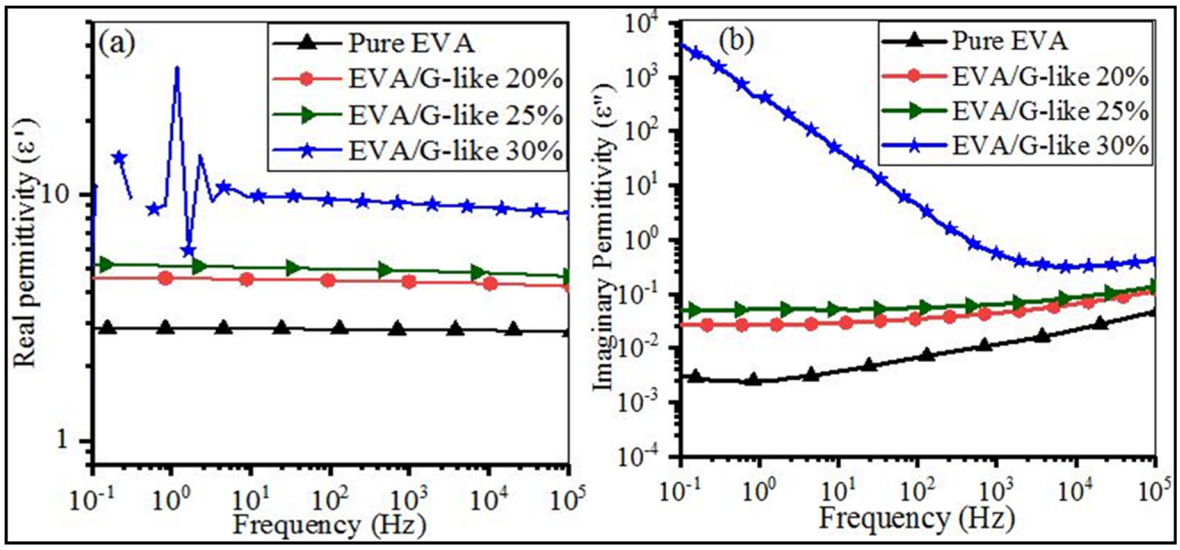

Figure AIII. 2 The BDS results of EVA/G-like: (a) the real permittivity and (b) the imaginary permittivity at room temperature

The frequency-domain dielectric response of CG-based composites was also investigated at different temperatures from 30 to 80 ºC. The relative imaginary permittivity of pure EVA is depicted in Figure AIII. 3a in the form of a tridimensional plot showing the contribution of the charge carrier in the high temperature/low frequency corner and the beginning of the α relaxation process in the opposite corner. Both EVA/CG15% (Figure AIII. 3b) and EVA/CG15% S+E (Figure AIII. 3c) showed a constant or flat dielectric loss response with relatively high losses but no sign of direct conduction. This behavior is quite intriguing as materials presenting flat dielectric responses, such as polyethylene or polypropylene, are also usually characterized by low losses.

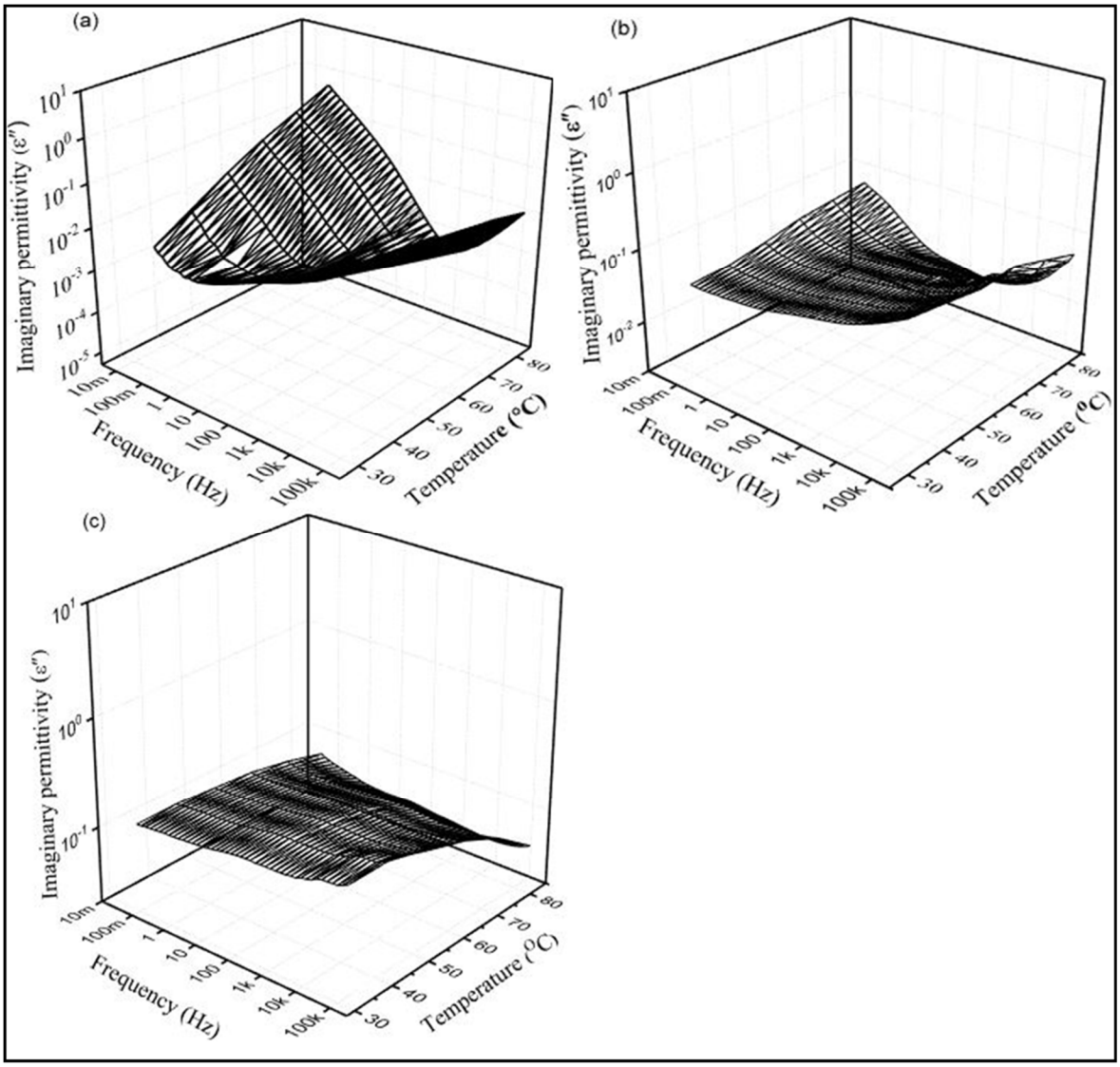

Figure AIII. 3 Tridimensional plots of dielectric losses of EVA polymer EVA/CG15% and EVA/CG15 S+E composites over a wide range of temperature

The EVA/CG20% (Figure AIII. 4a) sample exhibited a relaxation peak in the 1-10 Hz frequency range, which is related to interfacial relaxation processes between the matrix and the conductive aggregates (Kummali, Alegría, Miccio, & Colmenero, 2013). The peak was observed to slightly shift towards higher frequency as the temperature was increased, most likely leading to an increase of the agglomerate conductivity and consequently a decrease of the relaxation time. The rest of the dielectric response shown in Figure AIII. 4a is characterized by a rather flat-loss behavior similar to what was observed at 15wt%. One of the possible

explanations is that this behavior is the result of a large number of relaxation peak due to the heterogeneity of the size and properties of the aggregates and that the superposition of a multiple relaxation peaks leads to more or less constant dielectric loss response in the observed frequency range. At a loading of 25wt% of CG, a dominant contribution from charge carriers can be seen at low frequency and, surprisingly, at low temperature, as it can be seen in Figure AIII. 4b. As the temperature is increased, the conductivity was found to sharply decrease, possibly due to the thermal expansion creating a separation between the conductive particles otherwise in contact.

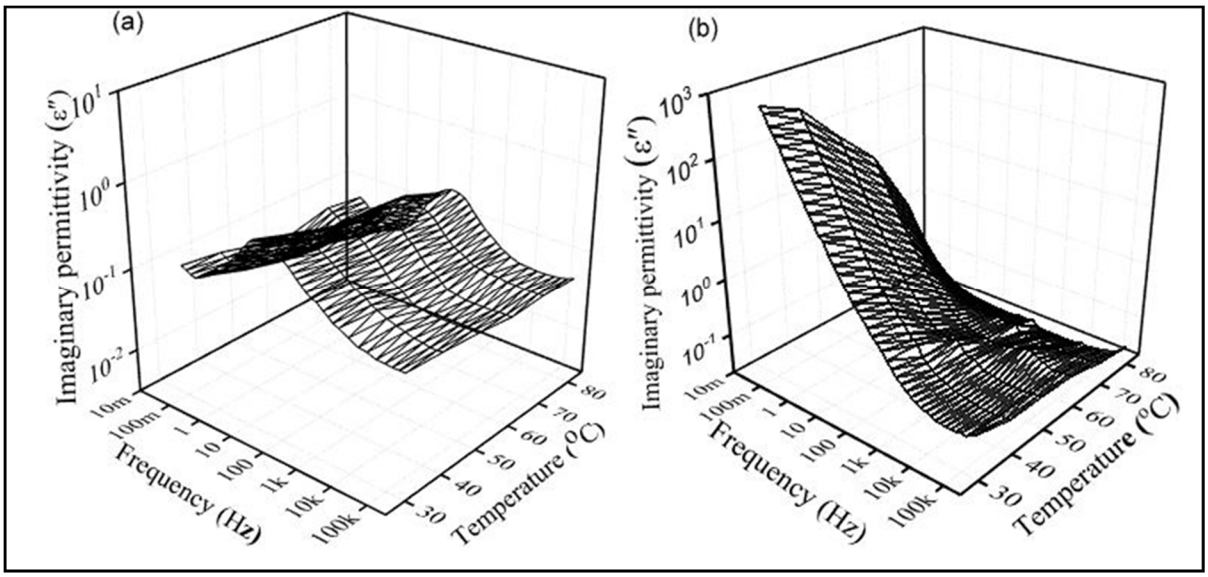

Figure AIII. 4 Tridimensional plots of dielectric losses of EVA/G20% S and EVA/CG25% composites over a wide range of temperature

Conclusion

Two types of graphene were compounded with ethylene vinyl acetate which led to different percolation threshold, the commercial graphene giving a lower percolation threshold than the graphene fabricated from clay and sugar. Graphene sheets observed by SEM micrographs revealed a significant tendency to re-agglomeration in the composite structure which might be possible to further disperse by using vigorous ultra-sonication. The dielectric response the

graphene composites at a concentration lower than the percolation threshold showed an intriguing constant-loss response over a large frequency and temperature range.

Acknowledgment

The Natural Sciences and Engineering Research Council of Canada (NSERC) is gratefully recognized for his financial support. The authors would also like to thank NanoXplore for providing the commercial graphene used in this report.

APPENDIX IV

EDUCATION

- **Doctor of Philosophy (Ph.D.) in engineering**. École de Technologie Supérieure (ÉTS). Supervisor: Prof. Claudiane M. Ouellet-Plamondon, Co-supervisors: Prof. Eric David, Dr. Michel Fréchette and Dr. Phuong Nguyen-Tri. From September 2016 to April 2019. Montréal, QC – Canada.

- **Master of Science (Msc.) in Polymer science and technology engineering**, Azad University, Supervisor: Prof. Ahmad Ramazani, Prof. Nouradin Goudarzian. From August 2013 to June 2015. Iran.

- **Bachelor of Science in Polymer Engineering**, Azad University, Supervisor: Prof. Nouradin Goudarzian. From August 2001 to June 2005. Iran.

AWARDS AND SCHOLARSHIPS

- 2019, SUBSTANCE award, selected research article.

- 2018. Centre de recherche sur les Systèmes Polymères et Composites (CREPEC) award, best poster presentation

- 2018. Conference on Electrical Insulation and Dielectric Phenomena (CEIDP). Conference travel award.

- 2016. Three years of ETS scholarship.

APPENDIX V

PERSONAL PUBLICATION LIST
JOURNAL PUBLICATIONS

- **Sohrab Azizi**, Eric David, Michel F. Fréchette, Phuong Nguyen-Tri, Claudiane M. Ouellet-Plamondon (2018). "Electrical and thermal phenomena in low-density polyethylene/carbon black composites near the percolation threshold." Journal of Applied Polymer Science: 47043.

- **Sohrab Azizi**, Eric David, Michel F. Fréchette, Phuong Nguyen-Tri, Claudiane M. Ouellet-Plamondon (2018). "Electrical and thermal conductivity of ethylene vinyl acetate composite with graphene and carbon black filler." Polymer Testing.

- **Sohrab Azizi**, Claudiane M. Ouellet-Plamondon, Michel F. Fréchette, Phuong Nguyen-Tri, Eric David (2018). "Electrical, thermal and rheological properties of low-density polyethylene/ethylene vinyl acetate/graphene-like composite, submitted to Composite Part B Journal.

- **Sohrab Azizi**, Éric David, Michel F. Fréchette, Claudiane M. Ouellet-Plamondon. Numerical Simulation of the Effective Permittivity of LDPE Composite Filled by Carbon Black. Submitted to IET Nanodielectrics journal.

CONFERENCE PUBLICATION

- **Sohrab Azizi**, Claudiane Ouellet-Plamondon, Eric David, Michel F. Fréchette (2017). Electrical and thermal properties of low-density polyethylene/graphene-like composite.

Electrical Insulation and Dielectric Phenomenon (CEIDP), 2017 IEEE Conference on, IEEE.

- **Sohrab Azizi**, Claudiane Ouellet-Plamondon, Eric David, Michel F. Fréchette (2018). Electric response and thermal properties of Ethylene Vinyl Acetate/Graphene-based Composite. CEIDP 2018

- Boussaboun, Zakaria, **Sohrab Azizi,** Claudiane Ouellet-Plamondon (2017). Conductive clay containing graphene layers. Nanotechnology (IEEE-NANO), 2017 IEEE 17th International Conference on, IEEE.

BIBLIOGRAPHY

Alegria, A., & Colmenero, J. (2016). Dielectric relaxation of polymers: segmental dynamics under structural constraints. *Soft matter, 12*(37), 7709-7725.

Amini, A., & Bahreyni, B. (2012). Behavioral model for electrical response and strain sensitivity of nanotube-based nanocomposite materials. *Journal of Vacuum Science & Technology B, Nanotechnology and Microelectronics: Materials, Processing, Measurement, and Phenomena, 30*(2), 022001.

Anh, T. T., Fréchette, M., David, É., & Ouellet-Plamondon, C. (2016). *Impact of nature and preparation method of graphene on the electrical behavior of LDPE/Graphene composites.* Paper presented at the Electrical Insulation and Dielectric Phenomena (CEIDP), 2016 IEEE Conference on.

Atif, R., & Inam, F. (2016). Modeling and simulation of graphene based polymer nanocomposites: advances in the last decade. *Graphene, 5*(2), 96-142.

Azizi, M., Ramazani, S. A., Etemadi, M. H., & Shirzaei, S. E. (2013). Simulation of viscoelastic fluid flows in expansion geometry using finite volume approach. *Chinese Journal of Polymer Science, 31*(12), 1599-1612.

Azizi, M., Zolfaghari Sharak, A., Mousavi, S. A., Bakhtiari Ziabari, F., Shariati, J., & Azizi, S. (2013). Study on the acetylene hydrogenation process for ethylene production: Simulation, modification, and optimization. *Chemical Engineering Communications, 200*(7), 863-877.

Azizi, S., David, E., Fréchette, M. F., Nguyen-Tri, P., & Ouellet-Plamondon, C. (2018). Electrical and thermal conductivity of ethylene vinyl acetate composite with graphene and carbon black filler. *Polymer Testing*.

Azizi, S., David, E., Fréchette, M. F., Nguyen-Tri, P., & Ouellet-Plamondon, C. M. (2018). Electrical and thermal phenomena in low-density polyethylene/carbon black composites near the percolation threshold. *Journal of Applied Polymer Science*, 47043.

Azizi, S., Ouellet-Plamondon, C., David, E., & Fréchette, M. Electric Response and Thermal Properties of Ethylene Vinyl Acetate/Graphene-based Composite.

Azizi, S., Ouellet-Plamondon, C., David, E., & Fréchette, M. (2017). *Electrical and thermal properties of low-density polyethylene/graphene-like composite.* Paper presented at the Electrical Insulation and Dielectric Phenomenon (CEIDP), 2017 IEEE Conference on.

Badiee, A., Ashcroft, I. A., & Wildman, R. D. (2016). The thermo-mechanical degradation of ethylene vinyl acetate used as a solar panel adhesive and encapsulant. *International Journal of Adhesion and Adhesives, 68*, 212-218. doi: 10.1016/j.ijadhadh.2016.03.008

Bahmanyar, M., Ramazani SA, A., & Baniasadi, H. (2015). Preparation and Properties of Ethylene-vinyl Acetate/linear Low-density Polyethylene/Graphene Oxide Nanocomposite Films. *Polymer-Plastics Technology and Engineering, 54*(11), 1152-1158.

Bakar, N. A., Chee, C. Y., Abdullah, L. C., Ratnam, C. T., & Ibrahim, N. A. (2015). Thermal and dynamic mechanical properties of grafted kenaf filled poly (vinyl chloride)/ethylene vinyl acetate composites. *Materials & Design (1980-2015), 65*, 204-211.

Bao, W., Meguid, S., Zhu, Z., & Meguid, M. (2011). Modeling electrical conductivities of nanocomposites with aligned carbon nanotubes. *Nanotechnology, 22*(48), 485704.

Bazaka, K., Jacob, M. V., & Ostrikov, K. (2015). Sustainable life cycles of natural-precursor-derived nanocarbons. *Chemical reviews, 116*(1), 163-214.

Bellucci, F., Fabiani, D., Montanari, G., & Testa, L. (2010). The processing of nanocomposites *Dielectric Polymer Nanocomposites* (pp. 31-64): Springer.

Borisova, B., & Kressler, J. (2003). Environmental Stress-Cracking Resistance of LDPE/EVA Blends. *Macromolecular Materials and Engineering, 288*(6), 509-515.

Boussaboun, Z., Azizi, S., & Ouellet-Plamondon, C. (2017). *Conductive clay containing graphene layers*. Paper presented at the Nanotechnology (IEEE-NANO), 2017 IEEE 17th International Conference on.

Bueche, F. (1973). A new class of switching materials. *Journal of Applied Physics, 44*(1), 532-533.

Burger, N., Laachachi, A., Ferriol, M., Lutz, M., Toniazzo, V., & Ruch, D. (2016). Review of thermal conductivity in composites: mechanisms, parameters and theory. *Progress in Polymer Science, 61*, 1-28.

Cai, Z., Wang, X., Luo, B., Hong, W., Wu, L., & Li, L. (2017a). Dielectric response and breakdown behavior of polymer-ceramic nanocomposites: The effect of nanoparticle distribution. *Composites Science and Technology, 145*, 105-113.

Cai, Z., Wang, X., Luo, B., Hong, W., Wu, L., & Li, L. (2017b). Nanocomposites with enhanced dielectric permittivity and breakdown strength by microstructure design of nanofillers. *Composites Science and Technology, 151*, 109-114.

Calegari, F., de Souza, L. P., Barsan, M. M., Brett, C. M., Marcolino-Junior, L. H., & Bergamini, M. F. (2017). Construction and evaluation of carbon black and poly (ethylene co-vinyl) acetate (EVA) composite electrodes for development of electrochemical (bio) sensors. *Sensors and Actuators B: Chemical, 253*, 10-18.

Carastan, D. J., & Demarquette, N. R. (2006). *Microstructure of nanocomposites of styrenic polymers*. Paper presented at the Macromolecular symposia.

Chen, B.-Y., & Hwang, K.-S. (2010). Comparative study of carbon black and graphite powder as carbon source for PM compacts. *Powder Metallurgy, 53*(1), 51-56.

Chen, G. H., Wu, D. J., Weng, W. G., He, B., & Yan, W. l. J. P. I. (2001). Preparation of polystyrene–graphite conducting nanocomposites via intercalation polymerization. *50*(9), 980-985.

Christen, T., Donzel, L., & Greuter, F. (2010). Nonlinear resistive electric field grading part 1: Theory and simulation. *IEEE Electrical Insulation Magazine, 26*(6).

Coelho, P. H. d. S. L., Armellini, V. A. d. D., & Morales, A. R. (2017). Assessment of Percolation Threshold Simulation for Individual and Hybrid Nanocomposites of Carbon Nanotubes and Carbon Black. *Materials Research, 20*(6), 1638-1649.

Coleman, M. (2017). *Specific interactions and the miscibility of polymer blends*: Routledge.

Çopuroğlu, M., & Şen, M. (2005). A comparative study of UV aging characteristics of poly (ethylene-co-vinyl acetate) and poly (ethylene-co-vinyl acetate)/carbon black mixture. *Polymers for Advanced Technologies, 16*(1), 61-66.

Costache, M. C., Jiang, D. D., & Wilkie, C. A. (2005). Thermal degradation of ethylene–vinyl acetate coplymer nanocomposites. *Polymer, 46*(18), 6947-6958.

Crompton, T. R. (2012). *Thermal Stability of Polymers*: Smithers Rapra.

Czaniková, K., Špitalský, Z., Krupa, I., & Omastová, M. (2012). *Electrical and mechanical properties of ethylene vinyl acetate based composites.* Paper presented at the Materials Science Forum.

Dakin, T. (2006). Conduction and polarization mechanisms and trends in dielectric. *IEEE Electrical Insulation Magazine, 22*(5), 11-28.

Dalai, S., & Wenxiu, C. (2002). Radiation effects on LDPE/EVA blends. *Journal of Applied Polymer Science, 86*(5), 1296-1302.

Dang, Z.-M., Yuan, J.-K., Zha, J.-W., Zhou, T., Li, S.-T., & Hu, G.-H. (2012). Fundamentals, processes and applications of high-permittivity polymer–matrix composites. *Progress in Materials Science, 57*(4), 660-723.

Dang, Z. M., Yuan, J. K., Yao, S. H., & Liao, R. J. (2013). Flexible nanodielectric materials with high permittivity for power energy storage. *Advanced Materials, 25*(44), 6334-6365.

Das, N., Chaki, T., & Khastgir, D. (2003). Effect of filler treatment and crosslinking on mechanical and dynamic mechanical properties and electrical conductivity of carbon black-filled ethylene-vinyl acetate copolymer composites. *Journal of Applied Polymer Science, 90*(8), 2073-2082.

Dash, B. K., Achary, P. G. R., & Nayak, N. C. (2015). Dielectric relaxation behaviour of ethylene-vinyl acetate–exfoliated graphene nanoplatelets (xGnP) composites. *Journal of Materials Science: Materials in Electronics, 26*(9), 7244-7254.

David, E., & Fréchette, M. (2013). Polymer nanocomposites-major conclusions and achievements reached so far. *IEEE Electrical Insulation Magazine, 29*(6), 29-36.

de Oliveira, M. C. C., Diniz, A. S. A. C., Viana, M. M., & Lins, V. d. F. C. (2017). The causes and effects of degradation of encapsulant ethylene vinyl acetate copolymer (EVA) in crystalline silicon photovoltaic modules: A review. *Renewable and Sustainable Energy Reviews*.

Di, W., Zhang, G., Xu, J., Peng, Y., Wang, X., & Xie, Z. (2003). Positive-temperature-coefficient/negative-temperature-coefficient effect of low-density polyethylene filled with a mixture of carbon black and carbon fiber. *Journal of Polymer Science Part B: Polymer Physics, 41*(23), 3094-3101.

Dissado, L. A., & Fothergill, J. C. (1992). *Electrical degradation and breakdown in polymers* (Vol. 9): IET.

Dong, Y., Umer, R., & Lau, A. K. T. (2015). *Fillers and Reinforcements for Advanced Nanocomposites*: Woodhead Publishing.

Donzel, L., Greuter, F., & Christen, T. (2011). Nonlinear resistive electric field grading Part 2: Materials and applications. *IEEE Electrical Insulation Magazine, 27*(2).

Dudić, D., Škipina, B., Dojčilović, J., Novaković, L., & Kostoski, D. (2011). Effects of charge trapping on the electrical conductivity of low-density polyethylene–carbon black composites. *Journal of Applied Polymer Science, 121*(1), 138-143.

Ezquerra, T. A., Connor, M. T., Roy, S., Kulescza, M., Fernandes-Nascimento, J., Baltá-Calleja, F. J. J. C. s., & technology. (2001). Alternating-current electrical properties of graphite, carbon-black and carbon-fiber polymeric composites. *61*(6), 903-909.

Faker, M., Aghjeh, M. R., Ghaffari, M., & Seyyedi, S. (2008). Rheology, morphology and mechanical properties of polyethylene/ethylene vinyl acetate copolymer (PE/EVA) blends. *European Polymer Journal, 44*(6), 1834-1842.

Fathi, A., Hatami, K., & Grady, B. P. (2012). Effect of carbon black structure on low-strain conductivity of polypropylene and low-density polyethylene composites. *Polymer Engineering & Science, 52*(3), 549-556.

Feller, J. F., Bruzaud, S., & Grohens, Y. (2004). Influence of clay nanofiller on electrical and rheological properties of conductive polymer composite. *Materials Letters, 58*(5), 739-745. doi: 10.1016/j.matlet.2003.07.010

Fim, F. d. C., Basso, N. R., Graebin, A. P., Azambuja, D. S., & Galland, G. B. (2013). Thermal, electrical, and mechanical properties of polyethylene–graphene nanocomposites obtained by in situ polymerization. *Journal of Applied Polymer Science, 128*(5), 2630-2637.

Foulger, S. H. (1998). *Reduced percolation thresholds of immiscible conductive blends of poly (ethylene-co-vinyl acetate) and high density polyethylene.* Paper presented at the Electrical Insulation and Dielectric Phenomena, 1998. Annual Report. Conference on.

Foulger, S. H. (1999). Reduced percolation thresholds of immiscible conductive blends. *Journal of Polymer Science Part B: Polymer Physics, 37*(15), 1899-1910.

Frache, A., Monticelli, O., Ceccia, S., Brucellaria, A., & Casale, A. (2008). Preparation of nanocomposites based on PP and PA6 by direct injection molding. *Polymer Engineering & Science, 48*(12), 2373-2381.

Fréchette, M., Vanga-Bouanga, C., Fabiani, D., Castellon, J., & Diaham, S. (2015). *Graphene-based polymer composites: What about it for the HV electrotechnical arena?* Paper presented at the 2015 IEEE Electrical Insulation Conference (EIC).

Fréchette, M., Veillette, R., Trudeau, M., Pirondelli, A., Fabiani, D., Anh, T. T., . . . Castellon, J. (2016). *Dielectric design of LDPE properties: With the help of double-core Si/SiO 2 and Carbon Black.* Paper presented at the Electrical Insulation and Dielectric Phenomena (CEIDP), 2016 IEEE Conference on.

Furushima, Y., Nakada, M., Murakami, M., Yamane, T., Toda, A., & Schick, C. (2015). Method for calculation of the lamellar thickness distribution of not-reorganized linear polyethylene using fast scanning calorimetry in heating. *Macromolecules, 48*(24), 8831-8837.

Gabbott, P. (2008). *Principles and applications of thermal analysis*: John Wiley & Sons.

Gaska, K., Xu, X., Gubanski, S., & Kádár, R. (2017). Electrical, Mechanical, and Thermal Properties of LDPE Graphene Nanoplatelets Composites Produced by Means of Melt Extrusion Process. *Polymers, 9*(1), 11.

George, J., & Bhowmick, A. K. (2008). Fabrication and properties of ethylene vinyl acetate-carbon nanofiber nanocomposites. *Nanoscale research letters, 3*(12), 508.

George, J. J., Bhadra, S., & Bhowmick, A. K. (2010). Influence of carbon-based nanofillers on the electrical and dielectric properties of ethylene vinyl acetate nanocomposites. *Polymer Composites, 31*(2), 218-225.

George, J. J., & Bhowmick, A. K. (2008). Ethylene vinyl acetate/expanded graphite nanocomposites by solution intercalation: preparation, characterization and properties. *Journal of Materials Science, 43*(2), 702-708.

Ghislandi, M., Tkalya, E., Marinho, B., Koning, C. E., de With, G. J. C. P. A. A. S., & Manufacturing. (2013). Electrical conductivities of carbon powder nanofillers and their latex-based polymer composites. *53*, 145-151.

Ghose, S., Watson, K. A., Working, D. C., Connell, J. W., Smith, J. G., & Sun, Y. P. (2008). Thermal conductivity of ethylene vinyl acetate copolymer/nanofiller blends. *Composites Science and Technology, 68*(7-8), 1843-1853. doi: 10.1016/j.compscitech.2008.01.016

Gil-González, E., Perejón, A., Sanchez-Jimenez, P. E., Medina-Carrasco, S., Kupčík, J., Šubrt, J., . . . Pérez-Maqueda, L. A. (2018). Crystallization kinetics of nanocrystalline materials by combined X-ray diffraction and differential scanning calorimetry experiments. *Crystal Growth & Design, 18*(5), 3107-3116.

Gill, P., Moghadam, T. T., & Ranjbar, B. (2010). Differential scanning calorimetry techniques: applications in biology and nanoscience. *Journal of biomolecular techniques: JBT, 21*(4), 167.

Gkourmpis, T., Svanberg, C., Kaliappan, S. K., Schaffer, W., Obadal, M., Kandioller, G., & Tranchida, D. (2013). Improved electrical and flow properties of conductive polyolefin blends: Modification of poly (ethylene vinyl acetate) copolymer/carbon black with ethylene–propylene copolymer. *European Polymer Journal, 49*(8), 1975-1983.

Göldel, A., Kasaliwal, G., & Pötschke, P. J. M. r. c. (2009). Selective localization and migration of multiwalled carbon nanotubes in blends of polycarbonate and poly (styrene-acrylonitrile). *30*(6), 423-429.

Gulrez, S. K., Ali Mohsin, M., Shaikh, H., Anis, A., Pulose, A. M., Yadav, M. K., . . . Al-Zahrani, S. (2014). A review on electrically conductive polypropylene and polyethylene. *Polymer Composites, 35*(5), 900-914.

Håkansson, E., Amiet, A., Nahavandi, S., & Kaynak, A. (2007). Electromagnetic interference shielding and radiation absorption in thin polypyrrole films. *European Polymer Journal, 43*(1), 205-213.

Han, Z., & Fina, A. (2011). Thermal conductivity of carbon nanotubes and their polymer nanocomposites: a review. *Progress in Polymer Science, 36*(7), 914-944.

Haurie, L., Fernández, A. I., Velasco, J. I., Chimenos, J. M., Cuesta, J.-M. L., & Espiell, F. (2007). Thermal stability and flame retardancy of LDPE/EVA blends filled with synthetic hydromagnesite/aluminium hydroxide/montmorillonite and magnesium hydroxide/aluminium hydroxide/montmorillonite mixtures. *Polymer Degradation and Stability, 92*(6), 1082-1087.

He, L. X., & Tjong, S. C. (2011). Nonlinear electrical conduction in percolating systems induced by internal field emission. *Synthetic metals, 161*(5-6), 540-543. doi: 10.1016/j.synthmet.2010.12.007

Heid, T., Fréchette, M., & David, E. (2015). Epoxy/BN micro-and submicro-composites: dielectric and thermal properties of enhanced materials for high voltage insulation systems. *IEEE Transactions on Dielectrics and Electrical Insulation, 22*(2), 1176-1185.

Helal, E., Demarquette, N. R., David, E., & Fréchette, M. (2016). *Evaluation of dielectric behavior of polyethylene/thermoplastic elastomer blends containing zinc oxide (ZnO) nanoparticles for high voltage insulation.* Paper presented at the IEEE Electrical Insulation Conference (EIC), 2016.

Helal, E., Pottier, C., David, E., Fréchette, M., & Demarquette, N. (2018). Polyethylene/Thermoplastic elastomer/Zinc Oxide nanocomposites for high voltage

insulation applications: Dielectric, mechanical and rheological behavior. *European Polymer Journal*.

Henderson, A. M. (1993). Ethylene-vinyl acetate (EVA) copolymers: a general review. *IEEE Electrical Insulation Magazine, 9*(1), 30-38.

Hindermann-Bischoff, M., & Ehrburger-Dolle, F. (2001). Electrical conductivity of carbon black–polyethylene composites. *Carbon, 39*(3), 375-382. doi: 10.1016/s0008-6223(00)00130-5

Hoang, L. T., Leung, S. N., & Zhu, Z. H. (2018). Eliminating common biases in modelling the electrical conductivity of carbon nanotube–polymer nanocomposites. *Physical Chemistry Chemical Physics, 20*(19), 13118-13121.

Hojjat, A., & Mahmood, B. (2015). Effect of EVA content upon the dielectric properties in LDPE-EVA Films. *International Journal of Engineering Research, 4*(2), 69-72.

Hotta, M., Hayashi, M., Lanagan, M. T., Agrawal, D. K., & Nagata, K. (2011). Complex permittivity of graphite, carbon black and coal powders in the ranges of X-band frequencies (8.2 to 12.4 GHz) and between 1 and 10 GHz. *ISIJ international, 51*(11), 1766-1772.

Hou, Y. H., Zhang, M. Q., & Rong, M. Z. (2003). Performance stabilization of conductive polymer composites. *Journal of Applied Polymer Science, 89*(9), 2438-2445.

Hou, Y. H., Zhang, M. Q., Rong, M. Z., Yu, G., & Zeng, H. M. (2002). Improvement of conductive network quality in carbon black-filled polymer blends. *Journal of Applied Polymer Science, 84*(14), 2768-2775.

Hu, E., Hu, X., Liu, T., Liu, Y., Song, R., & Chen, Y. (2013). Investigation of morphology, structure and composition of biomass-oil soot particles. *Applied Surface Science, 270*, 596-603.

Huang, C., Qian, X., & Yang, R. (2018). Thermal conductivity of polymers and polymer nanocomposites. *arXiv preprint arXiv:1805.05561*.

Huang, C. L., Chen, Y. C., Wang, C., Tu, C. F., & Liao, F. S. (2013). Structural variations and morphological features of polyethylene/carbon black conductive composites after processing in an internal mixer. *Journal of Applied Polymer Science, 130*(2), 1038-1046.

Huang, J. C., & Wu, C. L. (2000). Processability, mechanical properties, and electrical conductivities of carbon black-filled ethylene-vinyl acetate copolymers. *Advances in Polymer Technology, 19*(2), 132-139.

Huang, X., Jiang, P., & Tanaka, T. (2011). A review of dielectric polymer composites with high thermal conductivity. *IEEE Electrical Insulation Magazine, 27*(4).

Huang, X., & Zhi, C. (2016). Polymer Nanocomposites.

Huang, Y., Jiang, S., Wu, L., & Hua, Y. (2004). Characterization of LLDPE/nano-SiO 2 composites by solid-state dynamic mechanical spectroscopy. *Polymer Testing, 23*(1), 9-15.

Huang, Y., Krentz, T. M., Nelson, J. K., Schadler, L. S., Li, Y., Zhao, H., . . . Wu, K. (2014). *Prediction of interface dielectric relaxations in bimodal brush functionalized epoxy nanodielectrics by finite element analysis method.* Paper presented at the Electrical Insulation and Dielectric Phenomena (CEIDP), 2014 IEEE Conference on.

Isayev, A. I. (2016). *Encyclopedia of Polymer Blends, Volume 3: Structure* (Vol. 3): John Wiley & Sons.

Jacob George, J., Bandyopadhyay, A., & Bhowmick, A. K. (2008). New generation layered nanocomposites derived from ethylene-co-vinyl acetate and naturally occurring graphite. *Journal of Applied Polymer Science, 108*(3), 1603-1616.

Jia, L. C., Yan, D. X., Cui, C. H., Ji, X., & Li, Z. M. (2016). A unique double percolated polymer composite for highly efficient electromagnetic interference shielding. *Macromolecular Materials and Engineering, 301*(10), 1232-1241.

Jiang, X., & Drzal, L. T. (2012). Reduction in percolation threshold of injection molded high-density polyethylene/exfoliated graphene nanoplatelets composites by solid state ball milling and solid state shear pulverization. *Journal of Applied Polymer Science, 124*(1), 525-535.

Jin, Y., & Gerhardt, R. A. (2014). Percolation and Electrical Conductivity Modeling of Novel Microstructured Insulator-Conductor Nanocomposites Fabricated from PMMA and ATO. *MRS Online Proceedings Library Archive, 1692*.

Jonscher, A. K. (1996). *Universal relaxation law: a sequel to Dielectric relaxation in solids*: Chelsea Dielectrics Press.

Jonscher, A. K. (1999). Dielectric relaxation in solids. *Journal of Physics D: Applied Physics, 32*(14), R57.

Jylha, L., & Sihvola, A. H. (2005). Numerical modeling of disordered mixture using pseudorandom simulations. *IEEE Transactions on geoscience and remote sensing, 43*(1), 59-64.

Jyoti, J., Kumar, A., Dhakate, S., & Singh, B. P. (2018). Dielectric and impedance properties of three dimension graphene oxide-carbon nanotube acrylonitrile butadiene styrene hybrid composites. *Polymer Testing, 68*, 456-466.

Kalaitzidou, K., Fukushima, H., & Drzal, L. (2006). *Multifunctional nanocomposites made of polypropylene reinforced with exfoliated graphite nanoplatelets (xGnP)*. Paper presented at the NSTI Nanotech.

Khanam, P. N., AlMaadeed, M., Ouederni, M., Harkin-Jones, E., Mayoral, B., Hamilton, A., & Sun, D. (2016). Melt processing and properties of linear low density polyethylene-graphene nanoplatelet composites. *Vacuum, 130*, 63-71.

Khobragade, P. S., Hansora, D., Naik, J. B., Njuguna, J., & Mishra, S. (2017). Effect of multilayered nanostructures on the physico-mechanical properties of ethylene vinyl acetate-based hybrid nanocomposites. *Polymer Composites*.

Kim, C.-K., Sood, V. K., Jang, G.-S., Lim, S.-J., & Lee, S.-J. (2009). *HVDC transmission: power conversion applications in power systems*: John Wiley & Sons.

Kim, H., Abdala, A. A., & Macosko, C. W. (2010). Graphene/polymer nanocomposites. *Macromolecules, 43*(16), 6515-6530.

Kim, H. S., Bae, H. S., Yu, J., & Kim, S. Y. (2016). Thermal conductivity of polymer composites with the geometrical characteristics of graphene nanoplatelets. *Scientific reports, 6*, 26825.

Klaus Friedrich, U. B. (2014). Multifunctionality of Polymer Composites Challenges and New Solutions. *Elsivier*.

Kochetov, R., Andritsch, T., Morshuis, P. H. F., & Smit, J. J. (2012). Anomalous Behaviour of the Dielectric Spectroscopy Response of Nanocomposites. *IEEE Transactions on Dielectrics and Electrical Insulation, 19*(1), 107-117. doi: Doi 10.1109/Tdei.2012.6148508

Kondawar, S. B. (2015). *Conducting Polymer Nanocomposites for Supercapacitors*: Smithers Rapra.

Kontopoulou, M. (2011). *Applied polymer rheology: polymeric fluids with industrial applications*: John Wiley & Sons.

Koo, J. H. (2006). *Polymer nanocomposites*: McGraw-Hill Professional Pub.

Kremer, F., Huwe, A., Schönhals, A., & Rózanski, S. (2012). *6 Molecular Dynamics in Confining Space*: Springer.

Krishnamoorti, R., & Giannelis, E. P. (1997). Rheology of end-tethered polymer layered silicate nanocomposites. *Macromolecules, 30*(14), 4097-4102.

Kuila, T., Khanra, P., Mishra, A. K., Kim, N. H., & Lee, J. H. (2012). Functionalized-graphene/ethylene vinyl acetate co-polymer composites for improved mechanical and thermal properties. *Polymer Testing, 31*(2), 282-289.

Kuilla, T., Bhadra, S., Yao, D., Kim, N. H., Bose, S., & Lee, J. H. (2010). Recent advances in graphene based polymer composites. *Progress in Polymer Science, 35*(11), 1350-1375.

Kummali, M. M., Alegría, A., Miccio, L. A., & Colmenero, J. (2013). Study of the Dynamic Heterogeneity in Poly (ethylene-ran-vinyl acetate) Copolymer by Using Broadband Dielectric Spectroscopy and Electrostatic Force Microscopy. *Macromolecules, 46*(18), 7502-7512.

Kurusu, R. S., Helal, E., Moghimian, N., David, E., & Demarquette, N. (2018). The Role of Selectively Located Commercial Graphene Nanoplatelets in the Electrical Properties, Morphology, and Stability of EVA/LLDPE Blends. *Macromolecular Materials and Engineering*, 1800187.

le Reinders, A., Verlinden, P., & Freundlich, A. (2017). *Photovoltaic Solar Energy: From Fundamentals to Applications*: John Wiley & Sons.

Lei, H., Liu, Z., He, C., Zhang, S.-C., Liu, Y.-Q., Hua, C.-J., . . . Cai, R. (2016). Graphene enhanced low-density polyethylene by pretreatment and melt compounding. *RSC Advances, 6*(103), 101492-101500.

Li, B., Xu, X. B., Li, Z. M., & Song, Y. C. (2008). Manipulating the conductivity of carbon-black-filled immiscible polymer composites by insulating nanoparticles. *Journal of Applied Polymer Science, 110*(5), 3073-3079.

Li, X., Cai, W., Colombo, L., & Ruoff, R. S. (2009). Evolution of graphene growth on Ni and Cu by carbon isotope labeling. *Nano letters, 9*(12), 4268-4272.

Lisunova, M., Mamunya, Y. P., Lebovka, N., & Melezhyk, A. J. E. P. J. (2007). Percolation behaviour of ultrahigh molecular weight polyethylene/multi-walled carbon nanotubes composites. *43*(3), 949-958.

Long, G., Tang, C., Wong, K.-w., Man, C., Fan, M., Lau, W.-m., . . . Wang, B. J. G. C. (2013). Resolving the dilemma of gaining conductivity but losing environmental friendliness in producing polystyrene/graphene composites via optimizing the matrix-filler structure. *15*(3), 821-828.

Louis, P., & Gokhale, A. (1996). Computer simulation of spatial arrangement and connectivity of particles in three-dimensional microstructure: application to model electrical conductivity of polymer matrix composite. *Acta materialia, 44*(4), 1519-1528.

Ma, F. L., Han, B. Z., Wang, Y. J., & Jiang, H. (2009). Effect of Magnetic Field on Conductivity Properties of Carbon Filler/LDPE Composites. *Icpadm 2009:*

Proceedings of the 9th International Conference on Properties and Applications of Dielectric Materials, Vols 1-3, 1192-1195. doi: 10.1109/icpadm.2009.5252287

Mancinelli, P., Santangelo, V., Fabiani, D., Saccani, A., Toselli, M., & Frechette, M. (2014). *LDPE composite materials obtained from building blocks containing standardized graphene interfaces.* Paper presented at the Electrical Insulating Materials (ISEIM), Proceedings of 2014 International Symposium on.

Mazzanti, G., & Marzinotto, M. (2013). *Extruded cables for high-voltage direct-current transmission: advances in research and development* (Vol. 93): John Wiley & Sons.

Menard, K. P. (2008). *Dynamic mechanical analysis: a practical introduction*: CRC press.

Méndez, R., Constant, B., Garzon, C., Nisar, M., Nachtigall, S. M. B., & Quijada, R. (2017). Barrier, mechanical and conductive properties of polycaprolactam nanocomposites containing carbon-based particles: Effect of the kind of particle. *Polymer, 130*, 10-16.

Mensah, B., Gupta, K. C., Kim, H., Wang, W., Jeong, K.-U., & Nah, C. (2018). Graphene-reinforced elastomeric nanocomposites: A review. *Polymer Testing, 68*, 160-184.

Meszlényi, G., & Körtvélyessy, G. (1999). Direct determination of vinyl acetate content of ethylene-vinyl acetate copolymers in thick films by infrared spectroscopy. *Polymer Testing, 18*(7), 551-557.

Mittal, V. (2011). *In-situ synthesis of polymer nanocomposites*: John Wiley & Sons.

Moalleminejad, M., & Chung, D. (2015). Dielectric constant and electrical conductivity of carbon black as an electrically conductive additive in a manganese-dioxide electrochemical electrode, and their dependence on electrolyte permeation. *Carbon, 91*, 76-87.

Mofokeng, T. G., Ray, S. S., & Ojijo, V. (2018). Influence of Selectively Localised Nanoclay Particles on Non-Isothermal Crystallisation and Degradation Behaviour of PP/LDPE Blend Composites. *Polymers, 10*(3), 245.

Mondal, S., Ganguly, S., Rahaman, M., Aldalbahi, A., Chaki, T. K., Khastgir, D., & Das, N. C. (2016). A strategy to achieve enhanced electromagnetic interference shielding at low concentration with a new generation of conductive carbon black in a chlorinated polyethylene elastomeric matrix. *Physical Chemistry Chemical Physics, 18*(35), 24591-24599. doi: 10.1039/c6cp04274k

Mondal, S., Nayak, L., Rahaman, M., Aldalbahi, A., Chaki, T. K., Khastgir, D., & Das, N. C. (2017). An effective strategy to enhance mechanical, electrical, and electromagnetic shielding effectiveness of chlorinated polyethylene-carbon nanofiber nanocomposites. *Composites Part B-Engineering, 109*, 155-169. doi: 10.1016/j.compositesb.2016.10.049

Mora, A., Han, F., & Lubineau, G. (2018). Computational modeling of electrically conductive networks formed by graphene nanoplatelet–carbon nanotube hybrid particles. *Modelling and Simulation in Materials Science and Engineering, 26*(3), 035010.

Myroshnychenko, V., & Brosseau, C. (2005). Finite-element method for calculation of the effective permittivity of random inhomogeneous media. *Physical Review E, 71*(1), 016701.

Mysiukiewicz, O., Sterzyński, T., Ławniczak, P., & Rogodzińska, M. (2017). Electrical conductivity and mechanical properties of carbon black modified polyolefinic blends influenced by phase inversion. *Journal of Applied Polymer Science, 134*(46).

Nakamura, S., & Sawa, G. (1998). Percolation phenomena and electrical conduction mechanism of carbon black-polyethylene composites. *1998 International Symposium on Electrical Insulating Materials, Proceedings*, 333-336. doi: Doi 10.1109/Iseim.1998.741753

Nilsson, F., Gedde, U., & Hedenqvist, M. (2011). Modelling the relative permittivity of anisotropic insulating composites. *Composites Science and Technology, 71*(2), 216-221.

Nilsson, F., Krueckel, J., Schubert, D. W., Chen, F., Unge, M., Gedde, U. W., & Hedenqvist, M. S. (2016). Simulating the effective electric conductivity of polymer composites with high aspect ratio fillers. *Composites Science and Technology, 132*, 16-23.

Nisar, M., Bergmann, C. P., Geshev, J., Quijada, R., Maraschin, T., de Souza Basso, N. R., . . . Galland, G. B. (2017). Synthesis of high-density polyethylene/rGO-CNT-Fe nanocomposites with outstanding magnetic and electrical properties. *Journal of Applied Polymer Science, 134*(40).

Olabisi, O. (1981). Interpretations of polymer-polymer miscibility: ACS Publications.

Pajoumshariati, S. R., Azizi, M., Wesner, D., Miller, P. G., Shuler, M. L., & Abbaspourrad, A. (2018). Microfluidic-Based Cell-Embedded Microgels Using Nonfluorinated Oil as a Model for the Gastrointestinal Niche. *ACS applied materials & interfaces, 10*(11), 9235-9246.

Paredes, J., Villar-Rodil, S., Martínez-Alonso, A., & Tascon, J. (2008). Graphene oxide dispersions in organic solvents. *Langmuir, 24*(19), 10560-10564.

Paul, D., & Robeson, L. (2008). Polymer nanotechnology: nanocomposites. *Polymer, 49*(15), 3187-3204.

Peacock, A. (2000). *Handbook of polyethylene: structures: properties, and applications*: CRC Press.

Peon, J., Vega, J., Del Amo, B., & Martınez-Salazar, J. (2003). Phase morphology and melt viscoelastic properties in blends of ethylene/vinyl acetate copolymer and metallocene-catalysed linear polyethylene. *Polymer, 44*(10), 2911-2918.

Pirondelli, A., Fabiani, D., Fréchette, M., Bouanga, C. V., Guo, M., & David, È. (2016). *Electric and thermal properties of polyethylene-based nanodielectrics containing graphene-like additives*. Paper presented at the Electrical Insulation and Dielectric Phenomena (CEIDP), 2016 IEEE Conference on.

Pleşa, I., Noţingher, P. V., Schlögl, S., Sumereder, C., & Muhr, M. (2016). Properties of polymer composites used in high-voltage applications. *Polymers, 8*(5), 173.

Ponnamma, D., Sadasivuni, K. K., Wan, C., Thomas, S., & AlMa'adeed, M. A.-A. (2015). *Flexible and stretchable electronic composites*: Springer.

Psarski, M., Piorkowska, E., & Galeski, A. (2000). Crystallization of polyethylene from melt with lowered chain entanglements. *Macromolecules, 33*(3), 916-932.

Pu, S., Hao, Y.-B., Dai, X.-X., Zhang, P.-P., Zeng, J.-B., & Wang, M. (2017). Morphological, rheological, crystalline and mechanical properties of ethylene-vinyl acetate copolymer/linear low-density polyethylene/amphiphilic graphene oxide nanocomposites. *Polymer Testing, 63*, 289-297.

Qiu, H.-J., Guan, Y., Luo, P., & Wang, Y. (2017). Recent advance in fabricating monolithic 3D porous graphene and their applications in biosensing and biofuel cells. *Biosensors and Bioelectronics, 89*, 85-95.

Raju, G. G. (2016). *Dielectrics in electric fields*: CRC press.

Ratanakamnuan, U., & Aht-Ong, D. (2006). Preparation and characterization of low-density polyethylene/banana starch films containing compatibilizer and photosensitizer. *Journal of applied polymer science, 100*(4), 2717-2724.

Ratzsch, K. F., Cecen, V., Tölle, F., Wartig, K. A., Thomann, R., Mülhaupt, R., & Friedrich, C. (2014). Rheology, Electrical Properties, and Percolation of TRGO-Filled EVA-Copolymers. *Macromolecular Materials and Engineering, 299*(9), 1134-1144.

Ray, S. (2015). *Applications of graphene and graphene-oxide based nanomaterials*: William Andrew.

Reddy, K. R., Jeong, H. M., Lee, Y., & Raghu, A. V. (2010). Synthesis of MWCNTs-core/thiophene polymer-sheath composite nanocables by a cationic surfactant-assisted chemical oxidative polymerization and their structural properties. *Journal of Polymer Science Part A: Polymer Chemistry, 48*(7), 1477-1484.

Ren, D., Zheng, S., Wu, F., Yang, W., Liu, Z., & Yang, M. (2014). Formation and evolution of the carbon black network in polyethylene/carbon black composites: Rheology and conductivity properties. *Journal of Applied Polymer Science, 131*(7).

Renaudot, R., Daunay, B., Kumemura, M., Agache, V., Jalabert, L., Collard, D., & Fujita, H. (2013). Optimized micro devices for liquid-dielectrophoresis (LDEP) actuation of conductive solutions. *Sensors and Actuators B: Chemical, 177*, 620-626.

Rizvi, R., & Naguib, H. (2015). Effect of carbon nanoparticle type, content, and stress on piezoresistive polyethylene nanocomposites. *Polymer Engineering and Science, 55*(7), 1643-1651. doi: 10.1002/pen.24002

Rudolph, N., & Osswald, T. A. (2014). *Polymer rheology: fundamentals and applications*: Carl Hanser Verlag GmbH Co KG.

Ruiz-García, C., Darder, M., Aranda, P., & Ruiz-Hitzky, E. (2014). Toward a green way for the chemical production of supported graphenes using porous solids. *Journal of Materials Chemistry A, 2*(7), 2009-2017.

Ruiz-Hitzky, E., Sobral, M. M. C., Gómez-Avilés, A., Nunes, C., Ruiz-García, C., Ferreira, P., & Aranda, P. (2016a). Clay-Graphene Nanoplatelets Functional Conducting Composites. *Advanced Functional Materials*.

Ruiz-Hitzky, E., Sobral, M. M. C., Gómez-Avilés, A., Nunes, C., Ruiz-García, C., Ferreira, P., & Aranda, P. (2016b). Clay-Graphene Nanoplatelets Functional Conducting Composites. *Advanced Functional Materials, 26*(41), 7394-7405.

Ruvolo Filho, A., Menezes, A. J. d., & Scarpa, P. S. d. N. (2008). Correlation among volumetric conductivity, electrical threshold field and compensation plots by oxidation induction time on LDPE/CB composites. *Materials Research, 11*(2), 175-181.

Ryden, K. A., & Hands, A. D. (2017). Modeling of Electric Fields Inside Spacecraft Dielectrics Using In-Orbit Charging Current Data. *IEEE Transactions on Plasma Science, 45*(8), 1927-1932.

Sabet, M., Soleimani, H., & Hosseini, S. (2018). Effect of addition graphene to ethylene vinyl acetate and low-density polyethylene. *Journal of Vinyl and Additive Technology, 24*, E177-E185.

Sabu, T., Visakh, P., Jasma, D., & Nikolic, M. (2011). Handbook of Engineering and Speciality thermoplastics. *Hoboken*.

Sadasivuni, K. K., Ponnamma, D., Kim, J., & Thomas, S. (2015). *Graphene-based polymer nanocomposites in electronics*: Springer.

Schultz, J. M. (2017). On nucleation in miscible polymer blends. *Polymer, 108*, 301-304.

Sefadi, J. S., Luyt, A. S., Pionteck, J., Piana, F., & Gohs, U. (2015). Effect of surfactant and electron treatment on the electrical and thermal conductivity as well as thermal and mechanical properties of ethylene vinyl acetate/expanded graphite composites. *Journal of Applied Polymer Science, 132*(32).

Serdyuk, Y. V., Podoltsev, A. D., & Gubanski, S. M. (2005). Numerical simulations of dielectric properties of composite material with periodic structure. *Journal of electrostatics, 63*(11), 1073-1091.

Shafiee, M., & Ramazani, S. (2008). *Investigation of barrier properties of poly (ethylene vinyl acetate)/organoclay nanocomposite films prepared by phase inversion method.* Paper presented at the Macromolecular symposia.

Shen, L., Wang, F., Yang, H., & Meng, Q. (2011). The combined effects of carbon black and carbon fiber on the electrical properties of composites based on polyethylene or polyethylene/polypropylene blend. *Polymer Testing, 30*(4), 442-448.

Sheng, S., Liu, S., Zhang, L., & Chen, G. (2013). Graphene/poly (ethylene-co-vinyl acetate) composite electrode fabricated by melt compounding for capillary electrophoretic determination of flavones in Cacumen platycladi. *Journal of separation science, 36*(4), 721-728.

Shenogin, S., Lee, J., Voevodin, A. A., & Roy, A. K. (2016). *Multiscale modeling of electrical transport in carbon nanotube-metal-polymer composite materials.* Paper presented at the 24th AIAA/AHS Adaptive Structures Conference.

Shi, X., Zhang, J., Jin, J., & Chen, S. (2008). Non-isothermal crystallization and melting of ethylene-vinyl acetate copolymers with different vinyl acetate contents. *Express Polym Lett, 2*(9), 623-629.

Shokri, E., Yegani, R., Heidari, S., & Shoeyb, Z. (2015). Effect of PE-g-MA compatibilizer on the structure and performance of HDPE/EVA blend membranes fabricated via TIPS method. *Chemical Engineering Research and Design, 100*, 237-247.

Siemann, U. (2005). Solvent cast technology–a versatile tool for thin film production *Scattering methods and the properties of polymer materials* (pp. 1-14): Springer.

Sihvola, A. (2000). Mixing rules with complex dielectric coefficients. *Subsurface sensing technologies and applications, 1*(4), 393-415.

Silva, C., Caridade, S. G., Cunha, E., Sousa, M. P., Rocha, H., Mano, J. F., . . . Alves, N. M. (2018). Nanostructured Biopolymer/Few-Layer Graphene Freestanding Films with Enhanced Mechanical and Electrical Properties. *Macromolecular Materials and Engineering, 303*(4), 1700316.

Singh, K., Ohlan, A., & Dhawan, S. (2012). Polymer-graphene nanocomposites: Preparation, characterization, properties, and applications *Nanocomposites-New Trends and Developments*: InTech.

Soheilmoghaddam, M., Adelnia, H., Bidsorkhi, H. C., Sharifzadeh, G., Wahit, M. U., Akos, N. I., & Yussuf, A. A. (2017). Development of Ethylene-Vinyl Acetate Composites Reinforced with Graphene Platelets. *Macromolecular Materials and Engineering, 302*(2).

Son, D. R., Raghu, A. V., Reddy, K. R., & Jeong, H. M. (2016). Compatibility of thermally reduced graphene with polyesters. *Journal of Macromolecular Science, Part B, 55*(11), 1099-1110.

Song, Y., Zheng, Q., & Yi, X. S. (2004). Reversible nonlinear conduction in high-density polyethylene/acetylene carbon black composites at various ambient temperatures. *Journal of Polymer Science Part B: Polymer Physics, 42*(7), 1212-1217.

Sonnier, R., Viretto, A., Dumazert, L., Longerey, M., Buonomo, S., Gallard, B., . . . Freitag, A. (2016). Fire retardant benefits of combining aluminum hydroxide and silica in ethylene-vinyl acetate copolymer (EVA). *Polymer Degradation and Stability, 128*, 228-236.

Sopicka-Lizer, M. (2010). *High-energy ball milling: mechanochemical processing of nanopowders*: Elsevier.

Stankovich, S., Dikin, D. A., Dommett, G. H., Kohlhaas, K. M., Zimney, E. J., Stach, E. A., . . . Ruoff, R. S. (2006). Graphene-based composite materials. *Nature, 442*(7100), 282.

Stark, W., & Jaunich, M. (2011). Investigation of ethylene/vinyl acetate copolymer (EVA) by thermal analysis DSC and DMA. *Polymer Testing, 30*(2), 236-242.

Stepashkina, A., Tsobkallo, E., & Alyoshin, A. (2014). *Electrical conductivity modeling and research of polypropylene composites filled with carbon black.* Paper presented at the Journal of Physics: Conference Series.

Stoller, M. D., Park, S., Zhu, Y., An, J., & Ruoff, R. S. (2008). Graphene-based ultracapacitors. *Nano letters, 8*(10), 3498-3502.

Sumita, M., Sakata, K., Asai, S., Miyasaka, K., & Nakagawa, H. (1991). Dispersion of fillers and the electrical conductivity of polymer blends filled with carbon black. *Polymer Bulletin, 25*(2), 265-271.

Sun, X., Ramesh, P., Itkis, M. E., Bekyarova, E., & Haddon, R. C. (2010). Dependence of the thermal conductivity of two-dimensional graphite nanoplatelet-based composites on the nanoparticle size distribution. *Journal of Physics: Condensed Matter, 22*(33), 334216.

Suñer, S., Joffe, R., Tipper, J., & Emami, N. (2015). Ultra high molecular weight polyethylene/graphene oxide nanocomposites: Thermal, mechanical and wettability characterisation. *Composites Part B: Engineering, 78*, 185-191.

Takidis, G., Bikiaris, D., Papageorgiou, G., Achilias, D., & Sideridou, I. (2003). Compatibility of low-density polyethylene/poly (ethylene-co-vinyl acetate) binary blends prepared by melt mixing. *Journal of Applied Polymer Science, 90*(3), 841-852.

Tanaka, T., Kozako, M., Fuse, N., & Ohki, Y. (2005). Proposal of a multi-core model for polymer nanocomposite dielectrics. *IEEE Transactions on Dielectrics and Electrical Insulation, 12*(4), 669-681.

Tang, H., Chen, X., & Luo, Y. (1997). Studies on the PTC/NTC effect of carbon black filled low density polyethylene composites. *European Polymer Journal, 33*(8), 1383-1386.

Tang, H., Liu, Z., Piao, J., Chen, X., Lou, Y., & Li, S. (1994). Electrical behavior of carbon black-filled polymer composites: Effect of interaction between filler and matrix. *Journal of Applied Polymer Science, 51*(7), 1159-1164.

Tang, M., Qi, F., Chen, M., Sun, Z., Xu, Y., Chen, X., . . . Shen, R. (2016). Synergistic effects of ammonium polyphosphate and red phosphorus with expandable graphite on

flammability and thermal properties of HDPE/EVA blends. *Polymers for Advanced Technologies, 27*(1), 52-60.

Tarani, E., Wurm, A., Schick, C., Bikiaris, D., Chrissafis, K., & Vourlias, G. (2016). Effect of graphene nanoplatelets diameter on non-isothermal crystallization kinetics and melting behavior of high density polyethylene nanocomposites. *Thermochimica Acta, 643*, 94-103.

Thongruang, W., Spontak, R. J., & Balik, C. M. J. P. (2002). Correlated electrical conductivity and mechanical property analysis of high-density polyethylene filled with graphite and carbon fiber. *43*(8), 2279-2286.

Tian, F., Lei, Q., Wang, X., & Wang, Y. (2012). Investigation of electrical properties of LDPE/ZnO nanocomposite dielectrics. *IEEE Transactions on Dielectrics and Electrical Insulation, 19*(3).

Tjong, S. C., & Mai, Y.-W. (2010). *Physical properties and applications of polymer nanocomposites*: Elsevier.

Tkalya, E. (2012). *Graphene-based polymer nanocomposites.* PhD thesis, Technische Universiteit Eindhoven (Eindhoven).

Torquato, S. (2000). Modeling of physical properties of composite materials. *International Journal of Solids and Structures, 37*(1-2), 411-422.

Traina, M., Pegoretti, A., & Penati, A. (2007). Time–temperature dependence of the electrical resistivity of high-density polyethylene/carbon black composites. *Journal of Applied Polymer Science, 106*(3), 2065-2074.

Tsekmes, I., Kochetov, R., Morshuis, P., & Smit, J. (2013). *Thermal conductivity of polymeric composites: A review.* Paper presented at the Solid Dielectrics (ICSD), 2013 IEEE International Conference on.

Utracki, L. (1991). On the viscosity-concentration dependence of immiscible polymer blends. *Journal of Rheology, 35*(8), 1615-1637.

Utracki, L. A. (2010). Clay-containing polymeric nanocomposites and their properties. *IEEE Electrical Insulation Magazine, 26*(4).

Utracki, L. A., & Wilkie, C. A. (2002). *Polymer blends handbook* (Vol. 1): Springer.

Valentová, H., Ilčíková, M., Czaniková, K., Špitalský, Z., Šlouf, M., Nedbal, J., & Omastová, M. (2014). Dynamic mechanical and dielectric properties of ethylene vinyl acetate/carbon nanotube composites. *Journal of Macromolecular Science, Part B, 53*(3), 496-512.

Venkatesulu, B., Jonsson, B. L. G., Edin, H., & Norgren, M. (2013). Modeling of insulating nanocomposites-electric and temperature fields. *IEEE Transactions on Dielectrics and Electrical Insulation, 20*(1), 177-184.

Villacorta, B. S., & Ogale, A. A. (2014). Morphological influence of carbon modifiers on the electromagnetic shielding of their linear low density polyethylene composites. *Journal of Applied Polymer Science, 131*(24).

Villacorta, B. S., Ogale, A. A., & Hubing, T. H. (2013). Effect of heat treatment of carbon nanofibers on the electromagnetic shielding effectiveness of linear low density polyethylene nanocomposites. *Polymer Engineering & Science, 53*(2), 417-423.

Wang, K., Liang, S., Du, R., Zhang, Q., & Fu, Q. (2004). The interplay of thermodynamics and shear on the dispersion of polymer nanocomposite. *Polymer, 45*(23), 7953-7960.

Wang, Q., Meng, Q., Wang, T., & Guo, W. (2017). High-performance antistatic ethylene–vinyl acetate copolymer/high-density polyethylene composites with graphene nanoplatelets coated by polyaniline. *Journal of Applied Polymer Science, 134*(37).

Wang, S., Wu, Z.-S., Zheng, S., Zhou, F., Sun, C., Cheng, H.-M., & Bao, X. (2017). Scalable fabrication of photochemically reduced graphene-based monolithic micro-supercapacitors with superior energy and power densities. *ACS nano, 11*(4), 4283-4291.

Wang, X., Bi, B., Liu, J., Yang, S., Zhou, L., Lu, L., . . . Huang, R. (2018). Halogen-free intumescent flame-retardant ethylene-vinyl acetate copolymer system based on organic montmorillonite and graphene nanosheets. *Journal of Applied Polymer Science, 135*(23), 46361.

Wang, X., Zhao, Y., Jin, J., & Song, M. (2017). A comparative study on the effect of carbon fillers on electrical and thermal conductivity of a cyanate ester resin. *Polymer Testing, 60*, 293-298.

Wang, Z., Nelson, J. K., Hillborg, H., Zhao, S., & Schadler, L. S. (2013). Dielectric constant and breakdown strength of polymer composites with high aspect ratio fillers studied by finite element models. *Composites Science and Technology, 76*, 29-36.

Webb, A. J., Bloor, D., Szablewski, M., & Atkinson, D. (2014). Temperature dependence of electrical transport in a pressure-sensitive nanocomposite. *ACS Appl Mater Interfaces, 6*(15), 12573-12580. doi: 10.1021/am502515u

Wu, C., Huang, X., Wang, G., Lv, L., Chen, G., Li, G., & Jiang, P. J. A. F. M. (2013). Highly conductive nanocomposites with three-dimensional, compactly interconnected graphene networks via a self-assembly process. *23*(4), 506-513.

Wu, C., Liang, X., Dissado, L. A., Chalashkanov, N. M., Dodd, S. J., Gao, Y., & Xu, S. (2018). Dielectric response of nano aluminium tri-hydrate filled silicone rubber. *Composites Science and Technology, 163*, 56-62.

Wu, G., Zheng, Q., Zhang, M., & Hou, Y. (2006). Dynamic viscoelasticity of low-density polyethylene/in-situ-grafted carbon black composite. *Journal of Applied Polymer Science, 100*(5), 4127-4132.

Wu, H., Zhao, W., & Chen, G. (2012). One-pot in situ ball milling preparation of polymer/graphene nanocomposites. *Journal of Applied Polymer Science, 125*(5), 3899-3903.

Wycisk, R., Poźniak, R., & Pasternak, A. J. J. o. e. (2002). Conductive polymer materials with low filler content. *56*(1), 55-66.

Xiaoming, L. J. X. X. T., & Shuangnan, Y. W. Z. (2001). Effect of CPE on PTC Conductive PE/EVA/CB Composite [J]. *China Plastics Industry, 4*, 012.

Xu, J., Zhong, W., & Yao, W. (2010). Modeling of conductivity in carbon fiber-reinforced cement-based composite. *Journal of Materials Science, 45*(13), 3538-3546.

Xu, P., Luo, X., Zhou, Y., Yang, Y., & Ding, Y. (2017). Enhanced cold crystallization and dielectric polarization of PLA composites induced by P [MPEGMA-IL] and graphene. *Thermochimica Acta, 657*, 156-162.

Xue, Y., Li, X.-f., Zhang, D.-h., Wang, H.-s., Chen, Y., & Chen, Y.-f. (2018). Comparison of ATH and SiO2 fillers filled silicone rubber composites for HTV insulators. *Composites Science and Technology, 155*, 137-143.

Yacubowicz, J., & Narkis, M. (1986). Dielectric behavior of carbon black filled polymer composites. *Polymer Engineering & Science, 26*(22), 1568-1573.

Yan, D.-X., Pang, H., Xu, L., Bao, Y., Ren, P.-G., Lei, J., & Li, Z.-M. J. N. (2014). Electromagnetic interference shielding of segregated polymer composite with an ultralow loading of in situ thermally reduced graphene oxide. *25*(14), 145705.

Yan, Z., Martin, C. L., Guillon, O., & Bouvard, D. (2013). Effect of size and homogeneity of rigid inclusions on the sintering of composites. *Scripta Materialia, 69*(4), 327-330.

Yang, J., Liu, Y., Liu, S., Li, L., Zhang, C., & Liu, T. (2017). Conducting polymer composites: material synthesis and applications in electrochemical capacitive energy storage. *Materials Chemistry Frontiers, 1*(2), 251-268.

Yang, L., Toh, C. L., & Lu, X. (2014). In Situ Preparation of Conducting Polymer Nanocomposites. *Synthesis Techniques for Polymer Nanocomposites*, 211-240.

Yang, Q. Q., & Liang, J. Z. (2010). Electrical properties and morphology of carbon black-filled HDPE/EVA composites. *Journal of Applied Polymer Science, 117*(4), 1998-2002.

Yang, S., Taha-Tijerina, J., Serrato-Diaz, V., Hernandez, K., & Lozano, K. (2007). Dynamic mechanical and thermal analysis of aligned vapor grown carbon nanofiber reinforced polyethylene. *Composites Part B: Engineering, 38*(2), 228-235.

Ye, C. M., Shentu, B. Q., & Weng, Z. X. (2006). Thermal conductivity of high density polyethylene filled with graphite. *Journal of Applied Polymer Science, 101*(6), 3806-3810. doi: 10.1002/app.24044

Yin, S., Niu, Z., & Chen, X. (2012). Assembly of graphene sheets into 3D macroscopic structures. *Small, 8*(16), 2458-2463.

Yousefzade, O., Hemmati, F., Garmabi, H., & Mahdavi, M. (2016). Thermal behavior and electrical conductivity of ethylene vinyl acetate copolymer/expanded graphite nanocomposites: Effects of nanofiller size and loading. *Journal of Vinyl and Additive Technology, 22*(1), 51-60.

Youssef, H. A., Senna, M. M., & Eyssa, H. M. (2007). Characterization of LDPE and LDPE/EVA blends crosslinked by electron beam irradiation and foamed with chemical foaming agent. *Journal of Polymer Research, 14*(5), 351-357.

Yu, J., Zhang, L., Rogunova, M., Summers, J., Hiltner, A., & Baer, E. (2005). Conductivity of polyolefins filled with high-structure carbon black. *Journal of Applied Polymer Science, 98*(4), 1799-1805.

Yuan, N., Ma, F., Fan, Y., Liu, Y., & Ding, J. (2012). High conductive ethylene vinyl acetate composites filled with reduced graphene oxide and polyaniline. *Composites Part A: Applied Science and Manufacturing, 43*(12), 2183-2188.

Yuan, Q., & Wu, D. (2010). Low percolation threshold and high conductivity in carbon black filled polyethylene and polypropylene composites. *Journal of Applied Polymer Science, 115*(6), 3527-3534.

Zarandi, M. B., & Bioki, H. A. (2013). Thermal and mechanical properties of blends of LDPE and EVA crosslinked by electron beam radiation. *The European Physical Journal-Applied Physics, 63*(2).

Zare, Y., & Rhee, K. Y. (2017). Development of a Model for Electrical Conductivity of Polymer/Graphene Nanocomposites Assuming Interphase and Tunneling Regions in

Conductive Networks. *Industrial & Engineering Chemistry Research, 56*(32), 9107-9115.

Zazoum, B., David, E., & Ngô, A. D. (2014). Simulation and modeling of polyethylene/clay nanocomposite for dielectric application. *Transactions on electrical and electronic materials, 15*(4), 175-181.

Zhang, M. Q., Yu, G., Zeng, H. M., Zhang, H. B., & Hen, Y. H. (1998). Two-step percolation in polymer blends filled with carbon black. *Macromolecules, 31*(19), 6724-6726. doi: DOI 10.1021/ma9806918

Zhang, P., & Wang, B. b. (2018). Positive temperature coefficient effect and mechanism of compatible LLDPE/HDPE composites doping conductive graphite powders. *Journal of Applied Polymer Science*, 46453.

Zhang, Y., Tan, Y.-W., Stormer, H. L., & Kim, P. (2005). Experimental observation of the quantum Hall effect and Berry's phase in graphene. *Nature, 438*(7065), 201.

Zhang, Y., Wang, B., Sheng, H., Yuan, B., Yu, B., Tang, G., . . . Hu, Y. (2016). Enhanced fire-retardancy of poly (ethylene vinyl acetate) electrical cable coatings containing microencapsulated ammonium polyphosphate as intumescent flame retardant. *RSC Advances, 6*(88), 85564-85573.

Zhou, S., Hrymak, A., & Kamal, M. (2017). Electrical and morphological properties of microinjection molded polypropylene/carbon nanocomposites. *Journal of Applied Polymer Science, 134*(43).

Zhu, Y., Murali, S., Cai, W., Li, X., Suk, J. W., Potts, J. R., & Ruoff, R. S. (2010). Graphene and graphene oxide: synthesis, properties, and applications. *Advanced Materials, 22*(35), 3906-3924.